Author:
Leitch, A

Title:
Studies on living and fossil Charophyte oosporangia.

STUDIES ON LIVING AND FOSSIL CHAROPHYTE OOSPORANGIA

by

Andrew Leitch

Thesis submitted for the Degree of

Doctor of Philosophy at the

University of Bristol

July, 1986

Volume 1

Memorandum

The work reported in this thesis is the result of my own independant research under the supervision of Prof. F.E. Round and Dr. K.C. Allen.

Andrew Leitch

Acknowledgements

I thank my colleages and friends for useful discussion, advice, instruction and help in many aspects of this work, especially Drs. A. Beckett, R.E. Cambell, R.M. Crawford, M.H. Martin, N.P. Rowe, R.H. Thomas, M.A.J. Williams, A. Woods, P. Wright and Mr. A.J. Byfield. I am grateful to Mr. R. Porter for technical assistance in electron microscopy.

I am grateful to Drs. V.W. Proctor, P. DeDeckker, M. Feist, K. Wilbur and Mrs. J. Moore for their very useful correspondance.

I thank my family and particularly my wife for their help and encouragement throughout this work.

I thank my supervisors Prof. F.E. Round and Dr. K.C. Allen for their guidance and help at all stages of this work.

Finally, I thank the Natural Environment Research Council for sponsoring this work.

SYNOPSIS

The development of the oosporangium of the family Characeae from the first occurrence of the oosporangial primordium to oospore germination is presented in this work. A range of techniques for scanning electron microscopy, transmission electron microscopy and light microscopy were used to achieve this.

1. Cell division and cell differentiation leading to the formation of the oosporangium was studied. The morphological and ultrastructural events are documented.

2. A study was made on the development of a thick multilayered protective wall around the oospore, called the compound oosporangial wall; eight wall layers were identified.

3. The development of the calcified layer, or calcine, was studied.

4. The effect of germination on the compound oosporangial wall and the calcine was investigated. Germination is probably an entirely mechanical process.

5. The site of oosporangial calcification was identified; calcification is extracellular, occurring between the plasmalemma of the spiral cells and the compound oosporangial wall.

6. A comparative study was made of Chara and Lamprothamnium calcine. A number of similarities and differences have emerged. It is not known whether the differences are of taxonomic or ecological importance.

7. Calcine has an organic and mineral phase. The mineral phase was analysed and found to be low-magnesium calcite (Chara) or high-magnesium calcite (Lamprothamnium).

8. A number of parallels are drawn between calcification in charophytes and the formation of the gastropod (Mollusca) nacreous layer.

9. Various morphological forms of calcite are documented including some strange forms of recrystallised calcite.

10. The possible effects of diagenesis on fossil calcine is discussed with reference to a few examples.

11. A collection was made of fossils exhibiting interesting characteristics. These are discussed and compared where possible with extant oosporangia.

12. Modern oosporangia were used as a tool to help identify species in a fossil population from San Martinho do Porto (Upper Jurassic). A systematic appraisal of these fossils is presented; seven taxa are described of which one is new.

Contents

Chapter 1 - INTRODUCTION TO THE FAMILY CHARACEAE

Charophytes are a group of macrophytic green algae anchored to the sediment by colourless rhizoids. They occur in lakes and backwaters of streams and rivers, often forming high density "charophyte meadows". They favour oligotrophic calcareous water to a depth of 15m (see Spence 1982, Stross 1979); disappearing from lakes when they become eutrophic and more productive (Spence 1982). A few species are found in brackish water. One genus Lamprothamnium is exceptional in that it can survive highly saline conditions, but, it requires brackish water for the completion of its life cycle (DeDeckker & Geddles 1980).

The taxonomic affinities of the family Characeae remain controversial. They are a very homogenous group in their life history, reproduction, physiology and ecology. They were assigned divisional status by Round (1984). However, their supposed intermediary position between green algae and bryophytes has led workers to propose that they represent a subdivision of higher plants; perhaps the most recent reference to this is Bremer and Wantorp (1981). Like all green algae they possess chlorophyll a and b and α1-4 linked starch. Mattox and Stewart (1984) recognise 5 distinct classes of green algae of which one the Charophyceae, includes the orders Charales, Coleochaetales, Zygnematales, Klebsormidiales and Chlorokybales grouped together on the basis of flagella insertion, microtubular flagella root system, karyogamy

and cytokinesis. This is a new concept that will require many detailed studies to substantiate.

Most phycologists agree that there is a single extant family the Characeae, within the Charales, with 6 extant genera belonging to 2 subfamilies; the Nitelleae comprising Nitella and Tolypella and the Chareae comprising Chara, Lamprothamnium, Nitellopsis and Lychnothamnus (see Appendix IV). The group has most recently been monographed by Wood and Imahori (1964, 1965). The authorities of all the species mentioned in the text are given in Appendix V. Grambast (1974) reviewed the fossil history which remains distinct as far back as the Upper Devonian. He recognised 9 fossil families the Sycidiaceae, Chovanellaceae, Trochiliscaceae, Eocharaceae, Paleocharaceae, Clavatoraceae, Porocharaceae, Raskyellaceae and the Characeae (see Chapter 6).

In the family Characeae the life cycle commences with the germination of a resistant, resting zygote that produces an emergent prothallus or protonema. The process occurs after a period of dormancy (Takatori & Imahori 1971, Imahori & Iwasa 1965, Shen 1966, Proctor 1967) and is stimulated by red light suggesting a phytochrome system (Takatori & Imahori 1971). The mature thallus (Diag.1.1a) that bears male and female gametangia arises from the protonema (Pringsheim 1862, DeBary 1875, both cited in Sundaralingam 1954, Sundaralingam 1954, Ross 1959 and others). It has an erect habit that ranges in size from 0.5 - 200 cm (average 15-30 cm) (Wood & Imahori 1965) and has a main axis that bears whorls of branchlets at intervals.

Early botanists such as Braun (1852), Kuczewski (1906) and Walker (1929) detailed most of the vegetative and reproductive features encountered in charophytes. Later, Sundaralingam (1954, 1962a,b, 1963, 1965, 1966) made an important contribution with the elucidation of the fine detail of charophyte vegetative and reproductive morphology and ontogeny. His work confirmed conclusively that morphology and ontogeny were essentially the same for all species.

The main axis shows a marked complexity and consists of a regular alternation of tiny discoid cells, the nodal cells, with a large (up to 30 cm long in some species), highly vacuolate, coenocytic cell, the internodal cell. Growth is achieved by cell divisions of an apical dome-shaped cell which cuts off a linear sequence of cells. Each cell then divides into an upper biconcave cell and a lower biconvex cell (see Diag. 1.1b). The biconvex cell elongates to form the internodal cell, and the biconcave cell undergoes a complex sequence of cell divisions, to form the nodal cells. The first of these divisions divides the biconcave cell into two, this forms a wall termed the "halving wall". In each of the two cells produced, small peripheral cells are cut off to the outside producing the typical main axis nodal structure consisting of a ring of small peripheral cells (typically 6-12) surrounding two small central cells.

Growth and division of each peripheral cell produces a branchlet of limited growth which, like the main axis, has an alternating sequence of nodes and internodes. Unlike the main axis, however, no "halving wall" is formed. A number of vegetative structures of

taxonomic importance can occur, these include the development in some species of one or two spine-like outgrowths called stipulodes on either side of the branchlet and the development of a cortex on the branchlets and main axis (i.e. ranks of cells covering the internodal cell, see Diag. 1.1d). The branchlet cortex is generally much simpler than the main axis cortex. In corticate species the main axis cortex may be spinose (Diag. 1.1d). Traditionally, variants found in these features have been used to determine charophyte ancestφry. The interpretations have, however, been severely criticised by Proctor (1980).

The large size of the internodal cell has lent itself ideally to physiological and biochemical studies (Hope & Walker 1975, Lucas & Smith 1973, Lucas 1976a,b, 1977, 1979, 1983, Raven & Smith 1978, Spanswick 1981 and many others). Cytoplasmic streaming is especially marked in the internodal cell and this coupled with the advantage of its large size has led to many detailed studies (Allen 1980, Kamiya 1981, and others). The internodal cell nucleus divides amitotically, forming a coenocytic cell with over 1000 crescent shaped nuclei (Shen 1967a, Roberts & Chen 1975).

The gametangia usually arise from branchlet nodes following cell division of the first formed, oldest peripheral cell. The remaining peripheral cells may divide and elongate to form bract cells. Gametangia are also often associated with two elongate vegetative cells, called bracteoles which are derived from the same peripheral cell as the gametangia (Diag. 1.1c). In monoecious species the male and female gametangia are in close proximity and in some dioecious species an elongate bractlet cell can replace the male gametangium

in female plants.

The male gametangium when young is green, however, during maturation carotenoids accumulate causing the male gametangium to appear orange (Fritsch 1965). The male gametangium is a complex structure of 8 (rarely 4) curved and flattened cells (shield cells), each supported by a columnar cell (the manubrium). These cells enclose a cavity containing colourless spermatogenous filaments, each cell of the filament is an antheridium that gives rise to a single spermatozoan. The ultrastructural features of the male gametangium are described in Pickett-Heaps (1968a, 1975). The spermatozoan has two subapically inserted flagella and is covered in scales. The ultrastructural features of Chara spermatozoa (Pickett-Heaps 1968b, 1975, Möestrup 1970) have been used to speculate on the taxonomic position of the charophytes (Mattox & Stewart 1984).

Genetic examination of the spermatogenous filaments have shown that, in the species investigated, the subfamily Nitelleae has chromosome numbers in multiples of 3 (n = 6,9,12,18,36), and the subfamily Chareae in multiples of 7 (n = 14,21,42,56,70). In both Chara and Nitella a low chromosome number is related to dioecism and a high chromosome number to monoecism (Hotchkiss 1962, 1963, 1966, Tindall & Sawa 1964).

The female gametangium (Diag. 1.1c) is the subject of the forthcoming chapters, each chapter is involved with different aspects of its structure, development and fossil record.

DIAGRAM 1.1 CHARA DELICATULA

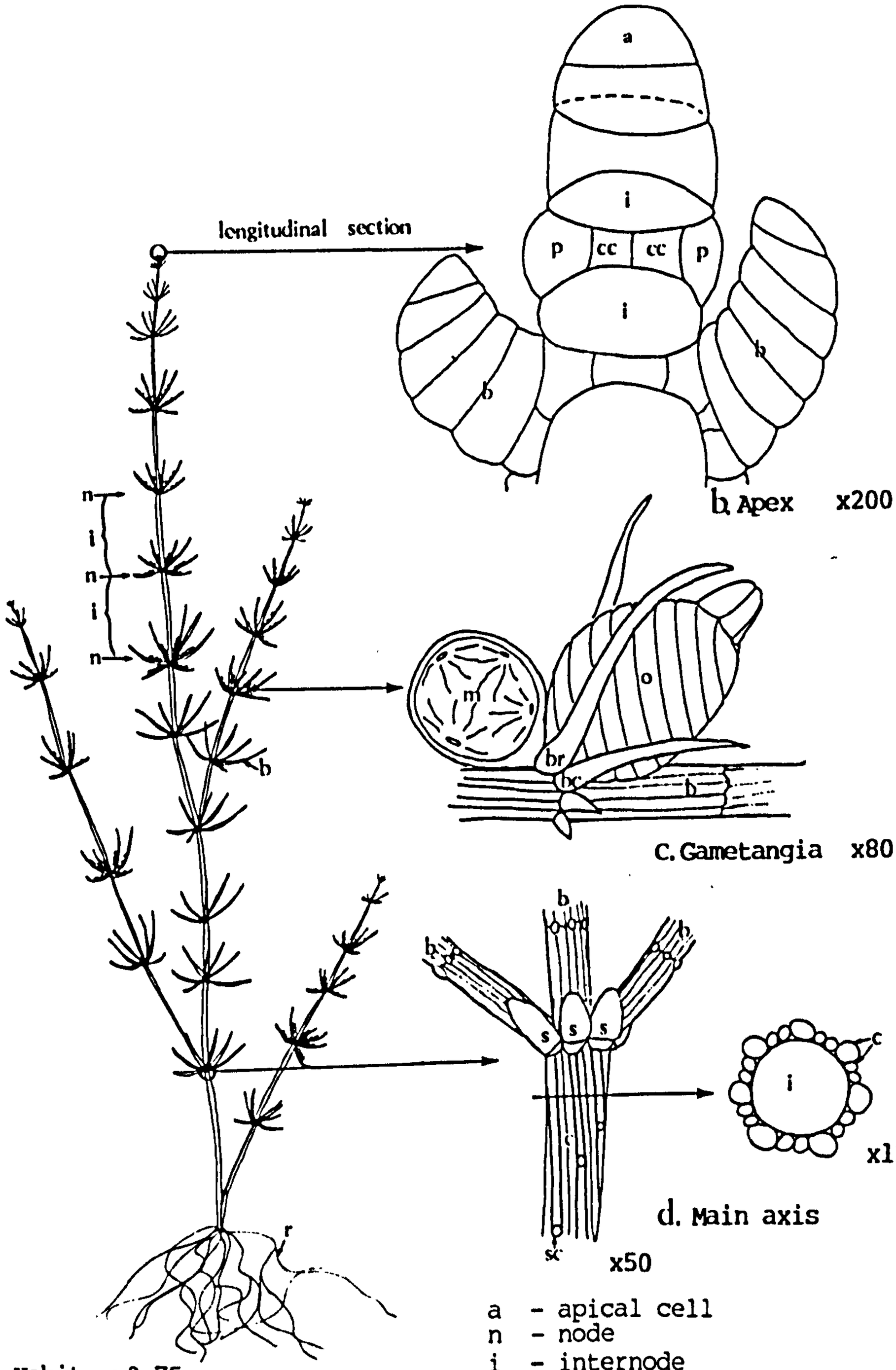

b. Apex x200

C. Gametangia x80

x120

d. Main axis x50

a. Habit x0.75

a - apical cell
n - node
i - internode
b - branchlet
br - bracteole
bc - bract cell
m - male gametangium
o - oosporangium
s - stipulode
c - cortical cell
sc - spine cell
r - rhizoid
p - peripheral cell } node
cc - central cell }

Chapter 2 - MATERIALS AND METHODS

Collection and Culture

Chara hispida and Chara delicatula were collected from drainage ditches in the Gordano Valley, Avon (ST 444 735) and Nitella opaca was collected from the University's Botanical Gardens (ST 558 731). They were cultured in plastic tanks (22x20x35cm) filled with unsterilised mud to a depth of 2cm and tap water. The tanks were illuminated by 4 x 5ft, 80W fluorescent tubes for a 15 hour day. Culturing was carried out at room temperature. Lamprothamnium papulosum was collected from a salt marsh near Lymington (SZ 328 939). Attempts to culture Lamprothamnium in water and mud taken from the collection site failed mainly because of the grazing activities of small crustaceans.

Harvesting Oosporangia for Storage

Fully calcified oosporangia were harvested following the method of Proctor (1967). Freshly collected plants were kneaded in a bowl filled with water. Slight agitation caused the fully developed oosporangia to settle. The plant remains were decanted and removed. Oosporangia of Chara hispida, Chara delicatula and Lamprothamnium papulosum were stored, both dry and under water, in the dark at $4^{o}C$.

Extraction of Fossils

Marls and limestones, collected by Dr. K.C. Allen from the Upper Jurassic of Portugal (locality: San Martinho do Porto) and soft marls from the Eocene of England (locality: Hordle Cliffs) were macerated in different ways according to their composition. The procedure follows the recommendations of Feist and Grambast-Fessard (unpublished).

a. Soft Marls: 1 kg of fragmented rock was placed in 30% hydrogen peroxide. The rock was macerated by adding 500g of sodium carbonate and leaving for 24 hours.

b. Harder Marls: 1 kg of fragmented rock was soaked in petrol for 30 minutes. The rock was macerated by adding water and leaving for one hour.

c. Limestone: 1 kg of fragmented rock was treated with a mixture of anhydrous copper sulphate in glacial acetic acid (100 g/l). At the first signs of disintegration ammonium hydroxide was slowly added (very exothermic reaction).

Siliceous charophyte petrifications from the Purbeck (Upper Jurassic) of Dorset (loose cherty pebbles taken from Stair Hole) were extracted from 1 kg of fragmented limestone by macerating the rock in 10% hydrochloric acid.

In all cases the macerates were sieved using Endecotts Ltd.

Laboratory Test Sieves (pore sizes 2mm, 500μm, 150μm). Fossils were extracted from the 500μm and 150μm sieve fractions and cleaned, if necessary, in an ultrasonic bath (30 seconds in warm water).

Specimen Collections

Specimens were examined from herbarium sheets ("Complete Vasculum of British Charophyta", Groves and Bullock-Webster (1934) collection) at Bristol University.

Oosporangia of Nitella translucens, from Shannagh, Donegal were kindly supplied by J. Moore (British Museum, Natural History).

Gyrogonites of Saportonella maslovi from the Maastrichtian (Upper Cretaceous) of France and Rantzieniella nitida from the Aquitanian (Miocene) of France were kindly supplied by Dr. M. Feist and Mme. N. Grambast-Fessard (Université des Sciences et Techniques du Languedoc, France).

Germination

Many attempts were made to germinate oospores, only Chara hispida was germinated successfully. The oosporangia were extracted from mud underlying a healthy Chara hispida sward. The mud was sieved using Endecotts Ltd. Laboratory Test Sieves (2mm, 500μm, 150μm pore sizes) and the oosporangia were extracted from the 150μm sieve

fraction. The oosporangia were stored at low temperature (4°C) in the dark for one month. Low temperature storage is known to break dormancy (Shen 1966).

Germination was carried out in 150x25mm tubes using aseptic techniques following the recommendations of Takatori and Imahori (1971). All media were autoclaved and all oosporangia were surface sterilised in 1% sodium hypochlorite for half an hour and rinsed three times in sterilised distilled water. Each tube contained autoclaved 1.2% agar to a depth of 20mm and a germination medium to a depth of 40mm. Germination was carried out at a constant temperature (21°C) in continuous light. A germination medium of distilled water and gibberellic acid (20ppm (w/v)) gave 17% germination and distilled water alone gave 10% germination.

Transmission Electron Microscopy (T.E.M.)

Sections were examined at 40-80 kV using either a Phi L.ips 300 or an AEB 6G transmission electron microscope. Sections were prepared as follows.

A. Preparation of Living Material.

1. Early stages in oosporangium differentiation were excised from the thallus under water. They were then transferred to a glass vial containing fixative.

2. Advanced stages in oosporangium differentiation

(immediately prior to fertilisation and post-fertilisation stages) were fixed in the following way.

a. Uncalcified oosporangia of all species examined were placed on a glass slide in a drop of fixative and pierced with fine entomological needles under the binocular microscope. They were then transferred to a vial containing fixative.

b. Calcified oosporangia of Chara were first decalcified by removing the calcine by micromanipulation. The oosporangia were then pierced in a drop of fixative and transferred to a glass vial containing fixative (as in a above).

c. Calcified oosporangia of Lamprothamnium papulosum were pierced in a drop of fixative by plunging a fine entomological needle through the weakly calcified apex. (This does not damage sub-apical calcine). The oosporangia were then transferred to a glass vial containing fixative.

d. Calcified oosporangia of Chara, with intact calcine, could only be fixed and embedded if they had germinated. The emergent protonema and the germ pore allowed the infiltration of fixatives and embedding resins. Germinated oosporangia were removed from the agar on which the emergent protonema was developing (see Germination above) and transferred to a glass vial containing fixative.

B. Fixing and Embedding the Specimens.

The following schedule proved satisfactory because it reduced plasmolysis to a minimum (plasmolysis was a problem in large cells) and the fixative penetrated the tissues well.

Spurr's (1969) resin (Taab Premix Kit) gave the best membrane preservation. However, LR White (medium grade) resin was favoured as the embedding resin for the following reasons:

a) it gave much better infiltration

b) it gave better contrast in the electron microscope

c) it was non-toxic.

The fixation and resin embedding schedule is shown below.

1. Preparation of fixative.

   a. Place 0.124g paraformaldehyde in 6.8 ml water, heat to 70°C. Clear the solution by adding drops of 0.1N sodium hydroxide and leave to cool.

   b. Add (i) 10.2 ml filtered pond water
   (ii) 3 ml 0.2M sodium cacodylate pH 7.2
   (iii) 10ml of 8% glutaraldehyde (aq).

2. Fix for 3 hours in glass vials.
   Wash for 3 x 8 minutes in sodium cacodylate buffer (0.2M, pH 7.2).

3. Post-fix for 3 hours in 2% osmium tetroxide in sodium cacodylate buffer (0.2M, pH 7.2) in the dark.
   Wash for: 3 x 10 minutes in sodium cacodylate
   3 x 10 minutes in distilled water.

4. Block stain overnight in 0.25% uranyl acetate (aq) in the dark at 4°C.
   Wash for 3 x 10 minutes in distilled water.

5. Dehydrate in ethanol (10 minutes).
   10%, 20%, 30%, 50%, 70%, 90%, 100%, 100%, 100%.

6. Embed in LR White (medium grade) resin.

100% ethanol	:	LR White	Time
3	:	1	30 minutes
1	:	1	1 hour
1	:	3	3 hours

LR White, 3 days, 6 changes.

7. Polymerise at 70°C for 24 hours in open dishes ensuring a depth of resin >1 cm.

8. All oosporangia having a high starch content, (i.e. those oosporangia which fall into sections 2 and 3 Preparation of Living Material for Fixing (above)), needed re-embedding before sectioning. Polymerised blocks were trimmed to expose the face to be sectioned, re-embedded for three days (6 changes) in LR White and re-polymerised at 70°C for 12 hours in open dishes ensuring that the resin adequately covered the specimen (top 2mm does not polymerise properly in air).

C. Sectioning.

Sections (80-100nm thick, i.e. silver sections) were cut with a Du Pont diamond knife using an LKB Ultrotome III.

Sections of large specimens were picked up on copper slot grids (slot size 2x0.05mm). The grids had been previously coated with 0.5% Formvar made up in ethylene dichloride and air dried on Whatman grade 50 filter paper. The sections, held in the grid's slot by surface tension of the water, were transferred onto a Formvar support film (prepared from 0.5% Formvar made up in ethylene dichloride dried over a molecular sieve). The sections and grids dried onto the Formvar support film and formed an intimate contact. Slot grids were then carbon stabilised (1.5 kV, 50mA for 10 seconds) using a Cressington Electron Beam Evaporator.

Sections of smaller specimens were picked up on copper mesh

grids (200 hexagonal) coated with a Formvar support film (prepared as above).

D. Staining.

All staining was carried out on a wax sheet in a petri dish by placing the grid (sections downwards) onto a drop of stain. All stains were injected through a Millipore Millex-GS 0.22µm filter unit onto the wax sheet. A small water reservoir ensured the atmosphere in the petri dish was saturated with water vapour. This reduced evaporation from the stain droplet. Reynolds' (1963) lead citrate staining was carried out in a carbon dioxide free atmosphere. Sodium hydroxide pellets should not be used to remove carbon dioxide as they are deliquescent and pull water from the atmosphere and then the stain (O'Brian & McCully 1981). The methods of staining are shown below.

1. All sections (except those in 2 and 3 below) were stained as follows:

   a. Reynolds' (1963) lead citrate for 5 minutes
   b. washed in a continuous stream of filtered distilled water for 1 minute
   c. uranyl acetate (2% in 30% alcohol) for 2 minutes in the dark.
   d. washed in a continuous stream of filtered distilled water and air dried.

2. Staining the calcine of Chara hispida using the procedure (1. above), partially decalcifies the section and exposes the organic matrix. Omitting the uranyl acetate staining (1c above) preserves more calcite but reduces contrast in the organic matrix.

3. Staining the organic matrix in Lamprothamnium papulosum required an exceptionally heavy staining procedure to provide sufficient contrast. The method of Hoch (1977) was modified to achieve this:

   a. 1% barium permanganate(aq) for 30 seconds
   b. washed in a stream of filtered distilled water for 1 minute
   c. 0.05% citric acid for 30 seconds
   d. washed in a stream of filtered distilled water for 1 minute
   e. Reynolds' (1963) lead citrate for 5 minutes
   f. washed in a stream of filtered distilled water for 1 minute
   g. 2% uranyl acetate (aq) in the dark for 2 minutes
   h. washed in a stream of filtered distilled water for 1 minute and air then dried.

X-Ray Microanalysis

The compound oosporangial wall of Chara hispida was isolated in a drop of fixative. The fixation procedure had to be free of heavy metals. Consequently, the fixative was prepared as for transmission electron microscopy (above), omitting the post-fix in osmium tetroxide (step 3) and the block staining in uranyl acetate (step 4).

Sections 80-120nm thick were cut using a Du Pont diamond knife on an LKB Ultrotome III and picked up on carbon coated slot grids. Carbon films were prepared on a sheet of freshly cleaved mica using a Cressington Electron Beam Evaporator (1.5kV, 50mA for 10 seconds). Sections were examined at 80 kV using a Jeol JEM 200CX TEM Scan fitted with a KEV EX5000A X-ray energy spectrometer. For spot analysis, the electron beam was focused (probe diameter = 10nm) for an analysis duration of 100 seconds. Control X-ray

emission spectra were obtained by analysing resin only regions of the section.

Mr. P. Heap (Bristol University) kindly operated all the equipment necessary to obtain X-ray emission spectra.

X-Ray Crystallography

The calcine of Chara hispida and Lamprothamnium papulosum was isolated and ground to a fine powder. This was mixed into a small drop of water on a freshly cleaned microscope slide and air dried.

Identification of the crystalline powder was carried out using a Phi Lips PW 1730/10 Powder Diffractometer with an automatic divergence slit. Scans were taken at 40kV, 40mA and at a scan speed of $1^{o}_{2\theta}$/min. Dr D. Robinson (Bristol University) kindly operated all the equipment necessary for the X-ray crystallography.

Light Microscopy

Material for light microscopy was examined using bright field and Nomarski interference contrast on an Olympus BHB compound microscope.

A. Thin sections

Material for sectioning was fixed as for transmission electron microscopy. Sections (>200nm) were cut with a freshly prepared

glass knife using an LKB Ultrotome III. They were then transferred to a glass slide using a wire loop and mounted onto the slide using a hot plate.

Sections were stained using a method adapted from Grimley (1964). The stain was devised for plastic embedded osmium-fixed tissues. Stain the sections as follows:

1. 4% toluidine blue (aq) and 4% malachite green (aq) in a 1:1 mix for 5 seconds. Wash in a continuous stream of water for 1 minute.

2. 4% basic fuschsin (aq) (freshly filtered through Whatman grade 50 filter paper) for 5 seconds. Wash in a continuous stream of water for 1 minute and air dry.

All sections except those that demonstrated calcine were permanently mounted in Elvacite dissolved in xylene. Sections showing calcine were not mounted in Elvacite because the mountant has a similar optical density to the organic material in the calcine and so it masks calcine detail.

Fossil calcine could not be sectioned.

B. Carborundum Ground Sections.

The method enables single oosporangia or gyrogonites to be ground into thin section. The technique was carried out on the extant species Chara hispida and Lamprothamnium papulosum and the fossil species Musacchiella palmeri and Musacchiella douzensis. The sections were prepared using the methods shown below.

1. An oosporangium/gyrogonite was embedded in LR White

(medium grade).

2. Polymerised at 70°C for 24 hours.

3. The resin block was trimmed under a binocular microscope.

4. The resin block was ground to a polished surface using Carborundum (grades 100, 500, 1000) under a binocular microscope. Excess Carborundum was removed with water and a soft paint brush. The block was air dried.

5. The polished surface of the block was stuck to a glass slide using Superglue Rapid.

6. The second side of the block was trimmed and the oosporangium/gyrogonite ground to a polished thin section using Carborundum (grades 100, 500, 1000). Excess Carborundum was removed with water and a soft paint brush.

7. The section was mounted in Elvacite dissolved in xylene.

Scanning Electron Microscopy (S.E.M.)

All specimens were examined on a Cambridge S4 or a Phillips 501B scanning electron microscope at 15-20 kV. Specimens were mounted onto S.E.M. stubs using double sided Sellotape and sputter coated with gold using a Polaron coating unit. If specimen charging was a problem then silver conductive paint was used as a mountant. This is a messy technique and was used as little as possible.

Critical Point Dried Specimens

Specimens to be critical point dried for S.E.M. were prepared using the following method.

1. Freshly collected material was fixed in 1% glutaraldehyde in 0.1M sodium cacodylate buffer pH 7.2 and 1% osmium tetroxide in 0.1M sodium cacodylate buffer pH 7.2 for 2 hours in the dark.

2. Washed 3 x 10 minutes in 0.1M sodium cacodylate pH 7.2.

3. Post-fixed in 1% osmium tetroxide in 0.1M sodium cacodylate pH 7.2 for 2 hours.

4. Washed 3 x 10 minutes in distilled water.

5. Dehydrated in acetone (10 minutes) 10%, 20%, 30%, 50%, 70%, 90%, 100%, 100%, 100%.

6. Material was transferred to a Samdri-780 critical point drier.

Acid Etched Specimens

The extant species Chara hispida and Lamprothamnium papulosum were acid etched using the following method.

1. The oosporangia were embedded in LR White (medium grade) resin.

2. Polymerised at 70°C in open dishes for 24 hours.

3. The resin block was trimmed under a binocular microscope.

4. The resin block was ground to a polished surface using Carborundum (grades 100, 500, 1000) under a binocular microscope. Excess Carborundum was removed with water and a soft paint brush.

5. The polished surface was etched with a continuous stream of acid (0.01%-0.1% hydrochloric acid) for varying amounts of time (5-30 seconds).

6. Air dried and mounted for S.E.M..

Laboratory Grown Calcite

Calcite crystals were grown on an S.E.M. stub by submerging the stub for 20 minutes in a beaker containing the reaction reagents sodium hydrogen carbonate(1M) and calcium chloride(1M) in a 1:1 mix. The stub was then air dried for S.E.M..

Fast Atom Beam Etching

Calcine removed from the oosporangia of Chara hispida was air dried and mounted onto two S.E.M. stubs using silver conductive paint. Two periods (20mins. and 2hrs.) of fast atom beam etching were carried out using a water cooled, Ion Tech Fast Atom Beam 26M Source mounted on a high-vacuum base. Etched calcine was examined at 15 kV using a Hitachi S-800 field emission scanning electron microscope. The operation of this equipment was kindly carried out by Mr D. Claugher (British Museum, Natural History).

Experiment to show the effects of bacterial action on the substructure of Chara and Lamprothamnium calcine.

The use of bacteria to hydrolyse the organic component in the calcine of Chara hispida and Lamprothamnium papulosum would, it was hoped, reveal the relationship of the inorganic and organic phases of the calcine. All glassware and agar were autoclaved prior to use.

1. Prepare the colonies of bacteria from pond water as follows:

   a. inoculate petri dishes containing 2% agar (made up in pond water) with serial dilutions of pond water

   b. incubate for 1 week to raise bacterial colonies. Subculture 4 colonies on to new petri dishes each containing 2% agar (made up in pond water).

2. Sterilise the calcine by using one of the following:

   a. ethylene dichloride vapour in a sealed autoclaved flask

   b. autoclave without the addition of any chemicals (the

calcine is autoclaved dry).

3. Inoculate the calcine with bacteria. Add sterilised calcine from each species to 3 sets of 5 flasks containing autoclaved distilled water. Inoculate 4 flasks from each set with one of the bacterial subcultures. The fifth flask in each set remains uninoculated as a control.

4. Incubate the flasks for 1 week, 2weeks or 3 weeks at 20°C.

5. After incubation the calcine is air dried on Whatman grade 50 filter paper and mounted on S.E.M. stubs.

Experiment to show the influence of water on isolated calcine.

Calcine removed from the oosporangia of Chara hispida and Lamprothamnium papulosum was soaked in water for varying lengths of time (hours to weeks). Four sources of water were used, each with a different calcium concentration; these are shown below.

1. Distilled water.
2. Tap water.
3. Distilled water standing over calcium carbonate powder for 1 week.
4. Distilled water standing over calcium carbonate powder for 2 months and considered to be saturated in calcium carbonate.

Experiment to show the effects of water on Glutaraldehyde fixed calcine.

Calcine removed from oosporangia of Chara hispida was fixed in 2% glutaraldehyde (in O.1M sodium cacodylate pH 7.2) for 3 hours. The calcine was then given three rinses in distilled water and soaked for varying time spans in distilled water (hours to days). After soaking the calcine was air dried on Whatman grade 50 filter paper and mounted on S.E.M. stubs.

Experiment to show the effects of Pronase on the substructure of Chara calcine.

The experiment was designed to use the enzyme pronase in a high pH buffer to hydrolyse any proteins, if present, in the calcine of Chara avoiding the problem of the calcite dissolving.

The calcine was removed from the oosporangia of Chara hispida and added to the enzyme/buffer medium (below). A buffer only control was carried out. The reaction was terminated by rinsing the calcine in distilled water 3 times. The calcine was then air dried on Whatman grade 50 filter paper and mounted on S.E.M. stubs.

Enzyme/buffer medium: pronase (1mg/ml) in the reaction buffer, 0.01M Tris-HCl pH 7.8, 0.01M EDTA, 0.5% sodium dodecyl sulphate. Incubate at 37°C for 17 hours.

Experiment to show the effects of Proteinase K and Zymolyase on the substructure of Chara and Lamprothamnium calcine.

The experiment was designed to use the enzymes proteinase K and zymolyase to hydrolyse organic material in the calcine of Chara and Lamprothamnium. Proteinase K hydrolyses proteins and zymolyase hydrolyses cell wall glucans.

Calcine removed from oosporangia of Chara hispida and Lamprothamnium papulosum was added to the proteinase K/buffer

medium (1 below) and then added to the zymolyase/buffer medium (2 below). Buffer only controls were carried out. The reactions were terminated by rinsing the calcine in distilled water three times.

The calcine was then air dried on Whatman grade 50 filter paper and mounted on S.E.M. stubs.

Preparation of the enzyme/buffer mediums are given below.

1. Proteinase K (1mg/ml) in the reaction buffer; O.OlM Tris-HCl pH 7.8, O.OO5M EDTA and O.5% sodium dodecyl sulphate. Incubate at 37°C for 30mins..

2. Zymolyase (1mg/ml) in the reaction buffer; 1.2M sorbital, O.OlM EDTA and O.1M sodium citrate. Incubate at 29°C for 30mins..

Experiment to show the effects of sodium hypochlorite on calcine substructure.

Calcine removed from the oosporangia of Chara hispida and Lamprothamnium papulosum was soaked in varying concentrations of sodium hypochlorite (1-10%) for varying time spans (10 secs-5 mins). After soaking the calcine was air dried on Whatman grade 50 filter paper and mounted on S.E.M. stubs using double sided Sellotape.

Measurements.

Gyrogonites and oosporangia were measured under an Olympus VMT binocular microscope at x20 and x80 using a calibrated eye piece graticule. The following measurements were taken (after Horn af Rantzien 1956).

(i) Length of the polar axis (LPA) = Linear distance between the poles passing through the gyrogonite/oosporangium centre.

(ii) Largest equatorial diameter (LED) = Greatest width that can be measured perpendicular to LPA.

(iii) Anisopolar distance (AND) = Linear distance from the apical pore to LED.

(iv) Width of the spirals (WS) = Measured perpendicular to the lateral wall of a spiral at the equator.

(v) Number of convolutions (NC) = Number of spirals that would be crossed by an imaginary line defining the LPA.

(vi) Apical pore (AP) = The maximum width of the apical pore in gyrogonites. Ungerminated oosporangia have no apical pore, but the position where the calcine will fracture on germination is marked by a sudden change in calcine thickness at the apex. The maximum diameter of the apical region of thin calcine is the AP in ungerminated oosporangia.

(vii) Basal pore (BP) = The maximum width of the basal pore.

(viii) Number of revolutions (NR) = Number of revolutions of a single spiral.

(ix) Isopolarity index (ISI) = Ratio of length and width as a percentage. A number which expresses how elliptical the oosporangium/gyrogonite is ("oblongness"):

ISI = LPA/LED x 100

	ISI
peroblate	<50
oblate	50-75
suboblate	76-88
oblate spheroidal	89-100
prolate spheroidal	101-114
subprolate	115-133
prolate	134-200
perprolate	>200

(x) Anisopolarity index (ANI) = Ratio of length to width as a percentage. A number expressing how oval the oosporangium/gyrogonite is ("ovalness"):

ANI = AND/LPA x 100

	ANI
perovoidal	<15
ovoidal	15-29
subovoidal	30-43
ellipsoidal	44-57
subobovoidal	58-71
obovoidal	72-85
perovoidal	>85

Computing and Statistics.

Cluster analysis (single link, centroid and average link) and principal component analysis carried out on gyrogonites and oosporangia were run on the University's main frame computer using programs written in the statistical package Genstat (see Appendices Ia and Ib). Miss S. Evans (University of Bristol) kindly wrote and

devised the programs to suit the requirements of the problem. Details of the language and the principles of the matrix algebra are complex and beyond the scope of this work.

Two tailed t-tests were carried out using the students statistical package (Bristol University) on a BBC microcomputer.

Measurements of Dry Weights.

Fresh material was dried for 24 hours at 100°C and weighed using a Cahn/Ventron Automatic Electrobalance.

Chapter 3 - DEVELOPMENTAL MORPHOLOGY OF THE CHAROPHYTE OOSPORANGIUM

(i) Prior to fertilisation

Introduction

The female gametangium, or oosporangium presents a complexity not encountered in any other algae; only in one other algal genus Coleochaete (Class Charophyceae sensu Mattox & Stewart 1984) is the zygote (oospore) known to be covered by outgrowths of surrounding vegetative cells.

The term oosporangium is used for the female fructification of the family Characeae following the recommendations of Horn af Rantzien (1956). The term oogonium frequently appears in the literature but it is inadequate largely because it usually refers to the unicellular egg cell in oogamous algae. I have extended Horn af Rantzien's (1956) definition of the oosporangium to include pre- and post- fertilisation stages in the fructification development (thereby ignoring his term for the pre- fertilisation stage, sporophydium).

Horn af Rantzien (1956) was the first to review the terminology applied to the charophyte oosporangium, his terms have not however been widely used and his opening comment is as applicable today as when he wrote it. "In spite of a considerable number of investigations devoted to the female reproductive bodies and

fructifications of the Charophyta there is no generally adopted system of terms". Here the terminology recommended by Horn af Rantzien (1956) has been adopted where applicable, in a few cases terms which are not useful for this work have simply been ignored while, in other cases, where stated they have been altered to avoid the confusion they generate.

Early development of the oosporangium proceeds by a complex series of cell divisions that give rise to a central reproductive cell, the oosphere (oospore after fertilisation), ensheathed by five sinistrally spiralling cells, the spiral cells and one or three basal, sterile cell(s) (Diag. 3.1 below). In the subfamily Chareae and the section Acutifolia of the genus Tolypella (subfamily Nitelleae) one cell division of an oosphere mother cell gives rise to an oosphere and one sterile cell (Sundaralingam 1954, 1962a,b, 1963, 1965, 1966, Sawa & Frame 1974). In the remaining members of the subfamily Nitelleae the oosphere mother cell divides to give rise to one oosphere and three basal sterile cells (Sawa & Frame 1974). In both subfamilies the sterile cell(s) remains basal and vestigial. The term "sterile cell" is a new term adapted from "sterile oogonial cell". The term sterile oogonial cell occurs frequently in the literature (Horn af Rantzien 1956, Daily 1975, Sawa & Frame 1974 and others); I have rejected it because it is a contradictory term. Each spiral cell undergoes one (Chareae) or two (Nitelleae) cell divisions giving rise to one or two small apical coronula cells (Sundaralingam 1954, 1962a,b, 1963, 1965, 1966). According to Goebel's (1902 -cited in Fritsch 1965) hypothesis the oosporangium represents a modified branchlet of limited growth.

The oosporangium is believed to become receptive to spermatozoa after small fertilisation slits appear between the spiral cells at the apex (DeBary 1871 -cited in Fritsch 1965). These slits allow entry of the spermatozoa which are then attracted to the oosphere at the receptive spot, an apical granular zone of cytoplasm. The oosphere nucleus is not located near the receptive spot but is basal (DeBary 1871 -cited in Fritsch 1965, confirmed by Pickett-Heaps 1975). It is assumed, therefore, that the spermatozoan nucleus must pass through the dense cytoplasm to effect nuclear fusion.

Only one ultrastructural study has previously examined the fine structure during the early ontogeny of the charophyte oosporangium. This study by Pickett-Heaps (1975) on Chara fibrosa produced some most fascinating data. Here a comparative and more extensive study on the early ontogeny and morphology of charophyte oosporangia is presented, using data from three species: Chara delicatula, Chara hispida and Nitella opaca (sensu Allen 1950). The work also includes new ultrastructural details of the earliest and latest pre-fertilisation stages.

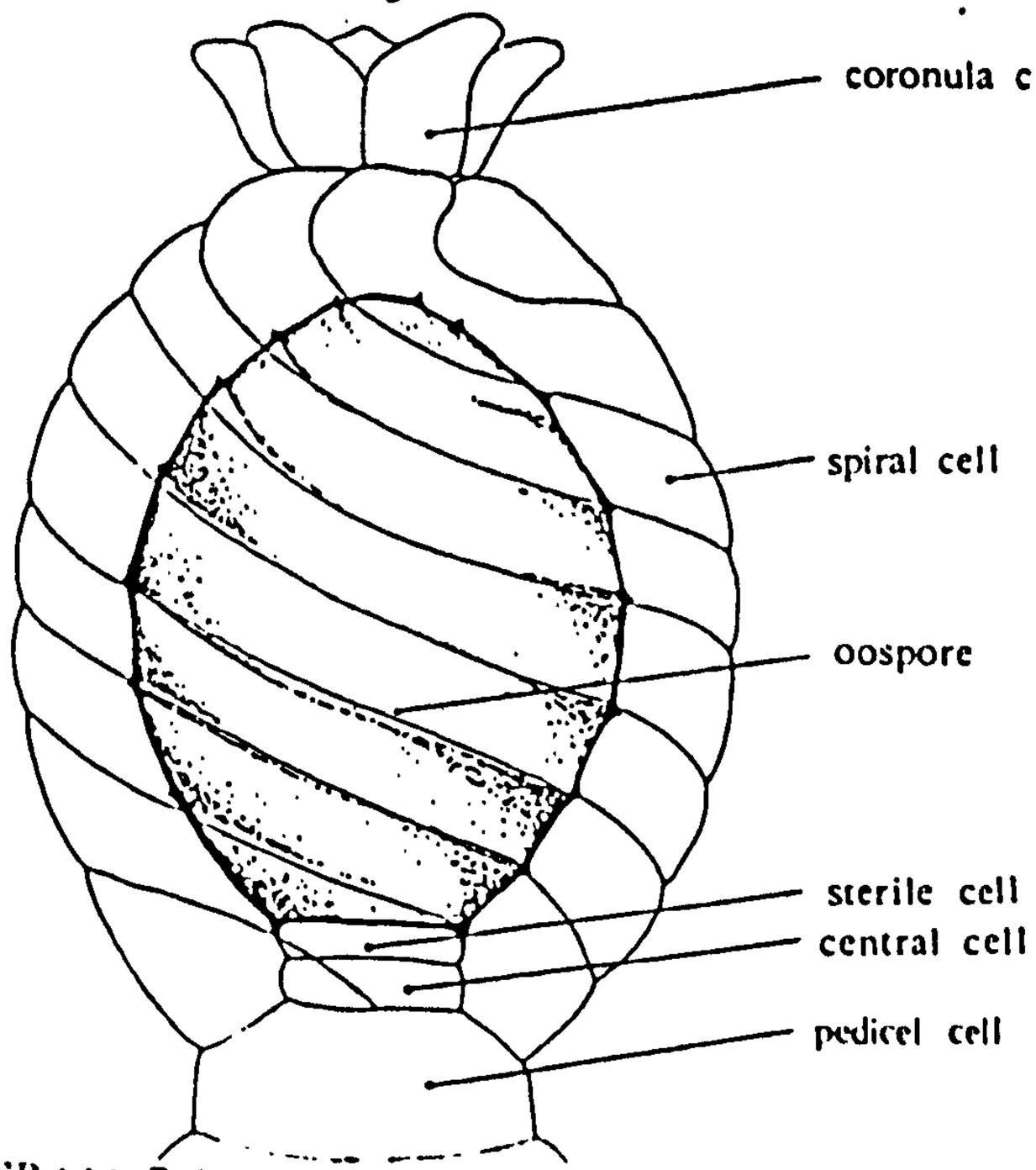

DIAGRAM 3·1 SHOWING THE OOSPORANGIUM OF *CHARA*

Results and Discussion

The results presented below are based on a study of Chara delicatula unless otherwise stated. In Chara delicatula the uppermost 2 - 4 cells of the branchlet do not divide into the node / internode sequence but elongate like internodal cells. This is also encountered in many other species (see Wood & Imahori 1964). Usually, the lowest four branchlet nodes (excluding the basal node) are involved in the formation of the gametangia. The oldest and first formed branchlet node is usually at the base of the branchlet and each successive more distal branchlet node being formed subsequently (Kuczewski 1906). This was referred to as centrifugal development. This age sequence of node formation is reflected in a developmental sequence of gametangia along the branchlet's length (i.e. the oldest gametangia are basal). However, some individuals exhibit the reverse developmental sequence (centripetal development) and the oldest gametangia are the most distal. Therefore, Chara delicatula exhibits both centrifugal and centripetal development; a feature that traditionally carries no taxonomic weight per se.

The gametangia develop from the first formed peripheral cell of each branchlet node. Since there is no developmental rotation in successive branchlet nodes (as occurs in nodes of the main axis) these first formed peripheral cells lie in the same relative position (i.e. adaxial along the longitudinal centre of the branchlet). As the peripheral cells give rise to gametangia, the

gametangia are also adaxial and in a straight line (Pl.1, Figs.1a,b,c).

In Chara delicatula the peripheral cell involved in gametangial formation enlarges, becoming considerably larger than the other, younger peripheral cells in the node and an apical cell is cut off. This apical cell is the male gametangial primordium (Pl.1, Fig. 1a, Diag. 3.2a). Following karyogamy in the lower cell, cell plate formation occurs between two well separated telophasic nuclei (Pl.1, Figs.1a,4). This forms a row of three cells; the male gametangial primordium, the gametangial node and the basal cell (Pl.1, Fig.1b, Diag. 3.2b). The row of cells can be considered as a branchlet of the second order (being borne on a branchlet of the first order).

The development of the male gametangial primordium has not been followed in this work; however, the interested reader is referred to Pickett-Heaps (1968a,b, 1975) for a detailed account of the development of the male gametangium in Chara fibrosa. The basal cell is no longer involved in gametangial development and becomes highly vacuolate (Pl.1, Figs.2,3). The gametangial node acts as a branchlet node and in Chara delicatula five cells are cut off in a ring. The first cell of this ring is the oosporangial primordium seen in Pl.1, Fig.1c and Diag.3.2c.

The oosporangial primordium is located towards the branchlet apex (Pl.1, Fig.1c; Diag.3.2c). Its position results in the oosporangium facing away from the main vegetative axis. The division that forms the oosporangial primordium is seen occurring in Pl.1, Fig.5; the

cell plate forms perpendicularly to the last formed wall. The development and position of the charophyte oosporangium led Goebel (1902 -cited in Fritsch 1965) and Sundaralingam (1954) to suggest that the oosporangium represents a modified branchlet of limited growth. In Lamprothamnium the oosporangium faces the main axis; this is diagnostic of the genus (Groves 1916).

The second and third cells cut off in the gametangial node of Chara delicatula flank the oosporangial primordium; they elongate, and grow to form bracteoles on each side of the developing oosporangium (Pl.1, Fig.2; Pl.9, Fig.4). The fourth and fifth cells of the node (facing the main axis) elongate to provide branchlet cortication (Pl.1, Fig.2; Pl.4, Figs. 1,6).

The oosporangial primordium expands and large vacuoles containing flocculent matter appear (Pl.1, Fig.2). The extent of vacuolation differs from earlier (Pl.1, Fig.1c, Diag. 3.2c) and later (Pl.2, Fig.1, Diag. 3,2e) developmental stages which have small spherical vacuoles also containing flocculent matter. Vacuoles are known to alter from few and large to many and small (and vice versa) in single cells; this results in the surface area to volume ratio being altered greatly (Atkinson et al. 1974, Gunning & Steer 1975). A tonoplast membrane can be discerned within the vacuole of the oosporangial primordium (Pl.1, Fig.2), suggestive of the incomplete fusion of two smaller vacuoles. It must, however, be emphasised that it is pure speculation to predict dynamic events from electron micrographs.

Growth and development of the oosporangial primordium occurs first

by the cutting off of an apical cell; the subapical cell then undergoes a cell division. Together, this forms a row of three cells (Pl.1, Fig.3; Pl.2, Fig.1, Diag. 3.2e). Each cell has characteristic curved walls (Pl.2, Fig.1). The apical cell is the oosphere mother cell; the basal cell does not divide further and is the pedicel cell of the oosporangium. The subapical cell is the oosporangial node and it cuts off, sequentially, five peripheral cells around the "central cell" (Pl.2, Figs.5,6, Diag. 3.2f). The five peripheral cells (Diag. 3.2f) elongate around the enlarging oosphere mother cell (Pl.3, Fig.1; Diag. 3.2h); as they elongate they become known as spiral cells (Diag. 3.2h).

Nuclear division is much like that in higher plants. Each nucleus has at least one prominent nucleolus, although it may not always be in the plane of section (Pl.2, Fig.1 and elsewhere). Pickett-Heaps (1967, 1975) reports that at prophase the nucleolar material in Chara fibrosa disperses over the chromatin and does not disappear as in the majority of higher plants. No specific nucleolar stains were used to test this in Chara delicatula.

During cell division in the oosporangial node, the nuclear envelope disperses completely (Pl.2, Figs.2,4), the chromosomes pair on the metaphase plate (Pl.2, Figs.2,4) and organelles are pushed towards the outside of the cell (Pl.2, Fig.2). In higher plants, microtubules have been seen proliferating around the cell wall at the position of the metaphase plate and corresponding to the position of the future cell plate (Pickett-Heaps 1975 and references within). Pickett-Heaps (1975) noted that these microtubules were not encountered in Chara fibrosa, a feature

shown to be consistent with this study of Chara delicatula (Pl.2, Fig.3).

The process of cytokinesis in charophytes is achieved by a cell plate organised as a phragmoplast (Pickett-Heaps 1975) (i.e. a cell plate and its associated microtubules, the microtubules lying at right angles to the plate and hence parallel to the old spindle fibres). In higher plants, it is believed that microvesicles secreted by dictyosomes, are pulled to the site of the cell plate by the microtubules, where they coalesce into the cell plate (see review in Gunning & Steer 1975). In Chara delicatula, dictyosomes are seen in association with the cell plate (Pl.1, Fig.5). This system of cytokinesis is also encountered in the green algal genus Coleochaete but is most typical of higher plants (Pickett-Heaps 1975). However, the phragmoplast of charophytes is not entirely typical of higher plants because development occurs from the outside wall towards the centre (centripetal development) rather than the reverse (centrifugal development); also microtubules are less prolific (Pickett-Heaps 1975).

The cell plate into which the wall precursors are presumed to be secreted provides the pattern for plasmodesmata formation (Pl.1, Fig.5). All the crosswalls which occur during gametangial formation of Chara have simple plasmodesmata (Pl.7, Fig.5 in longitudinal section, Pl.7, Fig.7 in transverse section), i.e. unbranched cytoplasmic connections between two adjacent cells through the intervening common cell wall. Vegetative cells of Chara and Nitella, have simple or branched plasmodesmata

(Spanswick & Costerton 1967, Fischer et al. 1974, Pickett-Heaps 1966, 1975). The branched plasmodesmata are complex, anastomosing and typically with a median sinus in the wall (Pl.7, Fig.6). Endoplasmic reticulum has been found associated with plasmodesmata of charophyte vegetative cells (Spanswick & Costerton 1967), however, in this work only during cell plate formation has an association with endoplasmic reticulum been established (Pl.1, Fig.5).

Further development of the oosporangium proceeds by a series of cell divisions. These divisions are shown in Chara in longitudinal section using light microscopy (Pl.4, Figs.1,3,5) and in whole preparation using S.E.M. (Pl.4, Figs.2,4,6,7). In the apical region of the thallus of Nitella opaca a mixed age sequence in oosporangial development is shown (Pl.9, Fig.1). The spiral cells grow by sinistral elongation around the oosphere mother cell (Pl.4, Figs.1,2; Diag.3.2h,i). Their growth is faster than the oosphere mother cell and they come to ensheath it. At the same time, one cell division occurs at the apex of each spiral cell and a cell, the coronula cell, is cut off (Pl.4, Figs.1,2; Diag.3.2i). Thus, a ring of five coronula cells is seen at the apex of the mature oosporangium (Pl.4, Fig.6). The subfamily Chareae is characterised by having one coronula cell per spiral cell. The subfamily Nitelleae, is characterised by two cell divisions in each spiral cell, resulting in ten coronula cells, seen as five tiers of two cells (Pl.9, Fig.3).

The oosphere mother cell in Chara (Pl.3, Fig.1; Pl.4, Fig.1, Diag. 3.2i) undergoes one cell division and a small basal cell is

cut off (Pl.4, Figs.3,5; Diag.3.2j). This cell is termed the sterile cell. Its sister cell, the oosphere, enlarges enormously (linear increase is 40-600µm). As it does so growth of the spiral cells continues until the mature oosporangium has a single large oosphere ensheathed in the spiral cells, with a single sterile cell at its base and coronula cells 'crowning' the apex of the structure (Pl.4, Figs.5,6; Diag. 3.1k).

Development in Nitella and Tolypella subsection Obtusifolia is slightly different; three small sterile cells have been observed at the base of the oosphere (Sawa & Frame 1974). Two of the three sterile cells found in Nitella opaca are shown in Pl.9, Fig.2. A speculative hypothesis (Soulié-Märsche 1979 unpublished thesis) suggests that in Nitella and Tolypella subsection Obtusifolia, the oosphere mother cell divides meiotically to form a quadrat of cells; three cells remain vestigial and basal, the sterile cells, and one cell, the oosphere, develops. In the remaining species of Tolypella and in the subfamily Chareae the oosphere mother cell undergoes a single mitotic division to form the oosphere and one sterile cell. Shen (1967b,c) showed by measuring the amount of nuclear DNA in Chara zeylanica that no meiosis took place during the process of spermatogenesis and that the sperm contained the haploid amount of DNA. By analogy, this would imply that the oosphere of Chara is also not derived by a meiotic division. Traditionally it has been considered that fertilisation of the oosphere by the spermatozoan resulted in the diploid stage and that germination of the zygote commenced with meiosis (DeBary 1875 -cited in Fritsch 1965). While this may well be true for Chara no study has been made on Nitella.

Once the spiral cells have ensheathed the oosphere mother cell (Diag. 3.2i) and in all subsequent stages of development, sections through oosporangia show intercellular spaces at the junctions between any two spiral cells and the oosphere / oosphere mother cell. This appears as a triangle in cross section (Pl.5, Fig.1; Pl.6, Figs.3,6). The intercellular space is occupied by flocculent amorphous matter (Pl.6, Fig.6) and is continuous with the environment just prior to fertilisation (see later).

Once the oosporangium has reached its maximum length it expands in width by the accumulation of large quantities of starch and lipid in the oosphere (Mirande 1919 -cited in Fritsch 1965, Pickett-Heaps 1975). The lipid forms into lipid droplets called sphaerosomes (Pl.7, Fig.1; Pl.8, Fig.1,3). They are sometimes found in association with endoplasmic reticulum (Pl.7, Fig.2). At the same time starch accumulates in elongate amyloplasts (Pl.6, Figs.5,6).

The plastids in the newly formed oosphere mother cell (Pl.6, Fig.1) are simple, having agranal thylakoids. During maturation of the oosphere mother cell, the plastids become characteristically rounded in section and have vestigial or no thylakoids (Pl.6, Figs.2,3). After cell division of the oosphere mother cell, the plastids accumulate starch (Pl.6, Fig.4 -note the oosphere plastid depicted here is unusual in showing a plastoglobular droplet). With maturation the oosphere plastids elongate and starch accumulates at either or both ends, forming in the latter case "dumb-bell"

shaped amyloplasts (Pl.6, Figs.5,6; Pl.7, Fig.1). As more and more starch accumulates extremely large grains can form (Pl.8, Figs.2,4). Starch exhibits varying degrees of electron densities in micrographs (Pl.5, Fig.1; Pl.8, Figs.2,4). This change in density is probably artifactual. Pickett-Heaps (1968c, 1975) found oosphere plastid microtubules in Chara fibrosa, however, no plastid microtubules were seen in any sections in this work.

In all cells examined, the mitochondria were circular or oblong in section with no suggestion of any branching system, and they possessed well differentiated cristae (Pl.7, Figs.3,4; Pl.8, Fig.3 and elsewhere).

Mitochondria, ribosomes and endoplasmic reticulum are squeezed into the interstitial spaces beween the starch and lipid in the swelling oosphere (Pl.8, Figs.1-4). The starch and lipid reserves are shown at an early stage of accumulation in Chara delicatula (Pl.5, Fig.1) and in a fully developed oosphere of Nitella opaca (Pl.9, Fig.2). The accumulation of storage products occurs to such a degree that fixation, embedding and sectioning is very difficult. Only at the apex of the oosphere is a clear zone observed (Pl.8, Fig.6); this is devoid of any amyloplasts or sphaerosomes and the cytoplasm is diffuse (Pl.8, Fig.5). The apical or fertilisation zone is believed to be the point where fertilisation is effected (DeBary 1875 -cited in Fritsch 1965).

The mature oosphere is never vacuolate (Pl.8, Figs.1-4; Pl.9, Fig.2), although vacuoles are encountered in the oosphere mother cell (Pl.3, Fig.1; Pl.6, Fig.1) and young oospheres (Pl.6, Fig.5).

The spiral cells and the coronula cells on the other hand become increasingly vacuolate during development forming a single cylindrical vacuole that occupies the largest part of the cell volume (Pl.5, Fig.1). The other organelles are pushed to the periphery of the cell and at the ultrastructural level the cells appear like internodal cells (see Pickett-Heaps 1975). However, the organelle unique to charophytes, the charosome (Barton 1965, Crawley 1965, Franceschi & Lucas 1980, 1981), that is found in internodal cells, is completely absent from all cells of the oosporangium.

During development of the spiral and coronula cells, the proplastids become more complex and convert to chloroplasts. Initially, the proplastids are simple, with a few agranal thylakoids and plastid ribosomes in the stroma (like oosphere mother cell plastids described above). At cell maturation they take on a more complex form, becoming considerably larger; converting to chloroplasts. The chloroplasts become aligned into long spiralling rows at the periphery of the cell. The grana and thylakoids never proliferate as they do in higher plant chloroplasts (see Gunning & Steer 1975). The stroma accumulates small starch grains and plastoglobular droplets (Pl.7, Figs.3,4). Plastogobular droplets are unbound by a membrane and can be considered as chloroplast sphaerosomes. They are often associated with chloroplast senescence. In Chara delicatula, the plastoglobular droplets proliferate in the spiral cells (Pl.6, Fig.6) and give the mature unfertilised oosporangium a brownish colouration.

Just prior to fertilisation the apex of each spiral cell expands and elongates. This causes them to separate and the intercellular space between the spiral cells and the oosphere becomes continuous with the external environment. The spiral separation forms the fertilisation slits (Pl.9, Fig.4) at the apex of the oosporangium. Spermatozoa are thought to enter the oosporangium through these fertilisation slits (DeBary 1871 -cited in Fritsch 1965). Once fertilised the oosphere is convered into the oospore. Sundaralingam (1954) records spermatozoa swarming around the oosporangium apex but does not see any entry through the slits. After fertilisation the slits close, presumably due to changes in the cell turgor; no evidence of them is seen in post-fertilisation stages.

The post-fertilisation events are dramatic; complex organic and inorganic layers are deposited around the oospore. Pre- and post-fertilisation stages of Chara oosporangia are shown in Pl.10, Figs.1,3 and Pl.10, Figs.2,4 respectively. These events are dealt with more fully in the fourth chapter "Developmental Morphology of the Charophyte oosporangium (ii) Post-fertilisation maturation".

DIAGRAM 3.2 SHOWING THE DEVELOPMENT OF THE OOSPORANGIUM IN CHARA

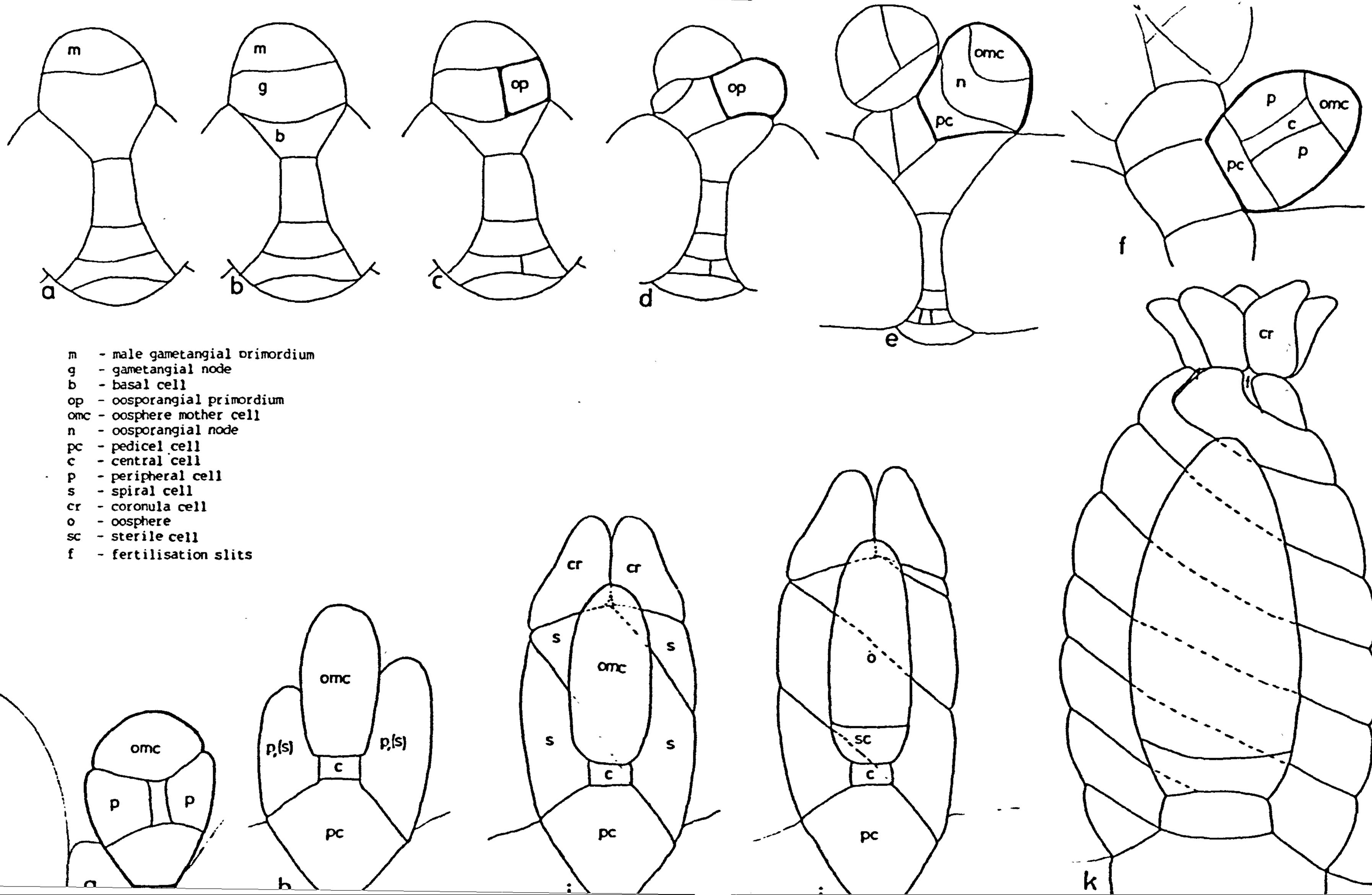

m - male gametangial primordium
g - gametangial node
b - basal cell
op - oosporangial primordium
omc - oosphere mother cell
n - oosporangial node
pc - pedicel cell
c - central cell
p - peripheral cell
s - spiral cell
cr - coronula cell
o - oosphere
sc - sterile cell
f - fertilisation slits

Chapter 4 - DEVELOPMENTAL MORPHOLOGY OF THE CHAROPHYTE OOSPORANGIUM

(ii) Post-fertilisation maturation

Introduction

Post-fertilisation events in the charophyte oosporangium are complex and at the ultrastructural level remain little studied. Two unpublished Ph.D. theses (Soulié-Märsche 1979, Dyck 1970) attempted to model the wall structure of the mature oosporangium, but the data were contradictory. Pickett-Heaps (1975) states "The differentiation of the oogonial complex cannot yet be fully studied at the ultrastructural level. The quantity of reserve material in older oogonia render them totally impossible to fix using present day methods". However, some methods are now available to help solve this and other problems.

The post-fertilisation events documented here concern the development and morphology of a thick multilayered wall around the oospore. The thick multilayered wall is almost certainly protective (Groves & Bullock-Webster 1920,1924). During germination, the wall has to be penetrated by the emerging prothallus. The effect this has on the protective wall layers is also documented here.

The thick protective wall around the oospore has had various terms (see Horn af Rantzien 1956), but is most widely known as the "oospore membrane" (Wood & Imahori 1965, Sawa & Frame 1974, Groves

& Bullock-Webster 1920,1924, Allen 1950). However, this term is unsatisfactory because the protective wall is derived from several cells (Horn af Rantzien 1956) and wall layers should not be called membranes. A new term for the thick, protective, resistant wall is proposed, the compound oosporangial wall.

The compound oosporangial wall is often highly ornamentated. In describing the ornamentation, most workers have used descriptive terminology such as granulate, fibrous, reticulate, pitted or smooth, adding prefixes or combinations for intermediate forms (Wood & Imahori 1965, Allen 1950, Horn af Rantzien 1956). Williams (1959) tried to apply terminology derived from palynology to the ornamentation, an approach not favoured by Horn af Rantzien (1956). John (pers. comm.) has shown that in Nitella species, there is a great variety in ornamentation when observed in S.E.M. Ornamentation may be valuable for use in taxonomy, but until now, as far as the author is aware, only Caceres (1975) has erected a new taxon on the basis of ornamentation.

The compound oosporangial wall was recognised to be a multilayered structure by Horn af Rantzien (1956). He distinguished two inner layers (the endosporine and the ectosporine) that he considered to be derived from the oospore and, superimposed on these, two outer layers (the endosporostine and the ectosporostine) that he considered to be derived from the spiral cells. These terms are maintained in this work, but will be given much stricter definition. Parker and Dyck (1967) and Dyck and Parker (1967) analysed the chemical composition of the "oospore membrane" and found cellulose, protein (10%), waxes or solid fats (20-40%) and no

evidence for lignin, callose, sulphated or carboxylated polysaccharides. Neville et al. (1976) identified a helicoidal layer of cellulose microfibrils in the compound oosporangial wall but did not identify its position in relation to Horn af Rantzien's (1956) layers. A helicoid is formed by multiple plies of microfibrils, with the microfibrils in each ply running parallel and a progressive change in direction from ply to ply. This gives rise to arced patterns in oblique ultrathin sections (Bouligand 1965, Neville & Levy 1984, Neville et al. 1976, Neville 1985, 1986). Unsubstantiated reports suggest that silica might be present in the compound oosporangial wall (Pickett-Heaps 1975, Fritsch 1965).

In the subfamily Chareae and in the genus Tolypella section Acutifolia a calcified layer is deposited on the compound oosporangial wall (Horn af Rantzien 1956, Daily 1975). This layer has been termed calcine by Horn af Rantzien (1956). The calcified layer forms a coherent structure that readily fossilises. Calcification will be considered in Chapter 5; the fossil forms and their relationship to extant forms will be discussed in Chapter 6.

Results and Discussion

The post-fertilisation events in the oosporangium are presented here. Comparisons will be made between the pre-fertilisation form and the post-fertilisation forms of the oosporangium. To avoid unnecessary repetition the discussion is presented with the results.

Before fertilisation, the common primary wall between the sterile cell and the oosphere is seen to be distinctly different from the wall between the spiral cells and the oosphere (compare Pl.12, Fig.1 with Pl.11, Fig.1). This difference arises from their different developmental histories. The wall between the sterile cell and the oosphere forms after cell division and, as is typical of all cross walls in charophytes, it has plasmodesmata (Pl.12, Fig.1). In contrast there are no plasmodesmata between the spiral cells and the oosphere; the wall is microfibrillar and arises by the spiral cells growing, by upward elongation, to encase the oosphere. This wall is, therefore, a compound wall consisting of the spiral cell primary wall and the oosphere primary wall in intimate contact (Pl.11, Fig.1).

After fertilisation, the wall of the oosphere and the ensheathing cells (spiral cells and the sterile cell(s)) becomes thickened with secondary layers, forming the compound oosporangial wall (Pl.10, Figs.2,4). Under the light microscope four secondary wall layers are resolvable (Pl.10, Fig.4 layers a-d). However the compound oosporangial wall is much more complex; the layers which comprise

the compound oosporangial wall are shown diagramatically (Diag. 4.1). Ultrastructurally the profile is the same for Chara delicatula, Chara hispida and Lamprothamnium papulosum. The results presented here are for these species unless otherwise stated.

In the fully developed compound oosporangial wall, the primary wall of the oospore, the adjacent primary wall of the spiral cell, and the innermost part of the lateral walls of the spiral cell are electron dense (Pl.11, Figs.2,3,4). The common primary wall between the sterile cell and the oospore is seen as a uniform electron dense layer perforated by empty channels (Pl.12, Fig.2). These channels are interpreted as the original sites of the plasmodesmata.

The intercellular space (triangular in thin section) between adjacent ensheathing cells and the oospore appears electron dense with areolar inclusions (Pl.11, Figs.3,4). A transverse fracture through the compound oosporangial wall reveals that the intercellular space is not a cavity (Pl.11, Fig.6). It is therefore assumed to have been filled with a solid secretory product. This secretory product might be the wax or solid fat component reported by Dyck and Parker (1967) and may be comparable to the cutin and waxes secreted through the wall of higher plant epidermal cells (Norris & Bukovac 1968).

Three secondary layers are deposited onto the inner and part (inner one-fifth) of the lateral primary wall of the ensheathing cells (Diag.4.1; Pl.11, Figs.2,3). The first layer to be deposited has

an electron dense matrix supporting small crystals about 1 μm long and oriented parallel to the spiral cell wall (Pl.12, Fig.6). This layer is the endosporostine. Often, these small crystals are pulled out of section and become heaped together by the sectioning process (Pl.12, Fig.5). This leaves holes in the supporting matrix (Pl.13, Fig.1). The endosporostine is about 10 μm thick and is laid down outside the plasmalemma often in association with endoplasmic reticulum, (Pl.13, Figs.2,3). The cell is highly vacuolate at this stage (Pl.13, Fig.3).

The second layer to be deposited is a helicoidal layer. This layer is deposited onto the endosporostine and is termed the ectosporostine.(Pl.13, Fig.4). Pigmentation of the ectosporostine causes the compound oosporangial wall to appear black. The pigment is probably the same as that which makes the primary walls electron dense.

A third layer is deposited onto the ectosporostine and is called the ornamentation layer. The ornamentation layer gives rise to the tubercles, lumps and knobs seen on the compound oosporangial wall (Pl.11, Fig.6). The ornamentation layer like the ectosporostine is pigmented but it has no microfibrillar component and appears amorphous. The differential thickness of the layer (Pl.13, Fig.5) gives rise to the structures which comprise the ornamentation (Pl.13, Fig.6). In Lamprothamnium papulosum the ornamentation takes on the form of lumps which can show complex patterns (Pl.15, Fig.6). In some species of Nitella the ornamentation is very complex and shows a network of interconnecting ridges (Pl.15, Fig.5).

In Nitella opaca the endosporostine has a different complexity. The endosporostine appears as a three zoned layer; the inner zone is electron dense and areolar, giving a granular appearance; the middle zone shows striations (possibly microfibrillar) parallel to the cell wall axis; the outer zone has a strange ridged appearance which is believed to be artifactual (Pl.14, Fig.1).

In all genera examined secondary wall deposition is simultaneously occurring on the oospore primary wall (Pl.11, Figs.2,3). The first layer to be deposited is a thin electron dense and amorphous layer (Pl.11, Figs.2,3; Pl.14, Figs.3,4) called the amorphous layer. A helicoidal layer, termed the endosporine is deposited on the amorphous layer (Pl.11, Figs.2,3; Pl.14, Figs.3,4). The helicoidal endosporine does not have an electron dense matrix like the ectosporostine. It appears very similar to the helicoidal wall of vegetative internodal cells of Nitella and of many other plant cells (Levy & Neville 1984 and references within). This layer is almost certainly the helicoidal layer previously reported in Chara oospores (Neville et al. 1976).

A random microfibrillar layer is deposited onto the endosporine (Diag. 4.1, Pl.11, Figs.2,3). This layer is the ectosporine and it is the final layer to be deposited within the oospore.

In the fully developed oosporangium three helicoidal layers are found, two have already been described, the ectosporostine, and the endosporine. The third helicoidal layer is a post-fertilisation layer deposited on the innerside of the outer wall of the spiral

cells (Diag. 4.1, Pl.11, Fig.5). All the helicoidal layers are secondary walls. Neville (pers. comm.) considers that all helicoidal walls with a uniform repeated deposition pattern, as in these three helicoidal layers, are formed against a constraining wall. Two helicoidal layers are deposited in each spiral cell, each with localised depositional regions around the cell. Localised control over helicoidal wall formation in plants is, as far as the author is aware, unique to spiral cells.

In summary, the whole compound oosporangial wall is an integral structure which is derived from both the oospore and the ensheathing cells. It is built up of at least 8 discrete layers; the ectosporine, the endosporine, the amorphous layer, the oospore primary wall, the ensheathing cell primary wall, the endosporostine, the ectosporostine and the ornamentation.

Onto the compound oosporangial wall the calcine forms (Pl.14, Fig.2; Pl.13, Fig.6). This is a complex organic and mineral layer and is examined in detail in the next chapter. In a fully developed oosporangium of Chara hispida (with calcine layer) over 10% of the oosporangium's dry weight is the compound oosporangial wall and over 70% of the oosporangium's dry weight is calcine (mean total dry weight of calcified oosporangium is 0.25 mg (n= 50)).

The ensheathing cells die after the full development of the post-fertilisation layers. With cell death, the outer wall sloughs away, either by bacterial degradation or mechanical action (Pl.10, Fig.4, Diag. 4.1). This exposes to the environment the last formed, ensheathing cell derived layer. In Chara this is the

calcine, whilst in Nitella which does not produce calcine, this is the ornamentation layer. Quite often, the lateral walls of the spiral cells are covered extensively in the ornamentation layer (Pl.13, Fig.6). This mechanically strengthens and gives rigidity to the lateral walls. In Nitella, when the outer wall of the spiral cell sloughs away, the lateral wall, covered in the ornamentation layer can be seen standing in profile, appearing like spiralling lamellae (Pl.15, Fig.5).

A section through a fully calcified oosporangium of Chara hispida shows the lateral wall of two spiral cells sandwiched between two calcine layers (Pl.14, Fig.5). The ornamentation layer on the lateral wall of the spiral cells is seen as small lumps (Pl.13, Fig.6) which when sectioned shows no structure (Pl.14, Fig.5).

The lateral walls that separate the sterile cell(s) from the spiral cells are cross walls and have plasmodesmata (Pl.12, Fig.3). In a calcified oosporangium the calcine is deposited against these walls. A section through these walls shows cavities in the wall which represent the position occupied by the plasmodesmata (Pl.12, Fig.4). Note that in the individual depicted on Pl.12, Fig.4 no ornamentation layer is present.

In Chara, exposing the outer layer of the compound oosporangial wall requires the removal of the calcine. With its removal, the lateral wall of the ensheathing cells break away. Deposition of the secondary layers on the lower part of the lateral wall of the ensheathing cells forms a ridge (Pl.11, Fig.6, Diag. 4.1). The top

of each ridge is where the lateral walls breaks on the removal of the calcine. As the lateral wall is very thin in relation to the ridge of secondary thickening there is little or no sign of the fracture (Pl.11, Fig.6; Pl.15, Fig.8).

The ridges on the compound oosporangial wall stand out clearly (Pl.15, Fig.1), showing the position the ensheathing cells occupied in relation to the oospore during life. A ridge describing a spiral represents the secondary thickening on the lateral walls of the spiral cells; shown in Chara (Pl.15, Fig.1) and Nitella (Pl.15, Fig.3). A ridge describing a circle or a rounded pentagon represents the thickened lateral walls of a single sterile cell; this is shown in Lamprothamnium (Pl.15, Fig.2). A ridge describing a trapezium adjacent to a ridge describing a triangle represents the thickened lateral walls of two sterile cells; this is shown in Nitella (Pl.15, Fig.4). Sawa and Frame (1974) report seeing "3 sterile oogonial cell imprints" in Nitella. It is assumed that the third sterile cell on the individual depicted on Pl.15, Fig.4 is not represented because it was not involved in the development of the compound oosporangial wall. This could occur if the third sterile cell was pushed away from intimate contact with the oospore by the growth of the other two sterile cells. No data supports this assumption.

In Lamprothamnium the ridges on the compound oosporangial wall vary in thickness (Pl.15, Fig.8) and height (Pl.15, Fig.7). This differential secondary thickening of each ridge appears to be unique to the genus. The variation in thickness and height of each ridge is directly reflected in the calcine deposited onto the

compound oosporangial wall. This is further discussed in Chapter 6 (iv. Pillars).

X-ray microanalysis carried out on ultrathin sections of the compound oosporangial wall of Chara hispida yielded little useful data. Only in the endosporostine were trace quantities of calcium, chlorine and aluminium recorded above background concentrations (see Trace 4.1 and control Trace 4.2). Silica has been reported in the compound oosporangial wall of charophytes (Fritsch 1965, Pickett-Heaps 1975); however, no evidence was found of silicon. It is quite possible that during fixation, embedding and sectioning of the compound oosporangial wall, elements were leached out of the wall. For this reason, in the absence of high concentrations of any elements, no conclusions of any significance can be drawn.

On germination the emerging prothallus has to penetrate both the compound oosporangial wall and the calcine (Pl.16, Fig.1). The action that penetrates these layers is entirely mechanical. There is no evidence of enzymic or chemical damage to the wall layers.

The process of germination involves the apical expansion of the oospore (Pl.10, Fig.2), a process which requires the growth of the innermost layer, the ectosporine. The ectosporine is continuous with the emergent prothallus (Pl.16, Fig.5, Pl.10, Fig.2). The oospore organelles migrate into the emergent oospore apex (Pl.16, Figs.3,5). The storage products (Pl.8, Figs.1-4) are broken down, the cytoplasm becomes more diffuse (Pl.16, Fig.4), until with time the oospore becomes completely depleted of all its

storage products (Pl.14, Fig.2).

After germination the endosporine shows a ragged edge, a feature considered to be indicative of mechanical rupture (Pl.16, Figs.5,6). Chemical degradation would, it is believed, have given a more rounded amorphous edge to the split layer. The spiral cell derived layers split apart on germination; the line of fracture passes along and through the spiral ridges at the oosporangium's apex (Pl.16, Figs.2,3). The layers are then bent backwards by the emerging prothallus, like the peeling of a banana.

The fracturing properties of calcine on oospore germination and the processes involved in its formation are discussed in Chapter 5; "Calcification of the Charophyte Oosporangium".

DIAGRAM 4·1 SHOWING POST-FERTILISATION EVENTS IN *CHARA*

before fertilisation

after fertilisation

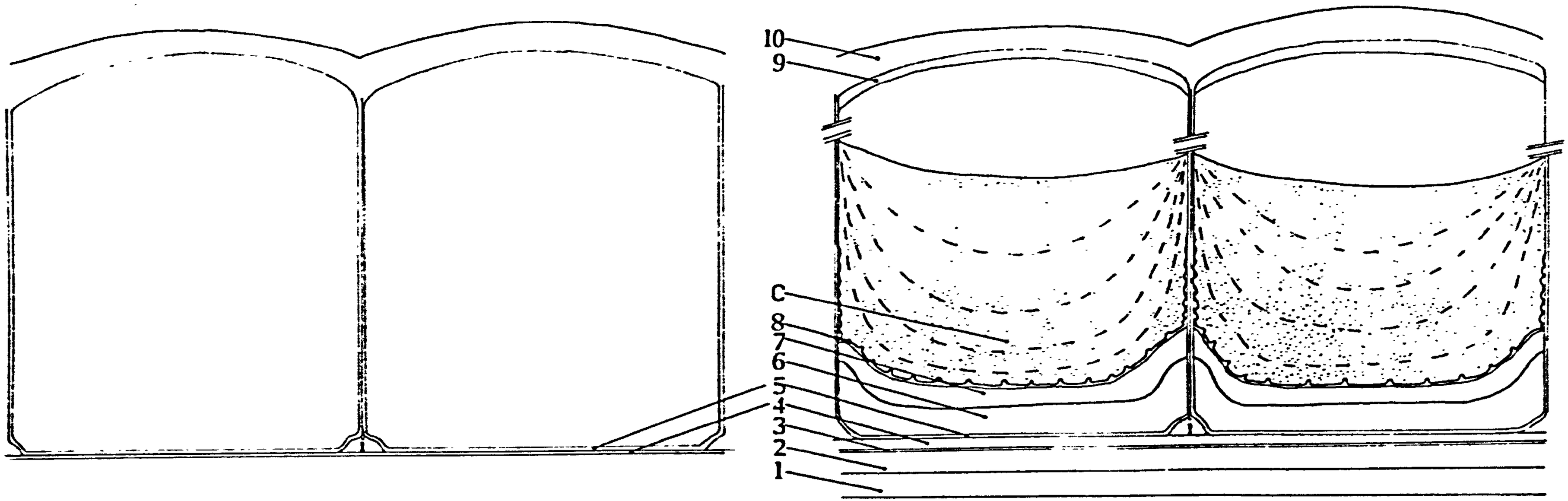

oospore derived

1 - ectosporine (random microfibrillar)
2 - endosporine (helicoidal)
3 - amorphous layer
4 - primary wall

spiral cell derived

5 - primary wall
6 - endosporostine (crystalline)
7 - ectosporostine (helicoidal)
8 - ornamentation layer
9 - helicoidal wall
10 - outer primary wall
C - calcine

i - intercellular space

X-RAY MICROANALYSIS TRACES

TRACE 4.1 CHARA HISPIDA, ENDOSPOROSTINE

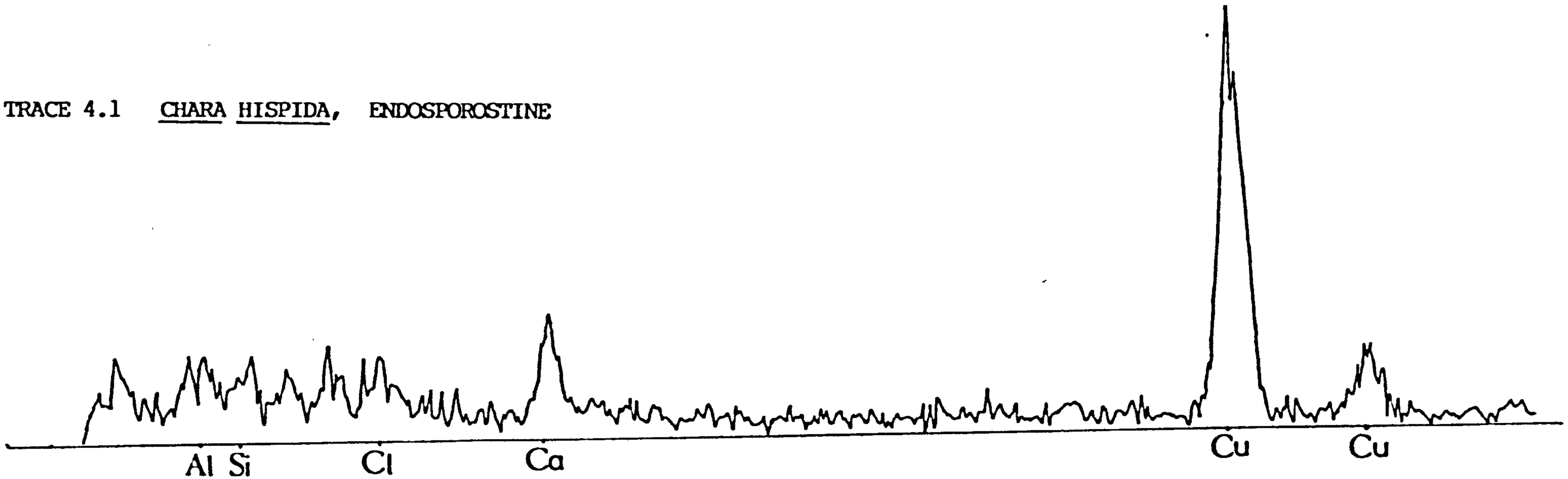

TRACE 4.2 CONTROL, RESIN

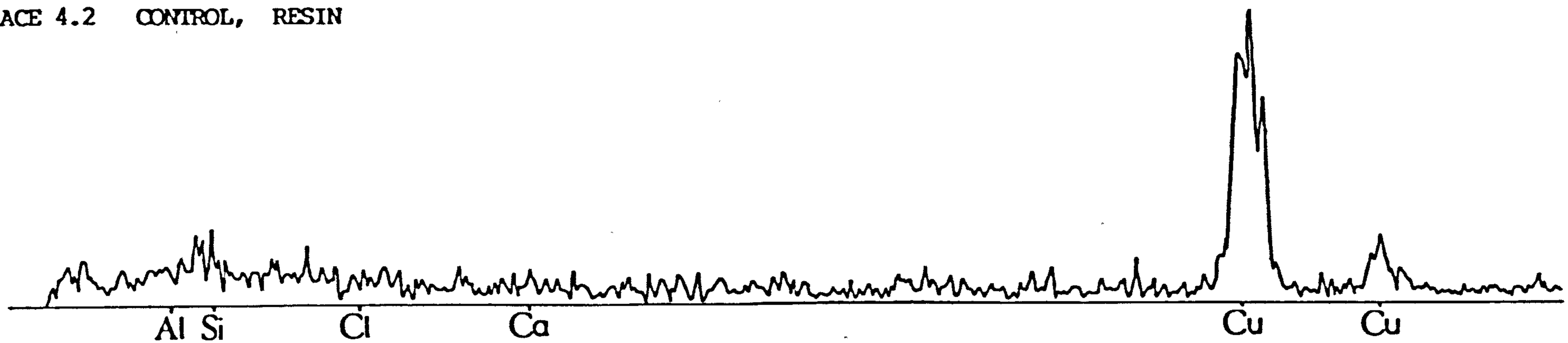

Chapter 5 - CALCIFICATION OF THE CHAROPHYTE OOSPORANGIUM

Introduction

Mineral deposition in biological systems (biomineralisation) can be beneficial to an organism leading to the formation of, for example, bones, teeth, and shells. Biomineralisation can also be pathological, for example, the thickening of arterial walls (Ross & Glomset 1973, and many others).

Various salts can be precipitated in cells and tissues. The group 2A elements are usually involved Ca^{2+}, Mg^{2+}, Ba^{2+}, Sr^{2+} reacting with CO_3^{2-}, PO_4^{2-}, P_2O_4, oxalate and SO_4^{2-}. Iron and manganese are also found in the form of oxides and sulphides. In addition, silica deposition represents an important mineral deposit. It occurs in the form $(SiO_2)_n$ and predominantly in the Bacillariophyta and the Chrysophyta. Amongst the green algae, small amounts are found in the cell wall of a few groups, including the Hydrodictyaceae (Pediastrum, Hydrodictyon) the Chlorococcaceae (Tetraedron) and the Scenedesmeaceae (Scenedesmus) (Millington & Gawlik 1967, Parker 1969). Unsubstantiated reports suggest that silica may be found in the walls of charophytes (Fritsch 1965, Pickett-Heaps 1975). However, no evidence of this has been found in this work (see Chapter 4).

The mineral barium sulphate is widespread in the Charophyceae (sensu Mattox & Stewart 1984)(see Raven et al. 1986 and references within). Within charophytes themselves, it is found in the rhizoids and is thought to be directly involved in a geotropic response (Schröter et al. 1975). The crystals occur near the apex as membrane bound statoliths. The statoliths sink in the cytoplasm to lie adjacent to the lowermost rhizoid wall; here they inhibit the wall's growth. This causes differential upper:lower wall development and so effects a positive geotropic response (Seivers 1965,1967a,b, Seivers & Schröter 1971, Pickett-Heaps 1975, Hejnowicz & Seivers 1981).

Calcium carbonate is the commonest of all deposits occurring in bacteria, myxomycetes, fungi, algae, higher plants, protozoa, sponges, annelids, echinoderms, bryozoans, brachiopods, ascidians, coelenterates and molluscs (see references in Borowitzka 1977). Calcification is a common phenomenon in eukaryotic algae. There are over 100 genera of calcareous algae with representatives in most algal phyla (Borowitzka 1977). In algae, calcification involves the precipitation of calcium carbonate within or around algal cells or thalli. A number of reviews deal with algal calcification (Borowitzka 1977, 1982a,b, Raven et al. 1986, Westbroek et al. 1983,1984, Johansen 1981).

Calcareous algae occur in freshwater and marine environments. The worldwide Upper Cretaceous chalky deposits are largely composed of coccoliths, the calcareous skeletons of coccolithophorids (Prymnesiophyta). The encrusting, calcareous red algae

(Rhodophyta) are of major importance in the formation of reefs, particularly in the surf zone (Womersley & Bailey 1969, Round 1981). The effect of selective removal of calcium by precipitation of $CaCO_3$, mainly by foraminifera and coccolithophorids, has drastically reduced the calcium concentrations in oceanic sea water. The ratio has changed from Mg/Ca <2:1 in Palaeozoic oceans to a ratio of 5:1 in modern oceans (Sandberg 1975a and references within).

Amongst the green algae with which the charophytes have their closest affinity (see Chapter 1), a number of classes are thought to calcify. These include, the Chlorophyceae (orders Chlorococcales; Chaetophorales) the Oedogoniophyceae (order Oedogoniales), the Bryopsidophyceae (orders Cladophorales; Dasycladales; Caulerpales; Derbesiales) and the Zygnemophyceae (order Zygnematales), (see Borowitzka 1982b). However, Round (pers. comm.) considers that calcification is not so widespread and many of the "calcareous algae" have only superficial precipitates on their cells or thalli. Within the charophytes there is calcification as an extracellular deposit on the internodal cells and calcification of the oosporangium (Daily 1975, Horn af Rantzien 1956). It is the calcareous deposits which give charophytes their common names, stoneworts or brittleworts.

Calcification in some of these algae has resulted in a remarkable fossil record, for instance, the Dasycladales have a range from the Precambrian to Recent and the charophytes from the Upper Silurian to Recent.

Two isomorphs of calcium carbonate can be precipitated in algae; namely an orthorhombic crystal, aragonite, and a hexagonal rhombohedral crystal, calcite. In animals a third isomorph (the least stable isomporph), vaterite, is infrequently found (Watabe & Dunkelberger 1979). Calcite is the most stable isomorph and is the crystal which is preferentially precipitated. However, in marine environments, a number of ions inhibit calcite crystal formation. The most important, due to its abundance in seawater, is Mg^{2+} (Simkiss 1964a). It acts by inhibiting calcite nucleation, the initial phase in any crystal's growth, consequently, aragonite is favoured (Pytkowicz 1965). There are however, two groups of marine algae which precipitate calcite, the coccolithophorids (Prymnesiophyta) (see reviews by Westbroek et al. 1983, 1984) and the Corallinaceae (Rhodophyta) (see review by Johansen 1981).

After crystal nucleation has occurred, magnesium ions can be incorporated into the growing calcite crystal lattice. Less than 4 mol percent magnesium carbonate is considered as low magnesium calcite, greater than 4 mol percent is considered as high magnesium calcite (Sandberg 1975b, Towe & Hemelben 1976); equal parts of magnesium to calcium forms dolomite. Where calcite forms in marine environments it is likely to be high magnesium calcite (Sandberg 1975b).

The study of calcification in lower plants and animals has led to a number of generalisations. The generalisations concerning the mechanism of precipitation involve a four compartment model as proposed by Simkiss (1986). The four categories of the model can be defined as follows:

1. modification of ion activity
2. diffusion limited site
3. nucleating surfaces
4. lattice modifiers and crystal inhibitors.

Sometimes these four categories occur as a byproduct of biological reactions (e.g. photosynthesis) and anatomical peculiarities of the organism. In these cases calcification can be considered as a purely physical process (e.g. on charophyte internodal cells). In other cases the process is a metabolically controlled biological system (e.g. in coccolith formation in prymnesiophytes). Often, however, the calcification process lies somewhere between these two extremes (e.g. in Halimeda and the Corallinaceae).

In order for mineral precipitation to occur in an otherwise stable aqueous solution the first category in Simkiss's (1986) four compartment model must be satisfied: the modification of ion activity. Biological reactions, particularly photosynthesis and ion pumping mechanisms, change the concentrations of ions and alter pH. This can cause the solubility product of a mineral to be exceeded and the mineral precipitates. Involved in calcification is a complex equilibrium between the following: Ca^{2+}; HCO_3^-; CO_3^{2-}; OH^-; H^+; $CO_2(aq)$; $CO_2(g)$. The reaction which causes calcium carbonate precipitation being:

$$Ca^{2+} + CO_3^{2-} \xrightarrow{Ksp} CaCO_3(s) \qquad \text{equation 1}$$

Ksp = solubility product of $CaCO_3(mol/dm^3)$

Details of the reactions and equilibria constants involved in calcification are given in Borowitzka (1982b).

The precipitation of calcite on charophyte internodal cells is from none to total incrustation depending on environmental factors and the physical condition of the algal thallus (Wood & Imahori 1965). The extent of calcification is directly related to the photosynthetic rate and the saturation state of the environment with respect to the relevant ions (Pentecost 1984). Charophytes, like many aquatic plants, may utilise as their carbon source either CO_2 (aq) or HCO_3^- (aq) (Arens 1939, Lucas 1975a, 1983, Walker 1983, Walker & Smith 1977, and others). If HCO_3^- is taken up it will be converted to CO_2 and OH^- by the activity of carbonic anhydrase, a process that is thought to occur in charophyte internodal cells (Borowitzka 1982b). The OH^- generated must be removed or neutralised either by OH^- efflux or H^+ influx (Lucas 1975b, Lucas & Nuccitelli 1980). In charophyte internodal cells this occurs in isolated regions giving rise to a profile of alkaline bands (pH 8-10) to acid bands (pH 5-6) (Lucas & Smith 1973, Lucas 1979). In the alkaline bands, a region of OH^- efflux (or H^+ influx), the solubility product of calcium carbonate is locally exceeded and calcite precipitates outside the cell wall (Borowitzka 1982a,b, Lucas & Smith 1973). The calcite is deposited as pyramidal to rectangular crystals 6-10 µm wide and 6-27 µm long, with random orientation (Borowitzka et al. 1974). The whole process of internode calcification has been modelled by Borowitzka (1982b) below:

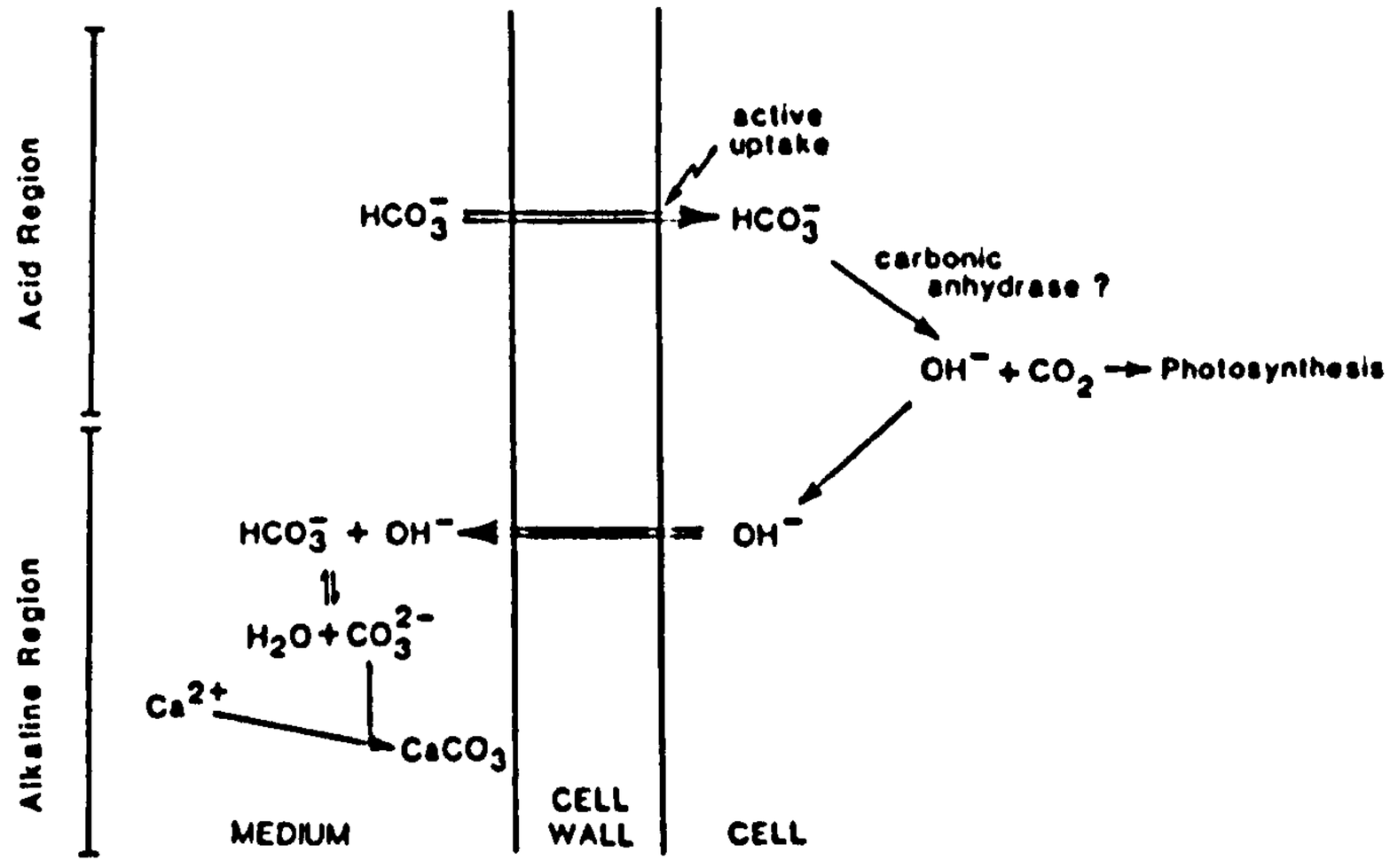

Chara corallina. Schematic representation of the major ion fluxes associated with HCO_3^- uptake in the acid region of the cell wall and OH^- efflux in the alkaline regions which results in $CaCO_3$ precipitation if sufficient Ca^{2+} is present. Borowitzka (1982b).

The effect of biological activity on ion concentrations is minimised by diffusion. By limiting diffusion, small ion fluxes can have a large influence on the position of reaction equilibria. The diffusion limited site (boundary layer) around the internodal cell of Chara can be 30-150 µm (Walker et al. 1979, Smith & Walker 1980). This is sufficient to allow ion fluxes across the cell wall to have a significant effect on mineral deposition. A diffusion limited site is the second generalisation of Simkiss's (1986) four compartment biomineralisation model.

The third generalisation of Simkiss's (1986) four compartment model concerns crystal nucleation. The activation energy for the formation of a crystal nucleus is a rate limiting step. The crystal nucleus is highly soluble and exists as amorphous, solid calcium carbonate. The formation of a crystal nucleus can be very slow; in sea water it can take up to 10^5 years to form (Pytkowicz 1965). Only after crystal nucleation has occurred can the crystal lattice form. The lattice then provides the site onto which additonal ions

can attach allowing the crystal to grow rapidly.

Crystal nucleation can be stimulated by organic molecules that either concentrate calcium ions or form a template onto which calcium carbonate crystals grow. The organic matrix or template has charged calcium binding sites spaced at similar distances and angles to the Ca^{2+} in the lattice of calcite or aragonite (Weiner & Traub 1984). This stimulates the crystals to grow on the organic matrix, a process called epitaxis or oriented crystal overgrowth. The position of the charged sites could explain why calcite instead of aragonite is precipitated in the coccolithophorids and the Corallinaceae (Borowitzka 1977). Any organic matrix which is able to act as an epitaxial substrate must be crystalline in nature (Degens 1976).

The fourth generalisation in Simkiss's (1986) biomineralisation model concerns lattice modifiers and crystal inhibitors. A crystal grown *in vitro* has a defined shape dictated by angles between ions. However, the crystals of biological systems are often varied and highly developed (e.g. coccoliths of Prymnesiophyta, Klaveness 1972, Van der Wal *et al*. 1983, Westbroek *et al*. 1983, 1984) and the oosporangia of charophytes (see later in this chapter). The "biomineral" shows no apparent relation to the physical crystal. The normal growth of a crystal can also be poisoned by organic crystal lattice modifiers and crystal inhibitors. A crystal poison interrupts the orderly array of ions on the surface of the crystal lattice and so stops crystal growth (see Simkiss 1964b). Crystal growth might then be restimulated but in a new direction, a process called crystal shaping (Simkiss 1986).

The oosporangia of charophytes represent a nearly unstudied biomineralisation system. The mode of calcification is very different from that of the internodal cell. Oosporangial calcification is restricted to the genus Tolypella section Acutifolia (subfamily Nitelleae) and the subfamily Chareae (Daily 1975). The mineral layer deposited on the compound oosporangial wall has been termed calcine by Horn af Rantzien (1956). It forms a coherent and complete structure around the oospore.

Calcification begins by deposition on the compound oosporangial wall, and proceeds to fill the lumen of the ensheathing cells. This process continues until cell death (Horn af Rantzien 1956). Daily (1975) considered the mechanism as representing intracellular calcification, however the work presented in this chapter does not vindicate this. The mineral component of the calcine is calcium carbonate in the form of calcite (Horn af Rantzien 1956, Daily 1975) or high magnesium calcite for Lamprothamnium growing in saline lakes (Burne et al. 1980).

Using light microscopy Horn af Rantzien (1956) reported concentric laminations in the calcine in transverse section. Later Feist and Grambast-Fessard (1984) described this as "U-form" calcification which contrasted with the "Y-form" of calcification found in Lamprothamnium and a fossil genus Musacchiella (family Porocharaceae, see Chapter 6). Feist and Grambast-Fessard (1984) raised doubts as to whether the two types of calcification were of ecological or taxonomic importance. Wright (1985) considered that the differences were of ecological importance and used the

differences to predict palaeoenvironments. Horn af Rantzien (1956) also reported that in a few instances the calcine was not uniform, with an inner part possessing the concentric laminations, and the outer part being structureless. In such cases he defined the inner part as endocalcine and the outer as ectocalcine.

An account of oosporangial calcification in Chara (freshwater genus) and Lamprothamnium (brackish water genus) is presented here.

Results

Development of the calcine in the oosporangia of two genera Chara and Lamprothamnium has been studied using the techniques of S.E.M., T.E.M., and L.M.. The data was often difficult to interpret and many specimens showed aberrations. Results from different techniques are compared and a number of patterns have emerged.

The calcine develops on the compound oosporangial wall in intimate association with the ornamentation layer (Pl.17, Fig.1). Consequently, features of the ornamentation, such as protuberances (Pl.17, Fig.2), are reflected as pits in the adjacent calcine (Pl.17, Fig.4). The calcine is first laid down on the inside of the inner wall and part of the lateral wall of the ensheathing cells and it continues by deposition on the inside of the ensheathing cells until up to two thirds of the cell lumen is filled (the cell lumen being defined by the limits of the cell wall). Calcine development therefore reduces the volume of the cell. The development of the calcine layer is shown in diagram 5.1.

In highly calcareous waters, where calcium carbonate is precipitating out of the environment onto all substrates, the entire oosporangium may become caked in calcium carbonate. This forms a 'ghost layer' around the oosporangium which maintains the pre-fertilisation form of the oosporangium (Pl.17, Fig.3). This extracellular deposit is more prevalent in some species than in

others (e.g. Chara hispida growing side by side with Chara delicatula will tend to be more encrusted). Often the extracellular crystals deposited on the outer walls of the oosporangium appear like laboratory grown calcite showing the hexagonal rhombohedral form (Pl.17, Figs.5,6).

The physiological condition of the alga, the species of alga and the environmental conditions (particularly the calcium levels in the water) have an effect on how extensively oosporangial calcification occurs (Wood & Imahori 1965). With the death of the ensheathing cells calcification stops; termination of the process may occur at any stage for any species. After death of the ensheathing cells, mechanical abrasion and bacterial degradation results in the loss of the outer cell walls. This exposes the underlying calcine directly to the environment. The senescing coronula cells are sloughed off at this stage.

Once the walls of the ensheathing cells have sloughed away, the degree of calcification can be seen by examining the profile of the oosporangium (which is now only an oospore surrounded by its compound oosporangial wall and calcine). If it is weakly calcified (Pl.18, Fig.1), each spiral of calcine (called a spiral) has a concave profile (Pl.18, Fig.3), if more strongly calcified (Pl.18, Fig.2) the profile becomes increasingly flatter(Pl.18, Fig.4) until in extreme cases the profile is convex (Pl.16, Fig.2, Diag.5.1). Calcification of the sterile cell forms the basal plate (Pl.19, Fig.7; Pl.29, Fig.1; Diag.5.1). In all species of Chara examined, a basal / apical polarity was found to exist in the degree of calcification (specimens examined from the complete

vasculum of British Charophyta, Groves and Bullock-Webster 1934 collection). In each case the apex was more weakly calcified. In Lamprothamnium papulosum the apex is considerably more weakly calcified so much so, that this feature is diagnostic of the species (Pl.18, Figs.1,2). In many cases there is a sharp and noticable demarcation where calcine thickness alters (Pl.18, Fig.5).

On germination, the calcine fractures at the position where the calcine thickness alters (Pl.18, Fig.6). The spiral apices above the line of fracture splay out into 5 small peg-like structures (Pl.18, Fig.6). These fractured apices are then shed (Pl.18, Fig.7; Pl.16, Fig.1). The line of fracture runs more or less transversely across each spiral (Pl.18, Fig.8). The germination pore which results from the spirals fracturing at the apex has a form that is characteristic of the family Chareae (see Chapter 6; apical construction).

Calcine deposition occurs outside the plasmalemma (Pl.20, Fig.1). between the plasmalemma and the inner wall of the ensheathing cells (Pl.20, Fig.1). This is, therefore, extracellular calcification. It was the deposition of calcine within the confines of the cell wall that lead Daily (1975) to erroneously believe that calcification was intracellular. The calcine has a crystalline and an organic component (Pl.20, Fig.1). The crystals exhibit great order (discussed later); the control of this order must be from within the cell across the plasmalemma.

In Chara the latest formed calcine lies closest to the plasmalemma

(Pl.20, Fig.1), its form being very different from mature calcine. It appears as strands (probably representing sectioned sheets of an organic substrate). It is possible that this is secreted across the plasmalemma in the form of precursors which then polymerise (see discussion). Electron dense patches occur between the closely packed strands (sheets) (Pl.20, Fig.1), these are interpreted as calcite nucleation sites. In older calcine (further away from the plasmalemma) small electron transparent areas are seen (Pl.20, Fig.1). These are interpreted as holes where crystals have fallen out of section. These areas become larger, (the crystals were bigger) with increased distance from the plasmalemma. At the same time the organic strands (sheets) separate (as if being pushed apart by the growing crystals). Detail of the organic strands becomes obscured in the oldest calcine. The condition of the calcifying spiral cell (Pl.20, Fig.1) appears poor, this is probably due to the thick walls, mineral deposits and the highly vacuolate nature of the cell which prevented fast penetration and even fixation from occurring.

The structure of mature calcine is difficult to elucidate, and micrographs are difficult to interpret. However, from the data a few patterns have emerged. Horn af Rantzien (1956) described concentric laminations in transverse sections of Chara calcine, a condition which Feist and Grambast-Fessard (1984) described as "U-form" calcification. Feist and Grambast-Fessard (1984) also report a second type of calcification, "Y-form" calcification, typified in the extant genus Lamprothamnium by radiating lines in transverse sections of calcine. A comparison of the two forms of calcification in the two genera Chara and Lamprothamnium showed

that the calcine in each genus was not fundamentally different (see results below).

The calcine of Chara shows, in transverse section under the light microscope, concentric bands that describe a concave arc (Pl.19, Fig.1). In T.E.M. these bands are also seen (Pl.20, Fig.2). The bands have a similar electron density to the embedding resin which they might partly represent. In all the specimens of Chara examined the central area of calcine sectioned unsatisfactorily, revealing ill-defined calcine and no visible bands (Pl.20, Fig.2). This may be related to poor resin infiltration.

The bands exposed in thin section are also exposed when resin embedded specimens are acid etched (optimum for Chara hispida 0.1% HCl for 10secs.)(Pl.19, Fig.3). The acid removes the mineral component exposing the organic and/or the resinous component of the calcine. In Chara the regions that appeared as concave bands in section can now be seen as concave lamellae that are continuous through the length of the calcine (Pl.19, Figs.4,5). Between 7 and 9 of these lamellae can be seen in Chara hispida. Acid insoluble strands can be seen which traverse the cavity between the concave lamellae; they act to compartmentalise the calcine (Pl.19, Fig.5). The "compartments" in the centre of the calcine are larger than those at the periphery. This might well be artifactual, relating to the poor resin infiltration or the over-vigorous action of the acid.

As already stated the spiral apices are more weakly calcified; this manifests itself in Chara hispida by the more closely packed

concave lamellae (Pl.19, Figs.4,6). The number of lamellae remains the same but they are less disperse. The basal plate also shows concave lamellae (Pl.19, Fig.7).

Resin embedded oosporangia of Lamprothamnium papulosum react differently to acid etching. They show concave lamellae that describe a concave arc, as in Chara hispida, but, the lamellae are more delicate and closely packed (Pl.19, Fig.8). The mineral component of Lamprothamnium papulosum is also much more soluble and the concave lamellae can only be revealed by low acid concentrations (0.01% HCl for 10secs.).

Attempts to examine the calcine of Lamprothamnium papulosum in T.E.M. proved difficult since the methods of fixation and staining totally decalcified the calcine. Only vigorous staining using Hoch's (1977) method and exceptional contrast enhancement revealed the organic component. The organic material existed as an intricate, interconnecting mesh (possibly sectioned sheets) that describe indistinct concave bands in transverse section (Pl.21, Fig.1). Unlike the calcine of Chara hispida there are no wide concave bands. Instead a finer, more delicate organic component was seen; this is consistent with the data from acid etching (Pl.19, Fig.8). This organic component could only be revealed adequately under the light microscope using Nomarsky phase contrast. Using this technique the organic component appeared as concave bands describing a "U" in transverse section(Pl.19, Fig.2); the bands were less distinct than the concave bands of Chara (Pl.19, Fig.1).

In Chara an additional feature of the calcine is encountered in most, but by no means all, specimens. This is an inner zone of calcine (i.e. the layer which lies adjacent to the compound oosporangial wall) that does not appear to react to acid etching (Pl.19, Fig.5) and appears quite different in T.E.M. (Pl.21, Figs.2,3). This layer shows closely packed organic / resinous bands (Pl.20, Figs.3,4). In T.E.M. the bands are seen to have cavities (electron transparent areas) that cut them perpendicularly (Pl.20, Fig.4). These are interpreted as regions where calcite crystals have been pulled out of section. They remain as black fragments (electron dense chips) of calcite crystals scattered over the banded regions (Pl.20, Fig.4). This layer lies closest to the compound oosporangial wall and therefore represents the first formed calcine, as is confirmed in only weakly calcified oosporangia (Pl.14, Fig.2). The inner surface of this first formed calcine shows small crystals that are stacked perpendicularly to the surface; hence, each crystal has its long axis vertically aligned (Pl.23, Fig.8). The alignment of these crystals adds support to the view that the electon transparent areas which cut the concave bands perpendicularly (Pl.20, Fig.4) are holes left by calcite crystals.

A transverse fracture through the calcine of Chara hispida reveals that the first formed calcine has different fracturing properties from the rest of the calcine (Pl.23, Fig.7). A demarcation line can be seen separating the two calcine types (Pl.23, Fig.7). However, a few specimens show no such fracturing, indicating that the inner layer is either very thin or absent. It is possible that this inner layer of calcine when present is the layer Horn af Rantzien

(1956) described from light micrographs as endocalcine (see Introduction to this chapter). In this work the term endocalcine is used only when describing the inner layer, the term calcine refers to the outer layer in specimens where an endocalcine has been identified or the whole calcified layer where it has not.

The calcine of Chara hispida seen in transverse fracture appeared highly ordered. Long, thin and closely packed structures (called polycrystalline columns for reasons explained later) radiate diagonally from the lateral spiral walls (like theatre curtains across a stage) (Pl.22, Fig.1). From the basal (internal) spiral wall more polycrystalline columns take the form of vertically orientated fans or simple columns (Pl.22, Fig.2). They can blend into the diagonal columns or form a suture line demarcating the contact of the two column directions.

The fractured calcine of Lamprothamnium papulosum is similar but shows even greater uniformity in its substructure. From the lateral spiral walls, relatively longer and thinner polycrystalline columns arise (Pl.22, Fig.3). These interdigitate with the polycrystalline columns from the basal spiral wall (Pl.22, Figs.3,4). This results in a well defined suture marking the change in direction of the two sets of columns (Pl.22, Fig.5).

In both Chara hispida and Lamprothamnium papulosum the long axis of the polycrystalline columns are, more or less, perpendicular to the organic bands revealed in T.E.M. and L.M. and exposed by acid etching. However, in neither genera was there any evidence of a banding phenomenon in dry fractured calcine (Pl.22, Figs.1,3). The

form of the columns is similar between genera, but the suture between the columns in Chara is less well defined and less regular (see Diag.5.2).

The polycrystalline columns bear no resemblance to chemically grown crystals which are hexagonal rhombohedral in form (Pl.17, Fig.6). In Chara, at high resolution each column is seen to be composed of thin tabular crystals piled on top of each other (Pl.23, Fig.1). These crystals are tiny and will be referred to as crystallites. Each crystallite shows considerable lateral growth, hence the tabular form. In a single specimen an oblique fracture through a spiral revealed the multicrystalline property of calcine very clearly (Pl.23, Fig.2). Such demarcation between layers is, however, atypical. In Lamprothamnium papulosum, tabular crystals were not resolved in the calcine (Pl.22, Fig.5). However, the term polycrystalline column is maintained for this species because of the overall similarities in the calcine with that of Chara calcine.

The polycrystalline columns could be an artifact of the fracturing properties of calcine. It is, however, felt that this is unlikely because thin sections of calcine from both Chara hispida and Lamprothamnium papulosum reveal polycrystalline columns (Pl.19, Figs.1,2). They appear in transverse section under light microscopy as radiating lines. In Lamprothamnium they are very distinct (Pl.19, Fig. 2); this gives rise to the so called inverted "Y" that gives the "Y-form" of calcification. In Chara the polycrystalline columns appear more indistinct under the light microscope and this might be the reason why they were not

previously noticed (Pl.19, Fig.1).

If the columns are not artifactual then they must be considered to be an integral part of the calcine. Examining a transverse fracture of calcine, together with the latest formed (outer surface) calcine, gives some clues as to the development of the polycrystalline columns (Pl.23, Fig.3). At high resolution the outer surface is composed of clusters of small, rounded and conical stacks (Pl.23, Fig.3). At greater resolution each stack is shown to have a substructure of layered crystallites (Pl.23, Fig. 4). There is a polarity in the size of the crystallites in each stack such that each successive crystallite (increasingly younger crystallite) is smaller. This is consistent with data described earlier showing a sequence from calcite nucleation to increased crystal growth with distance from the plasmalemma (Pl.20, Fig.1). Above each polycrystalline column there is a cluster of stacks. It is possible that with crystallite growth, each cluster of stacks fuse together forming the polycrystalline column.

Relating these findings to T.E.M. micrographs of mature and developing Chara calcine is difficult. Ultrathin sections showed some hint of the direction of the polycrystalline columns in vertical bands of electron dense fragments (Pl.20, Figs.5,6). These fragments were probably chips of calcite. Electron transparent regions also reflected the direction of the polycrystalline columns; these may represent the sites where the tabular crystallites were pulled out of section (Pl.20, Fig.6). Ramifying throughout the calcine of Chara hispida and between the crystal fragments, a complex matrix is encountered. This is most readily

seen in uranyl acetate stained sections (Pl.21, Figs.2,3). Uranyl acetate staining tends to decalcify the section (compare Pl.21, Fig.3 with Pl.20, Fig.6).

An attempt was made to establish the precise relationship between the crystallites and the organic component of calcine. This involved trying to remove selectively the organic component by: bacterial degradation or enzyme digestion (zymolyase, proteinase K, and pronase) or sodium hypochlorite. The results were interesting but difficult to interpret.

To isolate the mineral component by bacterial degradation the methods of Cuif et al. (1983) and Frérotte et al. (1983) were used. The rationale was to use cultured bacteria to hydrolyse any organic component in the calcine. The approach led to some startling results. By repeated experimentation and the use of controls it was found that the results had nothing to do with bacteria. Water alone (i.e. water from the sources 1-3 in Materials and Methods section "Experiment to show the influence of water on isolated calcine") was having a great influence on the calcine structure. Consequently, a time course of soaking fractured calcine in water was set up. In any sample there was considerable variation in the influence of water on the calcine structure. The results are therefore necessarily selective to show the sequential stages.

A period of a few days in water caused the complete loss of the polycrystalline columns at the fractured surface of Chara calcine (Pl.24, Fig.3). It was found that unless the water was completely saturated with calcium carbonate (i.e. water from source 4 in

Materials and Methods section "Experiment to show the influence of water on isolated calcine"), the crystallites dissolved at the fractured surface. This must be related to the huge surface area that the crystallites expose. Fixing the calcine in glutaraldehyde to stabilise any organic component in the calcine had no effect on the results. The process is entirely related to the solubility of the crystallites.

The crystallites dissolved at the fractured surface exposing a plate-like concave banding (concave sheets) (Pl. 24, Figs.3,4,5). Between 10 and 12 of these concave bands were found in Chara hispida, they are almost certainly related to the 7-9 concave lamellae/bands exposed by acid etching and seen under T.E.M..

By carefully varying the soaking time in water the extent to which this banding phenomenon occurred was regulated. After a few hours (2-6hrs.) in water the process had only just begun. Polycrystalline columns were still seen but the first stages in their loss was apparent (Pl.22, Figs.7,8).

After more prolonged soaking (1day to 1 week) fimbriate, branched structures mimicking the direction of the polycrystalline columns were seen (Pl.24, Figs.1,2). These structures are believed to be recrystallised calcite, formed by precipitation from a supersaturated solution. Recrystallised calcite also formed on the outside of the lateral spiral walls (Pl.25, Figs.1,2). Here fans of crystals, with their origin at the base of the lateral wall radiate out and interdigitate with adjacent fans in such a way as to be reminiscent of ice crystals growing on glass (Pl.25, Fig.1). These

fans are, however, regularly interrupted by narrow bands (Pl.25, Fig.2).

After 1 week of soaking in water the concave bands (sheets) were revealed (Pl.24, Fig.3). Each band revealed an interwoven network of densely packed fibrils. Between these layers a more dispersed network of fibrils was found (Pl.24, Figs.4,5). After 2 weeks of soaking the dispersed network was lost and the layers became isolated along their length (Pl.24, Fig.6).

After a lengthy time in water (about 3 weeks) there were signs of gross deformation. Structure was lost entirely and a cavity was dissolved out of the spiral (Pl.24, Fig.7). The lateral spiral wall (which is the spiral cell lateral wall), the inner spiral wall (endocalcine) and the outer spiral wall (youngest calcine) were resistant to soaking. These 4 walls collapsed around the cavity left by the action of prolonged soaking; they appeared like an insoluble skin around the central cavity.

This collapsed condition was always encountered in Lamprothamnium papulosum and concave bands could not be isolated by soaking (Pl.24, Fig.8). It is clear that the calcine from this genus dissolves considerably faster.

The water acts only on the fractured exposed surface of the spiral. The same spiral that shows concave bands will at some depth be unaffected by water and revert back to the original polycrystalline column. This can be seen in a specimen which shows one spiral with the banding phenomenon and an adjacent specimen with

polycrystalline columns (Pl.22, Fig.6). During preparation of the specimen for S.E.M. the spiral showing the polycrystalline column refractured thereby removing the spiral portion showing the effects of water. The fact that the action of water is only on a fractured surface is not surprising since intact oosporangia left in water for three years showed, on examination, normal calcine with polycrystalline columns.

The failure to isolate the calcite crystals by removing the organic material with bacteria led to two further approaches; the use of enzymes in high pH buffers and the use of sodium hypochlorite. It was hoped that this would remove any organic component without the added complication of calcite dissolving.

The effect of sodium hypochlorite on Chara hispida and Lamprothamnium papulosum calcine was disappointing. In Chara hispida, tabular crystals in columns were found as in unprepared calcine (Pl.23, Figs.5,6). It is possible that greater periods in sodium hypochlorite would yield more data (i.e. > 10% NaOCl for 5mins).

Subjecting the calcine of Chara to the enzyme pronase for 17 hours revealed a sequence of tabular, pitted layers (Pl.25, Figs.3,4). These layers appeared chipped and were sometimes connected by strands (Pl.25, Fig.4). In addition a secondary layering is encountered (Pl.25, Fig.3). Wilbur (pers. comm.) suggests that this secondary layering might represent cyclic changes in metabolism during the period of mineralisation. The problem with the data was that the calcite showed signs of dissolving and local

recrystallisation. This also occurred in the buffer only control. The recrystallised crystals were of a fimbriate pattern with a vertical axis, as previously described (Pl.24, Fig.2).

The combined use of the two enzymes, zymolyase and proteinase K led to some odd aberrations on the fractured face of Chara calcine. A fibrous layer was seen to coat the fractured surface (Pl.25, Figs.7,8; Pl.26, Fig.1). There were signs of recrystallisation on bands along the fractured surface (Pl.25, Figs.7,8) and strands could also be seen interwoven with recrystallised calcite (Pl.26, Fig.1). Depositional calcite, not dissimilar to the recrystallised calcite reported here, has been found in the rock travertine (Folk et al. 1986) Travertine is deposited in hot sulphurous springs. However, very little is known about any of these strange crystal forms. The results with these two enzymes are difficult to understand and as with the pronase experiments, the buffer-only control gave similar data.

The effect of proteinase K and zymolyase on Lamprothamnium calcine for 17 hours was very different, a strong banding phenomenon was encountered (Pl.25, Fig.5). The bands had a considerable number of cross lamellae fibrils (Pl.25, Fig.6). No hint of calcite crystals remained. Once again, however, the effect of the enzyme could not be disentangled from the effects of the buffer-only control.

The action of F.A.S. (fast-atom source) has been used to elucidate substructure in the silica wall of diatoms, the wall of pollen and in the testae of Amoebae (Claugher 1984). It acts in the same way

as ion-beam etching but does not have the disadvantage of charging artifacts. Atoms are accelerated and used to erode surfaces (see Claugher 1984). Its action can be best visualised by considering the atomic beam as an atomic "sandpaper", stripping away layers systematically. Here F.A.S. served only to erode detail from the calcine of Chara (Pl.26, Fig.2). Following F.A.S. there was no hint of the tabular crystallites. The polycrystalline columns became rounded and abraided. The technique proved unsatisfactory.

The high solubility of the crystallites, particularly those of Lamprothamnium, led to the belief that perhaps in Lamprothamnium, the calcine was composed of aragonite. The brackish water habitat of Lamprothamnium would also indicate that this was possible. This was tested using X-ray diffraction on Chara and Lamprothamnium calcine.

The lattice planes in any crystal are precise distances apart. These distances (d) can be derived from peaks on the X-ray diffraction traces and can be used to fingerprint the crystals present (using the J.C.P.D.S. Search Manual 1980). The peaks in the X-ray diffraction trace (p on Traces 5.1 & 5.2) represent peaks in diffracted X-rays at various angles of X-ray incidence (2θ). The X-rays are being diffracted from the lattice planes in the crystals. Calcite shows three diffracted peaks, a main peak at 29.40^{o} (d=3.04Å), a second peak at 36.00^{o} (d=2.49Å) and a third peak at 23.00^{o} (d=3.89Å). Traces 5.1 & 5.2 show the X-ray diffraction trace for Chara and Lamprothamnium respectively. Chara shows a main peak at 29.50^{o} a second peak at 36.10^{o} and a third peak at 23.10^{o} (d=3.303Å, 2.49Å, 3.87Å respectively).

Lamprothamnium shows three peaks, a main peak at 29.90°, a second peak at 36.50° and a minor peak at 23.50° (d= 2.99Å, 2.46Å, 3.80Å respectively). Both traces showed the mineral to be calcite. The drift recorded in the three peaks when compared with pure calcite is due to magnesium substitution in the crystal lattice. Utilising Scholle's (1978) conversion table an approximate magnesium carbonate content of 3mol percent and 15mol percent was found for Chara and Lamprothamnium respectively. These values show Chara to have low-magnesium calcite and Lamprothamnium to have high-magnesium calcite. This is only an approximation, however, because other cations besides magnesium can cause lattice modifications and the data should be checked using techniques like spectrophotometry. These results do, however, conform with published data (Horn af Rantzien 1956, Daily 1975 and Burne et al. 1980).

Discussion

Speculation on the process of oosporangial calcification and comparisons of oosporangial calcification with other biomineralising systems mentioned in the literature are discussed below. As far as the author is aware no metabolic or ion flux experiments have ever been carried out on oosporangia of charophytes.

The calcine is laid down within the confines of the ensheathing cell walls, between the compound oosporangial wall and the ensheathing cell plasmalemma. This site of calcification can be considered as an example of Simkiss's (1986) diffusion limited site. The isolation of a compartment (bound by the cell walls and the plasmalemma) will influence the movement of ions. There is a possibility of 4 major calcium exchange pools in a system like this.

(1) The cell wall (compound oosporangial wall). (The cell walls of Halimeda are known to be directly involved in calcification (Borowitzka & Larkum 1976a,1977, Borowitzka 1982a,b)).

(2) The ensheathing cells themselves have a direct connection (via plasmodesmata) to all the cells of the thallus (see Chapter 3). The vacuoles in Chara internodal cells (which appear ultrastructurally similar to the ensheathing cells) are known to have large amounts of stored Ca^{2+} (Hoagland & Davis 1923, 1929, Hope & Walker 1975)

(3) The calcite crystals themselves.

(4) The plant's environment.

Which pools have the most significant influence on the calcium supply necessary for calcification remains unstudied.

In order for calcite nucleation and growth to occur it is required that the solubility product of calcium carbonate is exceeded. For continued calcification there must be a continuous supply of Ca^{2+} and HCO_3^- (see review Borowitzka 1982b). Borowitzka and Larkum (1976a,b) considered that passive diffusion of these ions from the environment was unlikely to effect calcification in Halimeda due to the speed of ion diffusion and the length of their diffusion path. In Chara the length of the diffusion path is of the same order as in Halimeda (i.e. about 50µm; the width of a spiral cell) and the calcification site is isolated from the environment. It would seem likely therefore, that the ions are under at least partial control of the ensheathing cells. If HCO_3^- is being utilised as the carbon source for photosynthesis, as it is in the internodal cells of the thallus (Lucas 1983, Walker 1983 and others), then the OH^- generated could be removed into the calcification site. This would effect a favorable pH shift for calcification to occur. The ion Ca^{2+} may be pumped into the calcification site; this is known to occur in coccolith formation. Coccolithophorids are able to pump $3x10^6$ Ca^{2+} ions per second from the environment into the coccolith vesicle during coccolith synthesis (Westbroek et al. 1983 Van der Wal et al. 1983). The biochemical and ionic events during calcification will remain speculative until work with ionic inhibitors, pH probes, labelled carbon and calcium has been carried out.

Degens's (1976) template model for calcification in mollusc shells, proposes that a carrier protein is being secreted by the organism across the plasmalemma and polymerising in the form of a sheet. The carrier protein acts as a binding site for an acid polysaccharide fraction called the mineralising matrix. The mineralising matrix has a strong affinity for calcium ions and is presumed to nucleate the calcium carbonate. It is tempting to draw parallels between this model and observations concerning the formation of charophyte calcine. The organic strands (sectioned sheets) seen outside the plasmalemma of the calcifying spiral cells might represent Degens's (1976) carrier protein. If this is so, it must be assumed that the mineralising matrix, if it exists in calcine, has been secreted at the first signs of crystal nucleation.

It has been suggested that organic molecules are involved in crystal shaping by inhibiting and stimulating crystal growth in specific directions (Simkiss 1986 and references within). Organic molecules are known to be crystal growth inhibitors (Simkiss 1964a). Wilbur and Bernhardt (1982) suggest that the carboxyl group on a protein is responsible for this. The protein interacts with the normal growth site of the crystal preventing additions to the crystal lattice. This inhibits normal crystal development, or stops crystal growth altogether (Degens 1976). By means of X-ray diffraction Weiner and Traub (1980, 1981, 1984) and Weiner et al. (1983) showed that the alignment of organic matrix components were reflected in the alignment of the crystallographic axis of the calcite in the nacreous layer (Mother-of-Pearl) of Nautilus (Gastropoda, Mollusca). It is quite possible therefore, that the

complex 3D network of organic material in calcine represents organic molecules involved in controlling crystal growth and shape.

The parallels in development and morphology of Chara calcine and gastropod nacreous layer is striking. These are presented below. (Details taken from review article Wilbur & Saleuddin 1983).

1. An organic matrix that is involved in mineral deposition is secreted. In molluscs a thin organ lining the inner shell surface, the mantle, is responsible for this secretion; in charophytes the ensheathing cells are responsible.

2. In gastropods and charophytes the organic matrix is involved in crystal nucleation. Evidence for this in charophyte calcine lies in electron dense amorphous areas in the newly formed organic matrix.

3. In both gastropods and charophytes, calcification proceeds by new crystals forming on top of older crystals. This gives rise to conical stacks. Growth of the crystal proceeds by lateral extension but not by increased thickness. This forms the crystal morphology in 4 (below).

4. Fully developed gastropod nacre and calcine have layers of crystals with uniform thickness. The crystalline layers in gastropod nacre are separated by matrix. The crystals in both systems are tabular and arranged in columns.

The precision with which the calcite crystallites are aligned and grow is highly controlled. The crystal size and growth direction is

controlled by the cell but occurs outside the cell's plasmalemma. This is a case of remote control no less complex than the orderly array of microfibrils in the plant cell wall.

Polycrystalline columns were found in freshly fractured calcine and in thin sections of calcine under light microscopy. Each polycrystalline column is composed of layers of tabular calcite crystals. The occurrence of polycrystalline columns in two quite different preparations suggests that they are a real structural feature of calcine. Calcine development occurs by the nucleation and growth of calcite. The developing crystals occur in clusters of stacks. It is possible that the fusion of the stacks in each cluster, by the lateral growth of the crystals, unifies the stacks into a polycrystalline column. This will remain pure speculation until a more detailed understanding of the calcite and its interaction with the organic phase has been elucidated.

Using light microscopy Feist and Grambast-Fessard (1984), and Soulié-Märsche (1979) proposed two distinct forms of calcification, "U-form" and "Y-form". They questioned whether the observed differences were of taxonomic or ecological importance. On the basis of their work, Wright (1985) suggested that the "Y-form" calcification should be used as a palaeoecological indicator of brackish water to saline habitat; thereby giving ecological importance to the observation. In order to be able to make a valid judgement on the taxonomic versus ecological question concerning the calcine differences, it is necessary to find Chara growing side by side with Lamprothamnium. Davies (pers comm) reports having seen this in the Coorong of Australia but unfortunately was

not able to supply any oosporangia. It is therefore considered to be too early to speculate on whether the observed differences between the calcine of the two genera are of taxonomic or ecological importance.

The calcine of both Chara and Lamprothamnium possess polycrystalline columns, an organic matrix and an experimentally inducible concave banding phenomenon at fractured spiral surfaces. Examining sections of calcine under the light microscope showed that the polycrystalline columns are seen in the "Y-form" calcification and the organic matrix is seen in the "U-form" calcification. The observed "U-form" or "Y-form" is therefore a matter of emphasis. Which is most visible under a light microscope, the organics or the polycrystalline columns? (see Diag. 5.3). The calcine of the two genera is not fundamentally different. However, the layers of tabular crystals seen in fractured calcine of Chara were not seen in Lamprothamnium. It is possible that they are present in Lamprothamnium but not resolvable.

The fate of fossil calcine during diagenesis is discussed in Chapter 6-calcification.

DIAGRAM 5·1 SHOWING CALCINE DEVELOPMENT IN *CHARA*

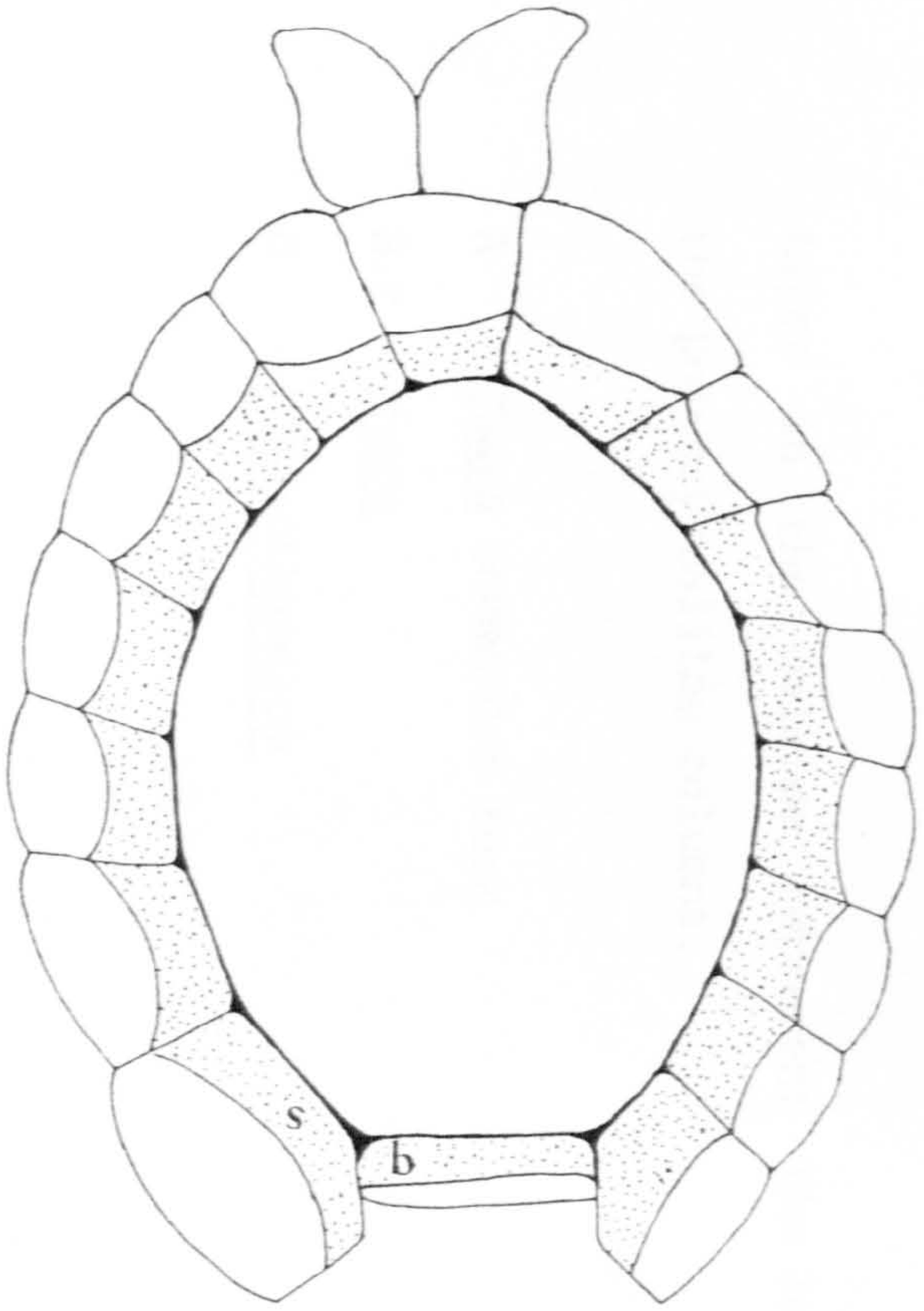

oosporangium in section

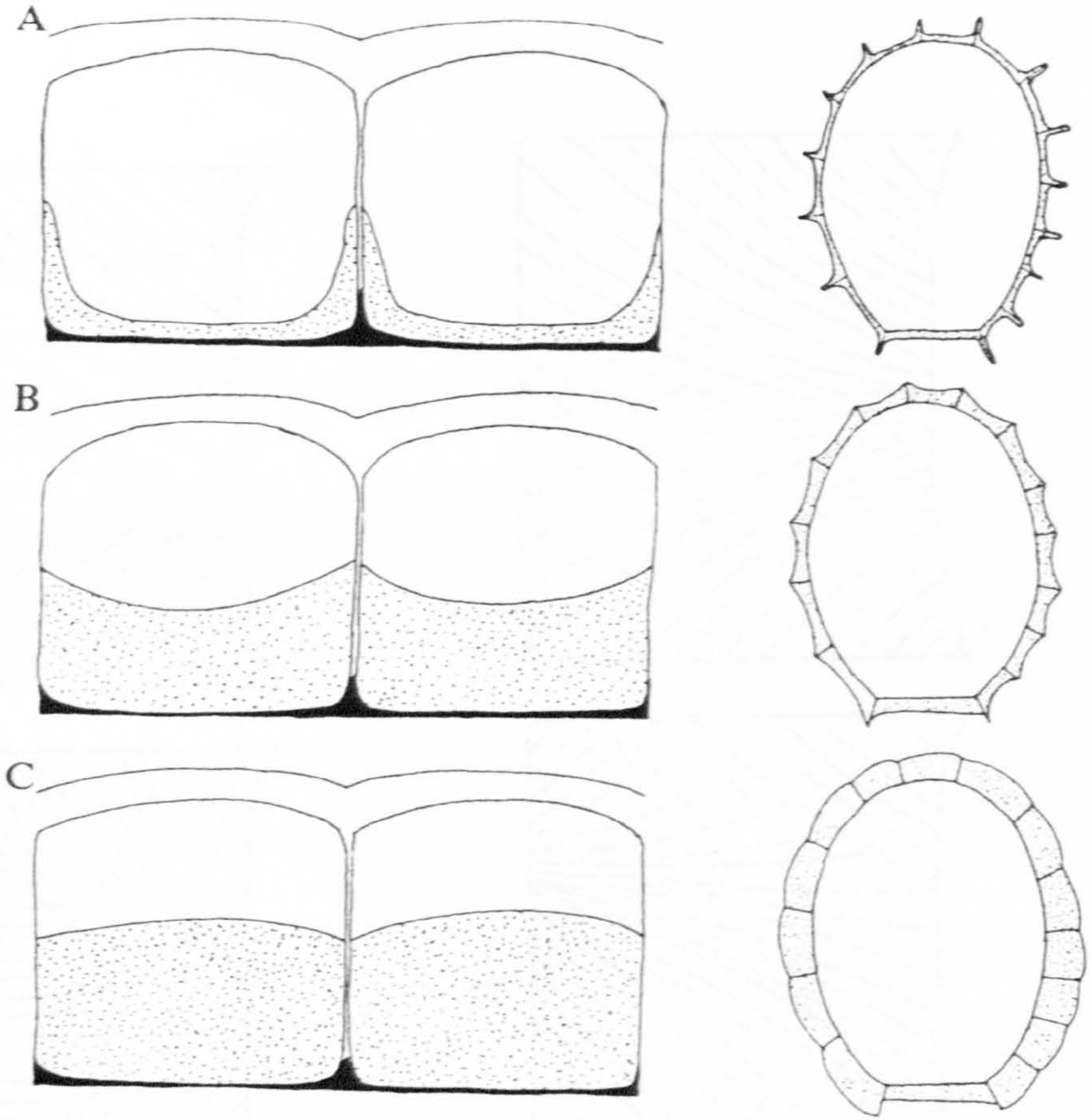

A–C progressive degrees of calcification

calcine (calcite + organic matrix)

DIAGRAM 5·2 SHOWING TRANSVERSE FRACTURE OF CALCINE

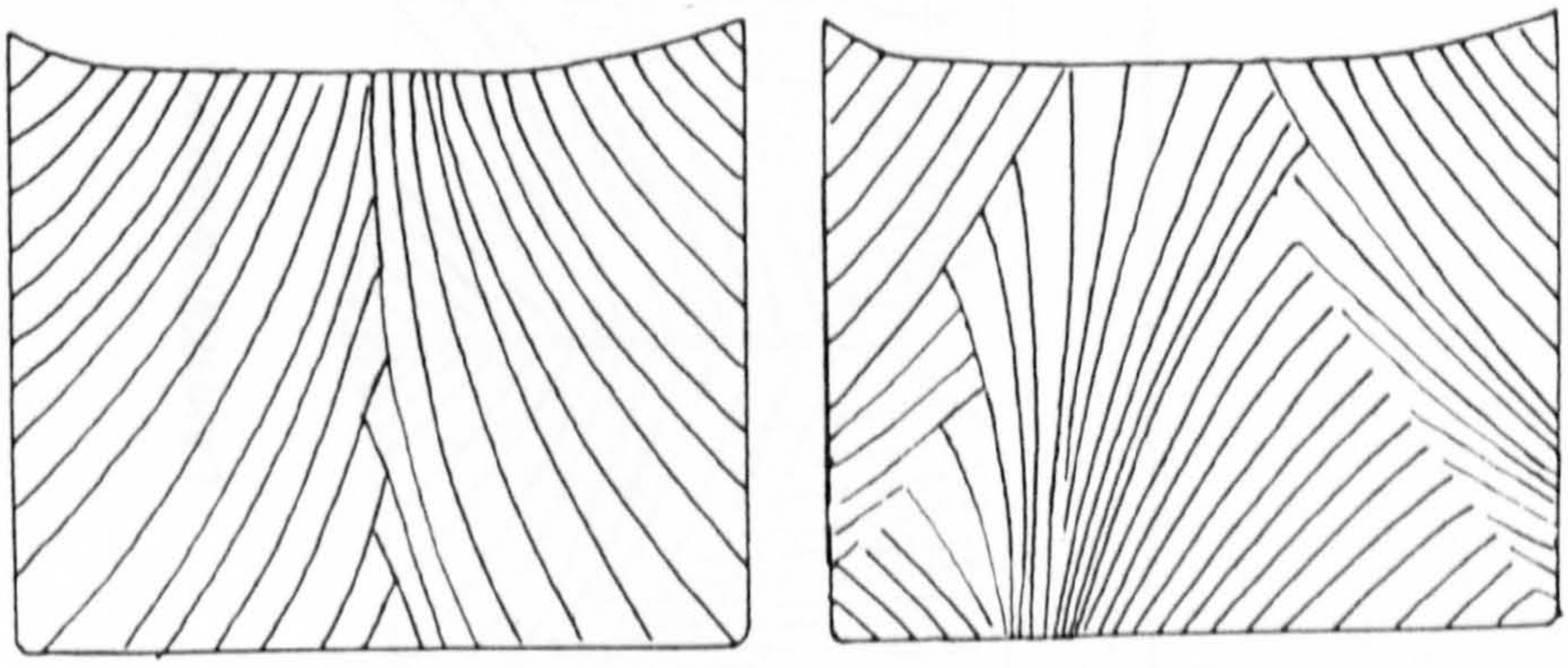

A B

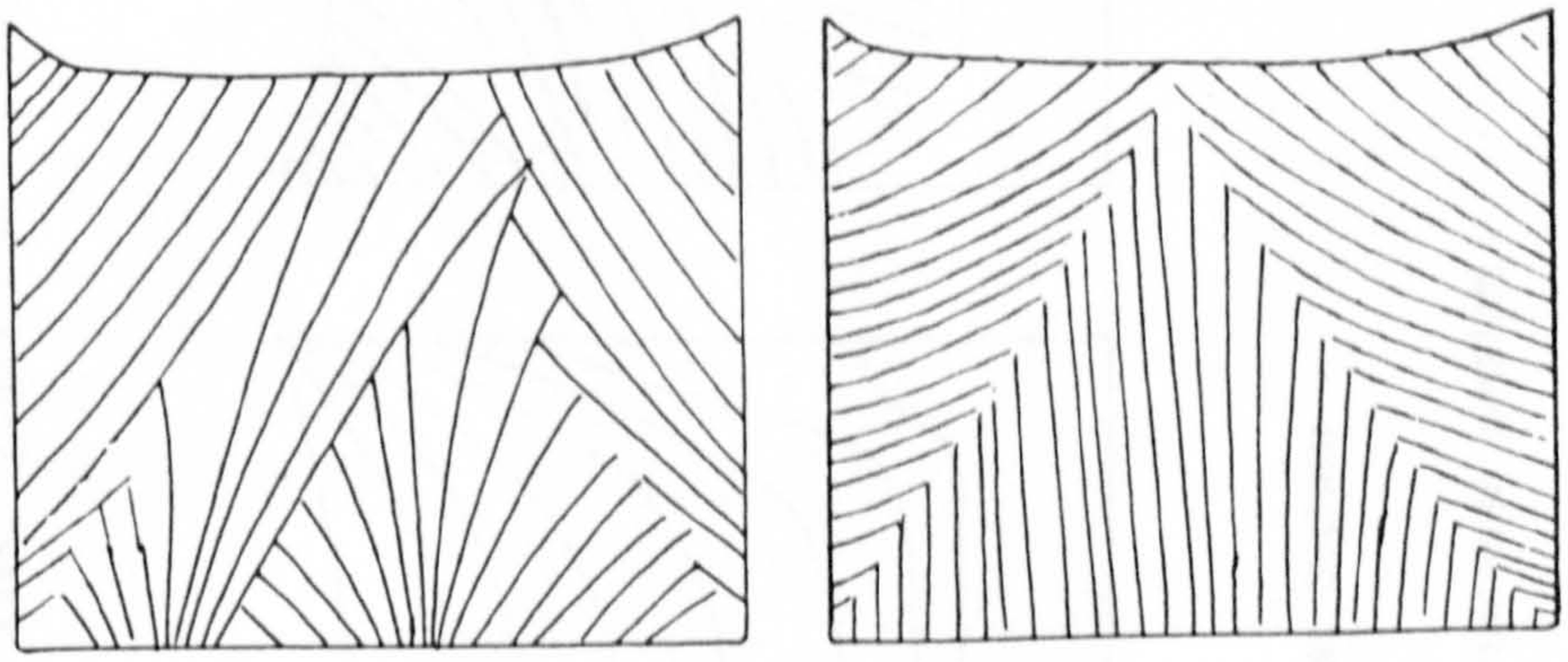

C D

Lines in the calcine represent the long axis of the polycrystalline columns.

A - Chara commonest form

B,C - Chara

D - Lamprothamnium

DIAGRAM 5·3 SHOWING THE RELATION OF ORGANIC MATRIX TO CALCITE IN THE CALCINE LAYER

CHARA

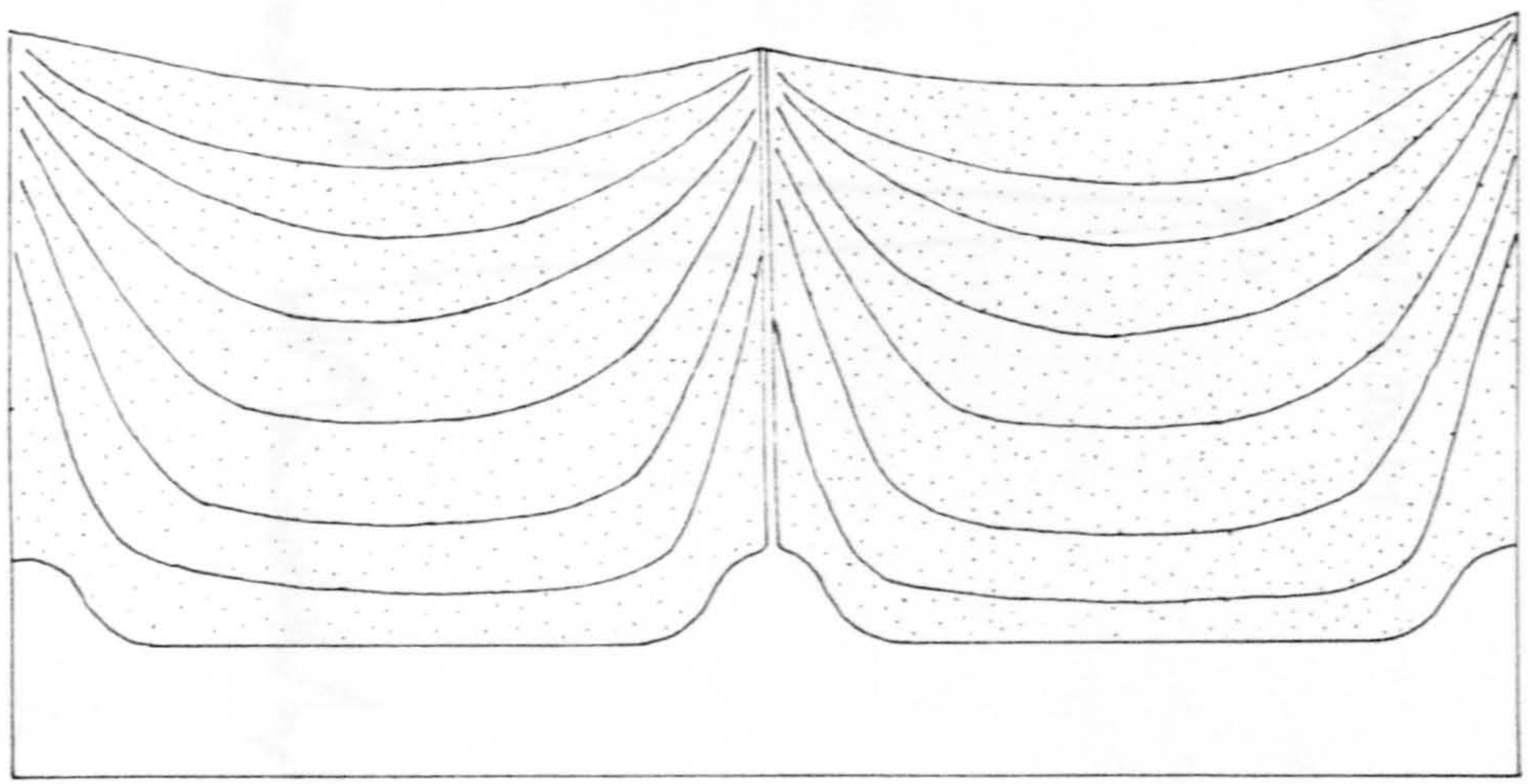

organic matrix describes a `U´ in transverse section

polycrystalline columns descibe an inverted `Y´ in transverse section

LAMPROTHAMNIUM

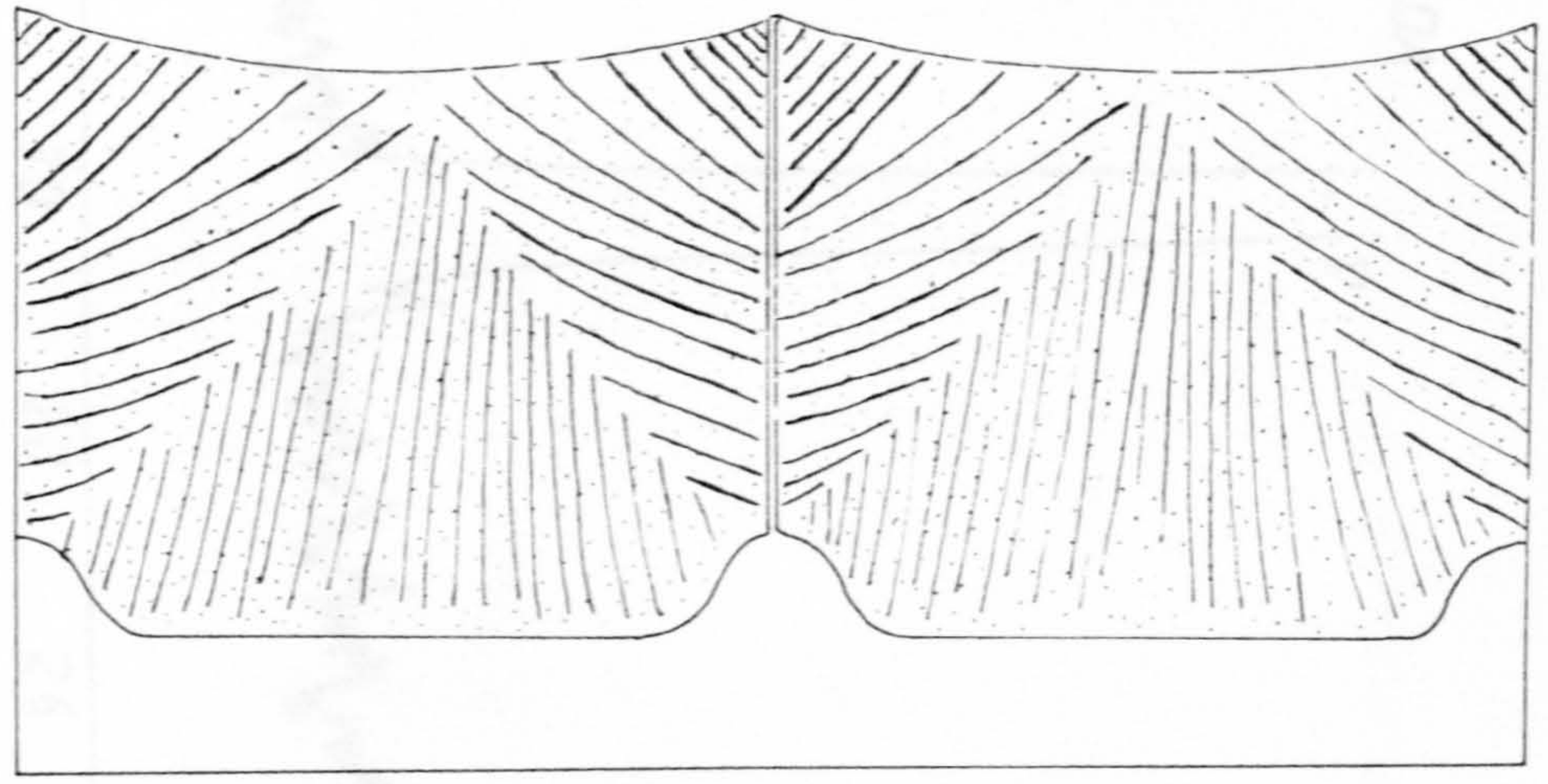

X-RAY DIFFRACTION TRACES

TRACE 5·1 *CHARA HISPIDA*

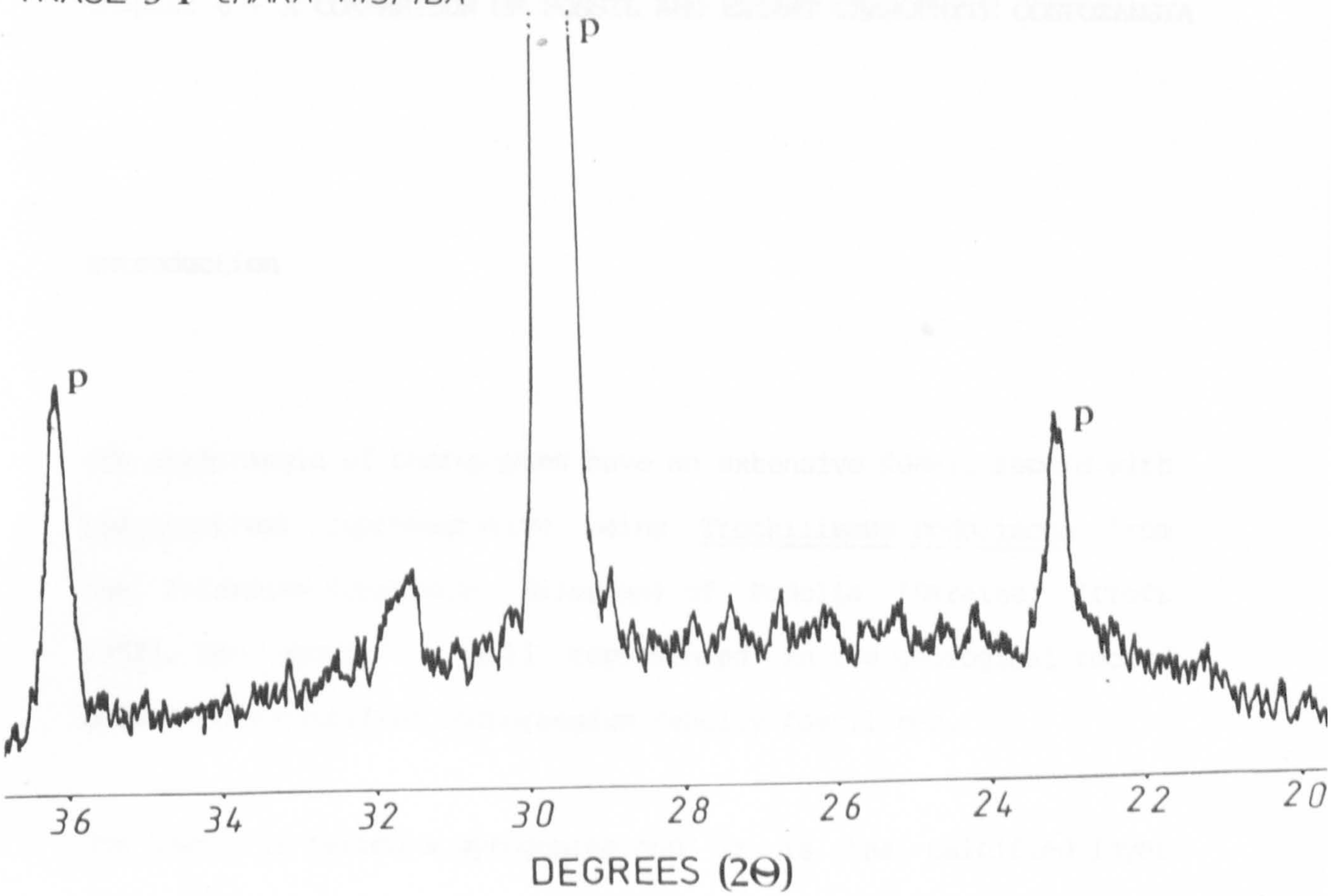

TRACE 5·2 *LAMPROTHAMNIUM PAPULOSUM*

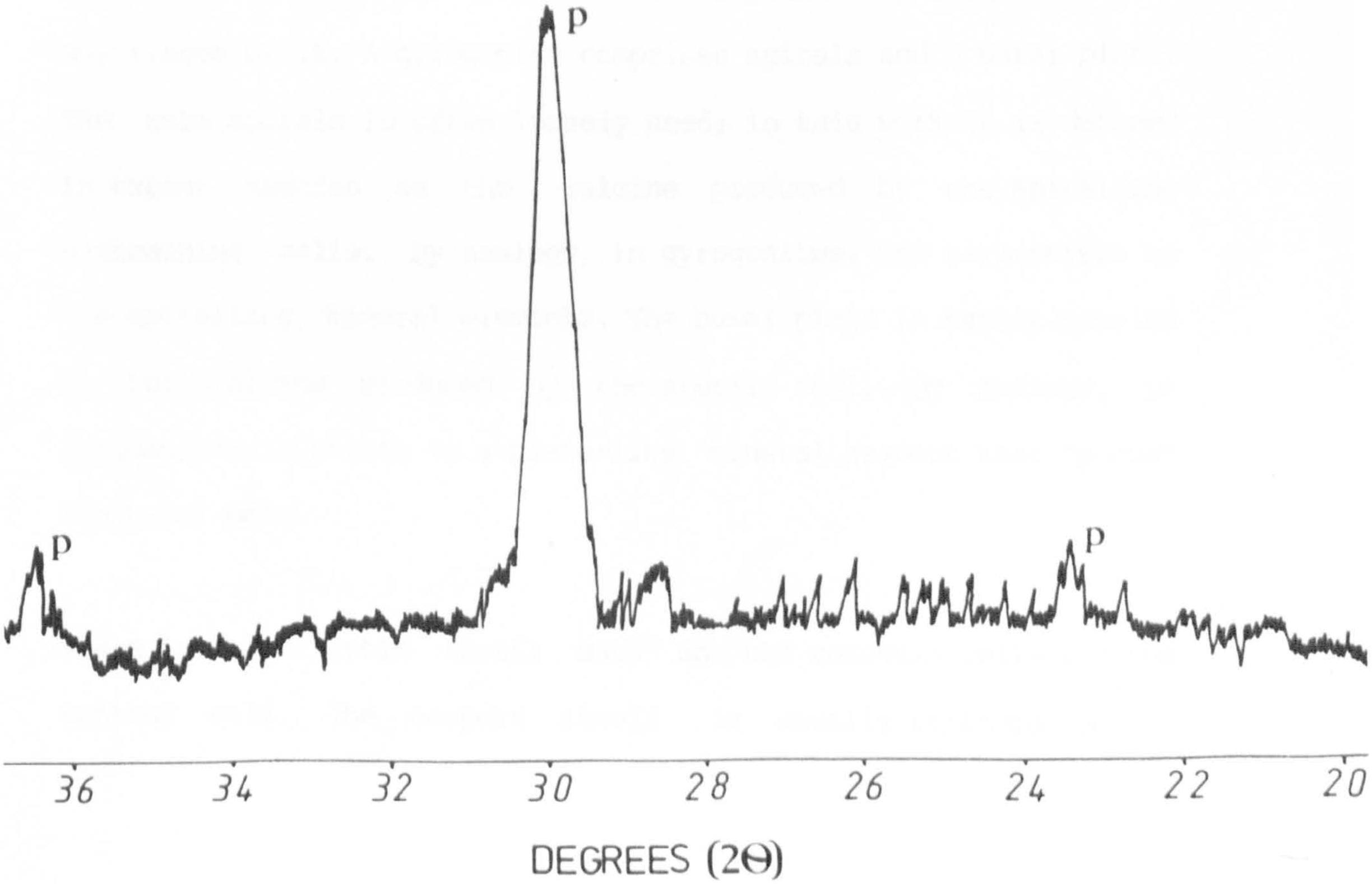

Chapter 6 - A COMPARISON OF FOSSIL AND EXTANT CHAROPHYTE OOSPORANGIA

Introduction

The oosporangia of charophytes have an extensive fossil record with the earliest representative being Trochiliscus podoliscus from the Pridolian (Uppermost Silurian) of Podolia (Ukraine) (Croft 1952). The group is well represented in the geological record because the calcified oosporangium readily fossilises.

The fossil is termed a gyrogonite and it is the calcified layer that would have surrounded the oospore; it is fossilised calcine. This definition differs from that of Horn af Rantzien's (1956) which includes the compound oosporangial wall or any traces of it. A gyrogonite comprises spirals and a basal plate. The term spirals is often loosely used; in this work it is defined in extant species as the calcine produced by the spiralling ensheathing cells. By analogy, in gyrogonites, the term refers to the spiralling mineral elements. The basal plate in extant species is the calcine produced by the sterile cell. By analogy, in gyrogonites it refers to a plate-like mineral segment that "plugs" the basal pore.

There is very little fossil data on the coronula cells and the central cell. The oospore itself is usually replaced by a

post-mortem deposit, usually of calcite or pyrite (Horn af Rantzien 1956). The fossil is usually encountered as a gyrogonite surrounding an internal mineralised cast. Sometimes traces of the compound oosporangial wall can be found on the innerside of the gyrogonite, usually preserved as post-mortem petrifications.

In more rarely encountered preservation conditions, the calcine is replaced by silica, the whole gyrogonite is then a silicious petrification. In some cases not only the gyrogonite but the whole plant becomes silicified. Such fossils have provided the opportunity to study antheridia, thalli, coronula cells and oosporangia (Sahni and Rao 1943 -cited in Horn af Rantzien 1956, Harris 1939).

Grambast (1974) has developed a fascinating gyrogonite phylogeny. This work has provided a sound foundation for an understanding of the major taxa and their evolutionary position. The evolutionary trends demonstrated by Grambast (1974) are shown in Diagram 6.1.

During the Devonian and Lower Mississippian the highest structural diversification in gyrogonites occurred. Three orders have been discovered, the extant order Charales (Middle Devonian to Recent), the fossil orders Sycidiales (Middle Devonian to Early Mississippian) and Trochiliscales (Upper Silurian to Early Mississippian).

Gyrogonites of the order Sycidiales lack the spirals found in the other orders, having vertically aligned elements that were either simple (family Chovanellaceae) or subdivided by horizontal

partitions (family Sycidiaceae). Gyrogonites of the order Trochiliscales had numerous (>6) dextrally spiralling spirals. Both fossil orders had an apical pore.

The first member of the order Charales, Eochara Choquette (Middle Devonian), showed a very similar structure to Trochiliscus Karpinsky (order Trochiliscales), with numerous (>6) spirals and an apical pore. However, the spirals showed sinistral spiralling, a feature that remained constant in all Post-Carboniferous forms.

Early evolution in the order Charales is characterised by a reduction and fixation in the number of sinistral spirals to five in Stomochara moreyi (Family Porocharaceae, Upper Carboniferous, Canada). The modern spiral form was therefore first seen in the Upper Carboniferous and has remained unchanged. Rare specimens of the genera Chara, Grambastichara Horn af Rantzien, Rhabdochara Mädler and Tectochara L & N Grambast have been found with four or six spirals (Glokhovskaya 1975 -cited in Tappan 1980). These are probably all mutants, but their occurrence question the validity of the family Palaeocharaceae (order Charales, Pensylvanian to Upper Carboniferous) which is characterised by six sinistral spirals and is known from only six specimens. (Bell 1922 -cited in Tappan 1980).

Later evolution in the order Charales was characterised by morphological changes in the apex. An open pore is seen in the families Palaeocharaceae, Porocharaceae (Upper Carboniferous to Lower Paleocene) and the Clavatoraceae (Upper Jurassic to

Cretaceous). A pore closed by five small units forming an operculum, perhaps derived from the coronula cells, is found in the family Raskyellaceae (Upper Cretaceous to Upper Oligocene). In the only extant family, Characeae (Triassic to Recent) the apex is closed.

The family Clavatoraceae represents a major group of Mesozoic charophytes which reached their zenith in the Cretaceous. They are characterised by having an external sheath of vegetative cells around the gyrogonite called the utricle. Grambast (1974) identified phylogenetic changes in the utricle of three Clavatoraceae lineages.

The family Characeae became abundant in the Middle Cretaceous and the most diverse in the Eocene and Oligocene. Since the Miocene the group diversity has decreased to reach its present, much reduced status. By the Middle Jurassic the two subfamilies of the Characeae, the Nitelleae and Chareae were distinguishable. The Chareae has a much more extensive fossil record.

Gyrogonites and extant charophytes are commonly found in association with ostracods, molluscs and fish-teeth. They are most frequently found in non-marine sediments, their rare occurrence in marine sediments is almost certainly due to transportation. For further reviews of fossil charophytes the reader is referred to Tappan (1980), Grambast (1974) and Feist & Grambast-Fessard (1982).

This chapter aims to examine structural features in extant

charophyte oosporangia and where possible to compare these with features found in fossils. Some of the features unique to the fossils are also presented. Fossil specimens illustrating structural features are necessarily limited to those which were collected and those which were kindly provided by other workers.

The following features are presented in turn .

1. Apical construction.
2. Basal cage.
3. Basal plate.
4. Spirals (i) concave vs. convex
   (ii) ornamentation
   (iii) lateral wall
   (iv) pillars.
5. Utricle.
6. Calcine.

Other features that vary within and between taxa include size, shape and number of spiral revolutions. These and other variable features and their bearing on systematics, are considered in the next chapter.

Apical Construction

The form and arrangement of the spirals at the apex is characteristic for all the charophyte families. Some of these differences are reviewed in Feist and Grambast-Fessard (1984). The spirals can meet at the apex or leave an apical pore; they can be apically expanded, contracted, elevated or truncated. The apical form can also be altered by dehiscence.

In the extant family Characeae the spirals come together at the apex (Pl.26, Fig.8). The apical tips of the spirals in Chara are expanded, a feature which is diagnostic of the genus (Feist & Grambast-Fessard 1982). On germination the spirals break subapically (behind the apical spiral expansions) to leave a fracture perpendicular to the lateral wall of the spiral (Pl.18, Fig.8). This gives rise to the so called "cog-wheel" form ("roué dentée") (Grambast 1956a). The zone where dehiscence is to occur is demarcated by an alteration in calcine thickness at the spiral apex (Pl.18, Figs.5,6). In Lamprothamnium, spiral apices are weakly calcified and appear to lie in a depression (Pl.18, Figs.1,2). Feist and Grambast-Fessard (1982) term this apex "type lamprothamnoide".

In any fossil population of the family Characeae, one would expect to find both germinated and/or ungerminated gyrogonites. From the Lower Headon beds (Eocene) of the Isle of Wight both forms are found in a fossil population of Gyrogona Lamark. The ungerminated

gyrogonite (Pl.27, Fig.1) has a closed apex and the germinated gyrogonite (Pl.27, Fig.2) has fractured spiral apices (Pl.27, Fig.3).

The family Raskyellaceae is characterised by having an apex which is not closed by the spirals but by five small calcine plates (Pl.27, Figs.5,6). These plates are considered to be the product of the calcification of the coronula cells (Grambast 1974); they can appear weakly (Pl.27, Fig.5) or strongly calcified (Pl.27, Fig.6). Together, the plates comprise the operculum. On germination the operculum is believed to be fractured off, resulting in a large apical pore (Pl.27, Fig.7) that is described as being of "rosette" form (Feist & Grambast-Fessard 1984).

In the family Porocharaceae the spirals do not extend apically. This results in an apical pore which is more or less round or rounded pentagonal (Pl.33, Figs.3,4). In Musacchiella there are slight variations in the apical pore morphology. For example, Musacchiella palmeri from the Middle Jurassic of England (see Chapter 7) has an apical pore that is of stellate form (Pl.27, Fig.8). Its characters seem to be intermediate between the "cog -wheel" form of the germinated Characeae (Pl.27, Fig.2) and the "rosette" form of the family Raskyellaceae (Pl.27, Fig.7).

Basal Cage

The basal cage is a loosely used term, here it is defined as being the downward extension of the spirals at their bases. Horn af

Ranzien (1956) also used the term basal cage to include the compound oosporangial wall in the basal region. In some individuals of some species (e.g. Chara hispida Pl.28, Fig.1) secondary wall deposits are laid down around the sterile cell and the central cell. This is an unusual aberration that does not fossilise and it will therefore not be included in this definition of a basal cage.

In the basal region of some individuals of Chara hispida the calcine extends sharply downwards (Pl.28, Fig.3). This is commonly found in weakly calcified oosporangia. In more strongly calcified oosporangia the additional calcine deposited by the spiral cells serves to mask the basal cage; consequently strongly calcified oosporangia usually show no signs of a basal cage (Pl.28, Fig.5).

In the fossil genus Harrisichara Grambast a basal cage is found (Pl.28, Fig.4) appearing as a column extending from the base. However, in most genera, a basal cage is not found, with most gyrogonites having a rounded base (Pl.36, Fig.4 & elsewhere).

Basal Plate

A review of the significance of the basal plate in charophyte oosporangia and their phylogenetic importance is given in Feist and Grambast-Fessard (1984). In the extant subfamily Chareae, and in the genus Tolypella section Acutifolia (subfamily Nitelleae) a single unsegmented basal plate is found (Daily 1975). This is

formed by calcification of the sterile cell (see chapter 5). It is best seen by internal inspection, appearing rounded/pentagonal (Pl.29, Fig.1). In fossils an unsegmented basal plate is most commonly found (e.g. Porochara westerbeckensis, Pl.29, Fig.4).

In the extant genera Nitella and Tolypella section Obtusifolia there are three sterile cells (Sawa & Frame 1974). Two of these cells are shown in a pre-fertilisation oosporangium of Nitella opaca (Pl.9, Fig.2). In both genera the oosporangium does not calcify, consequently no basal plate forms. However, fossil representatives of Tolypella section Obtusifolia have segmented basal plates that have either two (bipartite basal plates) or three (tripartite basal plate) segments (Daily 1969). Each segment is considered to be the calcine derived from a single sterile cell (Grambast 1956b).

Gyrogonites with segmented basal plates have now been ascribed to Tolypella (Upper Cretaceous to Lower Oligocene) and Musacchiella (family Porocharaceae, Middle Jurassic to Lower Cretaceous) (Feist & Grambast-Fessard 1982, 1984, Colin et al. 1985). The bipartite basal plate of two species of Musacchiella are shown on Pl.29, Figs.2,3. In Musacchiella douzensis (Pl.29, Fig.3), the basal plate is visible on external inspection (Pl.31, Figs.3,4) whilst in Musacchiella palmeri it is visible only on internal inspection (Pl.29, Fig.2).

Spirals

(i) Concave vs. convex

In living species the deposition of calcine can vary considerably from one individual to the next. If weakly calcified the spirals appear concave in profile and when strongly calcified convex (see Chapter 5, Pl.18, Figs.1-4). Sometimes an extant charophyte population is encountered with only concave spirals, but the author has never seen a population with individuals having only convex spirals. Most usually the condition is mixed. It would be expected therefore to find concave or mixed spiral forms in a single fossil population. In the author's experience this is true. From the Upper Jurassic of Portugal a population of gyrogonites with only concave spirals (e.g. Porochara raskyae, Pl.36, Fig.4 and several populations with mixed spiral forms (e.g. Porochara mundula Pl.35, Figs.5,6,7) were encountered.

(ii) Ornamentation

In all modern taxa the spirals show no ornamentation (e.g. Chara hispida (Pl.26, Figs.3-6). This is also the condition most commonly encountered in fossils (e.g. Gyrogona Pl.27, Figs.1-3). Quite often there is some contamination with calcite debris (e.g. Porochara obovata Pl.34, Fig.5) but there is no regularity to this. However, in a few genera (Harrisichara, Stephanochara Grambast, Nodosochara Madler and Microchara Grambast) the spirals do show ornamentation. In Harrisichara the spirals

can be seen to be concave, with protuberances or tubercles of calcine on the spirals. These protuberances can be of various sizes, isolated or combined and together they comprise the ornamentation (Pl.28, Figs.2,4,6).

(iii) Lateral Walls

In all the extant genera the lateral walls of the spirals are flat (Pl.25, Fig.1). When viewing the oosporangium from the inside or outside the lateral wall of the spiral is delimited by a spiralling suture (Pl.26, Figs.3-6; Pl.29, Figs.1,5). This is also the case in most fossil genera (e.g. Musacchiella douzensis Pl.31, Figs.1,5). However, in three species belonging to three genera Rantzienella nitida, Sphaerochara edda and Psilochara undulata the lateral wall of the spiral is not flat but ridged (see Feist-Castel 1973). In Rantzieniella nitida it is the inner region of the lateral wall that is strongly ridged (Pl.29, Fig.6). When this gyrogonite is viewed internally, the lateral wall appears to be sinusoidal with each spiral interdigitating with its neighbour (Pl.29, Fig.7).

(iv) Pillars

Feist-Castel (1973) was the first to describe these structures. In Lamprothamnium papulosum, "pillars" of calcine can be seen on internal inspection of the spirals and they occur at the base of the lateral walls of the spirals. (Pl.29, Fig.8). Each "pillar" is derived from two spirals. The occurrence of the "pillars" is a direct reflection of the altering thickness and height of the

spiralling ridge found on the compound oosporangial wall. The "pillars" correspond directly to regions of reduced height and thickness in the spiralling ridge because the calcine is deposited directly on top of the compound oosporangial wall. Feist-Castel (1973) reports similar pillars in the fossil genus Harrisichara. However, none of the specimens of this genus examined by the author exhibited "pillars".

Utricle

The utricle occurs only in the fossil family Clavatoraceae. Here a utricle of Clavator reidi from the Purbeck (Upper Jurassic) of Dorset is shown (Pl.30, Fig.1). It is preserved as a silicified petrification.

Calcine

The work carried out on the extant genera Chara and Lamprothamnium is presented in Chapter 5. This section concerns the fossil calcine morphology and the possible effects of diagenesis on the calcine.

The mineral component of all modern and fossil charophyte calcine is calcite or magnesium calcite (Horn af Rantzien 1956, Daily 1975, Burne et al. 1980, Chapter 5). This information, coupled with the

freshwater sediments in which most fossil charophytes are found, leads to the assumption that the likely mineral component of all gyrogonites is calcite or magnesium calcite. However, the possible occurrence of aragonite must be borne in mind.

Organisms that lay down aragonite are laying down an unstable isomorph of calcium carbonate (see Chapter 5). During diagenesis it slowly alters to the more stable isomorph calcite. With its change there is complete loss of the original crystal structure (Sandberg 1975a and references within).

The literature is unclear on the question as to whether or not the loss of magnesium from high magnesium carbonate (ie >4mol percent $MgCO_3$) during diagenesis is accompanied by the loss of primary crystal structure. Sandberg (1975b) considers that the process is accompanied by some textural change. However, Towe and Hemelben (1976) argue that the loss of magnesium is structurally non-destructive, but that once complete, further diagenesis results in the recrystallisation of the calcite into coarser more stable crystals.

If there is crystal alteration it can usually be detected using S.E.M (Sandberg 1975a,b, Towe & Hemelben 1976). Recrystallisation is a purely physical process, forming a tightly welded mosaic of coarse grained calcite called sparry calcite. Biological mineralisation is usually associated with fine structurally controlled crystals (see Chapter 5).

In conclusion therefore, if a fossil is encountered with fine

crystal structure and considerable crystal order it can be presumed that the mineral was formed under the influence of a biologically mediated process. If the fossil shows no fine crystal form and exists as a coarse sparry calcite, then it is probable that the original crystal form has been lost and secondary calcification effects are being seen.

The differences between the calcine of modern Chara and Lamprothamnium is only slight (see chapter 5). The calcine of both genera has polycrystalline columns, an organic matrix, and an experimentally inducible banding phenomenon. The most fundamental difference is that the layers of tabullar crystals in the calcine of Chara could not be resolved (if present at all) in Lamprothamnium. However, it is the similarities which give rise to considerable doubts as to whether two types of calcification can be identified in fossil forms, as is suggested by Feist and Grambast-Fessard (1984) and Wright (1985). The influence of diagenesis alone could account for all the variations seen in fossil forms. It is therefore considered that the fossil calcine substructure cannot as yet be used as an ecological or taxonomic indicator.

On examining gyrogonite ultrastructure three different preservational forms were found :

1. The calcine of Musacchiella palmeri (Pl.30, Figs.2,3); Rantzieniella nitida (Pl.30, Fig.4); Porochara mundula (Pl.30, Figs.5,6); Porochara westerbeckensis (Pl.33, Fig.9) and Porochara portoensis (Pl.36, Fig.7) had a fine crystal

morphology. Examination of single crystals showed them to be vertically aligned plates (Pl.30, Fig.6) in all species except Rantzieniella nitida. In Rantzieniella nitida the crystals were needle-like (Pl.30, Fig.4). No crystals showed any substructure , a feature most reminiscent of the polycrystalline columns seen in fractured Lamprothamnium calcine. On examining transverse sections of Musacchiella calcine under light microscopy a radiating fan of crystals could be seen; there was no evidence of any banding phenomenon (Pl.30, Fig.2). Feist & Grambast-Fessard (1984) considered Musacchiella to have the "Y-form" of calcine, because there was no concave banding phenomenon and the crystals were arranged in a fan. However, the absence of any detectable concave bands could be due to the loss of organic material and the retention of polycrystalline columns during diagenesis. This form of calcine could have arisen from either a Chara-like or Lamprothamnium-like calcine.

2. In the second preservational form the gyrogonite Saportonella maslovi showed concentric bands in the calcine substructure (Pl.30, Fig.8). The bands are gaps in the calcine. Bands of this sort are seen in transverse sections of Chara calcine observed by light microscopy. Similar bands can also be induced experimentally in Chara hispida and in Lamprothamnium papulosum (see Chapter 5). It is quite likely that the loss of organic material or only slight calcite recrystallisation during diagenesis could result in the preservation of a banded structure of this sort. This calcine form could have arisen from either a

Chara-like or Lamprothamnium-like calcine.

Both the above preservational forms are believed to represent only slight deviations from the original textural forms.

3. In the third preservation form seen in Gyrogona the calcine is considered to be secondary calcite. There is no fine structural detail, the crystals are typical of recrystallised calcite, being a coarse mosaic of calcitic spar (Pl.30, Fig.7).

Diagram 6.1 to show gyrogonite phylogeny (taken from Grambast 1974)

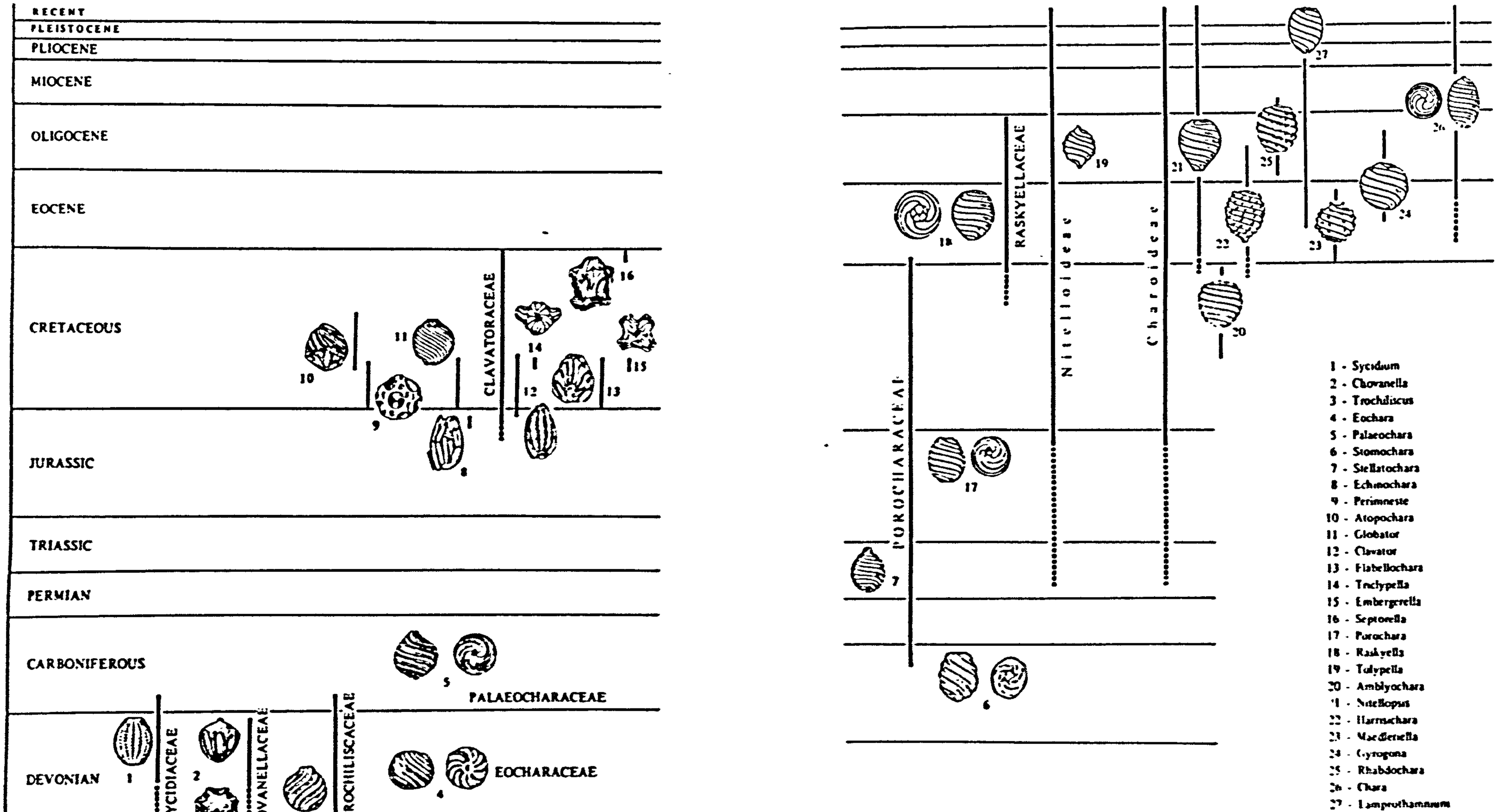

Chapter 7 - TRADITIONAL AND MODERN METHODS IN TAXONOMY, AS APPLIED TO FOSSIL CHAROPHYTES FROM THE OXFORDIAN/KIMMERIDGIAN (UPPER JURASSIC) OF SAN MARTINHO DO PORTO (PORTUGAL).

General Introduction

The charophyte oosporangium possess only a few characters useful to taxonomists. Most of these characters have been described in Chapter 6. They include such features as the structure of the apical region, the basal plate and the presence of a utricle. All of these are clearly definable and are most useful in designating higher levels of taxa. However, for lower levels of taxa, the most useful characters relate to size and shape, characters which tend to form a continuum. It is the interaction of these variable characters, and their relationship to the lower levels of taxa which are of interest in this Chapter.

The "species concept" is difficult enough to define in extant charophytes, since even here the taxonomic value of features is debatable. For example, Wood and Imahori (1965) reduced the number of extant species of Chara from 116 to 19. This concept of "macrospecies" was, however, severely criticised by Proctor (1980). He questioned the validity of using characters traditionally considered as "advanced" or "primitive".

Where morphological variation forms a continuum from one population to the next, then the problem of identifying species is largely a matter of subjectiveness on the part of the worker. The so called "lumpers" favour larger groups, fewer taxa and wider limits of variation and the so called "splitters" prefer the reverse. The matter is important and should not be at the whim of the worker.

Gyrogonites have been shown to be useful stratigraphically only when there is distinct resolution at the lower levels of taxa. For many years the value of charophytes for stratigraphy was obscured by too broad a species concept. Use of stricter limits for charophyte genera and species have shown that many had a short geological existence and therefore are of use as index fossils in non-marine beds (Grambast 1961, 1962a).

The charophytes in the Mesozoic of Portugal remain largely unstudied. Recently this shortcoming has been realised, and the first paper describing some Upper Jurassic charophytes from three Portuguese localities has been published (Grambast-Fessard & Ramalho 1985). Elsewhere, charophytes from the Mesozoic of Portugal have been documented (e.g. Wilson 1979, Wright 1985) but they remain undescribed.

Charophyte literature of the entire Jurassic remains sparce, publications include Peck (1937, 1957) Mädler (1952), Shajkin (1976), Bhatia and Mannikeri (1977), Grambast-Fessard and Ramalho (1985), Feist and Grambast-Fessard (1984), Brenner (1976) and Romaschkina (1975). Little attempt has been made in some of these papers to match species from quite separate localities, instead the

workers have opted for their own "species". This is an unsatisfactory solution because important information may be obscured.

This chapter attempts to minimise some of these problems. It is divided into two experimental subsections. Each subsection involves an approach to the problems in systematics. Fossils from a Portuguese locality, San Martinho do Porto are used in each subsection. Subsection I is a numerical taxonomic or morphometric approach to systematics. It examines the variables used in two extant species of charophyte and attempts to find a method by which the species can be separated mathematically. This information is then applied to the fossil population. Subsection II utilises the traditional approach to systematics and demonstrates the fossil taxa encountered.

Geology

The Upper Jurassic of Portugal consists of lacustrine carbonate and marginal marine shales (Wright 1985, Wilson 1979). These were deposited in the Lusitanian basin of Portugal within open shallow lakes, closed evaporitic lakes or lagoons (Wright 1985).

A summary of the Upper Jurassic stages mentioned in the text is shown in Fig. 7.3. The Upper Jurassic sequence at San Martinho do Porto is shown in the lithological log Fig. 7.4. The Pholadomya protei (Mollusca-bivalvia) beds (sensu Wilson 1979) are interpreted as open bay deposits (Wilson 1979) and were probably marginal marine in location. Wright (1985) noted that these beds contained gyrogonites which "possess 'Y' calcification structures" and stated, with reference to Feist and Grambast-Fessard (1984), that this may indicate tolerance to brackish water. However, I consider that this feature is not a satisfactory palaeoecological indicator (see Chapter 6 - calcification).

The exposure at San Martinho do Porto (Fig. 7.2) is located on the west coast of Portugal due north of Lisbon (Fig 7.1). The locality is a coastal exposure. The exact geological age is debatable, Wilson (1979) considers the section (Fig 7.4) to be Oxfordian, the end of the Oxfordian being marked by the end of the Pholadomya protei beds at about 1150m. However, Ellward (pers. comm.) considers the Pholadomya protei beds to end at 48m on the log, and so places the beginning of the Kimmeridgian lower in the

sequence.

Two horizons have been investigated for charophytes, a limestone horizon at 39m (Oxfordian) and a marl horizon at 50m (Oxfordian/Kimmeridgian). It is hoped that charophyte evidence will help to identify more accurately the boundary of the Oxfordian and the Kimmeridgian.

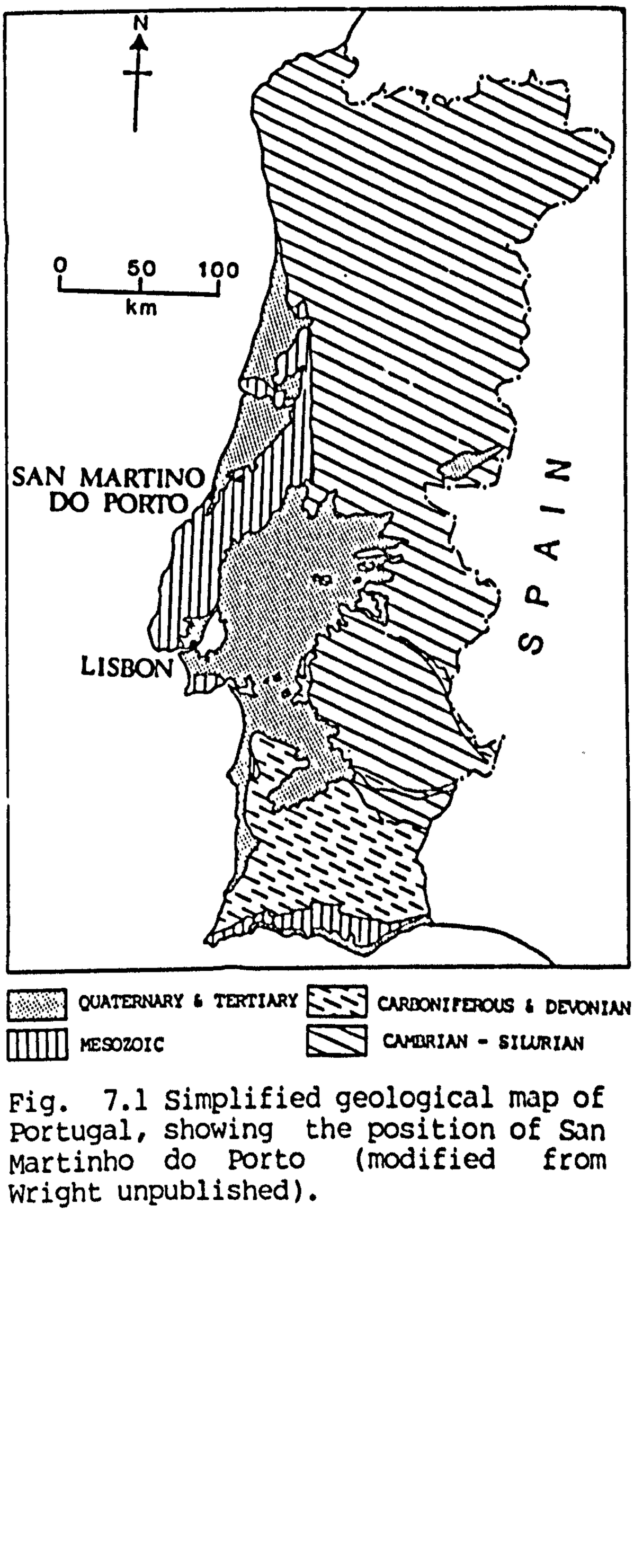

Fig. 7.1 Simplified geological map of Portugal, showing the position of San Martinho do Porto (modified from Wright unpublished).

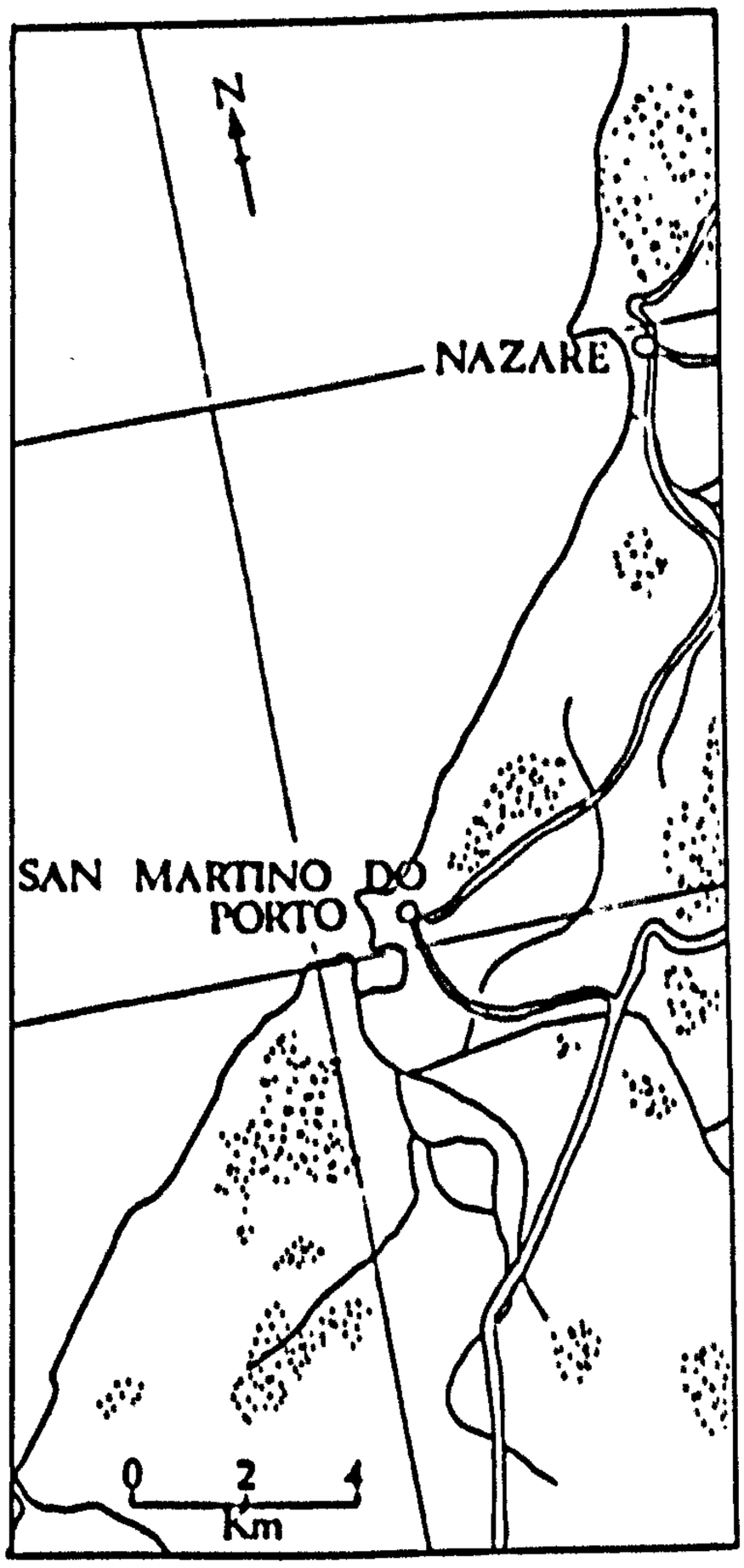

Fig. 7.2 Map showing San Martinho do Porto. Stipuled areas are land over 50m.

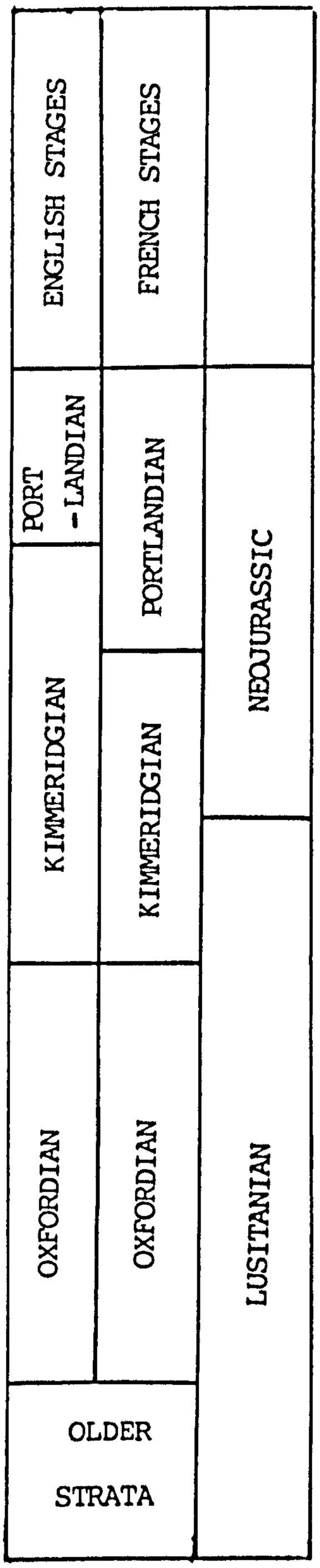

Fig. 7.3 Summary of the terminology of the Upper Jurassic of Portugal (taken from Wilson 1979)

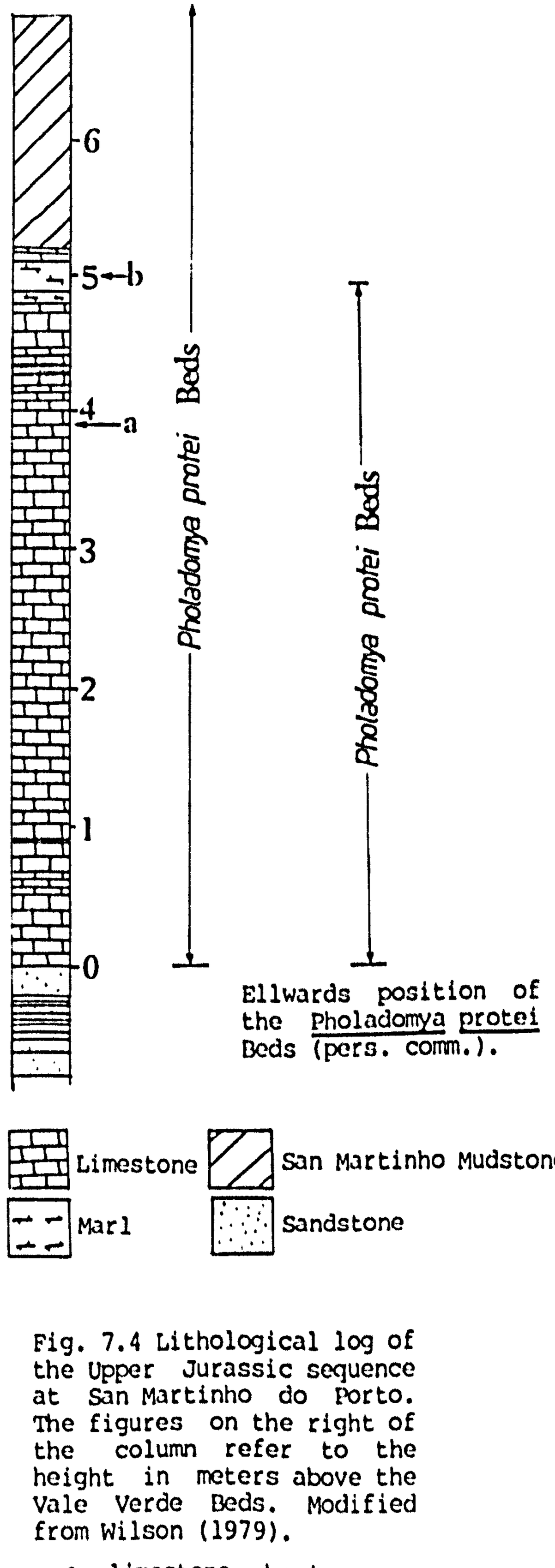

Fig. 7.4 Lithological log of the Upper Jurassic sequence at San Martinho do Porto. The figures on the right of the column refer to the height in meters above the Vale Verde Beds. Modified from Wilson (1979).

a - limestone horizon

b - marl horizon

Subsection I - A NEW APPROACH IN CHAROPHYTE SYSTEMATICS

Introduction

This subsection involves a numerical or morphometric analysis of 2 extant species of charophyte. The species used, Chara hispida and Chara delicatula, are considered distinct from each other in each of the systematic systems that have been proposed (Proctor 1980, Allen 1950, Wood & Imahori 1965, Groves & Bullock-Webster 1924). The information gained from this study will be applied to a fossil population in the hope that it will help in the systematic study of that population.

Ideally the method should delimit fossil taxa, with clear, easily defined limits. The systematic approach presented in this subsection was considered for the following reasons.

1. Size and shape can be described mathematically.

2. The characters which are regularly published can easily be used in a computer-based analysis. The characters are usually measured in accordance with the recommendations of Horn af Rantzien (1956) (see Chapter 2).

3. Modern oosporangia from unquestionably different species can be

tested in the numerical analysis to ensure accuracy of the analytical technique.

Modern oosporangia are also useful in understanding the range of variation in a measured character, so giving a clearer insight into the variability expected in fossil analogues. No work (as far as the author is aware) has been done relating gross morphology of extant oosporangia to specific systematics. This is probably because they are considered to have little diagnostic value. The neglect of extant oosporangia is surprising considering that the fossil history and fossil taxa are almost entirely based on gyrogonite morphology. Only Horn af Rantzien (1959) has gone some way to amend this shortcoming and details variation, similarities and differences in selected species from each extant genus.

One hundred gyrogonites from the limestone horizon at San Martinho do Porto were selected for morphometric analysis. These were not selected at random. The reason for this was to include all the taxa recognised using light microscopy (see Subsection II). Using a traditional approach to taxonomy it was considered that >95% were of one species (i.e. Porochara westerbeckensis - see subsection II). A random one hundred gyrogonites could exclude some of the taxa that might exist in the deposit. By entering data biased towards the existence of groups it enabled greater confidence to be placed on finding groups in the clustering techniques. The analysis was conducted with the belief that groups were present, the question was, could they be justified mathematically, and if so what were the mathematical parameters that delimited the groups? Further, if these groups could not be shown by mathematical

treatment of the data, what groups if any were present?

There are numerous programs and methods of entering data for morphometric analysis. Two methods were attempted; principal component analysis and cluster analysis.

The cluster analysis methods applied here are of a hierarchical nature. A hierarchical technique is probably best suited to taxonomic problems (Everitt 1974). This is because a hierarchical structure is assumed to exist in the data (e.g. specimens are in species and genera). In each method a similarity matrix, which compares each individual specimen with the next, is first generated. This information is then used to construct a dendrogram which involves the successive lumping of individuals into groups and then small groups are clustered into larger groups at different hierarchical levels. It is the formation of the dendrogram and the construction of the similarity matrix which varies between methods.

Three hierarchical methods of clustering were attempted; single link , average link and centroid cluster analyses. Single link cluster analysis (described by Sneath 1957 and Johnson 1967) forms clusters by fusing individuals which have the closest calculated similarity. The technique then finds the smallest distance between this cluster and the next individual and produces a larger cluster. (The distance between individuals, as calculated in the similarity matrix, is more properly termed the Euclidean distance).

Centroid cluster analysis (described by Sokal and Michener 1958) forms clusters by fusing the two closest individuals. Their data

is then averaged and the group average, the centroid, is treated as an individual. The next two closest individuals are fused and so on.

Average link cluster analysis (described by Lance and Williams 1966) calculates the Euclidean distance between one group (ie. > 1 individual) and another group by averaging the distance between all individuals in the two groups. The groups with the smallest averaged Euclidean distance are then fused together.

In all clustering methods the similarity matrix can be generated in a number of ways. Here the similarity matrix was constructed using the quantitative linear method. The method calculates the Euclidean distance between each pair of individuals and compiles the distance into the similarity matrix. The Euclidean distance between each pair of individuals is calculated utilising all the characters recorded. In each character the real data of each pair of individuals is directly compared. This is achieved by finding the ratio of the difference between the maximum and the minimum possible value with the actual difference of the values. The ratios derived by comparing the values of each character in this way are then summed to give the Euclidean distance between two individuals.

For further details of the techniques used in cluster analysis the reader is referred to Everitt (1974).

Individuals can also be clustered using principal component analysis. This method finds a set of computed variables (the

principal components) from the original data. The original data in this case involves eight variables. If it were possible, these would be plotted in eight dimensions, giving a multivariate data cloud. As this is not possible an analytical method has been devised which selects new variables, the principal components, which it is hoped, will express the data in far fewer variables (ie <8 in this case) without any significant loss of information. The analytical method finds an axis through the multivariate data cloud such that variance is maximised along it. This is the first principal component, the origin of which is at the centroid of the multivariate data. The second principal component maximises variance at a right angle to the first axis. The third, fourth ....nth principal components (where n = 8 in this case) are computed in the same way. The principal components are completely independent being uncorrelated with each other. They are linear combinations of the old variables and retain as much of the original information as possible. Results are presented graphically. Here only the first principal component is shown against the second, but any combination of components is possible.

Both standardised and non-standardised data was used in the principal component analysis. Standardisation was carried out using a computer program (see Appendix Ia), such that all data showed unit variance and a mean of zero. This enabled data with different or no units to be compared. The mathematical modelling involved in principal component analysis is beyond the scope of this work, the interested reader is referred to Davies (1971).

The computer programs necessary for this work are shown in Appendix I (a,b).

Results

The oosporangia of Chara delicatula (Pl.26, Figs. 7-9) and Chara hispida (Pl.26, Figs. 3-6) are morphologically distinct. Individuals can be identified by careful scrutiny under a binocular microscope. Some of the variations between individuals of Chara hispida are shown in Pl.26, Figs. 3-6.

All the characters measured were plotted as histograms (Fig. 7.5a-g). In both species, each character appeared to display normal distribution. This distribution was not however statistically tested for normality since the unpaired t-test which was applied to the data is robust enough to give satisfactory results even when there is some deviation from normality (Rayner pers.comm.). The t-test values for each character measured show that the two species have statistically distinct means ($p << 0.001$). However, many individual oosporangia share intermediary values and for these individuals univariate analysis of this sort is unsatisfactory in delimiting taxa. In such cases in order to assign the individual to a species more than one character has to be considered. The simultaneous examination of many characters is multivariate analysis and this can only be satisfactorily calculated using computer programs.

Single link cluster analysis was tested on 25 individual oosporangia of each species of Chara. The input data LPA, LED, AND, WS, NC, AP, BP, NR (see Materials and Methods section "Measurements" for the

definition of these terms) for Chara delicatula and Chara hispida is shown in Appendix II. The resulting clusters are demonstrated in the dendrogram (Fig. 7.6). They show inadequate species separation. Individuals of both species are shown clustered together (Fig.7.6 cluster A level 90).

Alteration of the input data improved the clusters generated by single-link cluster analysis. The linear measurement LED and AND were replaced by the ratios ISI and ANI. The two new parameters and the length (LED), together, mathematically describe the size and shape of the oosporangium profile (see Chapter 2). Employing ratios of original data is widespread in multivariate analysis of biological material (Minkoff 1965, Gipson et al. 1974, Moulton 1973). However, Atchley et al. (1976) warn that compounding continuous variables of this sort into ratios can lead to false correlations in the data (i.e. ISI and ANI might not be size independent). In this case, using ratios considerably improves the data output (Fig. 7.7). Cluster A' (level 90) is wholly that of Chara delicatula (excepting specimen 45), the remaining individuals being Chara hispida (excepting specimen 2). The analytical method is improved using ratios rather than raw data.

Complete separation of Chara delicatula using single-link cluster analysis was achieved using the ratios ISI, ANI and log transformation of the length variables WS, LPA, AP, BP (Fig. 7.8). Log transformations are often the best way to represent variables that change with size as these variables are often related logarithmically. Log-log plots were first used systematically by Huxley (1924, 1932) who found the method useful to describe changes

in proportions that occur with changes in absolute magnitude of the total organism. The study of size and its consequences is termed allometry (for more detailed insight into allometry the interested reader is referred to Gould 1966).

The clusters generated using log transformations and ratios is shown in the dendrogram Fig. 7.8. At level 85 (Fig. 7.8), cluster A'' is Chara delicatula and represents all individuals of that species and cluster B is Chara hispida. However, four specimens (Nos. 37, 35, 34 and 32) of Chara hispida fall outside cluster B and are not clustered together until the hierarchical level of 80 which contains the total number of individuals. The technique has therefore adequately clustered the group Chara delicatula but has inadequately clustered the group Chara hispida.

Hitherto, results have been obtained using single-link cluster analysis. This method proved most satisfactory when data was presented in the form of ratios and log transformations (Fig 7.8). For this reason data was presented in this form whilst the clustering method was altered.

Experimentation showed that average-link cluster analysis was ideally suited to clustering the two species Chara hispida and Chara delicatula into two easily defined clusters (Fig. 7.9 - clusters A''',B). At level 65 (Fig 7.9), two clusters are present, cluster A''' containing Chara delicatula and cluster B containing Chara hispida.

Average link cluster analysis with the input data modified into

ratios and log transformations (logLPA, logWS, logAP, logBP, ISI ANI NC NR) was able to discriminate between the two extant species. This technique was considered to be ideally suited to analyse fossiliferous material. The data from 100 gyrogonites (Appendix II) from the Upper Jurassic of Portugal (limestone horizon) was analysed in this way.

In the first method attempted the clusters produced (Fig. 7.10) were carefully examined and compared with the original specimens. However, the mathematical separation into clusters proved only partially satisfactory. Some groups, particularly groups D and E (level 75, Fig. 7.10) could not be justified by traditional microscopical methods. The remaining groups could be broken down essentially into groups A and B which contain the microscopically identified species Porochara westerbeckensis and Musacchiella palmeri (see Subsection II) and group C which contains Porochara obovata (see Subsection II).

Changing the form of the data input and/or the clustering method in any way produces a bewildering variation in the clusters produced. The second method attempted (Fig. 7.11) represents one such example. Here the clustering method remains the same as in Fig. 7.10 (i.e. average-link cluster analysis) but the data was entered unmodified (LPA, AND, LED, WS, NC, AP, BP, NR). This results in new clusters. A few examples illustrate this:

1. Specimens 1 and 2 (closed circles, Figs. 7.10, 7.11) which were clustered together in the first method (Fig. 7.10) and became widely separate in the second method (Fig. 7.11) and did not

cluster until all specimens were grouped together at level 65. They therefore moved from being very similar to very dissimilar.

2. Two specimens (Nos. 7 and 67, (open circles, Figs. 7.10, 7.11)) are clustered together at level 95 in the first method (Fig. 7.10). Therefore, this technique considers the two specimens as being similar. Using traditional microscopical techniques (see Subsection II) the two specimens are, however, considered as different (i.e. specimen 7 represents Musacchiella palmeri and 67 represents Porochara westerbeckensis). Modification of the data input (Fig. 7.11) produced clusters which widely separated specimens 7 and 67, and they only cluster at level 75.

3. Five specimens (Nos. 8, 12, 14, 20, 22, (stars, Figs.7.10, 7.11)) are considered by traditional microscopical means to represent Musacchiella palmeri (see Subsection II). In the dendrogram (Fig. 7.10), they are clustered together at level 95. However, in the dendrogram (Fig. 7.11) none of the individuals are grouped together above level 90 and they only all become grouped at level 75.

On the basis of the five specimens of Musacchiella palmeri the first method (Fig. 7.10) represents the most satisfactory analytical technique. However, using specimens 67 and 7 as markers the second method (Fig. 7.11) is the most satisfactory. No technique clustered specimens 3, 4 and 5 (dashed line, Figs. 10,11) together - specimens that are believed to represent Musacchiella

douzensis (see Subsection II).

The dendrogram (Fig. 7.10) presents the clusters generated using the same method as that which proved most successful in clustering Chara delicatula and Chara hispida and so was given greatest consideration. The method produces two clusters at level 65, five clusters at level 75 and eleven clusters at level 85. It would be expected that at any of these levels clusters representing the natural groupings which could be designated genera or species would be found. However with no confidence in the analytical method these groupings could not confidently be considered as representative of taxa.

Principal component analysis provedto be no more satisfactory than cluster analysis in demonstrating natural groupings in the fossil population. Using standardised data (s.d.=1, x=0) the technique could delimit, although not clearly, the two extant species Chara delicatula (group A, Fig. 7.12) and Chara hispida (group B, Fig. 7.12). However, it could not delimit any recognisable groups in the fossiliferous material (Fig 7.13). This could be for a number of reasons.

1. The technique could not find any groups because there were none.

2. The technique is not discriminatory enough to detect natural groupings.

3. There is significant overlap in the characters of each group

that clusters are obscured.

4. There are so many natural groupings that, with this sample size, they are being missed.

5. The measurements are inadequate.

6. The material is eroded and/or damaged making exact measurements difficult.

7. Important features have been lost in fossilisation.

Fig. 7.5 DISTRIBUTION OF VARIABLES IN TWO SPECIES OF CHARA

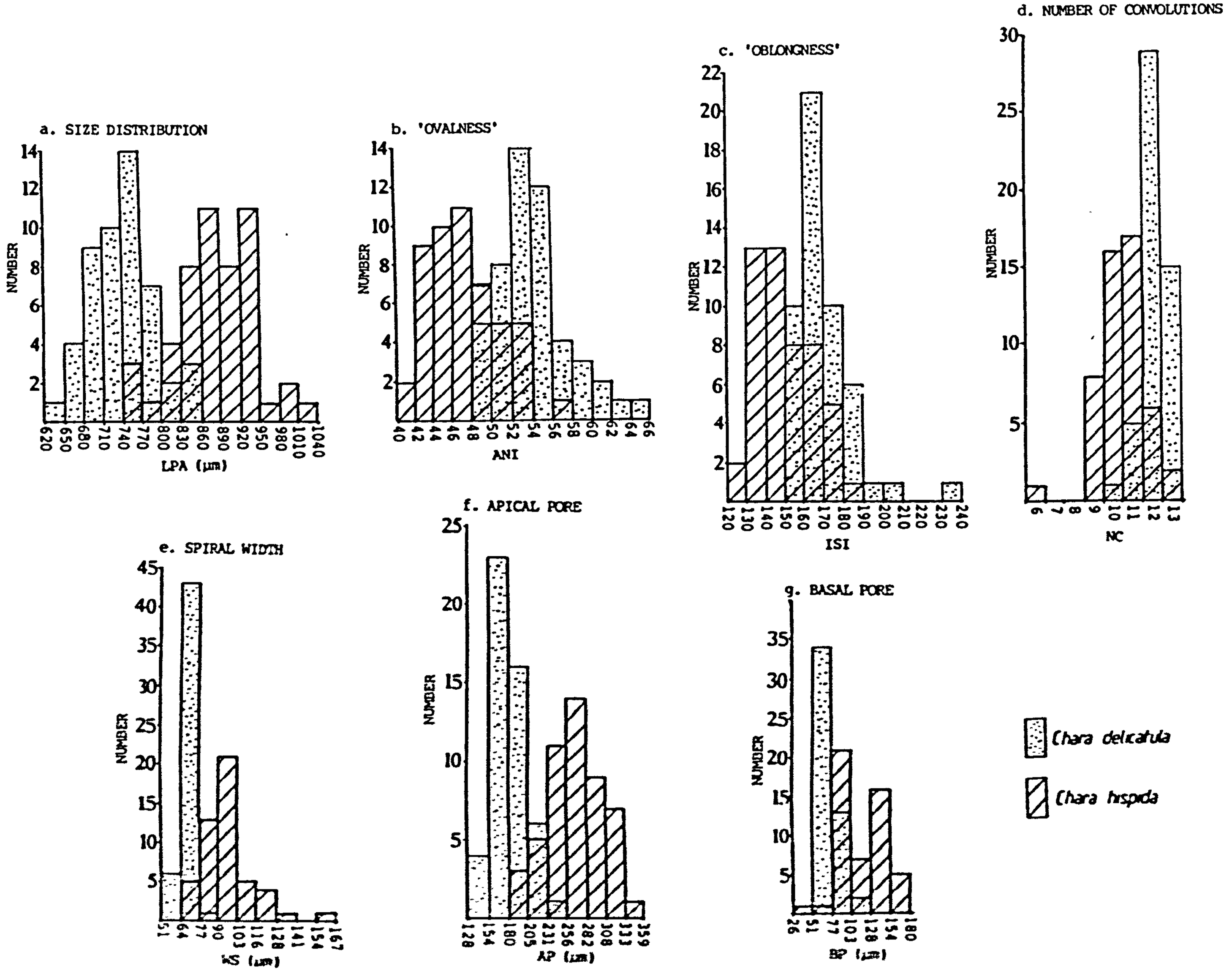

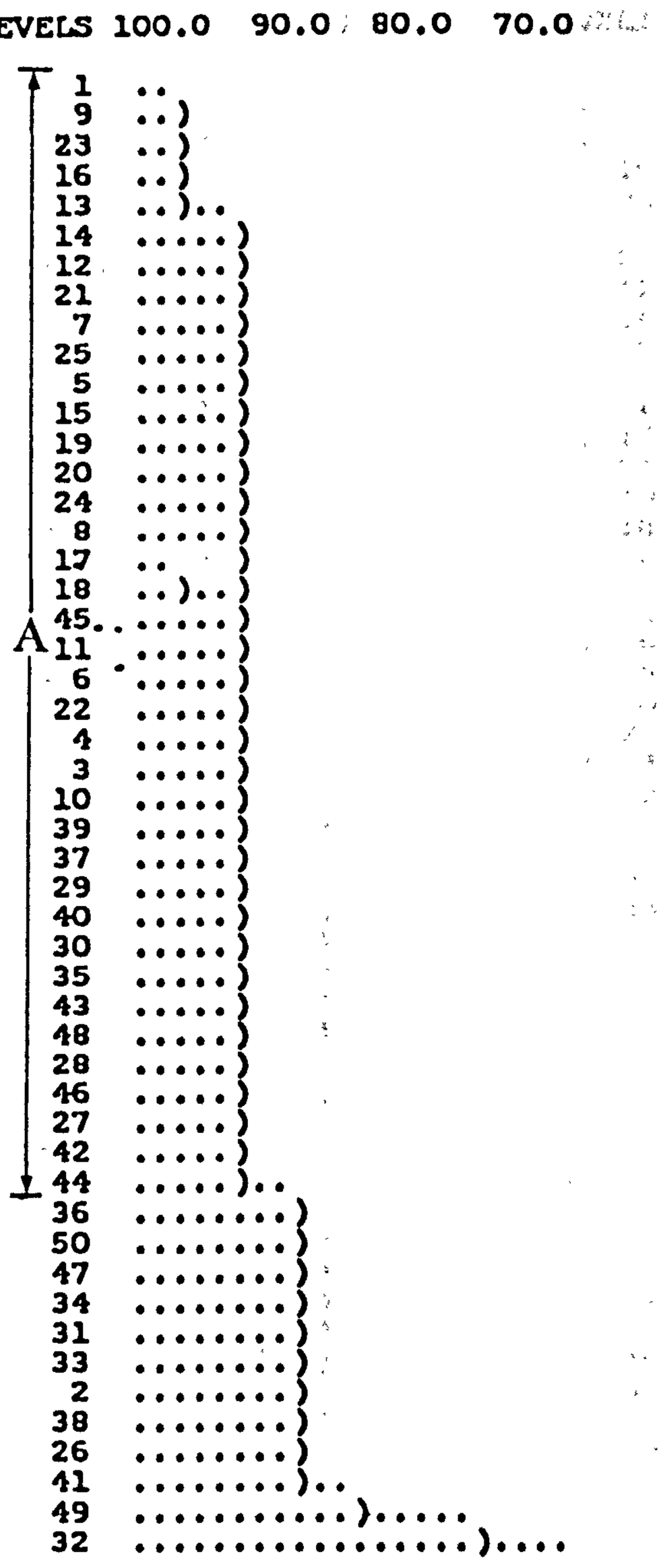

Fig. 7.6 Single link cluster analysis, using the input data, LPA, LED, AND, WS, NC, AP, BP, NR. The letter designating the cluster is described in the text.

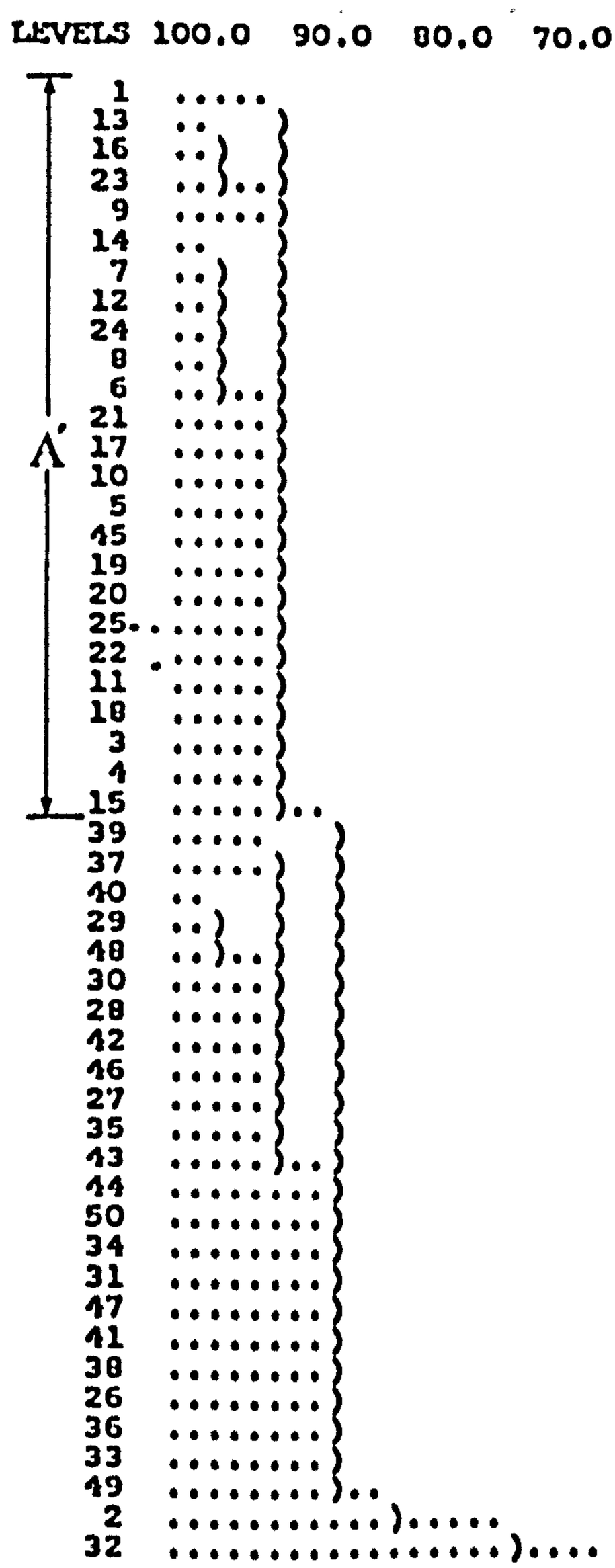

Fig. 7.7 Single link cluster analysis, using the input data, LPA, ISI, ANI, WS, NC, AP, BP, NR. The letter designating the cluster is described in the text.

Numbers 1-25 Chara delicatula Agardh
26-50 Chara hispida L.

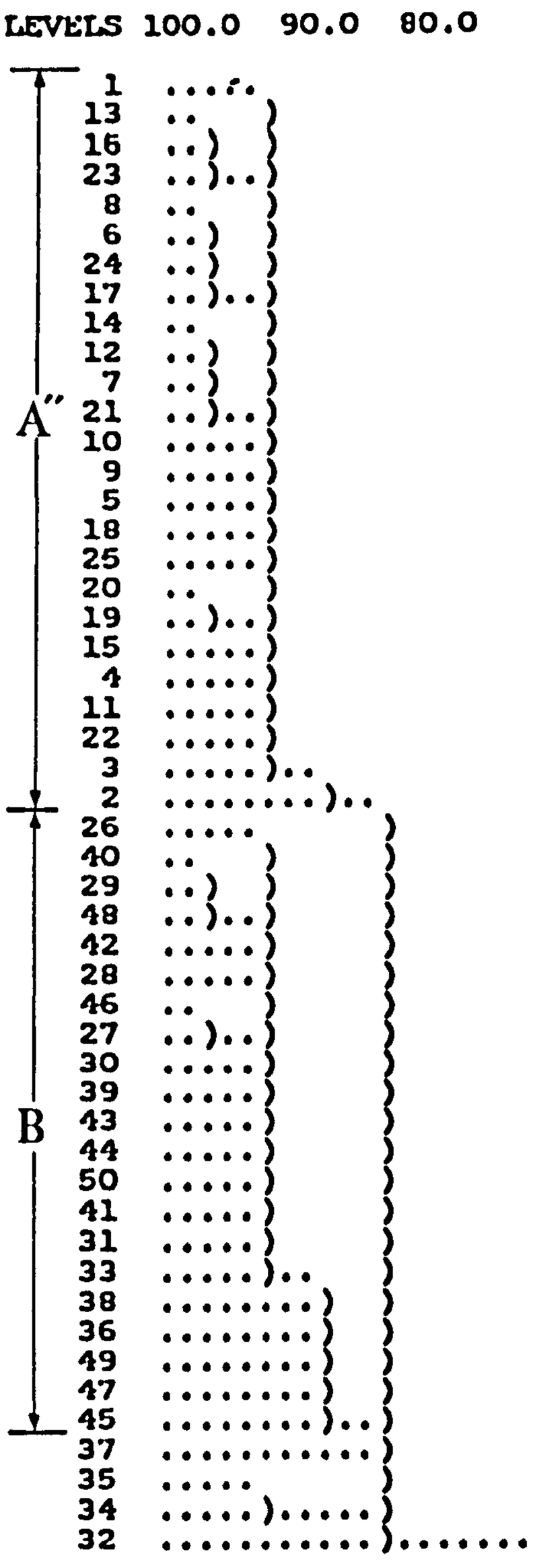

Fig. 7.8 Single link cluster analysis, using the input data logLPA, ISI, ANI, logWS, NC, logAP, logBP, NR. The letter designating the cluster is described in the text.

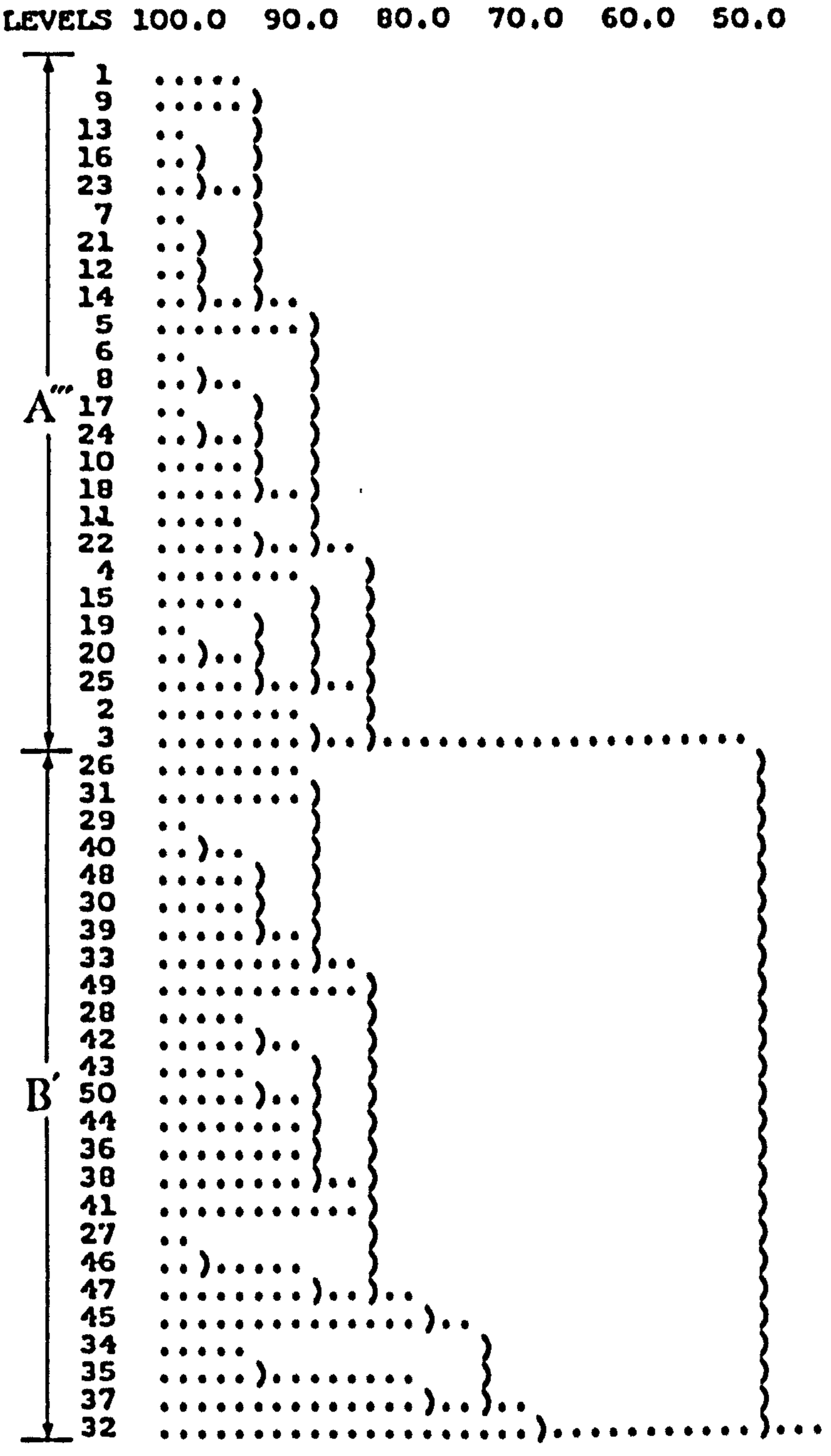

Fig. 7.9 Average link cluster analysis, using the input data logLPA, ISI, ANI, logWS, NC,logAP, logBP, NR. Letters designating clusters are described in the text.

Numbers 1-25 Chara delicatula Agardh
26-50 Chara hispida L.

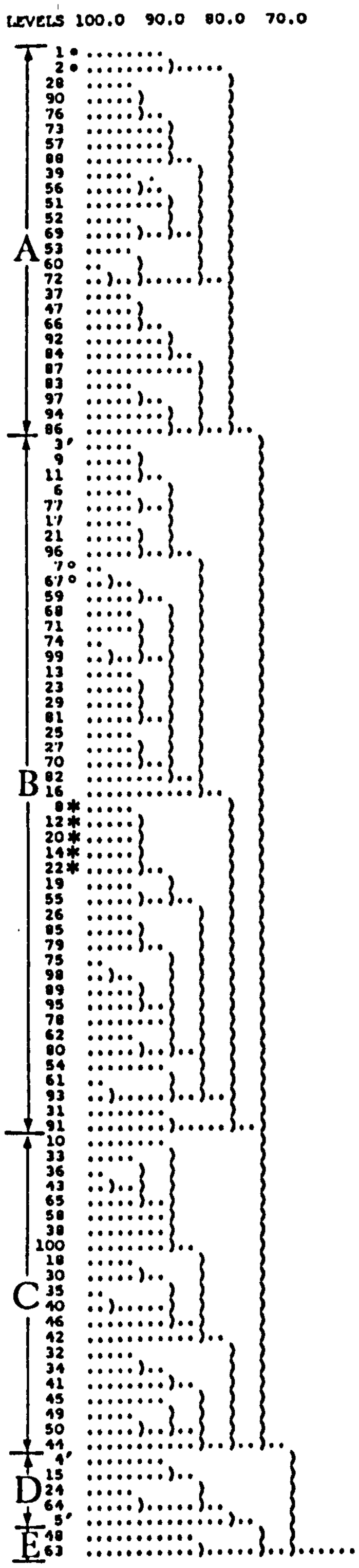

Fig. 7.10 Average link cluster analysis, using the data input logLPA, ISI, ANI, logWS, NC, logAP, logBP, NR. Letters designating clusters are described in the text. Numbers 1-100 are gyrogonites from the Upper Jurassic of Portugal (Limestone Horizon). Symbols against gyrogonites represent individuals mentioned in the text.

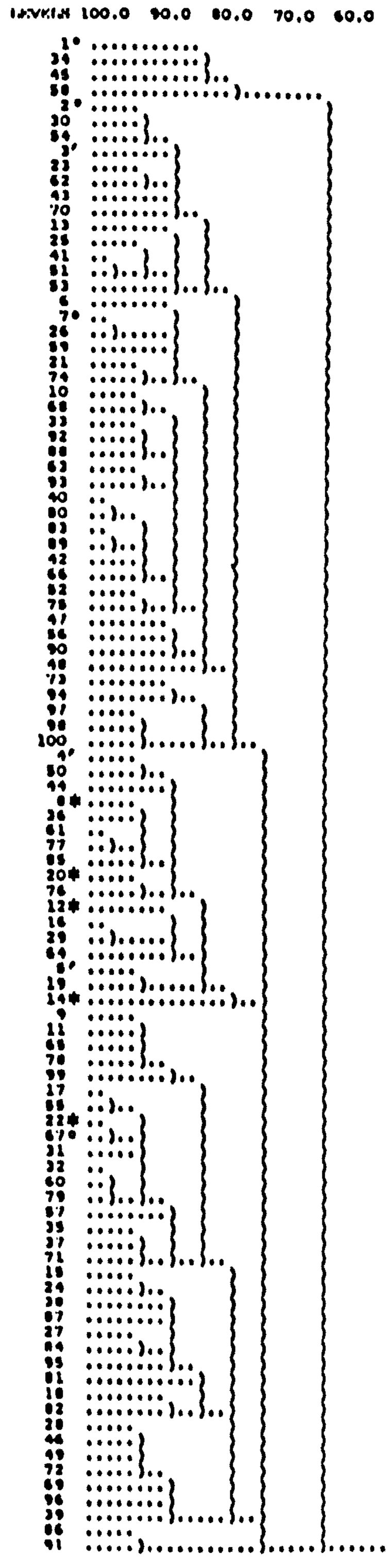

Fig. 7.11 Average link cluster analysis, using the input data LPA, LED, AND, WS, NC, AP, BP, NR. Letters designating clusters are described in the text. Numbers 1-100 are gyrogonites from the Upper Jurassic of Portugal (Limestone Horizon). Symbols against gyrogonites represent individuals mentioned in the text.

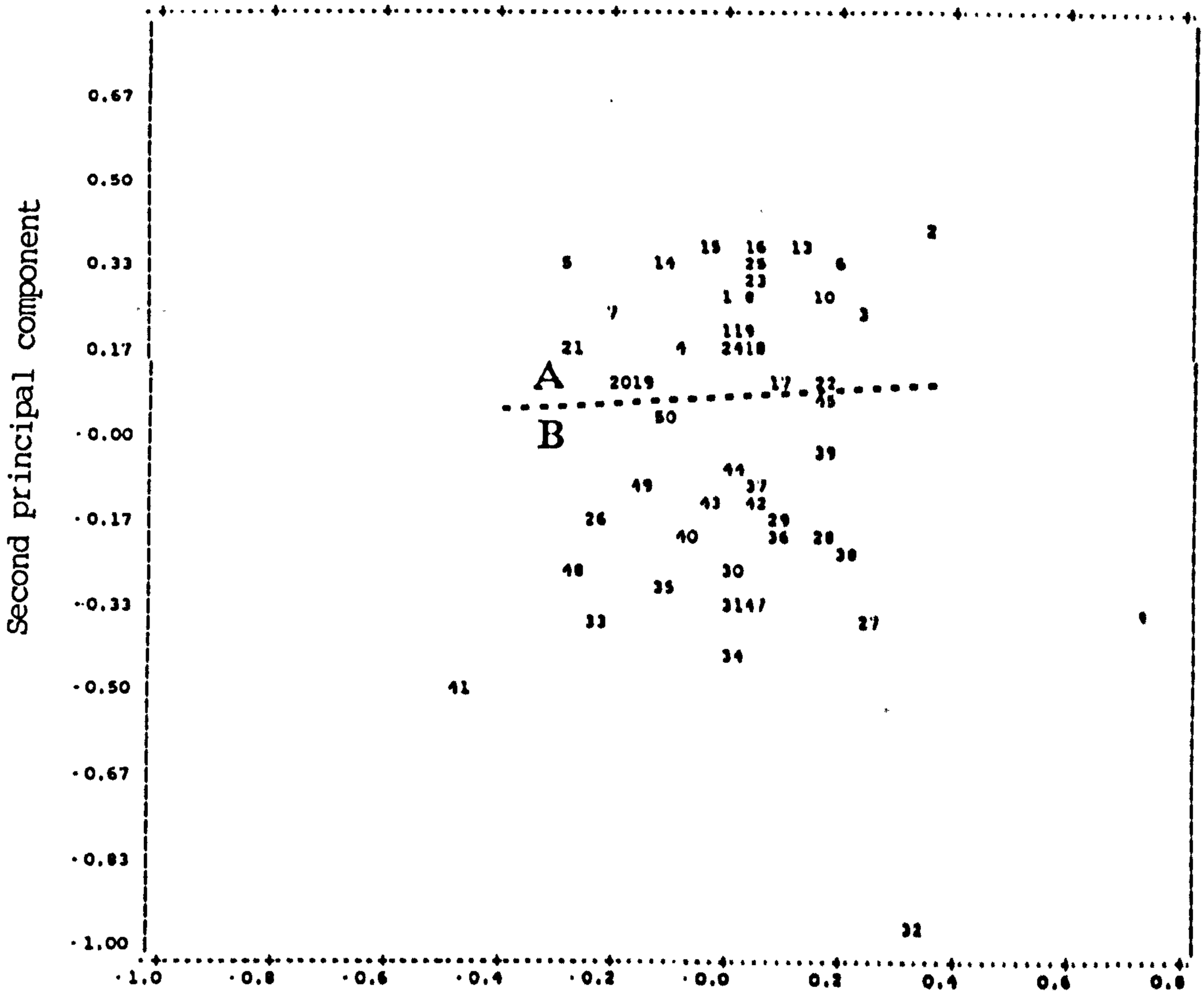

Fig. 7.12 Principal component analysis using the standardised input data LPA, LED, AND, WS, NC, AP, BP, NR. Group A (above the doted line) contains individuals of Chara delicatula and group B (below the dotted line contains individuals of Chara hispida.

Numbers 1-25 Chara delicatula Agardh
26-50 Chara hispida L.

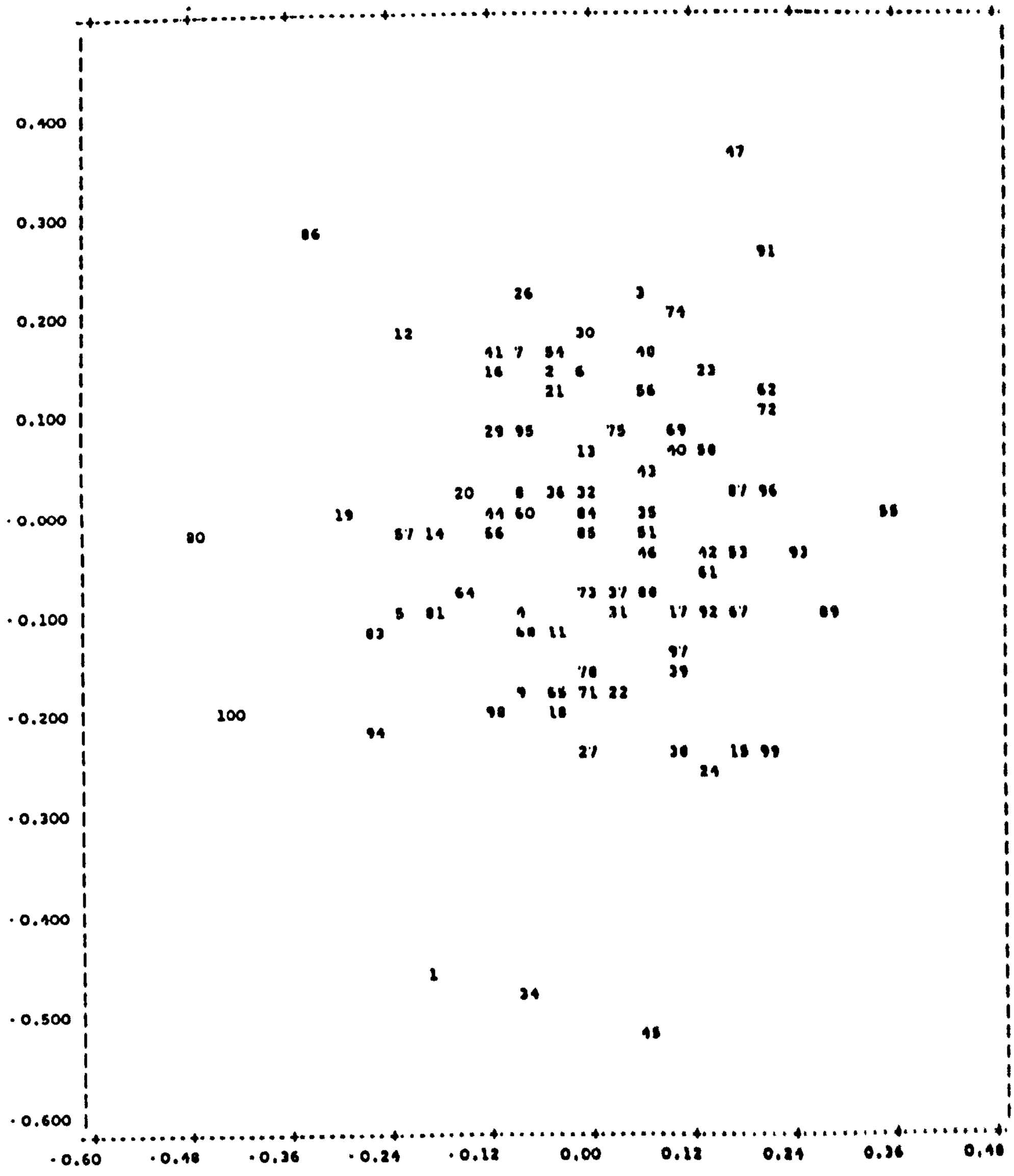

Fig. 7.13 Principal component analysis using the standardised input data LPA, LED, AND, WS, NC, AP, BP, NR. Numbers 1-100 are gyrogonites from the Upper Jurassic of Portugal (Limestone Horizon).

Discussion

All the values plotted (LPA,ISI,ANI,WS,WR,AP,BP) show distributions which approximate to normality. In each character recorded for Chara hispida and Chara delicatula the differences in their means (as indicated by t-tests) were highly significant ($p << 0.001$) and each character in each species showed quite a large degree of variability (e.g. Chara hispida LPA ranged from 740-1046µm, n=50). Variability of this sort must be borne in mind whenever a systematic survey of living or fossil groups is carried out. Within palaeobotanical literature, graphs depicting the size distribution of a measured character for a new species occur regularly (eg Horn af Rantzien 1954, Peck 1957, Grambast & Gutierrez 1977, Feist-Castel 1977 and many others), but not universally (e.g. Feist & Grambast-Fessard 1984). However, as far as the author is aware there are no published graphs showing the size distribution of variables in extant species. Plotting size distribution is considered to be very useful in determining the value of a measured character for taxonomic purposes. For instance, a bimodal plot might well indicate two distinct populations.

Very little useful information was obtained from the computer analysis. Program quality was improved for the extant species when the data was entered as logarithms. This suggests that the variables are related logarithmically as is predicted by allometric studies (see Gould 1966). However, no variables were plotted together to prove this.

The technique of numerical taxonomy as a means to identify natural groupings or taxa in this fossil population is therefore rejected for the present. Numerous alternative approaches to the problem have not been pursued, approaches which would perhaps refine the quality of the clusters produced. If work is to continue, it is recommended that the main thrust should proceed by finding an analytical technique which could discriminate between a large and variable number of extant species (i.e. more than the two presented here). This work is not however recommended for the following reasons:-

1. The computer clusters once generated must be directly compared with the original specimens. Only if the comparison is considered satisfactory by the worker can the clusters be trusted (i.e. the clusters are not an end in themselves).

2. Unless there are rigorous safeguards, the decision that the computer cluster is "real" is subjective; it is as subjective as examining a specimen by traditional means and assigning it to a certain taxon.

3. With the complexity of computer analysis comes a less than precise understanding of what the data output represents.

4. The returns on time and effort are not considered adequate.

Computer analysis has been rejected in favour of the traditional methods (see Subsection II).

Subsection II - A TRADITIONAL APPROACH TO CHAROPHYTE SYSTEMATICS

Introduction

The approach to taxonomy attempted here is, I am sure, the approach that many taxonomists have used from the beginning and hence the subsection title " A Traditional Approach". It initially involves studying the population as a whole and clustering it into groups by eye. Then the variability of form and extreme types within each group are assessed. Finally, detailed measurements of individuals in each group are made and these are compared with those for published taxa. An insight into the variability of the measured characters of Chara hispida and Chara delicatula proved invaluable in assessing the taxonomic merits of fossil groups (see subsection I). The taxa identified from the marl horizon and the limestone horizon are presented in the results of this subsection.

Results and Systematics

Amongst the gyrogonites from the marl horizon there were only a few individuals with compression artifacts. About 50% of the gyrogonites from the limestone horizon showed signs of compression, although only a few were seriously deformed. Gyrogonites from the marl horizon were dark brown, those from the limestone horizon were white and had the most easily isolated calcine. The gyrogonites are stored at Bristol University (Botany Department). The symbols designating the collections are: CB+number = collection box number

SB+number = S.E.M. stub number

MS+number = microscope slide number

Order Charales

Family Porocharaceae Grambast (1962b)

Subfamily Porocharoideae Grambast (1961)

Genus **Musacchiella** Feist and Grambast-Fessard (1984)

Type sp Musacchiella douzensis Feist and Grambast-Fessard (1984)

Musacchiella douzensis Feist and Grambast-Fessard (1984)

Plates: Pl.31, Figs. 1-7; Pl.29, Fig.3

Collection: CB1; MS11(9)

Material: 3 specimens

Horizons and Locality: Limestone horizon from the Oxfordian, Upper Jurassic, San Martinho do Porto, Portugal.

Description

	spec.1	spec.2	spec.3	mean	Type-material Feist & G-Fessard (1984) n = 300
LPA(µm)	672	705	744	707	625 - 975
LED(µm)	576	590	744	707	500 - 550
AND(µm)	288	372	436	365	
ISI	117	119	126	121	110 - 140
ANI	43	53	59	52	~50
WS(µm)	84	77	90	84	
NC	10	9	9	9	10 - 13
AP(µm)	48	77	64	63	
BP(µm)	24	51	26	34	
NR	3.25	3	3.5	3.25	

The gyrogonites are subprolate and ellipsoidal (or subovoidal) (Pl.31, Fig.1). A segmented (bipartite) basal plate is visible on external inspection and it occurs in a shallow pit bordered by the truncation of the spirals (Pl.31, Figs.3,4). One segment of the basal plate is pentagonal and the other is rectangular (Pl.29, Fig.3). The apical pore is small and tightly enclosed by the rounded apex of the spirals (Pl.31, Fig.2). The calcine structure is of the "Y-form" as seen in thin section under light microscopy (Pl.31, Fig.6).

Remarks

All the specimens found had concave spirals (Pl.31, Figs. 1-5). This conforms with the type material that is described as being "frequently concave" (Feist & Grambast-Fessard 1984). The calcine appeared cracked and blocky from the outside (Pl.31, Figs.5,7); however, the calcine substructure is clearly definable as the "Y-form" with the crystals radiating in a fan. This probably represents primary or slightly altered primary calcification (see

Chapter 6-calcine). The genus Musacchiella was erected on the basis of a segmented basal plate. The basal plate of specimens 2 and 3 was obscured by calcitic debris, strictly speaking therefore, in the absence of a basal plate, these specimens should not be included in Musacchiella. However, they are included on the basis of their size and shape.

All the features described for these three specimens conform with the type-material except for the size of the LED (i.e. largest LED for the San Martinho do Porto population is 590µm and for the type-material is 550µm). This small discrepancy is ignored because of the inconsistencies that exist in the published data for the values of LPA, LED and their ISI ratio (see diagnosis above). None of the specimens had an apical pore with a "rose outline" as has been described in a few specimens of the type-material (Feist & Grambast-Fessard 1984).

Comparisons

Musacchiella differs from Porochara in the basal plate characteristics. Musacchiella douzensis closely resembles the following species; Porochara rotunda, Porochara raoi, Musacchiella maxima and Musacchiella palmeri.

Porochara rotunda from the Middle Jurassic of the USA is smaller and has fewer spiral convolutions than Musacchiella douzensis. Its basal plate has not been described.

Porochara raoi from the Callovian of India is smaller over all than Musacchiella douzensis and has an undivided basal plate.

Musacchiella maxima from the Berriasian (Purbeckian) of Cala d'Inferno (N.W Sardinia) differs from Musacchiella douzensis in being wider (i.e. larger LED) (Colin et al. 1985).

Musacchiella palmeri is smaller and more rounded than Musacchiella douzensis. The form of the segmented basal plate is different; Musacchiella palmeri has a hemispherical segment, whereas Musacchiella douzensis has a pentagonal segment.

Occurrence

Musacchiella douzensis was only previously known from the Bathonian (Middle Jurassic) of France (Feist & Grambast-Fessard 1984).

Musacchiella palmeri Feist & Grambast-Fessard (1984)

Plates:	Pl.32, Figs.1-9; Pl.30, Figs.2,3; Pl.29, Fig.2
Collections:	SB 8 (Cl).1; CB 2; MS 11(10)
Material:	24 specimens
Horizon and Locality:	Limestone horizon from the Oxfordian, Upper Jurassic, San Martinho do Porto, Portugal

Description

	M.palmeri San Martinho do Porto n = 24		Type-material Feist & Grambast -Fessard (1984) n ~ 250
	mean	range	range
LPA(µm)	617	538 - 679	275-650
LED(µm)	521	436 - 590	250-500
AND(µm)	308	256 - 359	
ISI	119	112 - 133	108-136
ANI	50	44 - 59	Ellipsoidal
WS(µm)	75	64 - 103	
NC	8	7 - 10	6-10
AP(µm)	90	64 - 103	
BP(µm)	48	26 - 64	
NR	3.4	3 - 4.5	

The gyrogonites are prolate spheroidal to subprolate and ellipsoidal (Pl.32, Figs.1,2). The basal plate is segmented and visible only on internal inspection. There are two segments, one hemispherical and one rectangular (Pl.29, Fig.2). The spirals are concave (Pl.32, Figs.2,8) to convex (Pl.32, Figs.1,9). The apex is truncate (Pl.32, Figs.1,2). The apical pore is round (Pl.32, Fig.5) or deeply lobed stellate (Pl.32, Fig.4). The calcine substructure is of the "Y-form" as seen in transverse fracture under S.E.M. (Pl.30, Fig.3) and in thin section under light microscopy (Pl.30, Fig.2).

Remarks

The apical pore appears deeply lobed and is here termed stellate (Pl.29, Fig.2). Gyrogonites with a stellate apical pore have an apical pore that is intermediate in character between the "rosette form" as described in Rantzieniella nitida and the "cogwheel form" seen in the germinated summit of the family Characeae (see Chapter 6-apical construction).

The basal plate is only visible on internal inspection. Externally it is obscured by the basal ends of the spirals and by contamination with calcite debris. Two specimens were shown to have a segmented basal plate. Others were examined but fractured badly and no basal plate could be isolated. The internal surface of the gyrogonite was usually contaminated by the internal sparry calcite cast. The genus Musacchiella was erected on the presence of a segmented basal plate. Specimens which have an obscured basal plate are nevertheless included in the species when shape and size conform with individuals known to possess a segmented basal plate.

The population described here has slightly larger representatives than the population described by Feist and Grambast-Fessard (1984) (see description above).

All specimens were well preserved.

Comparisons

Musacchiella palmeri resembles the following species; Musacchiella douzensis, Musacchiella sardiniae, Porochara sahnii, Porochara raoi and Porochara sublaevis

Musacchiella palmeri differs from Musacchiella douzensis in having a more rounded shape and in having a hemispherical rather than a pentagonal segment in the basal plate.

Porochara sublaevis from the Middle Jurassic of Montana USA is similar to Musacchiella palmeri but the basal plate remains

undescribed.

Porochara sahnii and Porochara raoi from Jaisalmer formation (Callovian-Oxfordian) of Western India are similar to Musacchiella palmeri, but both have a higher number of convolutions in lateral view and there is no mention of the basal plate. The apical morphology of both these species of Porochara is more or less rounded hexagonal.

Musacchiella sardiniae from the Berriasian (Purbeckian) of Cala d'Inferno (N.W. Sardinia) has a more rounded and extended apex in lateral view than Musacchiella palmeri; otherwise its size and shape are very similar.

Occurrence

Musacchiella palmeri was previously only known from the Bathonian (Middle Jurassic) of Oxford (England).

Genus **Porochara** Mädler (1955)

Type sp. **Porochara kimmeridgensis** (Mädler)

Porochara westerbeckensis (Mädler)

Aclistochara westerbeckensis Mädler (1952)

Plates: Pl.33, Figs.1-9, Pl.29, Fig.4

Collection: CB 3; SB 20(19,23,26,27,30); MS 11(3,4)

Material: About 300 specimens

Horizon and Locality: Limestone horizon from the Oxfordian, Upper Jurassic, San Martinho do Porto, Portual.

Description

	San Martinho do Porto		Type-material Mädler (1955)
	n = 75		n = 27
	range	mean	range
LPA(µm)	410 - 759	547	570 - 730
LED(µm)	359 - 590	468	460 - 670
ISI	100 - 143	117	
ANI	37 - 55	49	
WS(µm)	51 - 116	69	
NC	6 - 10	8	9 - 10
AP(µm)	51 - 154	108	100 - 140
BP(µm)	27 - 77	44	40 - 70

The gyrogonites are prolate spheroidal to prolate and ellipsoidal (a few specimens are subovoidal)(Pl.33, Figs.1-2). They are of medium size. The summit can be slightly elongated into a short stout neck or it can be truncated (Pl.33, Figs.1,2). The base is usually rounded (rarely truncated). The apical pore is more or less rounded or rounded pentagonal (Pl.33, Figs.3,4), of mean diameter 108µm. The basal plate is single and pentagonal (Pl.29, Fig.4). It is usually highly eroded, altered by diagenesis or obscured by mineral deposits on its outer surface. The internal surface of the

gyrogonite is difficult to isolate, seldom being free from contamination and often fracturing poorly. The spirals are concave or convex. The calcine substructure is of the "Y-form" as seen in transverse fracture under S.E.M. (Pl.33, Fig.9)

Remarks and Comparisons

This is the most abundant species in the limestone horizon. It is a quite variable species which closely resembles the following species; Porochara raoi, Porochara mundula, Porochara sublaevis, Porochara minsinae and Porochara kimmeridgensis. The characters of these species are shown below.

	P. raoi Bhatia & Mann -ikeri(1977)		P. mundula Peck(1941, 1957)		P. sublaevis Peck (1957)		P. minsinae Shajkin (1976)	P.kimm'gensis Mádler (1952)
	n = 7		n = 200		n = 8			n = 126
	range	mean	range	mean	range	mean	range	range
LPA(µm)	520-600	553	320-650	500	520-600	550	560-650	569-745
LED(µm)	400-500	463	280-450	360	420-500	465	400-480	500-675
AND(µm)	270-300	286						
ISI	115-130	120					123-150	
ANI	50-54	52	>50			70		
NC	10-12	11	9-11	10	8-9		8-10	8-9
WS(µm)	40-50	42		~50		70		70-90
AP(µm)	50-100	81					45-70	85-115
BP(µm)	20-40	33	<50					45-70

Porochara raoi and Porochara mundula are extremely similar and may be synonymous. They both have the same shape as Porochara westerbeckensis, but Porochara westerbeckensis tends to be larger. Porochara westerbeckensis, Porochara mundula and Porochara raoi have short, stout necks. However, Porochara raoi and Porochara mundula have narrow spirals (50µm) and a large number of convolutions (range 9-12 (both species)). This differs from Porochara westerbeckensis which has wider spirals (51-116µm) and fewer convolutions (6-10).

Porochara sublaevis has a similar spiral form to Porochara westerbeckensis, however its shape is somewhat different. Porochara sublaevis is described as being ovoid, subcylindrical barrel shaped with a truncated base. The overal shape and particularly the base shape is more rounded in Porochara westerbeckensis.

The size range of Porochara minsinae falls within the limits of Porochara westerbeckensis. However, diagrams and descriptions are difficult to interpret and the shape tends towards being longer and thinner.

Porochara kimmeridgensis is very similar to Porochara westerbeckensis and might well be a synonym.

Preservation.

About half the specimens were well preserved, many had fragments of calcitic debris over the outside. All specimens examined had internal casts of sparry calcite. Many specimens showed compression artifacts of which two are shown here, a basal apical compression (Pl.33, Fig.6) and a lateral compression (Pl.33, Fig.7).

A basal apical compression is characterised by an exaggerated width of the fossil and a decreased angle of spiralling. The fossil is abnormally globose. A lateral compression is easily identified by a

varying equatorial diameter depending on the fossil's profile. The apical pore becomes distorted and looses its circular/pentagonal profile.

Occurrence

This species was previously recorded from the Kimmeridgian of N.W. Germany (Mádler 1952), the Upper Jurassic of Dobrogia (USSR), (Shajkin 1976), the Oxfordian (Kimmeridgian of Lvov (Ukraine) (Shajkin 1976), the Kimmeridgian (Upper Jurassic) of Portugal (Grambast-Fessard & Ramalho 1985) and the Kimmeridgian of N.W.Spain (Brenner 1976).

Porochara obovata (Peck)Saidakovsky (1966)

Stellatochara obovata Peck (1957)

Aclistochara obovata Peck (1937)

Plates: Pl.34, Figs.1-6

Collection: CB 4, SB 8(C2)

Material: 19 specimens

Horizon and Locality: Limestone horizon from the Oxfordian, Upper Jurassic, San Martinho do Porto, Portugal.

Description

	San Martinho population n=19		Type-material Peck (1937,57) n=100	
	mean	range	mean	range
LPA(µm)	539	538 - 679	540	420 - 600
LED(µm)	431	372 - 475	435	360 - 500
ISI	125	108 - 144		
ANI	48	40 - 59		
WS(µm)	86.5	77 - 141		50 - 80
NC	6.5	5 - 9	9	7 - 11
AP(µm)	130	77 - 180	100	
BP(µm)	50	39 - 77		20 - 50

The gyrogonites are prolate spheroidal to prolate and ellipsoidal (Pl.34, Figs.1,2). They are of medium size with strongly projecting bases and truncate summits. The summit opening is wide and conical in cross section with the inner orifice being smaller than the outer (Pl.34, Fig.3). The basal pore is hexagonal in outline (Pl.34, Fig.4). The basal plate could not be isolated and in many cases it appeared to be missing. The spirals were concave (Pl.34, Fig.5) or convex (Pl.34, Fig.6), the basal regions tending to be most strongly concave.

Remarks

The individuals from the San Martinho do Porto locality are of a similar size to the type material tending towards being slightly larger. They differ from the type material in having fewer, wider spirals. In all other details, particularly shape they are very similar. The long tapering base is a diagnostic character.

Preparation of the gyrogonites to enable examination of the basal plate was problematic. The interphase between the gyrogonite and the internal mineral cast was ill defined. Consequently, the fractured gyrogonite had obscuring fragments of cast over the basal plate. As only a limited amount of material exists the search for an uncontaminated plate was necessarily limited.

Comparisons

Porochara obovata resembles the following species; Stellatochara höllvicensis and Porochara raoi. Stellatochara hollvicensis from the Triassic of Sweden, if reversed in orientation, would closely resemble the size and shape of Porochara obovata. Its projecting apex is superficially reminiscent of the projecting base in Porochara obovata

Porochara raoi is very similar in size but has a less projected base.

Occurrence

Peck (1957) recorded this species in the Undivided Morrison Formation and the Bushy Basin shale member of N. America (Kimmeridgian / Lower Portlandian). The species is also recorded from the Upper Jurassic (Kimmeridgian) of Central Asia (Romaschkina 1975).

Porochara mundula (Peck)Grambast (1966)

Aclistochara mundula Peck (1941)

Aclistochara symmetrica Loranger (1951)

Plates: Pl.34, Figs.1-7; Pl.30, Figs.5,6

Collection: CB 5, SB 37(C4,D1,D4)

Material: About 200 specimens

Horizon and Locality: Marl Horizon from the Oxfordian / Kimmeridgian, Upper Jurassic, San Martinho do Porto, Portugal.

Description

	P.mundula San Martinho do Porto n = 30		Type-material Peck (1941,57) n = 27	
	range	mean	range	mean
LPA(µm)	423 - 590	493	320 - 650	500
LED(µm)	305 - 462	365	280 - 450	360
AND(µm)	205 - 333	257		
ISI	106 - 152	136		
ANI	43 - 56	52	>50	
WS(µm)	47 - 55	50	40 - 50	
NC	7 - 11	9	9 - 11	10
AP(µm)	77 - 12	96	50 - 100	81
BP(µm)	26 - 51	39	20 - 40	33
NR	2 - 4.5	3.2		

The gyrogonites are prolate, spheroidal to prolate and ellipsoidal (Pl.35, Figs.1,2). They are of medium to small size. The summit is truncate and in some specimens is extended into a broad stout neck. The base is rounded (rarely truncate). The greatest diameter is at about the gyrogonite's midheight. The apical pore is more or less rounded (Pl.35, Fig.3), conspicuous and relatively large. The basal pore is rounded (Pl.35, Fig.4). The basal plate could not be isolated because of an intimate association of the calcine with the internal calcitic cast. The basal plate was not visible from the outside as it had been eroded and/or obscured by mineral deposits. The spirals were concave to convex (Pl.35, Figs.4-6). The calcine substructure was of the "Y-form" as seen in transverse fracture under S.E.M (Pl.30, Fig.5).

Remarks and Comparisons

This species was the most abundant gyrogonite in the soft marl horizon. Porochara mundula resembles the following species: Porochara arguta, Porochara westerbeckensis and Porochara raoi.

Porochara arguta from the Bushy Basin shale member of the Morrison Formation (Kimmeridgian), N. America, has fewer spiral convolutions than Porochara mundula and does not have a short stout neck on any individuals.

Porochara westerbeckensis from the Kimmeridgian of N.W. Germany has the same shape as Porochara mundula, but tends to be larger with fewer broader spirals.

Porochara raoi may be a synonym of Porochara mundula. They both have numerous spirals in lateral view, analagous shape and size and both have short broad apical necks with truncate summits.

Preservation

The majority of the specimens were well preserved, many had fragments of calcitic debris over the outside. A few specimens showed compression artifacts of the sort described for Porochara westerbeckensis.

Occurrence

This species is widespread and abundant in the Aptian and Albian (Lower Cretaceous) non-marine deposits of the Rocky Mountain Area and Central Alberta of North America (Peck 1957).

Porochara raskyae (Mädler)

Porochara cf raskyae Brenner (1976)

Porochara rasky Shajkin (1976)

Aclistochara raskyae Mädler (1952)

Plates: Pl.36, Figs.4,5,8,9

Collections: CB 6, SB 37(C5)

Material: 25 specimens

Horizon and Locality: Marl horizon from the Oxfordian / Kimmeridgian, Upper Jurassic, San Martinho do Porto, Portugal.

Description

	P.raskyae San Martinho do Porto n = 25 Range	Mean	Type-material Mädler (1952) n = 18 Range
LPA(µm)	526-641	592	500-630
LED(µm)	346-526	479	415-570
AND(µm)	256-359	302	
ISI	110-163	124	
ANI	47-57	51	
WS(µm)	51-77	62	60-65
NC	8-12	10	10-13
AP(µm)	64-128	106	85-130
BP(µm)	26-77	52	30-45
NR	3-5	4.1	

The gyrogonites are prolate spheroidal to prolate and ellipsoidal (Pl.36, Fig.4). They are of medium size with rounded hemispherical bases. The apical region is rounded or conical in profile and truncated. The apical pore is wide (mean 106 µm) and more or less rounded. (Pl.36, Fig.5). The basal plate could not be isolated despite sacrificing 15 (out of the 25) individuals. This

was because the internal calcite cast was intimately associated with the calcine. Externally the basal plate appeared eroded and/or altered by diagenesis and obscured by calcitic debris (Pl.36, Fig.8). The spirals were concave and narrow (51-77μm) and in lateral view showed numerous convolutions (8-12) (Pl.36, Fig.4). The calcine structure shows only indistinct vertically aligned crystals in transverse fracture under S.E.M. (Pl.36, Fig.9).

Remarks and Comparisons

This is a species easily identified by its rounded profile. The basal plate was not isolated, the genus Porochara exists for those gyrogonites with a single basal plate or an unknown basal plate. Porochara raskyae resembles the following species; Musacchiella palmeri, Porochara raoi and Porochara obovata.

Porochara raskyae is very similar in shape and size to Musacchiella palmeri, a genus which can only be confirmed by demonstrating a segmented basal plate. Musacchiella palmeri, however, tends to have fewer spiral in lateral view.

Porochara raoi is of a similar size to Porochara raskyae but has a short broad apical neck (as in Porochara mundula) and its base is projected not rounded.

Porochara obovata is of similar size to Porochara raskyae but differs substantially in shape.

Preservation

The specimens were all well preserved, many with calcitic debris on the outside. All had calcitic internal casts which were intimately associated with the basal plate and the spirals, this prevented their isolation.

Occurrence

The species is known to occur in the Kimmeridgian of N.W. Germany (Mádler 1952), the Kimmeridgian of Algarve, Portugal (Grambast-Fessard & Ramalho 1985) and the Kimmeridgian of N.W. Spain (Brenner 1976) This species is also recorded from the Upper Jurassic of Dobroyea, USSR (Shajkin 1976).

Porochara portoensis n.sp.

Plates: Holoytpe Pl.36, Fig.1

Paratypes Pl.36, Figs.2,3,6,7

Collection: CB 7; SB 37(C3a-c)

Material: 8 specimens

Type Horizon and Locality: Marl horizons from Oxfordian / Kimmeridgian, Upper Jurassic, San Martinho do Porto, Portugal.

Derivation of name: Type locality

Diagnosis

	range	mean
LPA(µm)	308 - 462	356
LED(µm)	193 - 556	223
AND(µm)	154 - 231	183
ISI	130 - 225	161
ANI	50 - 54	51.5
WS (µm)	33 - 39	38
NC	7 - 11	9
AP (µm)	51 - 103	73
BP (µm)	13 - 39	21
NR	2.3 - 4	3.3

The gyrogonites are small, subprolate to perprolate and ellipsoidal (Pl.36, Figs.1,2). The base is projected downwards by a downward extention of the spirals. The spirals have numerous convolutions(i.e. up to 11) and are very narrow. They are concave or convex and spiral up to four times. The apex is truncate, with an apical pore which is wide relative to the size of the gyrogonite (Pl.36, Fig.3). The basal plate was not isolated. External examination of the basal plate was not possible because it was masked by calcitic debris or eroded away during diagenesis (Pl.36, Fig.6). Three gyrogonites showed poor preservation with

many details obscured by erosion. The calcine is of the "Y form" as seen in transverse fracture under S.E.M. (Pl.36, Fig.7).The size distribution of LPA, ISI, NC and AP is shown below.

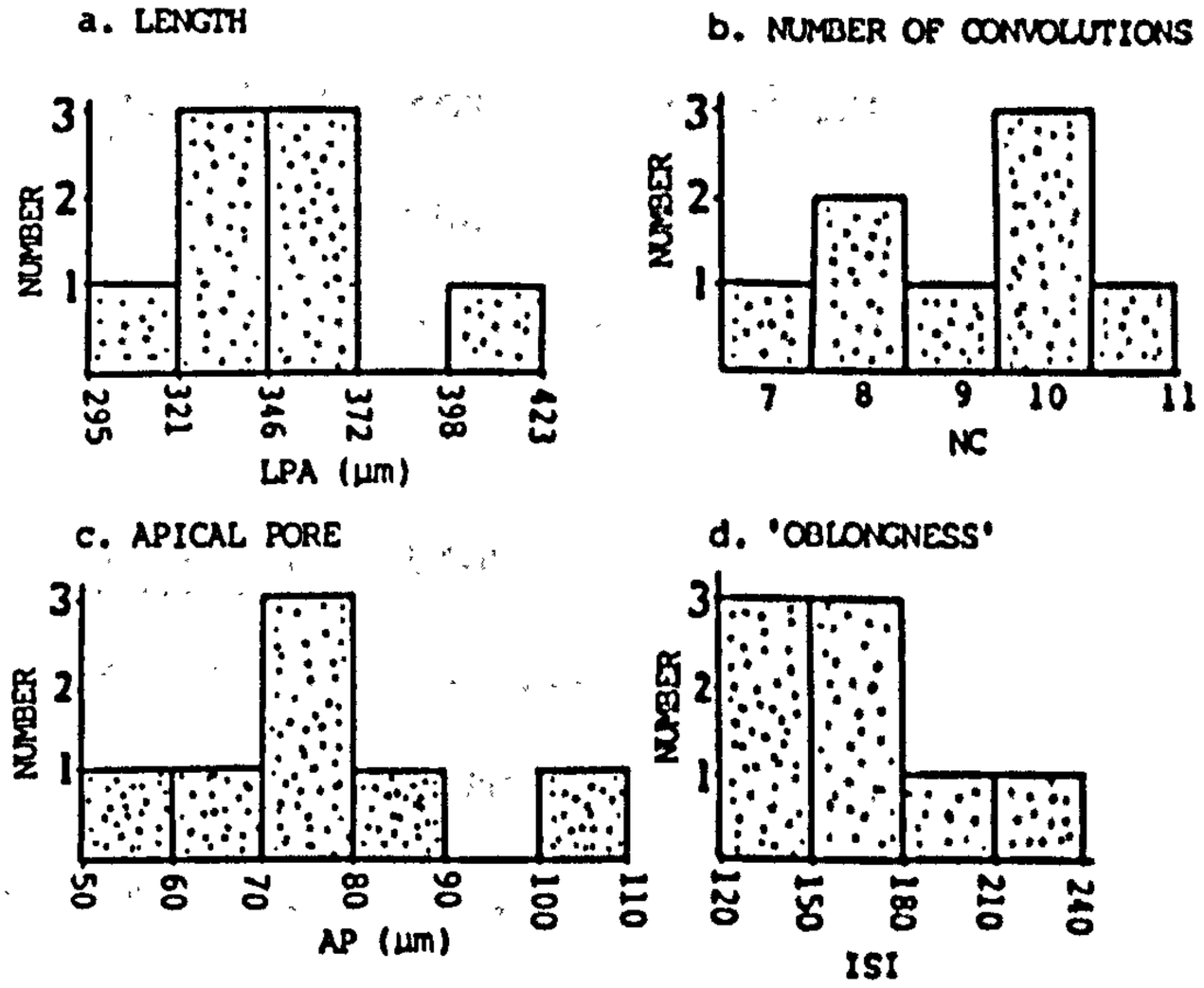

Remarks and Comparisons

This is a very small elongate gyrogonite with very narrow spirals. It has affinities with three species, Porochara jaisalmerensis, Porochara minima and Porochara polyspirator.

	P.jaislmerensis Bhatia&Mannikeri (1977) n = 3		P.minima Mädler (1952) n = 108	P.polyspirator Mädler (1952) n = 260
	range	mean	range	range
LPA(µm)	380-500	433	260-370	315-415
LED(µm)	280-350	310	200-285	250-350
AND(µm)	180-250	210		
ISI	136-143	140		
ANI	47-50	48		
NC	10-12	11	8-9	10-13
WS (µm)	30-40	37	40-50	35-45
AP (µm)	50-60	53	70-90	115-145
BP (µm)	20-25	22	25-30	35-45

Porochara jaislmerensis from the Morrison Formation (Upper Jurassic) of N.W. America is analagous to Porochara portoensis in details of the apical pore and spiral morphology. It falls in the top end of the size range of Porochara portoensis and exceeds it.

It differs in shape from Porochara portoensis which is relatively longer and thinner (reflected in a higher ISI) and has a wider diameter at or below the midpoint (higher ANI).

Porochara minima from the Kimmeridgian (Upper Jurassic) of N.W. Germany is smaller than the present species and is relatively wider, more rounded and has fewer, wider spirals.

Porochara polyspirator from the Kimmeridgian (Upper Jurassic) of N.W. Germany is similar in length to the present species but is a wider and a more rounded gyrogonite. Porochara polyspirator also has a wider apical pore.

Justification for erecting this species on so few individuals relates entirely to such a poor fit in characters with published taxa. Further work should proceed by extending the sample size to find a more complete distribution of measured characters.

Overall Discussion

Using the traditional methods of taxonomy seven taxa have been identified from San Martinho do Porto; six had previously been described and one is new. While it is accepted that this taxonomic approach has many limitations it still remains the most clearly understood and reliable method available. The distance between the "lumpers" and the "splitters" and the problem of worker's "pet" taxa is best closed by active communication, careful scrutiny and detailed observations.

It is considered that a paper reviewing the fossils from the Mesozoic, particularly the family Porocharaceae from the Middle and Upper Jurassic is needed. The workers in this field (i.e. Peck 1937,1957, Mädler 1952, Shajkin 1976, Bhatia & Mannikeri 1977 and Grambast-Fessard & Ramalho 1985, Romaschkina 1975, Brenner 1976, Feist & Grambast-Fessard 1984) each present new taxa. However, the variation within each taxon is often so great that some characters overlap substantially with those of other taxa. The two species Porochara mundula and Porochara westerbeckensis illustrate this. The description of the type material of Porochara mundula (Peck 1941, 1957) closely resembles a population from the marl horizons and so the population was assigned to that taxon. Likewise, the description of type material of Porochara westerbeckensis (Mädler 1952) closely resembles a population from the limestone horizons and so the population was assigned to that taxon. However, when the two species from the San Martinho do Porto locality are directly compared there is no obvious distinction between them due

to the variability within each taxon. It is necessary to return to the original material when problems of this nature arise. Until this is done it is best to conform to the published taxa but to be aware that a problem in the limits of the taxa might well exist. A review paper would, I am sure, reduce the number of species and give them clearly defined parameters.

On the basis of the charophyte evidence, the two horizons (limestone and marl) can only be described as being approximately Upper Jurassic in age. Species from the Middle Jurassic and the Lower Cretaceous make interpretation of the age confusing (see below).

SPECIES	LOCALITY		AGE
Musacchiella douzensis	France	*	Kimmeridgian/Oxfordian
Musacchiella palmeri	England	*	Bathonian(Mid.Jurassic)
Porochara obovata	Asia(Mongolia)	+	Kimmeridgian
	N. America	#	Kimmeridgian
	N.E. Spain	&	Kimmeridgian
Porochara mundula	N. America	#	Aptian/Albian(L.Cret.)
Porochara raskyae	N.W. Germany	$	Kimmeridgian
	Portugal	X	Kimmeridgian
	Ukraine	@	Oxfordian/Kimmeridgian
	U.S.S.R.	@	Upper Jurassic
	N.E. Spain	&	Kimmeridgian
Porochara westerbeckensis	N.W. Germany	$	Kimmeridgian
	U.S.S.R	@	Upper Jurassic
	Ukraine	@	Oxfordian/Kimmeridgian
	Portugal	X	Kimmeridgian
	N.E. Spain	&	Kimmeridgian

* Feist and Grambast-Fessard (1984)
+ Romaschkina (1975)
# Peck (1935, 1957)
& Brenner (1976)
$ Mädler (1952)
X Grambast-Fessard and Ramalho (1985)
@ Shajkin (1976)

The locality at San Martinho do Porto is recorded as being Oxfordian/Kimmeridgian (Wilson 1979). Unfortunately, this charophyte evidence adds nothing to determine the exact demarcation of the Oxfordian and the Kimmeridgian.

References

Allen, G.O. (1950). British Stoneworts (Charophyta). Published by: The Haslemere Natural History Society (Surrey).

Allen, N.S. (1980). Cytoplasmic streaming and transport in the characean alga Nitella.
Can. J. Bot. 58: 786-796.

Arens, K. (1939). Physiologische Multipolarität der Zelle von Nitella wahrend der Photosynthese.
Protoplasma 33: 295-300.

Atchey, W.R., Gaskin, C.T. and Anderson, D. (1976). Statistical properties of ratios I. Empirical results.
Syst. Zool. 25: 137-148.

Atkinson, A.W. Jr., John, P.C.L. and Gunning B.E.S. (1974). The growth and division of the single mitochondrion and other organelles during the cell cycle of Chlorella, studied by quantitative stereology and three dimension reconstruction.
Protoplasma 81: 77-109.

Barton, R. (1965). Electron microscope studies on surface activity in cells of Chara vulgaris.
Planta 66: 95-105.

Bell, W.A. (1922). A new genus of Characeae and new Merostomata from the coal measures of Nova Scotia.
Trans. R. Soc. Can. 16(3): 159-167.

Bhatia, S.B. and Mannikeri, M.S. (1977). Callovian Charophyta from Jaisalmer, Western India.
Geologica et Palaeontologica 11: 187-196

Borowitzka, M.A. (1977). Algal Calcification.
Oceanogr. Mar. Biol. Annu. Rev. 15: 189-223.

Borowitzka, M.A. (1982a). Morphological and Cytological Aspects of Algal Calcification.
Int.Rev. Cytol. 74: 127-162.

Borowitzka, M.A. (1982b). Mechanisms in algal calcification. Chp. 4: 137-177. Progress in Phycological Research 1. Elsevier Biomedical Press B.V.. Eds. Round/Chapman.

Borowitzka, M.A. and Larkum, A.W.D. (1976a). Calcification in the Green Alga Halimeda II. The Exchange of Ca^{2+} and the Occurrence of Age Gradients in Calcification and Photosynthesis.
J. Exp. Bot. 27: 864-878.

Borowitzka, M.A. and Larkum, A.W.D. (1976b). Calcification in the Green Alga Halimeda III. The Sources of Inorganic Carbon for Photosynthesis and Calcification and a Model of the

Mechanism of Calcification.
J. Exp. Bot. 27: 879-893.

Borowitzka, M.A. and Larkum, A.W.D. (1977). Calcification in the Green Alga Halimeda I. An Ultrastructure Study of Thallus Development.
J. Phycol. 13: 6-16.

Borowitzka, M.A., Larkum, A.W.D. and Nockolds C.E. (1974). A scanning electron microscope study of the structure and organization of the calcium carbonate deposits of algae.
Phycologia 13(3): 195-203.

Bouligand, Y. (1965). Sur une disposition fibrillaire torsadée commune a plusieurs structures biologiques.
C. R. Acad. Sci. Paris 261: 4864-4867

Braun, A. (1852). Ueber die Richtungsverhaltnisse der saftstrome in den Zellen der Charen.
Monatsber. Dtsch. Akad. Wiss., Berlin: 220-68.

Bremer, K. and Wantorp H.E. (1981). A cladistic classification of green plants.
Nord. J. Bot. 1: 1-3.

Brenner, P. (1976). Ostracoden und Charophyten des Spanischen Wealden.
Palaeontogr. 152A: 113-201.

Burne, R.V., Bauld, J. and DeDeckker, P. (1980). Saline lake Charophytes and their geological significance.
J. Sediment. Petrol. 50(1): 281-293.

Caceres, E.J. (1975). Novedades carologicas argentinas. I Una nueva especie de Nitella y tres adiciones al genero para la flora Argentina.
Kurtziana 8: 105-125.

Claugher, D. (1984). Ion and Fast Beam Etching of Biological Material for Scanning Electron Microscopy.
Proc. R.M.C. 19(3): 146-148

Colin, J.P., Feist, M., Grambast-Fessard, N., Cherchi, A. and Schroeder, R. (1985). Charophytes and Ostracods from the Berriasian (Purbeckian facies) of Cala D'inferno (Nurra region, N.W. Sardinia).
Estratto do Bollettino della Società Paleontologica Italiana 23(2): 345-354.

Crawley, J.C.W. (1965). A cytoplasmic organelle associated with the cell walls of Chara and Nitella cells.
Nature (Lond.) 205: 200-201.

Croft, W.N. (1952). A new Trochiliscus (Charophyta) from the Downtonian of Podolia.
Bull. Brit. Mus. (Nat.Hist.) Geol. 1: 189-220.

Cuif, J.P., Denis A. and Raguideau A. (1983). Observations sur les

modalites de mise en place de la couche prismatique du test de Pinna nobilis L. par l'etude des characteristiques de la phase minerale.
Haliotis 13: 131-141.

Daily, F.K. (1969). Some late glacial charophytes compared to modern species.
Proc. Indiana Acad. Sci. 78: 406-412.

Daily, F.K. (1975). A note concerning calcium carbonate deposits in Charophytes.
Phycologia 14(4): 331-2.

Davies, R.G. (1971). Computer programming in quantitative biology.
Academic Press inc. (London).

DeBary, A. (1871). Uber den Befruchtungsvorgang bei den Charen.
Monatsber. Dtsch. Akad. Weiss. Berlin: 277-239

DeBary, A. (1875). Zur Keimungsgeschichte der Charen.
Bot. Ziet. 33: 377-391 (English translation by Hemsley, W.B. (1875). J. Bot. (Lond.) 13: 298-313).

DeDeckker, P. and Geddles, M.C. (1980). Seasonal fauna of ephemeral saline lake near the Coorong Lagoon, South Australia.
Aust. J. Mar. Freshwater Res. 31: 677-700.

Degens, E.T. (1976). Molecular Mechanisms of Carbonate, Phosphate and Silica deposition in the Living Cell.
Top. Curr. Chem. 64: 1-112.

Dyck, L.A. (1970). Morphological, chemical and developmental studies of Chara oosporangial walls.
Thesis Washington University 145p.

Dyck, L.A. and Parker, B.C. (1967). Comparisons of Fossil and Extant Fructifications of Chara. 2. Physical and Chemical Characteristics.
J. Phycol. 3(suppl.): 10-11.

Everitt, B. (1974). Cluster Analysis.
Heinemann Educational Books (London).

Feist, M. and Grambast-Fessard, N. (1982). Clé de determination pour les genres de charophytes.
Paleobiologie Continentale (Montpellier) 13(2): 1-28

Feist, M. and Grambast-Fessard, N. (1984). New Porocharaceae from the Bathonian of Europe: Phylogeny and Palaeoecology.
Palaeontology 27(2): 295-305.

Feist-Castel, M. (1973). Observations nouvelles sur la paroi des fructifications chez les charophytes
Geobios 6: 239-242

Feist-Castel, M. (1977). Evolution of the Charophyte floras, in

the Upper Eocene and Lower Oligocene of the Isle of Wight.
Palaeontology 20(1): 143-157 pls. 21-22.

Fischer, R.A., Dainty, J. and Tyree, M.T. (1974). A quantitative investigation of symplasmic transport in Chara corallina. I Ultrastructure of the nodal complex cell walls.
Can.J. Bot. 52: 1209-1214.

Folk, R.L., Chafetz, H.S. and Tiezzi, P.A. (1986). Bizarre Forms of Depositional and Diagenetic Calcite in Hot Spring Travertines, Central Italy.
Carbonate Cements, Society of Economic Palaeontologists and Mineralogists Special Publication 36

Franceschi, V.R. and Lucas W.J. (1980). Structure and possible function(s) of Charosomes; complex plasmalemma-cell wall elaborations present in some Characean species.
Protoplasma 104: 253-271.

Franceschi V.R. and Lucas W.J. (1981). Characean charasome - complex and plasmalemma vesicle development.
Protoplasma 107(3/4): 255-268.

Frérotte, B., Raguideau, A. and Cuif, J.P. (1983). Dégradation in vitro d'un test carbonaté d'invertébré Crassostrea gigas (Thunberg), par action de cultures bacteriennes. Intérêt pour l'analyse ultrastructural
C. R. Acad. Sci. Paris 297(2): 383-388

Fritsch, F.E. (1965). The structure and reproduction of the algae.
Vol. 1 C.U.P.

Gipson, P.S., Sealander, J.A. and Dunn, J.E. (1974). The taxonomic status of wild Canis in Arkansas.
Syst. Zool. 23: 1-11.

Glukhovskya, N.B. (1975). Girogonity Semeystva Characeae s anomal'nym Kolichestvom spiraley (Gyrogonites of the family Characeae with anomalous numbers of spirals)
Dokl. Akad. Nauk. SSSR 224: 691-692

Goebel, K. (1902). Morphologische und biologische Bermerkungen II. Ueber die Homologie in der Entwicklung mannlicher und Weiblicher Sexualorgane.
Flora 90: 279-305.

Gould, S.J. (1966). Allometry and size in ontogeny and phylogeny.
Biol. Rev. 41: 587-640.

Grambast, L. (1956a). Sur la dehiscence de l'oospore chez Chara vulgaris L. et la systematique de certaines Characeae fossiles.
Rev. Gén. Bot. 63: 331-336

Grambast, L. (1956b). La plaque basale des Characées.
C. R. Hebd. Seanc. Akad. Paris 242: 2585-2587

Grambast, L. (1961). Remarques sur la systematique et la

repartition stratigraphique des characeae pré-tertiaires.
C.R. Somm. Seances Soc. Geol. Fr. :200-202.

Grambast, L. (1962a). Sur l'intérêt stratigraphique des Charophytes fossiles: exemples d'application au Tertiaire parisien.
C. R. Somm. Seances Soc. Geol. Fr. :207-209

Grambast, L. (1962b). Classification de l'embranchement des Charophytes.
Naturalia monspel. Ser. Bot. 14: 63-86.

Grambast, L. (1966). In Saidakovsky, L.Y. (1966).

Grambast, L.J. (1974). Phylogeny of the Charophyta.
Taxon 23(4): 463-481.

Grambast L. and Gutierrez, G. (1977). Espèces nouvelles de charophytes du Crétacé Supérieur terminal de la province de Cuenca (Espagne).
Paleobiologie Continentale, Montpellier 8(2): 1-34.

Grambast-Fessard, N. and Ramalho, M (1985). Charophytes du Jurassique supérieur du Portugal.
Revue de Micropaléontologie 28(1): 58-66.

Grimley, P.M. (1964). A tribasic stain for thin sections of plastic embedded OsO_4-fixed tissues.
Stain Technol. 39: 229-233

Groves, J. (1916). On the name Lamprothamnus Braun.
J. Bot. LIV: 336-337.

Groves, J. and Bullock-Webster, G.R. (1920). The British Charophyta.
Vol.I Nitelleae, Ray Society (London).

Groves, J. and Bullock-Webster, G.R. (1924). The British Charophyta.
Vol.II Chareae, Ray Society (London).

Gunning, B.E.S. and Steer, M.W. (1975). Ultrastructure and the Biology of Plant cells.
Edward Arnold (Publishers) Ltd.

Harris, T.M. (1939). British Purbeck Charophyta.
British Museum (Nat. Hist.) Lond.

Hejnowicz, Z. and Sievers, A. (1981). Regulation of the position of statoliths in Chara rhizoids.
Protoplasma 108: 117-137.

Hoagland, D.R. and Davis, A.R. (1923). The composition of the cell sap of the plant in relation to the absorbtion of ions.
J. Gen. Physiol. 5: 629.

Hoagland, D.R. and Davis, A.R. (1929). The intake and accumulation of electrolytes by plant cells.

Protoplasma 6: 610.

Hoch, H.C. (1977). Use of permanganate to increase electron opacity of fungal walls.
Mycologia LXIX (6): 1209-1213

Hope, A.B. and Walker, N.A. (1975). The Physiology of Giant algal cells.
C.U.P. Aberdeen.

Horn af Rantzien, H. (1954). Middle Triassic Charophyta of South Sweden.
Opera Bot. 1(2): 5-83.

Horn af Rantzien, H. (1956). Morphological terminology relating to female charophyte gametangia and fructifications.
Bot.Not. 109(2): 212-259.

Horn af Rantzien, H. (1959). Recent charophyte fructifications and their relations to fossil charophyte gyrogonites.
Ark. Bot., Ser.2, 4(7): 165-332

Hotchkiss A.T. (1962). A cytotaxonomic study of the Characeae Progress Report G-19449, Department of Biology, University of Louisville, Kentucky.

Hotchkiss, A.T. (1963). A first report of chromosome number in the genus Lychnothamnus (Rupr.) Leonh. and comparisons with the other charophyte genera.
Proc. Linn. Soc. N.S.W. 88(3): 368-372

Hotchkiss, A.T. (1966). Chromosome numbers in Lamprothamnium.
Proc. Linn. Soc. N.S.W. 91(2): 118-120

Huxley, J.S. (1924). Constant differential growth - ratios and their significance.
Nature (Lond.) 114: 895-6.

Huxley, J.S. (1932). Problems of relative growth.
Methuen and Co., Ltd. (London).

Imahori K. and Iwasa, K. (1965). Pure Culture and Chemical Regulation of the Growth of Charophytes.
Phycologia 4: 127-134.

J.C.P.D.S. Search Manual (1980). Mineral Powder Diffraction File.
International Centre for Diffraction Data

Johansen, H.W. (1981). Coralline Algae, A First Synthesis.
CRC Press, Inc. Florida.

Johnson, S.C. (1967). Hierarchical clustering schemes.
Psychometrika 32: 241-254.

Kamiya, N. (1981). Physical and chemical basis of cytoplasmic streaming.
Annu. Rev. Plant Physiol. 32: 205-36.

Klaveness, D. (1972). Coccolithus huxleyi (Lohmann) Kamptner I. - Morphological investigations on the vegetative cell and the process of coccolith formation.
Protistologica 8(3): 335-346.

Kuczewski, O. (1906). Morphologische und Biologische Untersuchungen an Chara delicatula f. bulbillifera A. Braun.
Beih. bot. Zbl. 20(1): 25-75.

Lance, G.N. and Williams W.T. (1966). Computer program for hierarchical polythelic classification.
Comp. J. 9: 60-64.

Loranger, D.M. (1951). Useful Blairmore microfossil zone in central and southern Alberta, Canada.
Am. Assoc. Pet. Geol. Bull. 35: 2348-2367

Lucas, W.J. (1975a). Photosynthetic Fixation of ^{14}Carbon by Internodal cells of Chara corallina.
J. Exp. Bot. 26: 331-346.

Lucas, W.J. (1975b). The Influence of Light Intensity on the Activation and Operation of the Hydroxyl Efflux System of Chara corallina.
J. Exp. Bot. 26: 347-360.

Lucas, W.J. (1976a). Plasmalemma Transport of HCO_3^- and OH^- in corallina: non-antiporter systems.
J. Exp. Bot. 27: 19-31.

Lucas, W.J. (1976b). The Influence of Ca^{2+} and K^+ on $H^{14}CO_3^-$ Influx in Internodal cells of Chara corallina.
J. Exp. Bot. 27: 32-42.

Lucas, W.J. (1977). Analogue Inhibition of the Active HCO_3^- Transport Site in the Characean Plasma Membrane.
J. Exp. Bot. 28: 1321-1336.

Lucas, W.J. (1979). Alkaline Band Formation in Chara corallina. Due to OH^- Efflux or H^+ Influx?
Plant Physiol. 63: 248-254.

Lucas, W.J. (1983). Photosynthetic Assimilation of Exogenous HCO_3^- by Aquatic Plants.
Ann. Rev. Plant Physiol. 34: 71-104.

Lucas, W.J. and Nuccitelli, R. (1980). HCO_3^- and OH^- transport across the plasmalemma of Chara.
Planta 150: 120-131.

Lucas, W.J. and Smith F.A. (1973). The Formation of Alkaline and Acid Regions at the Surface of Chara corallina cells.
J. Exp. Bot. 24: 1-14.

Mädler, K. (1952). Charophyten aus dem Nordwestdeutschen Kimmeridge.
Geol. Jahrb. 67: 1-46

Mädler, K. (1955). Zur Taxionomie der tertiären Charophyten. Geol. Jahrb. 70: 265-328 pl.23-26.

Mattox, K.R. and Stewart, K.D. (1984). Chapter 2. Classification of the Green Algae. A Concept Based on Comparative Cytology. In: Systematics of the Green Algae. The Systematics Association Special Volume 27. Ed. Irvine D.E.G. and John, D.M.. Academic Press.

Millington, W.F. and S.R. Gawlik (1967). Silica in the walls of Pediastrum.
Nature 216: 68

Minkoff, E.C. (1965). The effects on classification of slight alterations in numerical technique.
Syst. Zool. 14: 196-213.

Mirande, M. (1919). Sur la formation cytologique de l'amidon et de l'huile dans l'oogone de Chara.
C.R. Acad. Sci. Paris, 168: 528-9.

Möestrup, Ø. (1970). The fine structure of mature spermatozoids of Chara corallina, with special reference to microtubules and scales.
Planta 93: 295-308.

Moulton, T.P. (1973). Principal component analysis of variation in form within Oncaca confera Giesbreckt, 1891, a species of Copepod (Crustacea).
Syst. Zool. 22: 141-156.

Neville, A.C. (1985). Molecular and Mechanical Aspects of Helicoid Development in Plant Cell Walls.
BioEssays 3(1): 4-8.

Neville, A.C. (1986). The physics of helicoids. Multidirectional 'plywood' structures in biological systems.
Phys. Bull. 37: 74-76

Neville, A.C., Gubb, D.C. and Crawford, R.M. (1976). A New Model for Cellulose Architecture in some Plant Cell Walls.
Protoplasma 90: 307-317.

Neville, A.C. and Levy, S. (1984). Helicoidal orientation of cellulose microfibrils in Nitella opaca internode cells: ultrastructure and computed theoretical effects of strain reorientation during wall growth.
Planta 162: 370-384.

Norris, R.F. and Bukovac, M.J. (1968). Structure of the pear leaf cuticle with special reference to cuticular penetration.
Am. J. Bot. 55: 975-983.

O'Brian, T.P. and McCully M.E. (1981). The Study of Plant Structure. Principals and Selected Methods.
Termarcarphi Pty. Ltd., Australia.

Parker, B.C. and Dyck, L.A. (1967). Comparison of Fossil and

Extant Fructifications of Chara I. Histochemistry and Ultrastructure.
J. Phycol. 3 (suppl.): 10.

Parker, B.C. (1969). Occurrence of silica in brown and green algae.
Can. J. Bot. 47: 537-540.

Peck, R.E. (1937). Morrison Charophyta from Wyoming.
J. Paleont. 11: 83-90

Peck, R.E. (1941). Lower Cretaceans Rocky Mountain Non-Marine Microfossils.
J. Palaeontol. 15: 285-304.

Peck, R.E. (1957). North American Mesozoic Charophyta.
U.S. Geological Survey Prof. Paper 294: 1-44.

Pentecost, A. (1984). The growth of Chara globularis and its relationship to calcium carbonate deposition in Malham Tarn.
Field Studies 6: 53-58.

Pickett-Heaps, J.D. (1966). Ultrastructure and Differentiation in Chara sp. I Vegetative cells.
Aust. J. Biol. Sci. 20: 539-551.

Pickett-Heaps, J.D. (1967). Ultrastructure and Differentiation in Chara sp. II Mitosis.
Aust. J. Biol. Sci. 20: 883-94.

Pickett-Heaps, J.D. (1968a). Ultrastructure and Differentiation in Chara sp. III Formation of the Anthenidium.
Aust. J. biol. Sci. 21: 255-74.

Pickett-Heaps, J.D. (1968b). Ultrastructure and Differentiation in Chara (Fibrosa) IV Spermatogenesis.
Aust. J. biol. Sci. 21: 655-690.

Pickett-Heaps, J.D. (1968c). Microtubule-like structure in the growing plastids of chloroplasts of two algae.
Planta 81: 193-200.

Pickett-Heaps, J.D. (1975). Green Algae Structure Reproduction and Evolution in Selected Genera.
Sinauer Associates Inc., Publishers, Sunderland, Massachusetts.

Pringsheim, N. (1862). Ueber die Vorkeime der Charen.
Monatsber. Akad. Wiss. Berlin 225-31.

Proctor, V.W. (1967). Storage and germination of Chara oospores.
J. Phycol. 3: 90-92.

Proctor, V.W. (1980). Historical biogeography of Chara (Charophyta): an appraisal of the Braun-Wood classification plus a falsifiable alternative for future consideration.
J. Phycol. 16: 218-233.

Pytkowicz, R.M. (1965). Rates of inorganic calcium carbonate nucleation.
J. Geol. 73: 196-199.

Raven, J.A. and Smith, F.A. (1978). Effect of Temperature and External pH on the Cytoplasmic pH of Chara corallina.
J. Exp. Bot. 29: 853-66.

Raven, J.A., Smith, F.A. and Walker, N.A. (1986). Biomineralization in the Charophyceae sensu lato. In: Biomineralization in lower Plants and Animals.
Eds. Leadbeater, B.S.C. and Riding, R.. O.U.P.

Reynolds E.S. (1963). The use of lead citrate at a high pH as an electron opaque stain in electron microscopy.
J. Cell Biol. 17: 208-212

Roberts, G. and Chen, J.C.W. (1975). Chromosome analysis and amitotic nuclear division in Nitella axillaris.
Cytologia 40: 151-156.

Romaschkina, K. (1975). Iskop Fauna Flora Mongol. 2: 188, pl.I figs. 4 a-b.

Ross, M.M. (1959). Morphology and physiology of germination of Chara gymnopitys A. Braun. (i) Development and morphology of the sporeling.
Aust. J. Bot. 7: 1-11.

Ross, R. and Glomset, J.A. (1973). Atherosclerosis and Arterial Smooth Muscle Cell.
Science 180: 1332-1339.

Round, F.E. (1981). The ecology of algae.
C.U.P. Cambridge.

Round, F.E. (1984). Chapter I. The Systematics of the Chlorophyta: An Historical Review leading to some Modern Concepts (Taxonomy of the Chlorophyta III) in Systematics of the Green Algae.
Eds. Irvine, D.E.G. and John, D.M.. Systematics Association Special Volume 27

Sahni, B. and Rai, S.R.N. (1943). On Chara sausari sp.nov., a Chara (sensu stricto) from the Intertrappean Cherts at Sausar in the Deccan
Proc. Nat. Akad. Sci. Ind. 13(3): 215-223

Saidakovsky, L.Y. (1966). Biostratigraphiya triasovykh otlozhenii yuga russkoi platfory. In: Iskopaemye Kharofily SSSR. (Biostratigraphy of the triassic deposits in the southern Russian platform).
Trudy Geol. Inst. 143: 93-144

Sandberg, P.A. (1975a). New interpretations of Great Salt Lake ooids and of ancient non-skeletal carbonate mineralogy.
Sedimentology 22: 497-537.

Sandberg, P.A. (1975b). Bryozoan Diagenesis: Bearing on the Nature of the Original Skeleton of Rugose Corals. J. Paleont. 49(4): 587-618.

Sawa, T. and Frame, P.W. (1974). Comparative anatomy of Charophyta: 1. Oogonia and oospores of Tolypella - with special reference to the sterile oogonial cell. Bull. Torr. Bot. Club 101(3): 136-144.

Scholle P.A. (1978). A colour illustrated guide to carbonate rock constituents, textures and porosities. Amer. Assoc. Pet. Geol. Mem. 27: 288

Schröter K., Läuchli, A. and Sievers, A. (1975). Mikroanalytische Identifikation von Barium Sulfat - Kristallen in den Statolithen der Rhizoide von Chara fragilis Desv. Planta (Berl.) 122: 213-225.

Shajkin, I.M. (1976). New data on the biostratigraphy of the Jurassic and Cretaceous deposits of the Fore-Dobrogean trough. Geol. Zh. 36(2): 77-86.

Shen, E.Y.F. (1966). Oospore germination in two species of Chara. Taiwania 12: 39-46.

Shen, E.Y.F. (1967a). Amitosis in Chara. Cytologia 32: 481-488.

Shen, E.Y.F. (1967b). Microspectrophotometric analysis of nuclear D.N.A. in Chara zeylanica. J. Cell Biol. 35: 377-384.

Shen, E.Y.F. (1967c). The amount of nuclear D.N.A. in Chara zeylanica measured by microspectrophotometry. Taiwania 13: 111-114.

Sievers, A. (1965). Elektronenmikroskopische Unteruchungen zur geotropischen Reaktion. I Über Besouderheiten im Feinbau der Rhizoide von Chara foetida. Z. Pflanzenphysiol. Bd 53: 193-213.

Sievers, A. (1967a). Elektronenmikroskopische Untersuchungen zur geotropischen Reaktion. II Die polare Organisation des normal wachsenden Rhizoids von Chara foetida. Protoplasma 64: 225-253.

Sievers, A. (1967b). Elecktonenmikroskopische Untersuchungen zur geotropischen Reaktion. III Die transversale Polarisierung der Rhizoidspitze von Chara foetida nach 5 bis 10 Minuten Horizontallage. Z. Pflanzenphysiol. 57: 462-473 Bd.

Sievers, A. and Schröter, K. (1971). Versuch einer kausalanalyse der geotropischen Reaktionskette im Chara-Rhizoid. Planta 96: 339-353.

Simkiss, K. (1964a). Variations in the Crystalline form of Calcium Carbonate Precipitated from Artificial Sea Water.

Nature 201(1): 492-3.

Simkiss, K. (1964b). Phosphates as crystal poisons of calcification.
Biol. Rev. 39: 487-505.

Simkiss, K. (1986). The processes of biomineralization in the lower plants and animals - an overview. In: Biomineralization in Lower Plants and Animals. Eds. Leadbeater, B.S.C. and Riding, R.. O.U.P..

Smith, F.A. and Walker N.A. (1980). Photosynthesis by aquatic plants: effects of unstirred layers in relation to assimilation of CO_2 and HCO_3^- and to carbon isotopic discrimination.
New Phytol. 86: 245-259.

Sneath, P.H. (1957). The application of computers to taxonomy.
J. Gen. Microbiol. 17: 201-226.

Sokal, R.R. and Michener, C.D. (1958). A statistical method for evaluating systematic relationships.
Univ. Kans. Sci. Bull. 38: 1409-1438.

Soulié-Märsche, I. (1979). Etude comparée de gyrogonites de Charophytes actuelles et fossiles et phylogénie des genres actuels.
Thèse, Montpellier 320 p. dactylo, 45 pl.

Spanswick, R.M. (1981). Electrogenic ion pumps.
Ann. Rev. Plant Physiol. 32: 267-289.

Spanswick, R.M. and Costerton, J.W.F. (1967). Plasmodesmata in Nitella translucens: structure and electrical resistance.
J. Cell Sci. 2; 451-464.

Spence, D.H.N. (1982). The zonation of plants in freshwater lakes.
Adv. Ecol. Res. 12: 37-125.

Spurr, A.R. (1969). A low-viscosity epoxy resin embedding medium for electron microscopy.
J. Ultrastruct. Res. 26: 31-43

Stross, R.G. (1979). Density and boundary regulations of the Nitella meadow in Lake George, New York.
Aquat. Bot. 6: 285-300.

Sundaralingam, V.S. (1954). The developmental morphology of Chara zeylanica Willd.
J. Ind. Bot. Soc. 33: 272-297.

Sundaralingam, V.S. (1962a). Studies on Indian Charophytes - I. Lychnothamnus.
Proc. Ind. Acad. Sci. 55B: 131-151.

Sundaralingam, V.S. (1962b). Studies on Indian Charophytes - II. Developmental morphology of Nitella Agardh.
Phykos 1: 61-75.

Sundaralingam, V.S. (1963). Studies on Indian Charophytes - III. Developmental morphology of 2 ecorticate species. Phykos 2: 1-14.

Sundarlingam,V.S. (1965). Studies on Indian Charophytes - IV. Developmental morphology of three more species of Nitella Agardh. Phykos 4: 19-39.

Sundaralingam, V.S. (1966). Studies on Indian Charophytes - V. Developmental morphology of two more species of Chara Linn.. Phykos 5: 198-215.

Takatori, S. and Imahori, K. (1971). Light reaction in the control of oospore germination. Phycologia 10: 221-228.

Tappan, H (1980). The paleobiology of plant protists W.H. Freeman and Co., San Francisco

Tindall, D.R. and Sawa, T. (1964). Chromosomes of the Characeae of the Woods Hole (Massachusetts) Region. Am. J. Bot. 51(9): 943-949.

Towe, K.M. and Hemleben, C. (1976). Diagenesis of Magnesium Calcite: Evidence for Miliolacean Foraminifera. Geology 4: 337-339.

Van der Wal, P., DeJong, L. and Westbroek, P. (1983). Calcification in the Coccolithophorid Alga Hymenomonas carterae. Ecol. Bull. (Stockholm) 35: 251-258. Environmental Biogeochemistry. Ed. Hallberg, R..

Walker, E. (1929). Entwicklungsgeschichtliche und cytologische Untersuchungen an einigen Nitellen. Arch. Jul. Klaus-Stiflung 4: 23-121.

Walker, N.A. (1983). The uptake of inorganic carbon by freshwater plants. Plant Cell Environ. 6: 323-328.

Walker, N.A., Beilby, M.J. and Smith, F.A. (1979). Amine uniport at the plasmalemma of Charophyte cells. I. Current-voltage curves, saturation kinetics and effects of unstirred layers. J. Membr. Biol. 49: 21-55.

Walker, N.A. and Smith F.A. (1977). Circulating Electric Currents between Acid and Alkaline Zones Associated with HCO_3^- Assimilation in Chara. J. Exp. Bot. 28: 1190-1206.

Watabe, N. and Dunkelberger, D.G. (1979). Ultrastructural studies on calcification in various organisms. Scanning Electron Microsc. II 403-416.

Weiner, S., Talmon, Y. and Traub, W. (1983). Electron diffraction

of Mollusc shell organic matrices and their relationship to the mineral phase.
Int. J. Biol.. Macromol. 5: 325-328.

Weiner, S. and Traub, W. (1980). X-ray diffraction study of the insoluble organic matrix of Mollusk shells.
Fed. Eur. Biochem. Soc. 111: 311-316.

Weiner, S. and Traub, W. (1981). Organic-matrix-mineral relationships in mollusc shell nacreous layers. In: Structural Aspects of Recognition and Assembly in Biological Macromolecules. Ed. Balaban, M., Sussman, J.L., Traub, W. and Yonath, A.. Rehovot and Philadelphia, Balaban ISS.

Weiner, S. and Traub, W. (1984). Macromolecules in Mollusc shells and their function in biomineralization.
Phil. Trans. R. Soc. London. B 304: 425-434.

Westbroek, P., DeJong, E.W., Van der Wal, P., Borman, T., DeVrind, J.P.M., Van Emburg, P.E. and Bosch, L. (1983). Calcification in Coccolithophoridae - wasteful or functional? Ecol. Bull (Stockholm) 35: 291-299.
Environmental Biogeochemistry. Ed. Hallberg, R.

Westbroek, P., DeJong, E.W., Van der Wal, P., Borman, A.H., DeVrind, J.P.M., Kok, D., DeBruijn, W.C. and Parker S.B. (1984). Mechanism of calcification in the marine alga Emiliania huxleyi.
Phil. Trans. R. Soc. Lond. B 304,

Wilbur, K.M. and Bernhardt, A.M. (1982). Mineralisation of Molluscan shell: Effects of free polyaminoacids on crystal growth rate in vitro.
Am. Zool. 22: 952.

Wilbur, K.M. and Saleuddin, A.S.M. (1983). Chp. 6 Shell Formation in the Mollusca, Vol. 4 Physiology Part 1.
Ed. Saleuddin, A.S.M. and Wilbur, K.M., Academic Press, Inc. (Lond.) Ltd.,

Williams, M.B. (1959). A revision of Nitella cristata Braun (Characeae) and its allies. Part II Taxonomy.
Proc. Linn. Soc. N.S.W. LXXXIV(3): 346-355.

Wilson, R.C. (1979). A reconnaissance study of Upper Jurassic sediments of the Lusitanian Basin.
Ciencias da Terra (UNL) Lisboa 5: 53-84.

Wood, R.D. and Imahori, K. (1964). A revision of the Characeae: Iconograph of the Characeae - Vol. 2.
Weinheim Verlag Von J. Cramer.

Wood, R.D. and Imahori, K. (1965). A revision of the Characeae: Monograph of the Characeae - Vol. 1.
Weinheim Verlag Von J. Cramer.

Womersley H.B.S. and Bailey, A. (1969). The Marine algae of the Solomon Islands and their place in biotic reefs.

Phil. Trans. Roy. Soc. B 255: 433-442.

Wright, P. (1985). Lacustrine carbonates and source rocks from the Upper Jurassic of Portugal.
IAS European Meeting (Spain) Abstract.

APPENDIX Ia Program written for principal component analysis

```
'reference' princmpts
'unit' $100
'input' 2
'read/prin-dom' spec,lpa,led,and,wce,nc,ap,bp,nr
'input' 1
'run'
'matrix' cmpts $100,3
'pcp/prin-ltrs,corr-y' lpa,led,and,wce,nc,ap,bp,nr;scores-cmpts
'equa' x,y,z-cmpts$(1,2x)50,x
'fact' f$100
'gene' f
'graph/nrf-55,ncf-91,eqxy-y' x;y$;f
:  x;z$;f
:  y;z$;f
'run'
'close'                    For unstandardised data delete corr-y
'stop'
```

APPENDIX Ib Program written for cluster analysis

```
'refe' cluster
'unit' $100
'input'2 'read' spec,lpa,led,and,wce,nc,ap,bp,nr
'input'1
'run'
'symmat' simmat $100
'into' types-0(3)
'into' corder $100
'vari' ranges-0(-1)
'smat' simmat;lpa,led,and,wce,nc,ap,bp,nr;types;ranges
'smprint'simmat
'smprint/pr-2'simmat
'hier/cm-4 (or -1)' simmat;corder
'run'
'close'
'stop'                     For: single link cluster analysis use  cm=1
                                centroid cluster analysis use     cm=3
                                average link cluster analysis use cm=4
```

Numbers 1-25 Chara delicatula Agardh
26-50 Chara hispida L.

spec. Nº.	LPA (µm)	LED (µm)	AND (µm)	WS (µm)	NC	AP (µm)	BP (µm)	NR
1	757	462	385	64	13	180	51	3·7
2	653	321	359	51	12	180	51	2·5
3	666	436	385	64	12	154	64	2·5
4	844	436	436	64	12	154	51	3·0
5	744	462	436	64	13	154	51	4·5
6	666	410	359	64	12	141	64	3·5
7	759	475	436	51	13	180	64	3·7
8	718	436	398	64	12	128	64	3·5
9	731	487	385	64	12	180	51	3·7
10	692	410	359	51	13	205	77	3·5
11	718	462	385	51	11	180	77	4·3
12	795	449	436	64	13	180	51	3·8
13	692	433	359	64	13	154	51	3·8
14	744	436	410	51	13	180	51	3·8
15	757	410	385	64	12	154	39	4·3
16	692	436	385	64	13	154	51	3·8
17	744	449	385	64	12	205	77	3·5
18	692	462	385	64	12	193	77	3·8
19	839	462	436	64	12	180	64	3·5
20	839	462	436	64	12	154	77	3·8
21	795	475	462	64	13	180	64	3·8
22	718	475	359	64	10	180	77	4·0
23	705	436	385	64	12	154	51	3·8
24	744	448	410	64	12	180	64	3·5
25	744	410	385	51	12	154	64	3·8
26	870	564	436	64	11	205	99	4·0
27	832	564	359	90	9	269	77	2.8
28	819	513	359	77	10	244	90	3.3
29	857	538	359	77	11	256	77	3·5
30	844	564	410	77	10	256	77	3·0
31	819	590	410	90	10	231	99	3·5
32	921	692	410	154	6	282	77	1·5
33	883	628	410	77	11	308	90	4·3
34	973	590	410	90	9	231	77	2·8
35	921	538	410	90	10	256	77	3·8
36	896	487	372	77	10	205	99	3·5
37	744	538	385	90	11	231	77	3·8
38	870	513	359	103	10	180	77	3·0
39	744	513	359	77	11	231	77	3·5
40	870	551	410	77	11	256	77	3·5
41	1011	590	487	103	11	308	77	3·8
42	844	538	372	64	12	256	90	3·3
43	870	513	385	90	12	231	77	3·8
44	870	487	398	64	12	205	90	3·0
45	744	423	385	64	10	180	77	3·3
46	808	564	359	90	9	256	90	3·0
47	795	641	385	90	9	256	77	3·8
48	921	564	462	77	11	256	77	3·5
49	896	615	423	77	12	205	51	3·3
50	844	513	372	64	13	205	90	4·3

'eod'

APPENDIX III Data used in morphometric analysis. All gyrogonites were taken from the Upper Jurassic of Portugal (Limestone Horizon).

spec. Nº.	LPA (µm)	LED (µm)	AND (µm)	WS (µm)	NC	AP (µm)	BP (µm)	NR
1	718	590	333	103	8	77	39	3.0
2	551	475	205	77	6	103	51	1.5
3	513	423	218	77	6	141	51	1.8
4	564	487	282	64	8	77	39	3.5
5	590	500	295	77	8	77	26	2.3
6	513	487	218	64	7	128	26	2.8
7	513	462	256	64	7	128	26	1.5
8	513	475	269	64	9	103	26	3.0
9	615	487	308	64	10	77	51	2.3
10	487	436	244	64	8	128	26	3.0
11	551	462	308	64	10	77	51	3.0
12	500	436	231	64	7	77	26	2.0
13	513	449	231	64	9	77	64	2.5
14	577	462	269	103	7	103	39	1.5
15	590	564	295	64	10	128	51	3.5
16	513	423	244	64	9	103	26	2.0
17	615	475	295	64	9	128	51	2.5
18	615	526	308	51	10	90	39	3.0
19	564	423	282	90	8	77	26	2.0
20	538	436	256	77	7	90	26	3.5
21	538	436	244	77	7	128	39	2.0
22	615	462	308	64	9	103	51	3.5
23	487	449	256	77	7	154	51	2.0
24	615	577	282	77	9	128	51	3.5
25	487	436	244	64	9	90	51	3.3
26	500	410	256	64	7	128	26	1.7
27	628	564	308	64	9	103	39	3.0
28	564	487	282	77	9	128	51	3.0
29	538	423	256	64	9	103	26	2.5
30	513	449	205	64	8	103	51	1.7
31	577	475	295	64	9	103	51	2.7
32	538	436	282	64	8	103	51	2.7
33	513	436	231	64	8	103	39	2.7
34	666	564	359	116	7	77	64	3.5
35	526	436	282	51	9	103	51	3.5
36	538	423	269	64	9	103	39	3.0
37	564	462	282	51	10	103	39	3.7
38	590	538	308	90	8	128	51	3.5
39	557	513	273	77	9	128	39	4.3
40	487	487	244	64	8	128	39	3.3
41	487	398	244	64	8	77	51	2.3
42	564	462	256	64	9	128	51	3.5
43	513	487	244	77	7	103	64	2.5
44	538	410	282	77	8	90	39	3.0
45	692	615	333	103	9	103	64	3.5
46	538	449	295	77	8	128	51	2.8
47	423	398	193	64	7	154	51	2.0
48	475	436	205	90	7	128	51	3.0
49	538	475	260	77	8	141	39	3.0
50	513	462	282	64	8	77	39	2.5
51	487	410	244	64	8	103	51	2.5
52	513	449	244	64	7	103	51	3.3
53	526	410	244	64	8	103	77	3.0
54	500	449	244	64	6	103	51	1.7
55	603	462	282	64	9	128	51	2.3
56	410	410	205	64	6	141	39	2.7
57	538	436	282	51	8	128	51	2.3
58	603	475	308	90	8	64	64	3.0
59	500	475	256	64	7	154	39	2.5
60	577	462	282	64	8	103	51	2.7
61	564	500	282	64	9	103	39	2.7
62	500	410	256	77	7	103	51	2.0
63	449	385	231	64	8	128	51	3.0
64	513	359	256	64	7	51	26	2.7
65	577	487	282	64	10	77	51	3.5
66	526	487	282	64	8	128	51	3.5
67	577	487	282	64	9	103	51	3.5
68	475	436	244	51	9	141	26	3.0
69	538	526	282	77	8	128	26	3.0
70	538	436	269	64	6	103	64	2.0
71	557	475	282	51	9	90	39	3.5
72	557	462	269	77	8	128	39	2.5
73	423	513	205	51	9	103	51	2.0
74	564	487	244	90	7	128	39	2.7
75	500	462	244	64	6	128	51	3.5
76	526	423	269	64	8	77	26	3.3
77	564	526	282	64	8	103	39	3.0
78	564	462	295	64	9	77	51	3.7
79	577	410	282	64	8	103	51	3.0
80	513	475	244	64	8	128	39	3.5
81	718	590	359	64	10	103	51	3.5
82	628	526	308	64	8	90	26	3.5
83	500	449	231	64	9	116	39	3.5
84	641	564	308	64	9	116	64	3.0
85	538	487	256	64	8	103	39	3.0
86	564	513	282	77	6	141	51	2.0
87	666	513	346	77	9	128	51	3.5
88	513	410	231	51	8	116	51	3.0
89	500	462	231	64	9	116	39	3.5
90	462	436	218	51	7	128	39	2.5
91	615	513	321	64	6	154	51	2.0
92	475	410	231	51	8	103	39	2.7
93	462	449	218	64	8	128	51	3.5
94	410	398	205	51	9	90	51	3.3
95	653	564	333	64	8	141	51	3.0
96	590	423	295	77	8	128	26	3.7
97	500	385	244	46	9	128	51	2.5
98	500	410	256	51	10	103	51	2.7
99	590	436	282	64	12	103	51	2.7
100	487	372	231	46	10	97	51	2.0

Appendix IV Classification of the extant genera of the family Characeae

The levels of taxa at or above order follow Mattox and Stewart (1984).

Division	Chlorophyta
Class	Charophyceae
Order	Charales
Family	Characeae Agardh
Subfamily 1.	Chareae (Leonh.) Zanev
Genera	Chara L.
	Lamprothamnium Groves
	Nitellopsis Hy
	Lychnothamnus (Rupr.)Leonh.
Subfamily 2.	Nitelleae Gant.
Genera	Nitella Agardh
	Tolypella Braun
Sections of genus Tolypella	a. Acutifolia Allen
	b. Obtusifolia Allen

Appendix V Species mentioned in the text

Chara delicatula Agardh
Chara fibrosa Agardh
Chara hispida L.
Chara zeylanica Willd.
Clavator reidi Groves
Lamprothamnium papulosum Groves
Musacchiella douzensis Feist & Grambast-Fessard
Musacchiella maxima (Donze) Feist & Grambast-Fessard
Musacchiella palmeri Feist & Grambast-Fessard
Musacchiella sardiniae Colin
Nitella opaca Agardh
Nitella translucens Agardh
Porochara arguta (Peck) Grambast
Porochara jaisalmerensis (Bhatia and Mannikeri) Feist and Grambast-Fessard
Porochara kimmeridgensis Mädler
Porochara minima (Mädler) Shajkin
Porochara minsinae Shajkin
Porochara mundula (Peck) Grambast
Porochara obovata (Peck) Saidakovsky
Porochara polyspirator (Mádler) Shajkin
Porochara portoensis n.sp.
Porochara raoi (Bhatia and Mannikeri) Feist and Grambast-Fessard
Porochara raskyae (Mádler)
Porochara rotunda (Peck) Shajkin
Porochara sahnii (Bhatia and Mannikeri) Feist and Grambast-Fessard
Porochara sublaevis (Peck) Grambast
Porochara westerbeckensis (Mädler)
Psilochara undulata (Pia) Grambast
Rantzieniella nitida Grambast
Saportonella maslovi Grambast
Sphaerochara edda Soulié-Märsche
Stellatochara höllvicensis Horn af Rantzien
Stomachara moreyi Peck
Trochiliscus podoliscus Croft

STUDIES ON LIVING AND FOSSIL CHAROPHYTE OOSPORANGIA

by

Andrew Leitch

Thesis submitted for the Degree of

Doctor of Philosophy at the

University of Bristol

July, 1986

Plates

PLATE 1

Fig. 1 Transverse section of a young branchlet of Chara delicatula, showing 3 stages in gametangial development at 3 successive nodes. Note the internode (i) and node (a,b,c) sequence of the branchlet.

a. The peripheral cell at the node has enlarged and an apical cell, the male gametangial primordium (m) has been cut off. Note the 2 telophasic nuclei (n) in the subapical cell.

b. A row of 3 cells is formed at the node; the male gametangial primordium (m), the gametangial node (g) and the basal cell (b).

c. The first cell cut off at the gametangial node is the oosporangial primordium (op) and it faces away from the main axis.

All the cells have small vacuoles (v) containing flocculent matter.
T.E.M. x1,340.

Fig. 2 Section showing an enlarged and highly vacuolate oosporangial primordium (op) and a male gametangial primordium (m). The vacuoles (v) contain flocculent matter and are often seen with internal tonoplast membranes (arrows). Note the multicellular nature of the node; cell (c) is involved in branchlet cortication and cell (b) will form a bracteole. Chara delicatula, T.E.M. x1,150.

Fig. 3 Section showing developing gametangia. Note the oosphere mother cell (o), the oosporangial node (n), the pedicel cell (p) and the characteristic curved walls between the cells. Initial development of the male gametangial primordium (m) and the branchlet cortication (c) has commenced. Note also the large vacuole (v) in the basal cell. Chara delicatula, L.M. x400.

Fig. 4 Section through a cell undergoing cytokinesis. Note the cell plate (p), its centripetal development and 2 well separated telophasic nuclei (n). Chara delicatula, T.E.M. x7,300.

Fig. 5 Section showing cell plate formation. The cell being cut off is the oosporangial primordium (op). Note the abundance of dictyosomes (d), the initial signs of plasmodesmata (p), and the association of endoplasmic reticulum (er) with the cell plate.
Chara delicatula, T.E.M. x10,700.

1
a
b
c
m
n
g
op
i
h
v
2
m
c
op
h
v
3
m
o
n
p
c
v
4
n
p
h
5
n
op
p

PLATE 2

Fig. 1 Section showing a developing oosporangium. Note the oosphere mother cell (o), the oosporangial node (n) and the pedicel cell (p). There is a nucleolus (nu) in the oosporangial node. Chara delicatula, T.E.M. x2,000.

Fig. 2 Section showing a developing oosporangium. Note that the nuclear envelope in the oosporangial node (n) has dispersed and that the organelles are at the periphery of the cell (arrows). Chara delicatula, T.E.M x1,700.

Fig. 3 Section of an oosporangial node undergoing cell division. The chromosomes (c) are arranged on the metaphase plate. Note that there are no signs of any microtubules. Chara delicatula, T.E.M. x14,100.

Fig. 4 Increased magnification of the oosporangial node depicted in Fig. 2. Note the metaphase chromosomes (c). Chara delicatula, T.E.M. x6,100.

Fig. 5 Section of a developing oosporangium showing the oosphere mother cell (o), the pedicel cell (pc) and two peripheral cells (p) cut off at the oosporangial node. Note the large nucleolus (n). Chara delicatula, T.E.M. x1,710.

Fig. 6 Section of a developing oosporangium showing the oosphere mother cell (o), the pedicel cell (pc) and 3 peripheral cells (p) cut off at the oosporangial node. Chara delicatula, T.E.M. x1,350.

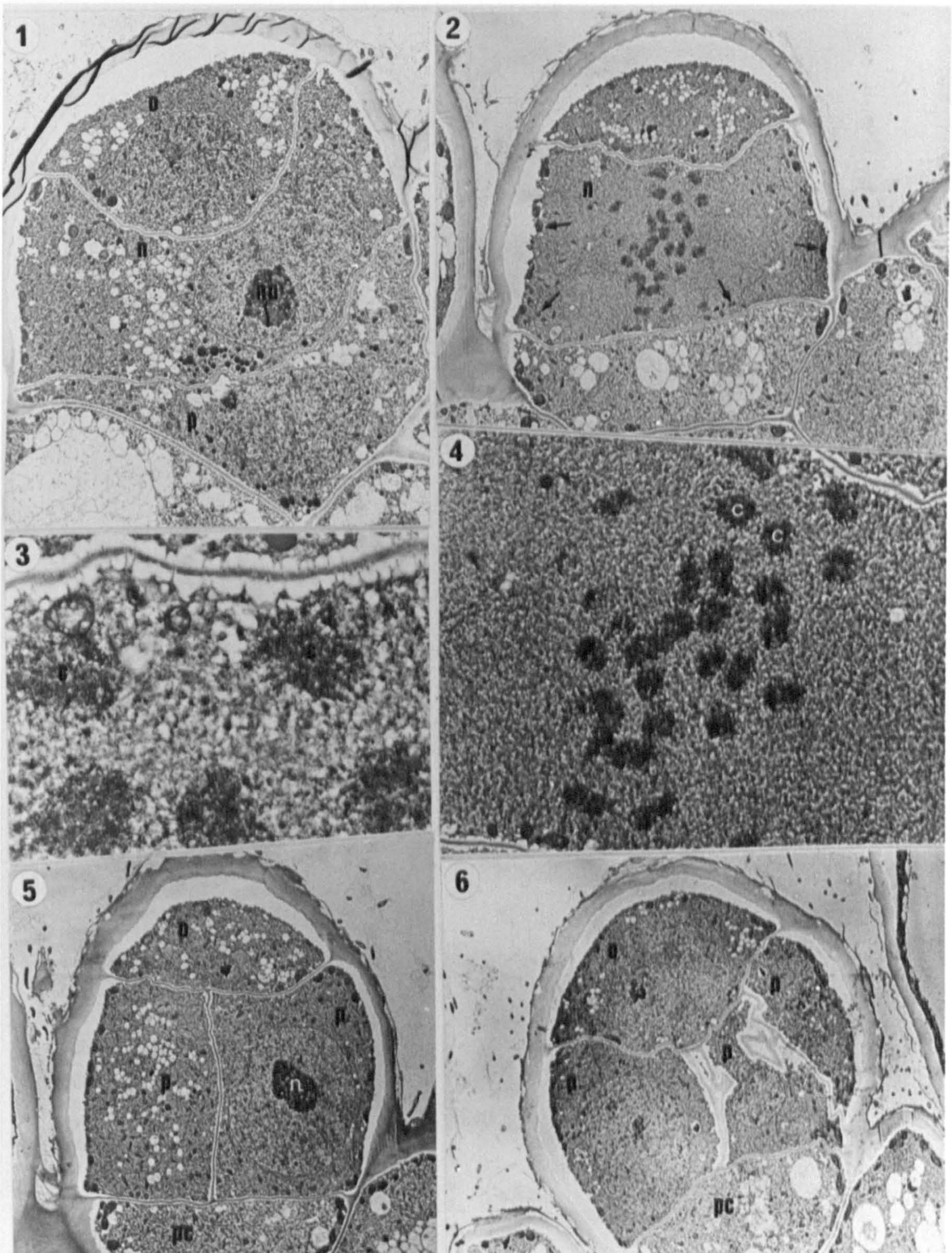
1
D
n
nu
R
2
n
4
C
C
3
C
5
p
n
p
n
pc
6
p
p
p
n
pc

PLATE 3

Fig. 1 Section through a young oosporangium showing the elongating spiral cells (s), the central cell (cc), the oosphere mother cell (omc) and the pedicel cell (pc). Note the vacuoles (v) in all the cells and the prominent nucleoli (n). Chara delicatula, T.E.M. x2,500.

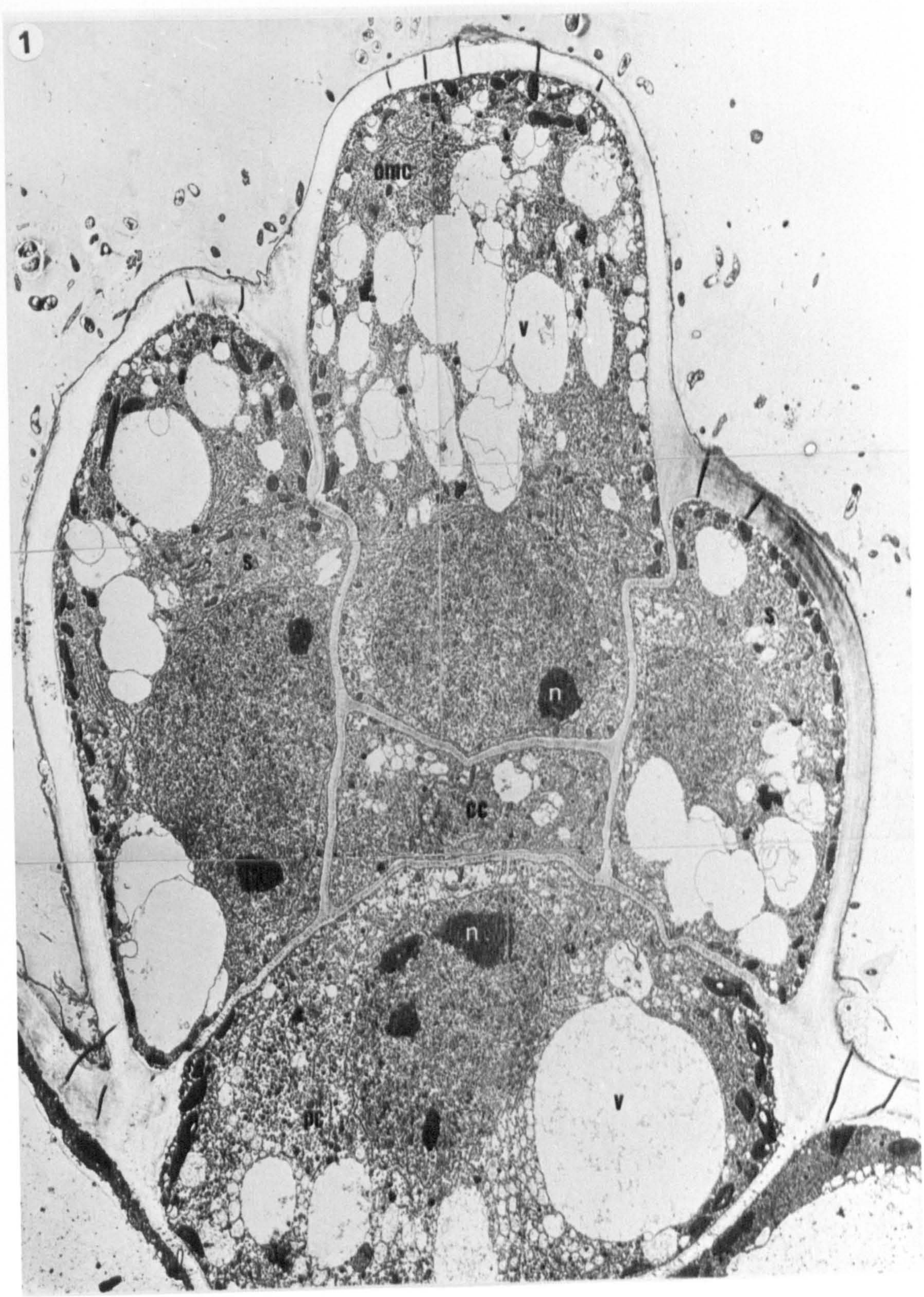
1
OMC
V
S
n
CC
n
V
PC

PLATE 4

Fig. 1 Section through a developing oosporangium showing coronula cells (c), the spiral cells (s) and the oosphere mother cell (om). Note the male gametangium (m) and the branchlet cortication (bc). Chara delicatula, L.M. x200.

Fig. 2 Critical point dried oosporangium at the same stage of development as the specimen shown in Fig. 1 above. Note the spiral cells (s), the coronula cells (c) and the male gametangium (m). Chara delicatula, S.E.M. x250.

Fig. 3 Section through a developing oosporangium. Note the sterile cell (sc) at the base of the oosphere (o). Chara delicatula, L.M. x200.

Fig. 4 Critical point dried specimen of an oosporangium at a similar stage of development as the specimen shown in Fig.3 above. Note the spiral cells (s) and the coronula cell (c). Chara delicatula, S.E.M. x250.

Fig. 5 Section through a developing oosporangium. The oosphere (o) has accumulated storage products and the oosporangium has become more rounded. Note the basal nucleus (n) in the oosphere, the sterile cell (sc) and the central cell (cc). Chara delicatula, L.M. x200.

Fig. 6 Critical point dried oosporangium (o) of Chara hispida. Note that with the accumulation of storage products the oosporangium becomes more rounded. Note the male gametangium (m), the branchlet cortication (bc) and the coronula cells (c). S.E.M x80.

Fig. 7 Critical point dried oosporangium of Chara hispida showing that with further accumulation of storage products the oosporangium (o) becomes more rounded. Note the bract cells (b) and the bracteole (br). Chara hispida, S.E.M. x60.

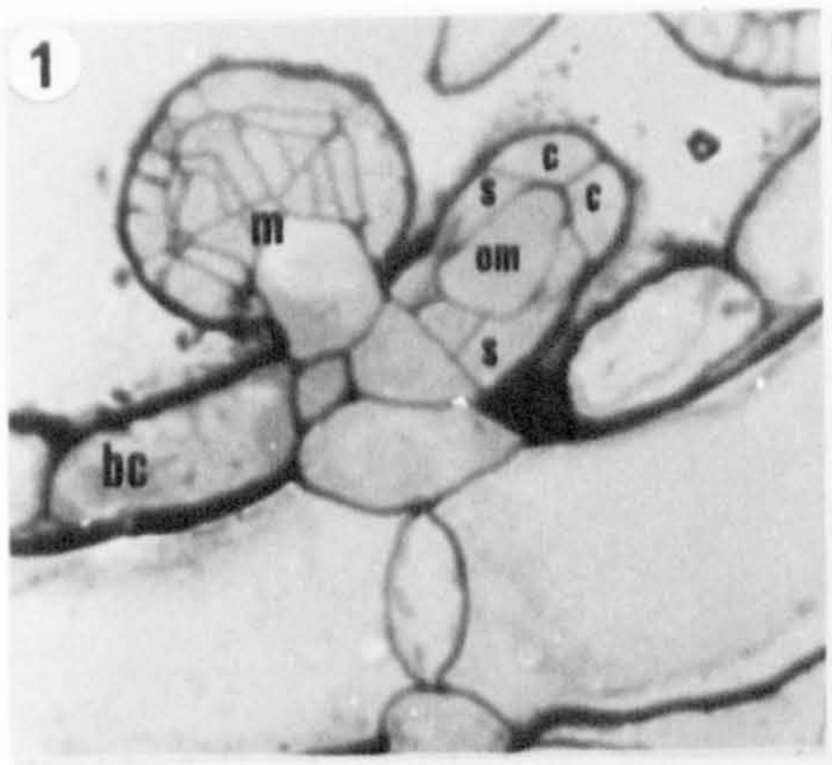
1
m
c
s
c
om
s
bc

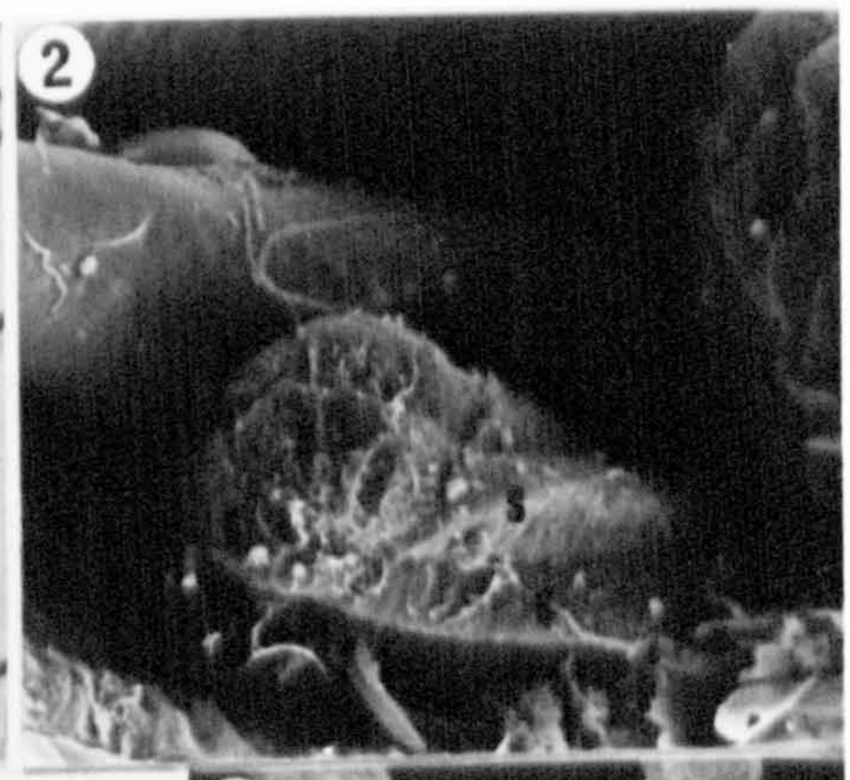
2
s


3
sc

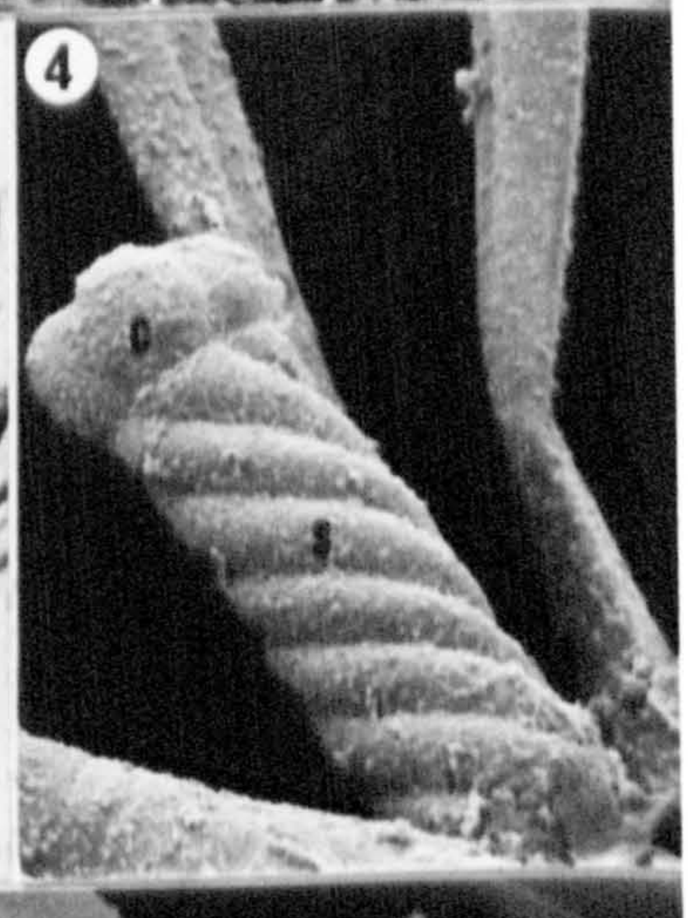
4
c
s

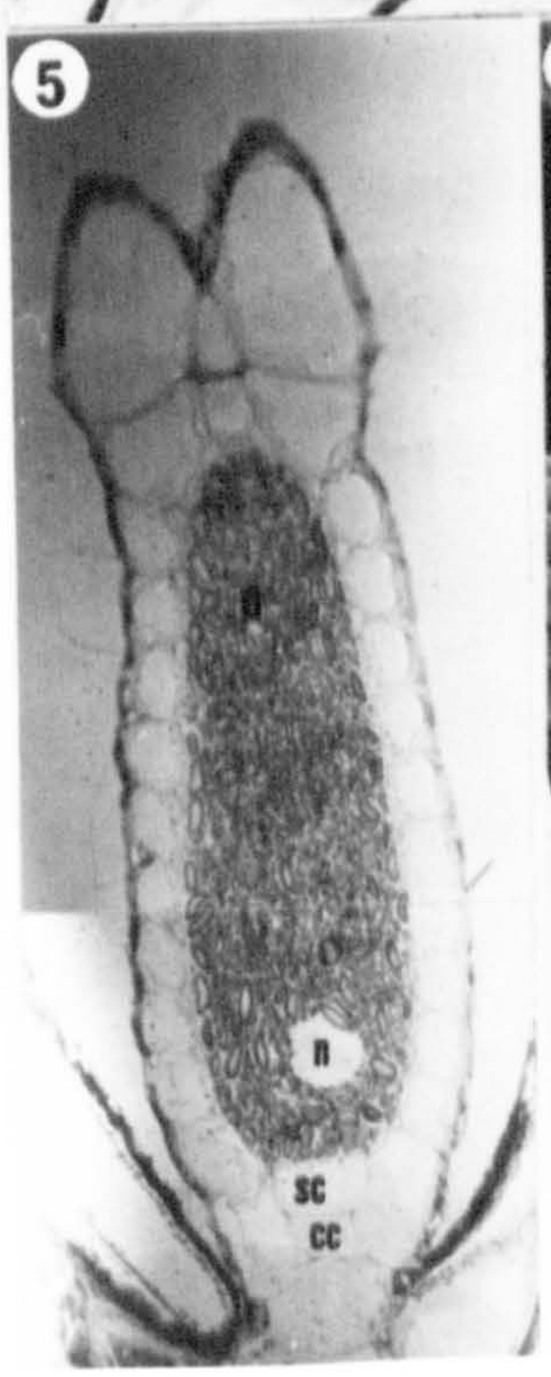
5
n
n
sc
cc

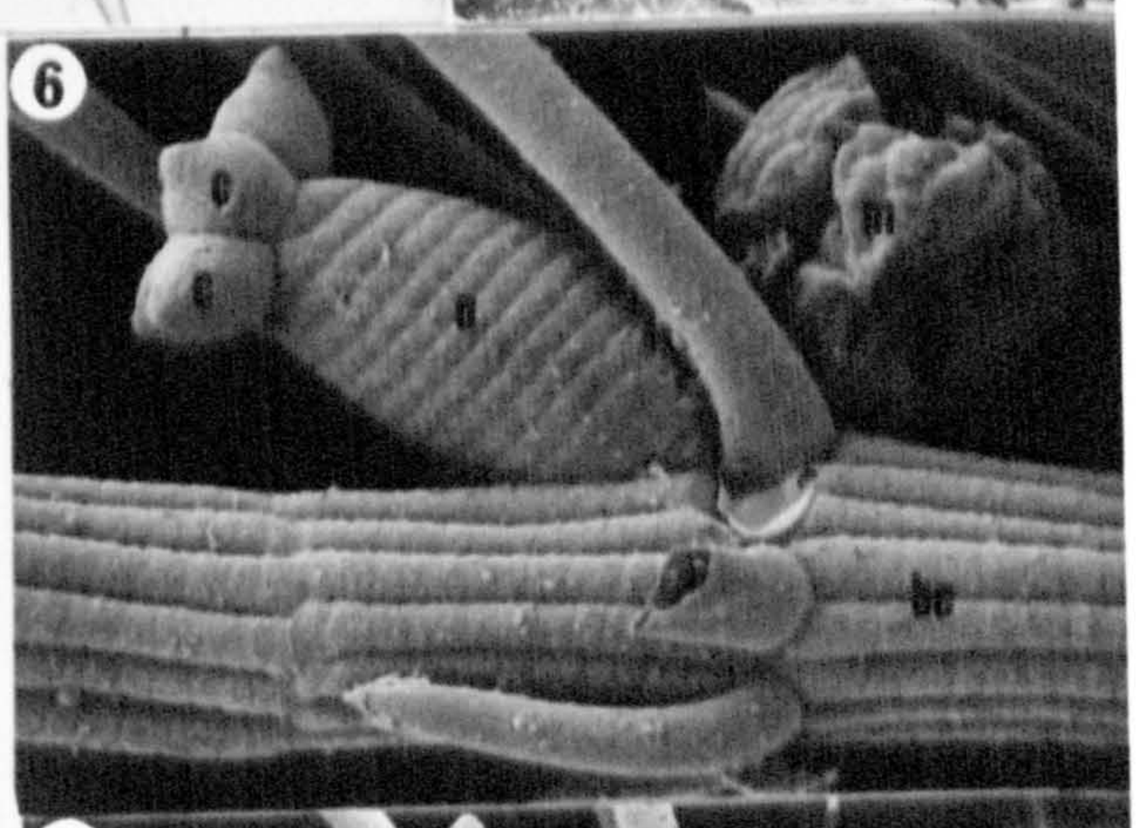
6
c
n
bc

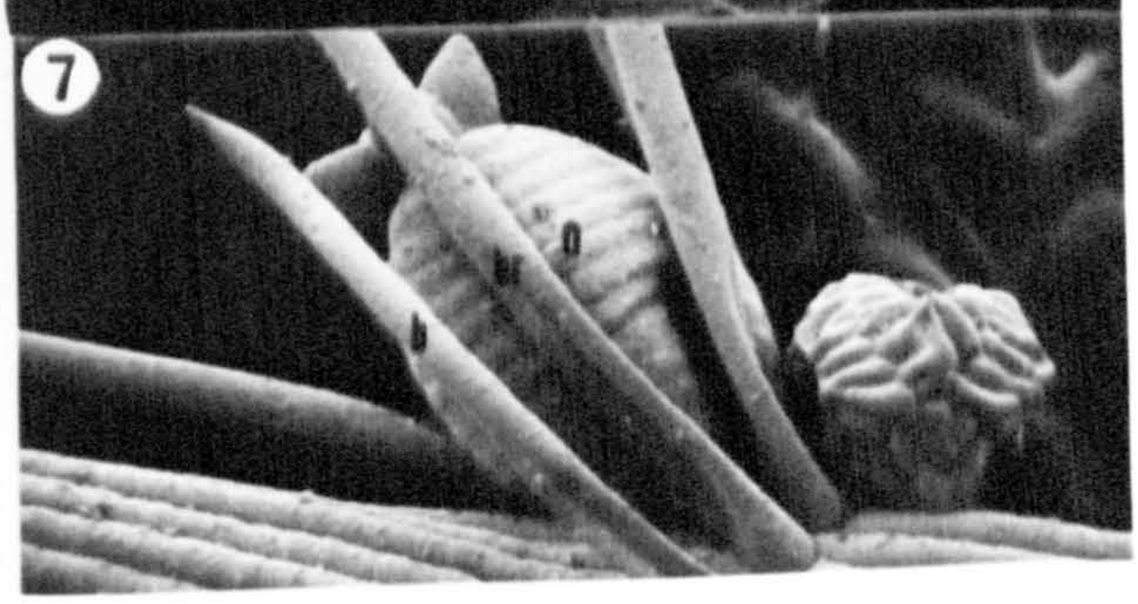
7
c
bc

PLATE 5

Fig. 1 Section through a developing oosporangium. Note the oosphere is accumulating storage products and has large starch grains (s). The spiral cells (sp) and the sterile cell (sc) are highly vacuolate and organelles are at the cell periphery. The intercellular space (i) between the spiral cells and the oosphere is triangular in section. Note the central cell (cc) and the pedicel cell (pc). Chara delicatula, T.E.M. x 1,190.

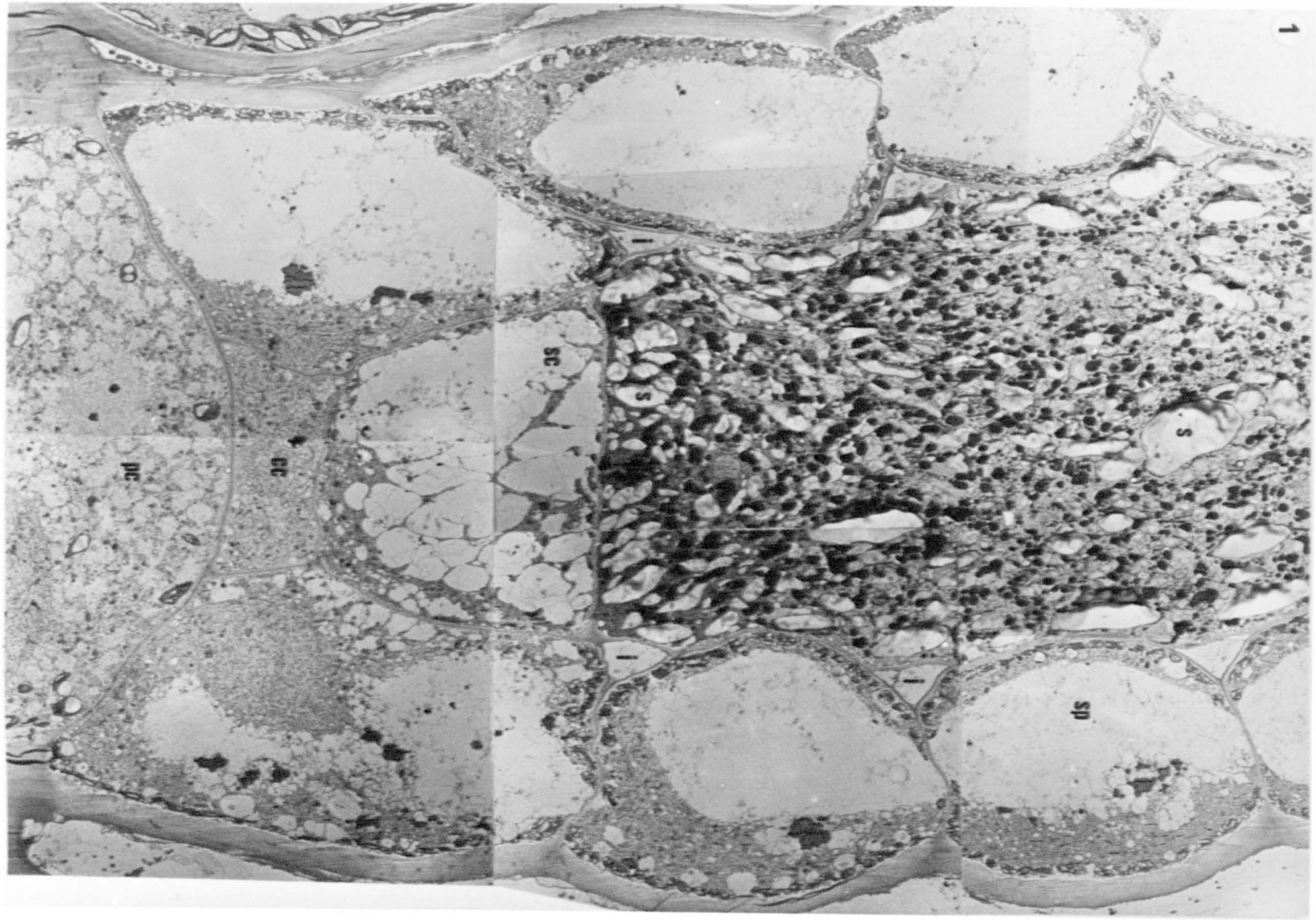
1
S
sp
sc
sc
B

PLATE 6

Fig. 1 Section showing the wall between an early oosphere mother cell (omc) and the oosporangial node (n). Note the wall has plasmodesmata (p) and that the oosphere mother cell proplastids have agranal thylakoids (arrow). Note also the vacuoles (v) containing flocculent matter. Chara delicatula, T.E.M. x13,550.

Fig. 2 Section through an oosphere mother cell (omc) showing proplastids (p). Chara delicatula, T.E.M. x23,800.

Fig. 3 Section through a young oosporangium showing an oosphere mother cell (omc) and spiral cell (s). Compare the proplastids (p) in the oosphere mother cell which have only vestigial thylakoids (arrows) with the chloroplasts (c) in the spiral cell (s) which have agranal thylakoids (arrow).,Chara delicatula, T.E.M. x13,000.

Fig. 4 Section through a developing oosporangium showing a spiral cell (sc) and an oosphere (o). The chloroplasts in the spiral cell have a few small grana (g). The plastids in the oosphere have vestigial thylakoids (t) and show early stages in starch accumulation (s). Note the mitochondria (m) and the plastoglobular droplets (p). Chara delicatula, T.E.M. x19,000.

Fig. 5 Section through an oosphere (o) and a sterile cell (sc). Note the plasmodesmata (arrows) between the two cells and the vacuoles (v) in the oosphere. The plastids in the oosphere have differentiated into "dumb-bell" shaped amyloplasts that accumulate starch (s). Chara delicatula, T.E.M. x18,200.

Fig. 6 Section through an oosphere (o) and its ensheathing spiral cells (sp). The spiral cell chloroplasts have plastoglobular droplets (p). The oosphere has amyloplasts (a) and sphaerosomes (s). Note the intercellular space (i) containing flocculent matter. Chara delicatula, T.E.M. x21,800.

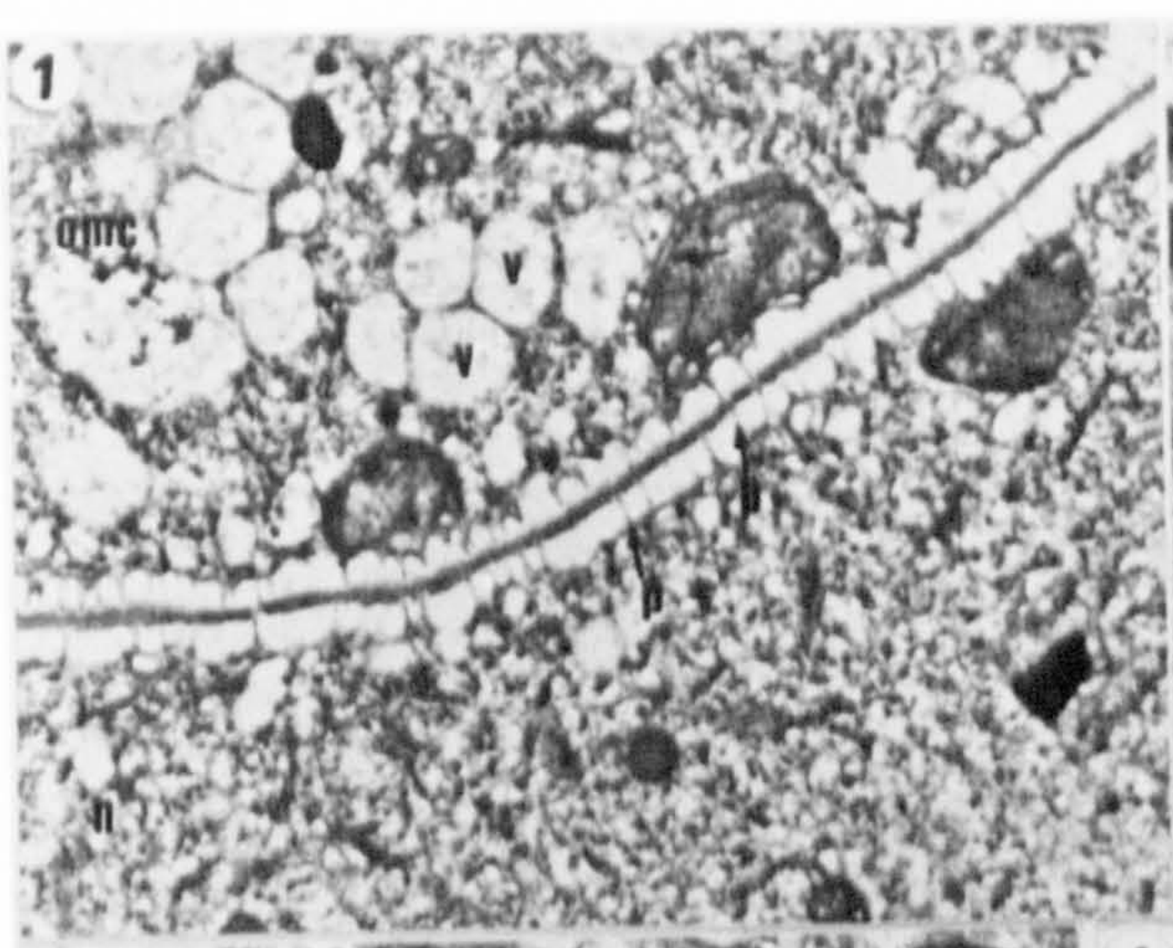
1
omc
v
v
n

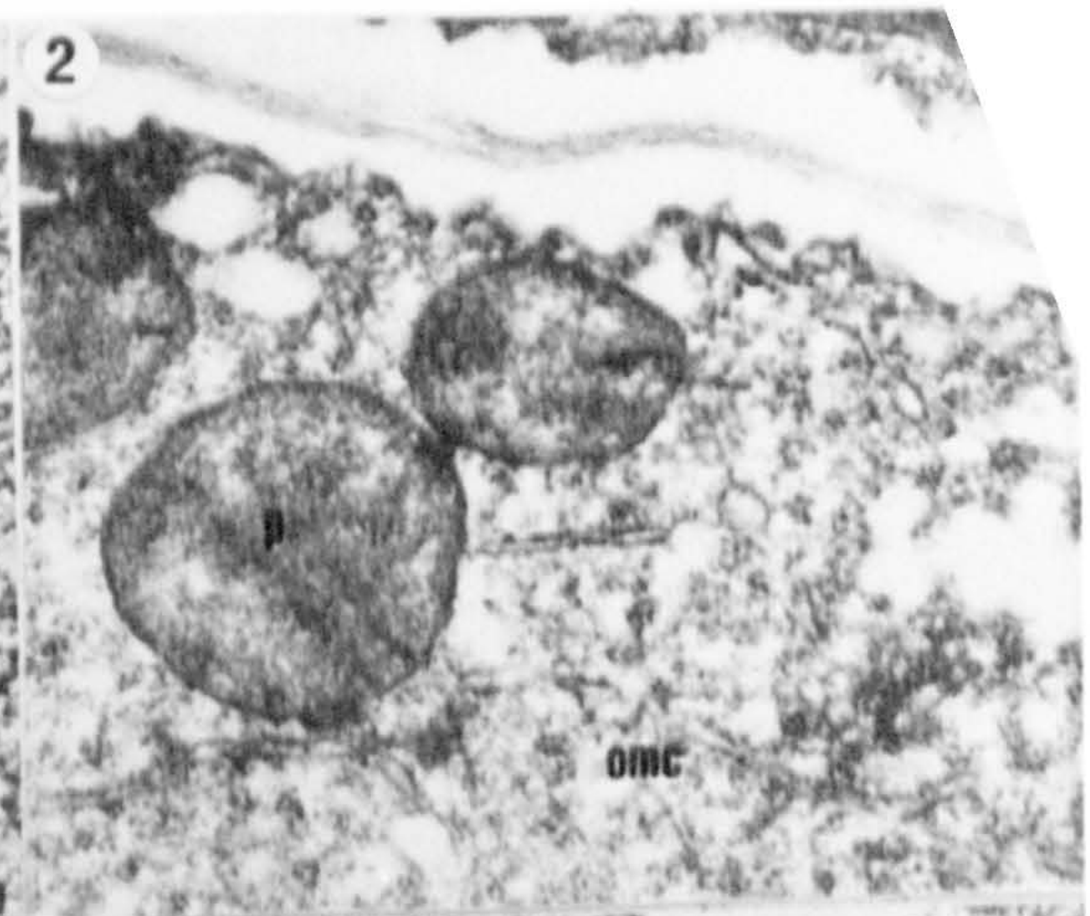
2
p
omc

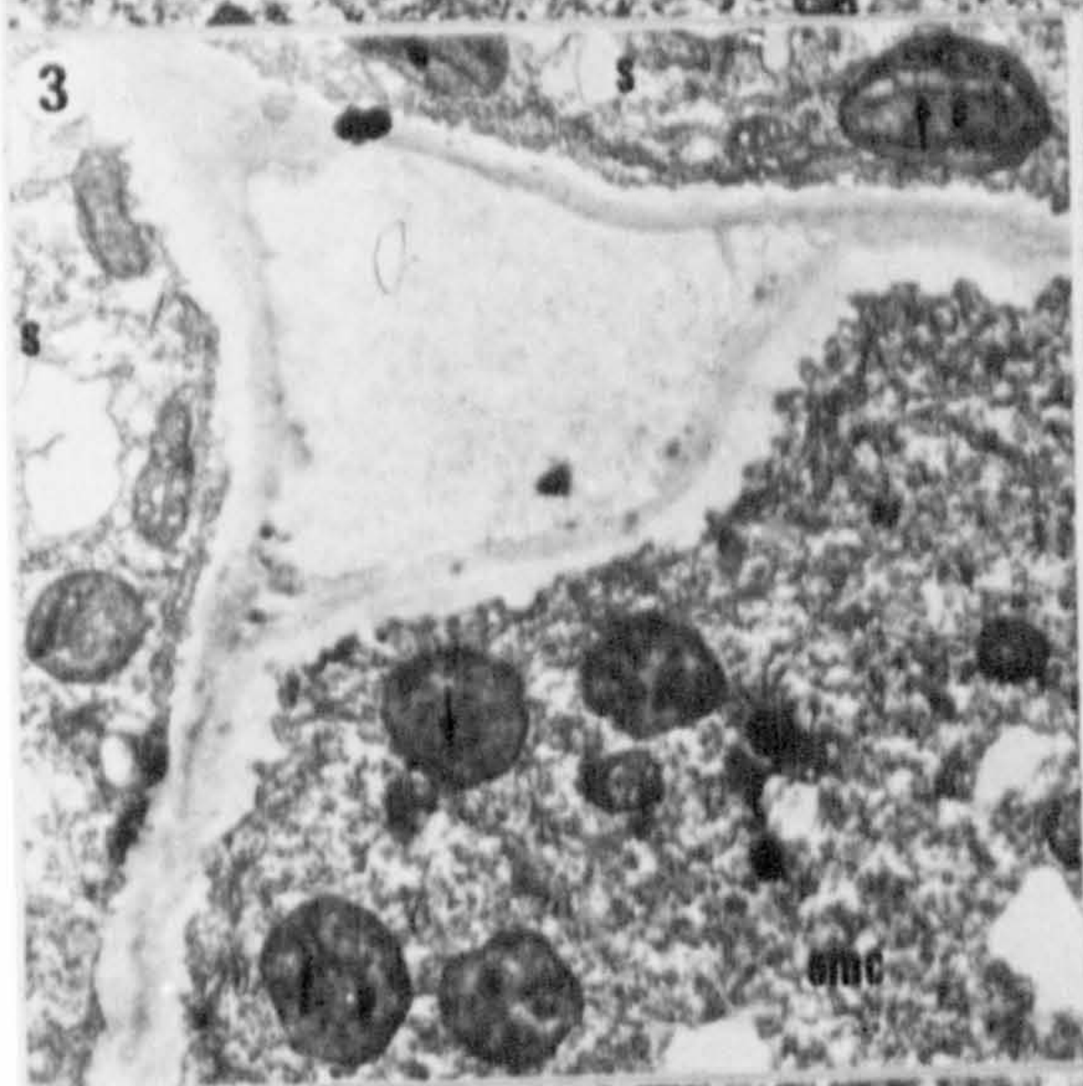
3
s
s
omc


4
sc
o

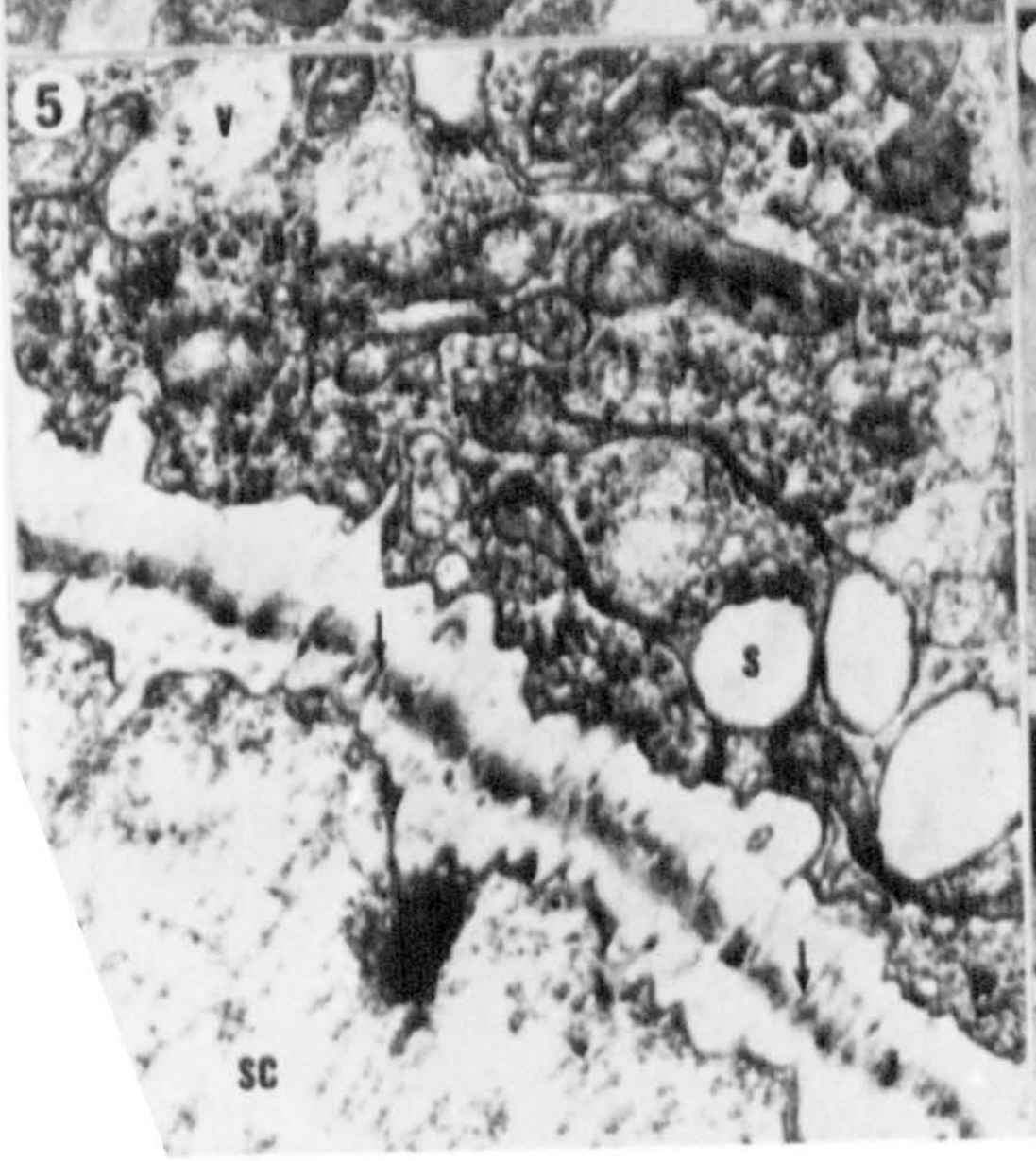
5
v
s
SC


6
sp
l
a
s
o

PLATE 7

Fig. 1 Section through a young oosphere of Chara delicatula. Note the sphaerosomes (s) and the amyloplasts (a) which contain stored starch (st). Chara delicatula, T.E.M. x13,550.

Fig. 2 Section through a young oosphere of Chara delicatula showing sphaerosomes (s) associated with endoplasmic reticulum (er). Chara delicatula, T.E.M. x23,800.

Fig. 3 Section showing a coronula cell (c) and its subtending spiral cell (sc). Note the similarity in the chloroplasts between the two cells. Both have thylakoids, grana (g), plastoglobular droplets (p) and starch grains (s). The mitochondrium (m) in the spiral cell has cristae. Chara delicatula, T.E.M. x19,000.

Fig. 4 Section showing two coronula cells (c) with their subtending spiral cells (sc). The spiral cell chloroplasts have grana (g) and starch grains (s). Note the mitochondrium (m). Chara delicatula, T.E.M. x19,000.

Fig. 5 Longitudinal section through simple, unbranched plasmodesmata (p). Chara delicatula, T.E.M. x30,000.

Fig. 6 Longitudinal section showing branched, anastomosing plasmodesmata (p) between vegetative cells of Nitella opaca. Note the median sinus (s). T.E.M. x32,100.

Fig. 7 Transverse section through simple unbranched plasmodesmata (p). Chara delicatula, T.E.M. x28,200.

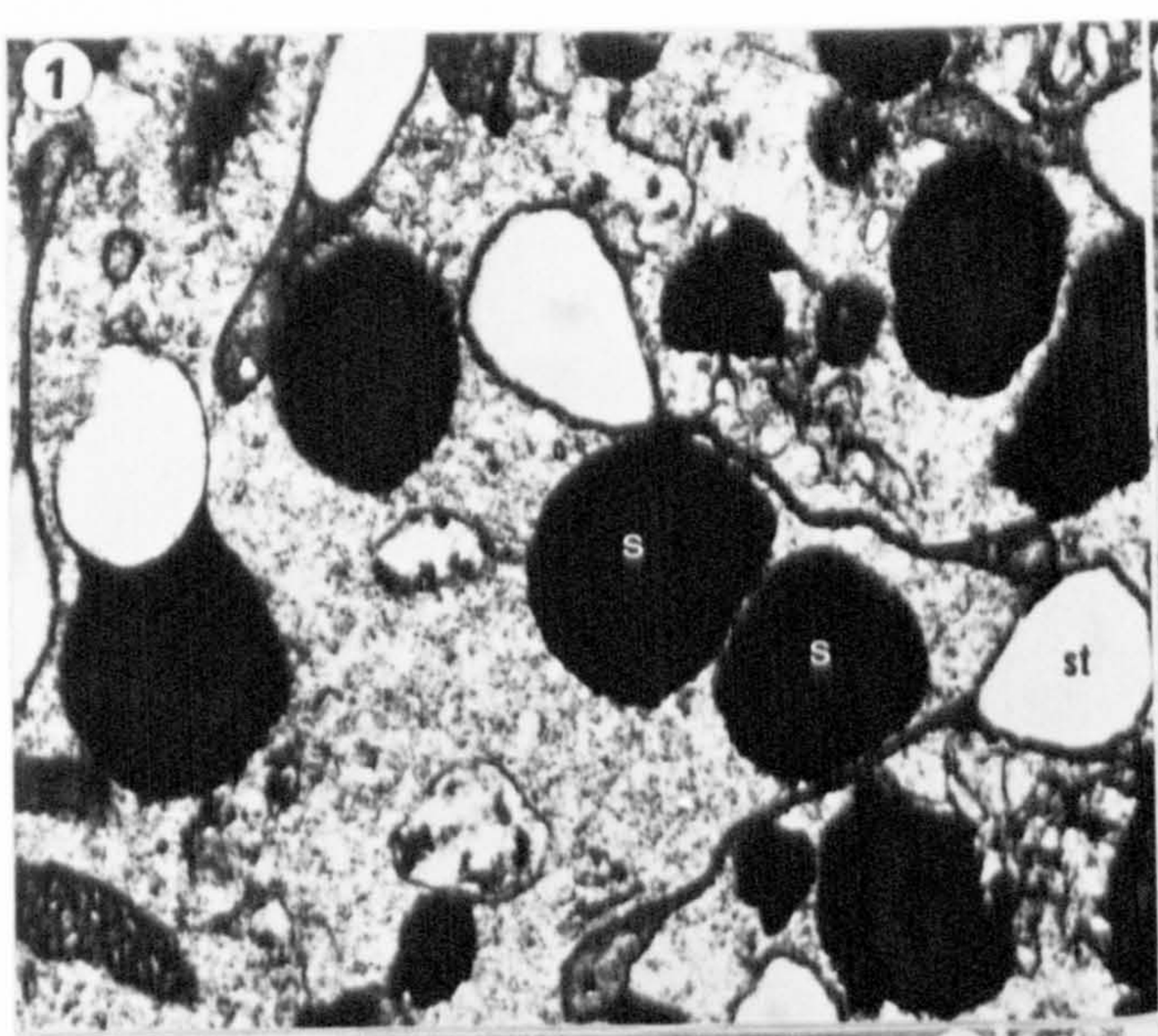
1
s
s
st

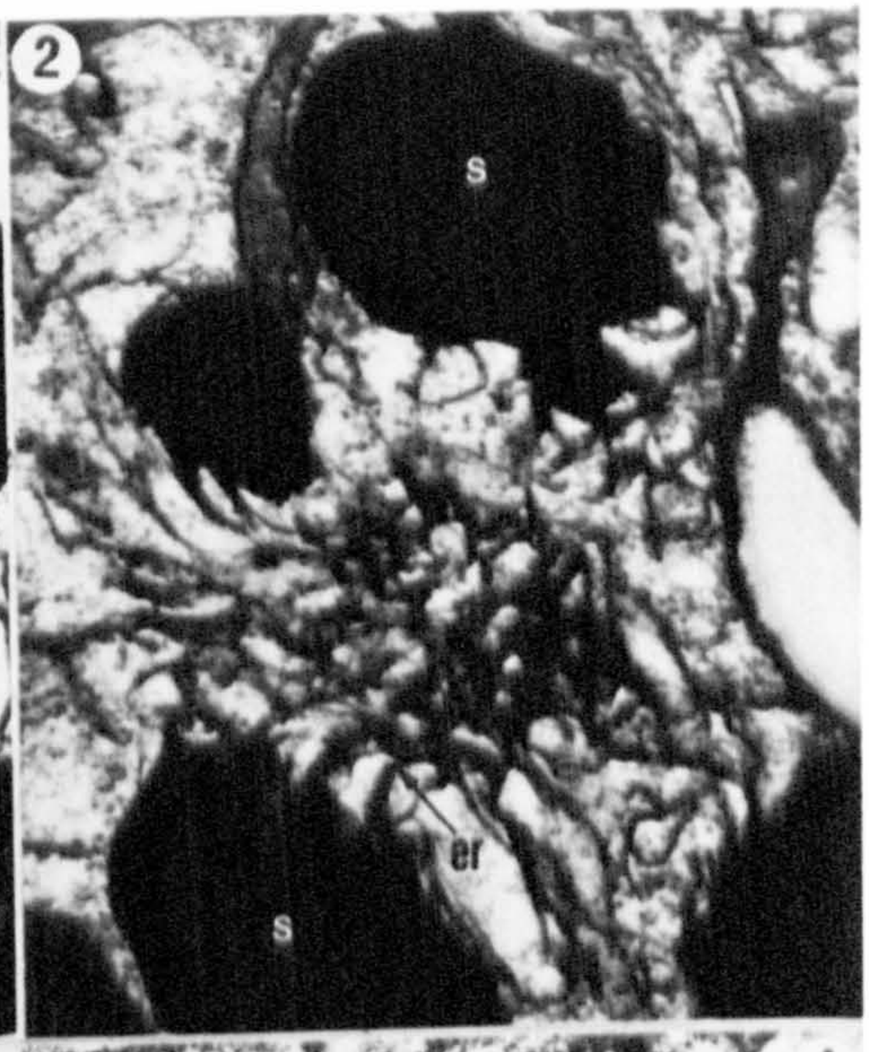
2
s
er
s


3
s
p
p
SC
m
s
c


4
c
SC
s
c
SC

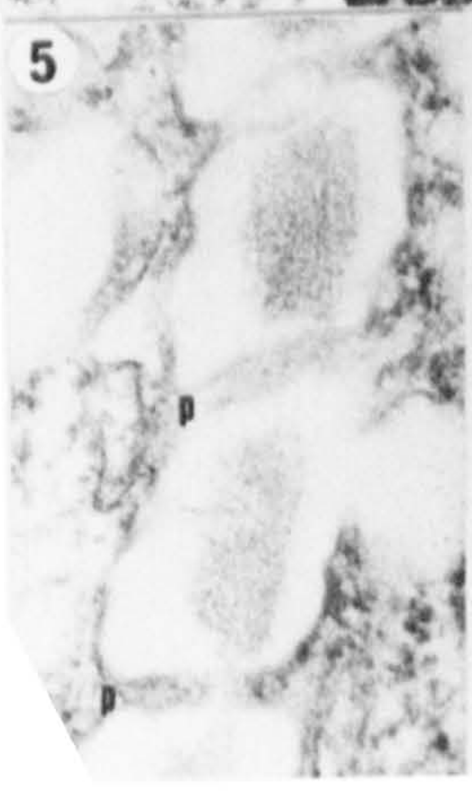
5
p

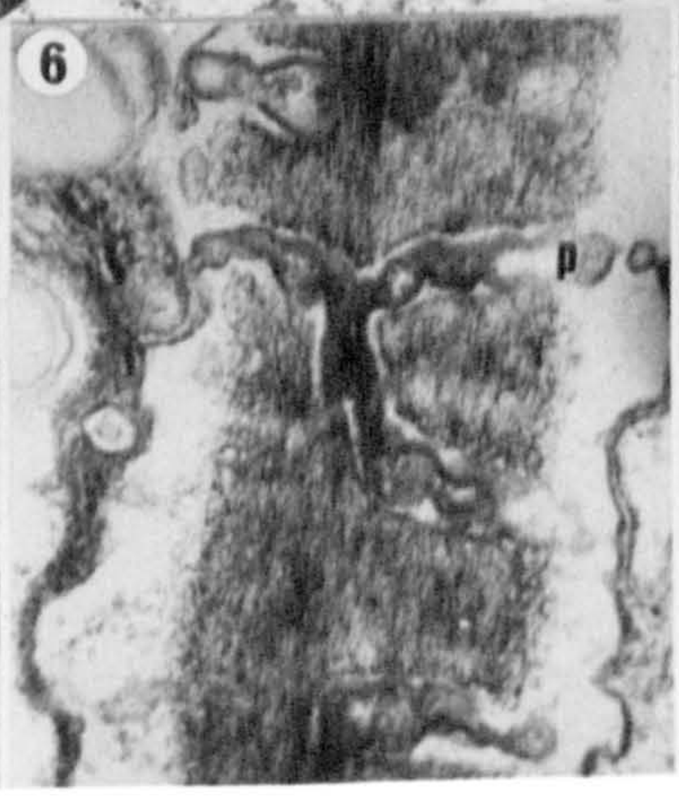
6
p

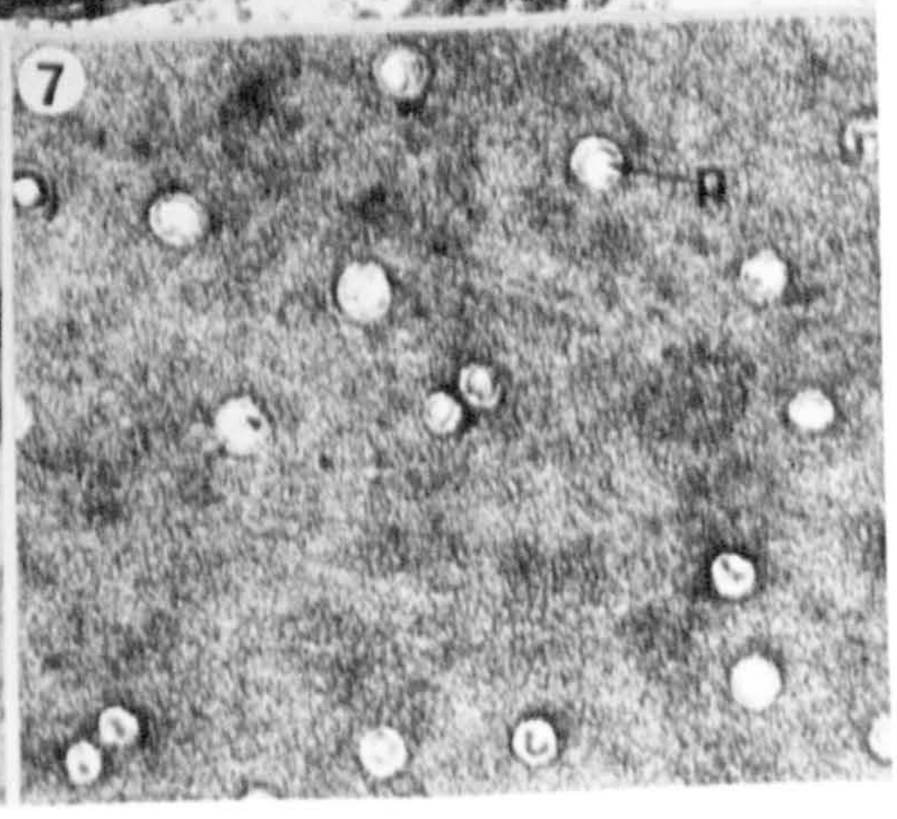
7
p

PLATE 8

Fig. 1 Section through a mature oosphere; organelles are pushed between the large sphaerosomes (sp). The electron transparent area (t) is probably artifactual. Chara delicatula,T.E.M. x19,000.

Fig. 2 Section through a mature oosphere. Note the starch grains (st), the sphaerosomes (sp) and the mitochondrium (m) with ill defined cristae. Chara delicatula, T.E.M. x19,000.

Fig. 3 Section through a mature oosphere. Note the starch grain (st), the sphaerosome (sp) and the endoplasmic reticulum (er). The mitochondria show cristae (arrows). Chara delicatula, T.E.M. x19,000.

Fig. 4 Section through a mature oosphere, organelles are pushed into the interstitial spaces between extremely large starch grains (st). Note the mitochondrium (m). Chara delicatula, T.E.M. x19,000.

Fig. 5 Apical fertilisation zone (f) of the oosphere is devoid of amyloplasts (a) and sphaerosomes (sp). Chara delicatula, T.E.M. x7,950.

Fig. 6 Section showing the apical fertilisation zone (f) of the oosphere (o). The intercellular space (i) between the oosphere and spiral cells (s) is largest above the fertilisation zone. Chara delicatula, L.M. x 1,500.

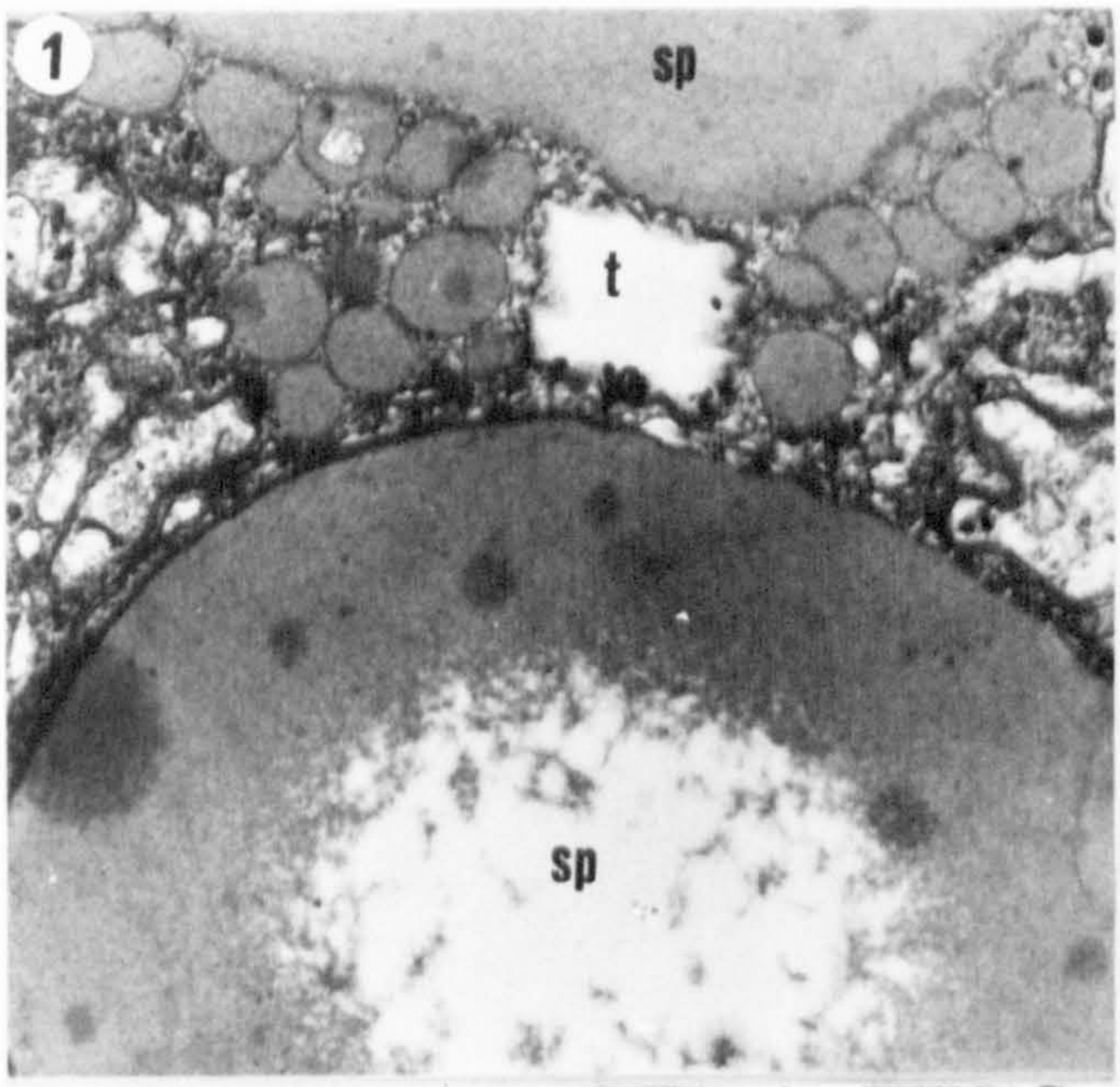
1
sp
t
sp

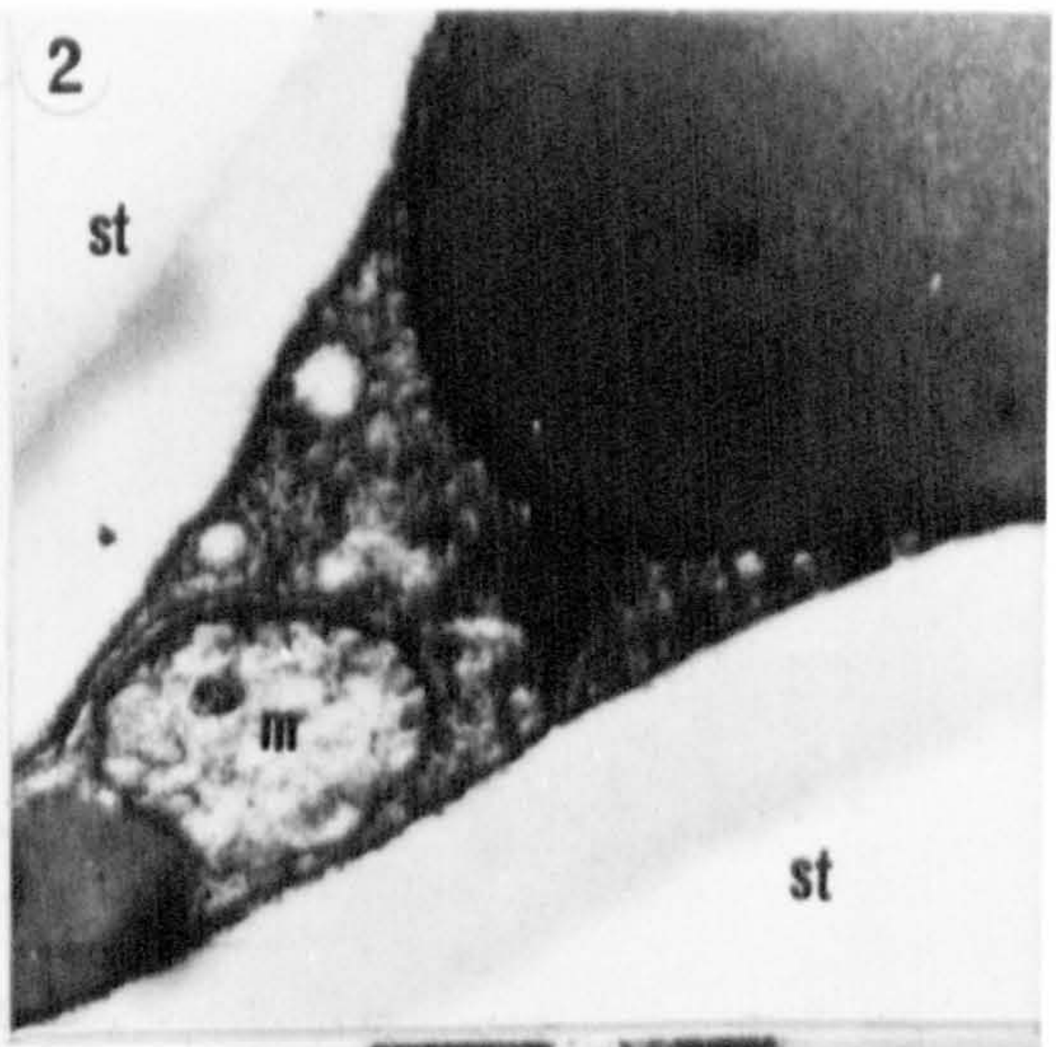
2
st
m
st

3
st
er


4
st
st

5
sp

6
s

PLATE 9

Fig. 1 Critical point dried thallus of Nitella opaca showing the apical region with a number of developmental stages in oosporangial ontogeny. These stages range from an oosporangial primordium (p) to a fully developed, unfertilised oosporangium (o). S.E.M. x700.

Fig. 2 Section through an oosporangium of Nitella opaca showing the accumulated reserves in the oosphere (o). Note the two sterile cells (s), each with peripheral chloroplasts (c). T.E.M. x 1,300.

Fig. 3 Critical point dried oosporangium of Nitella opaca. Note there are 2 coronula cells (c) per spiral cell (s) at the apex of the oosporangium. S.E.M. x700.

Fig. 4 Critical point dried oosporangium of Chara delicatula. The oosporangium is fully developed and unfertilised. Note the fertilisation slits (f), the elongate bracteoles (b) and the branchlet cortication (bc). S.E.M. x80.

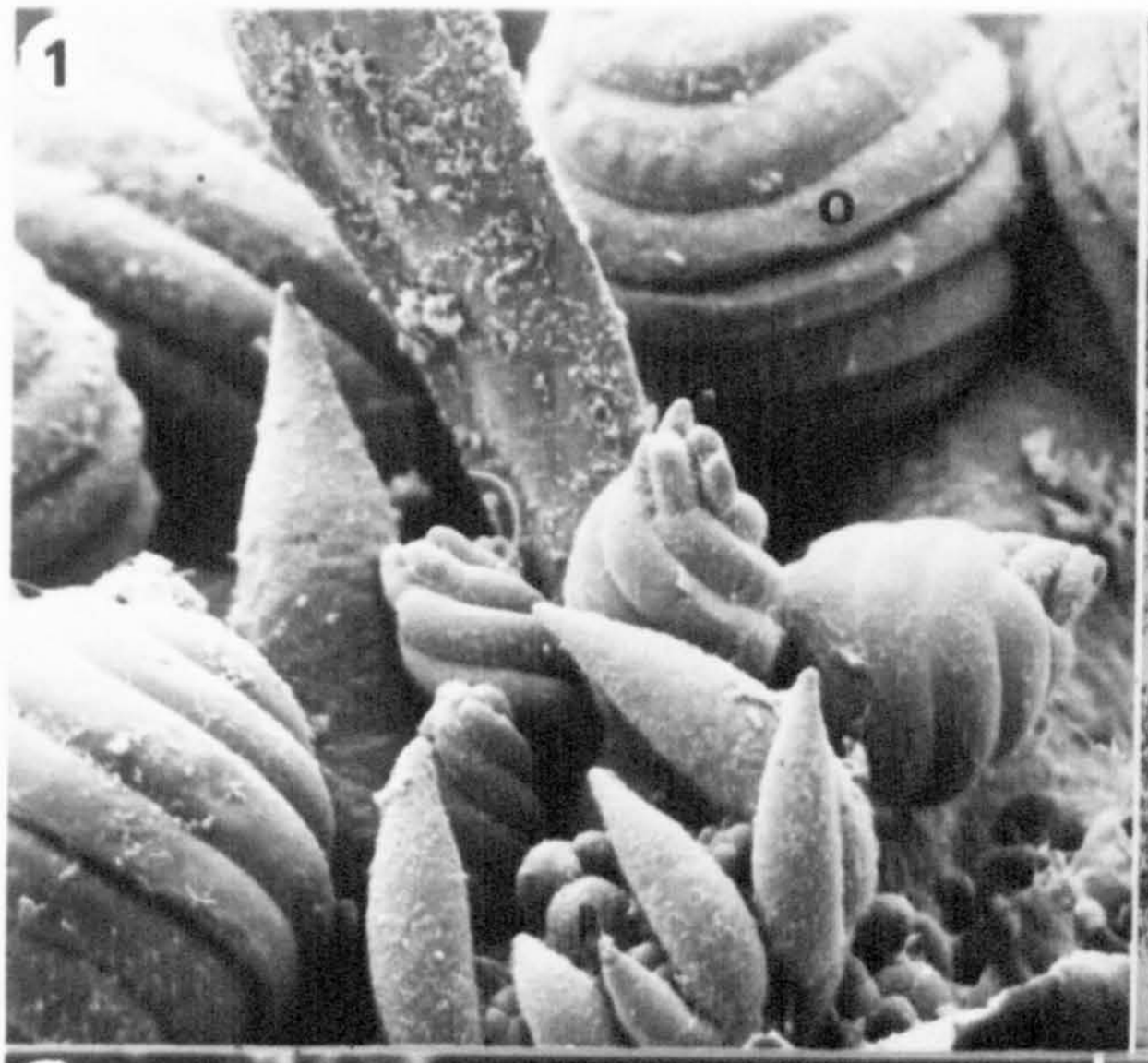
1
O

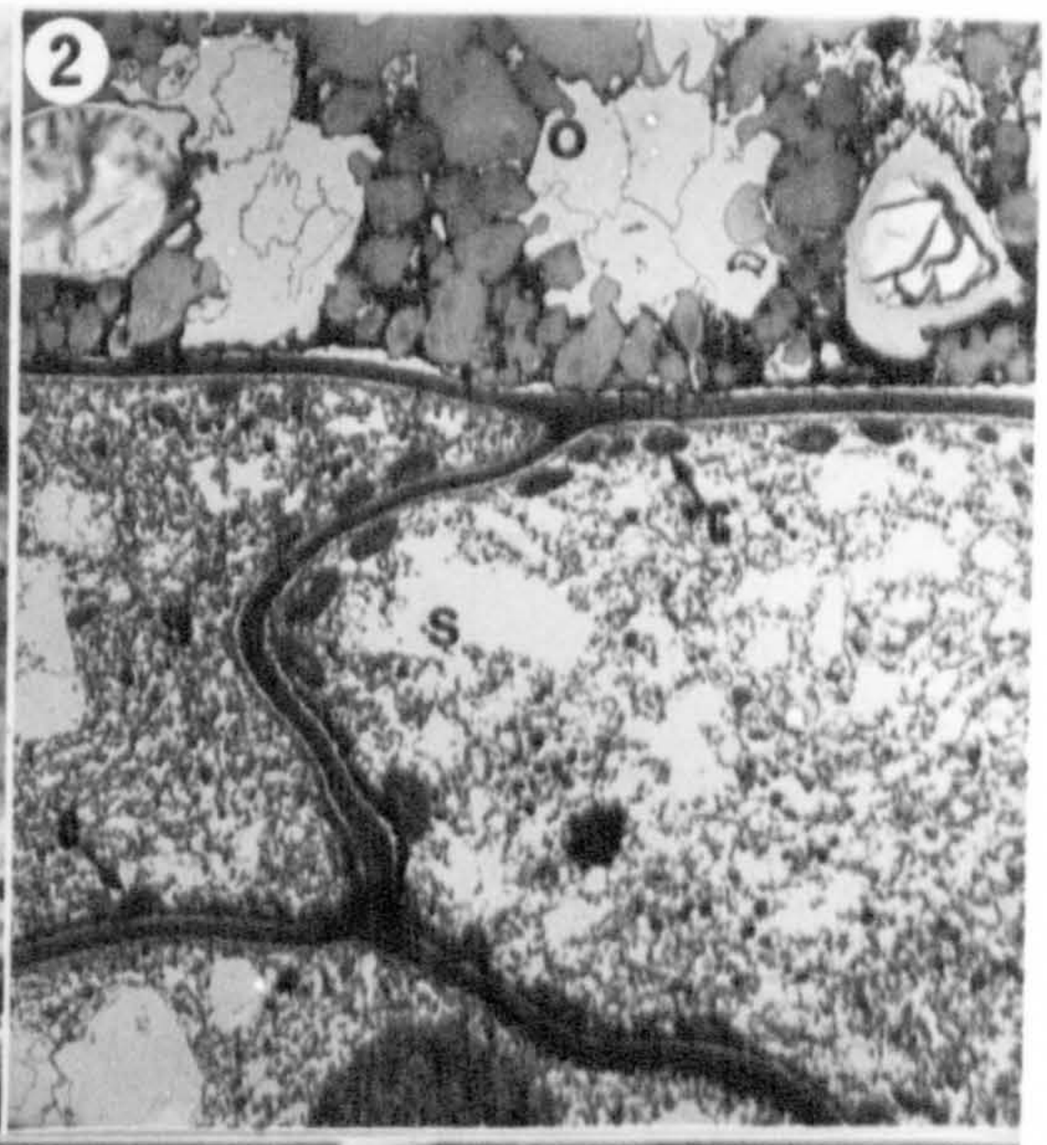
2
O
S

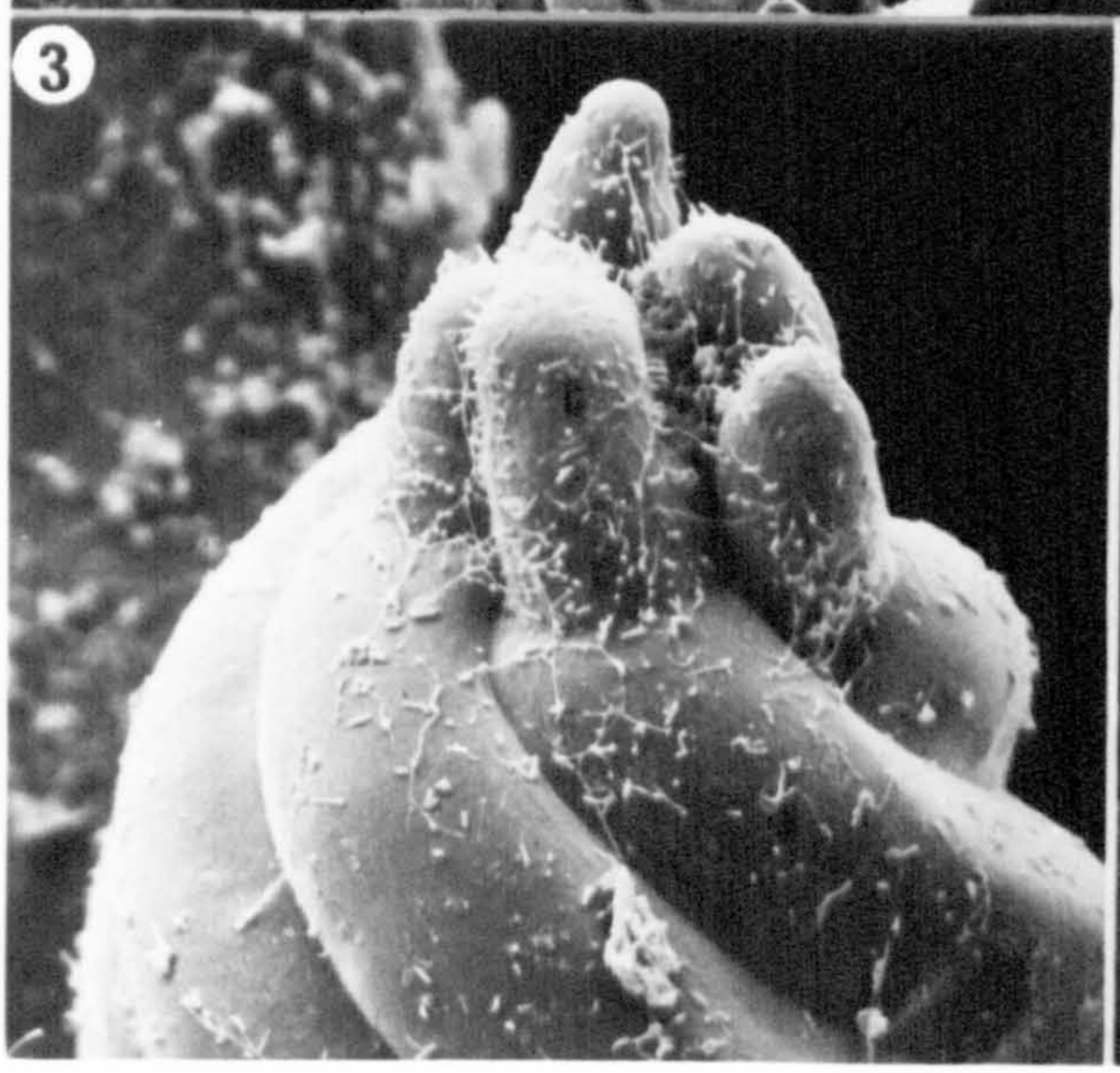
3

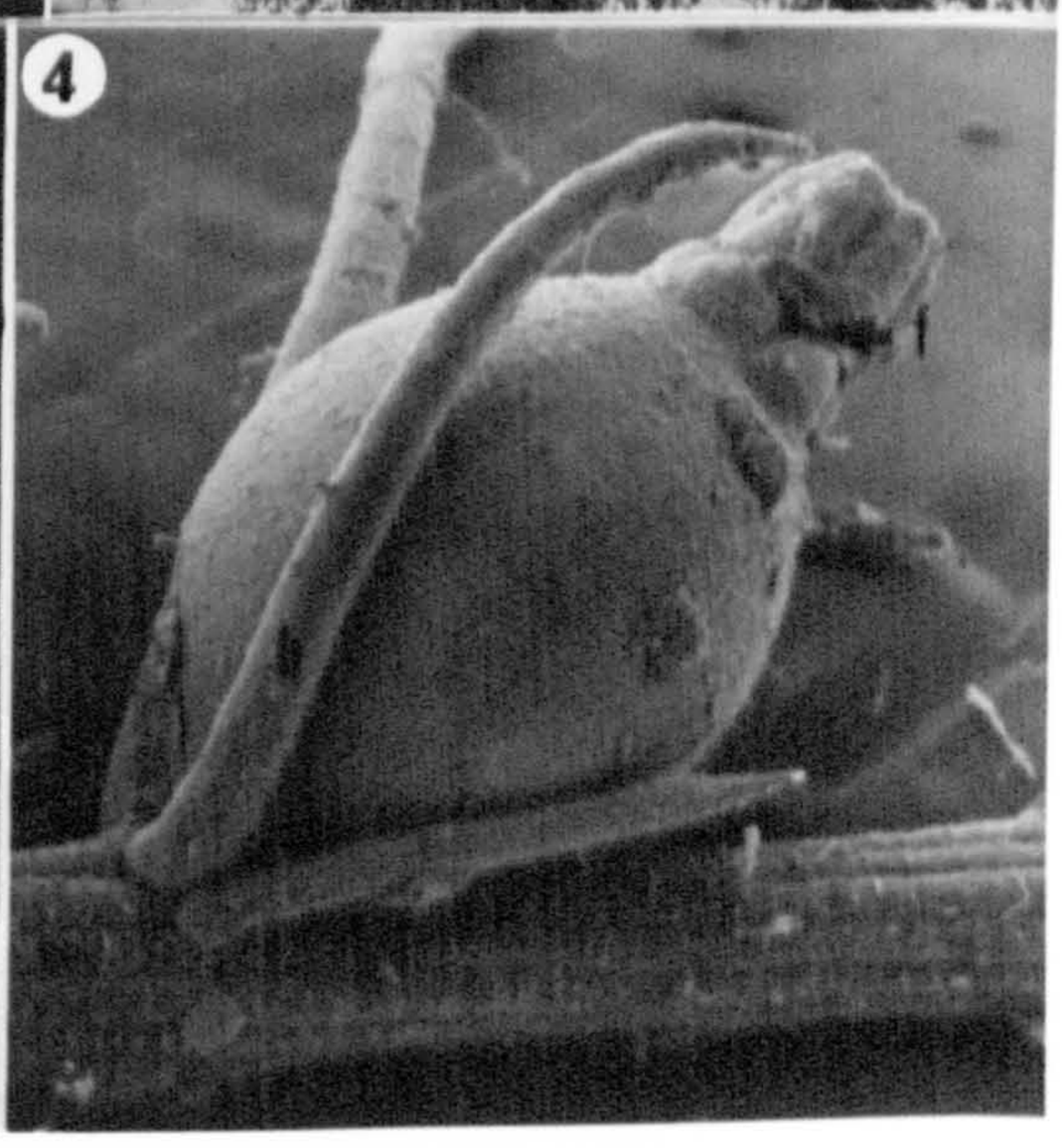
4

PLATE 10

Fig. 1 Section through a fully developed, unfertilised oosporangium of Chara delicatula. Note the oosphere (o), the sterile cell (s), the spiral cells (sp), the central cell (c) and the pedicel cell (p). L.M. x190.

Fig. 2 Section showing a germinated oospore of Chara hispida. Note the apical protrusion of the oospore (a), the secondary wall thickening around the oospore (w), and the calcified layer or calcine layer (c) L.M. x160.

Fig. 3 Detail of the spiral cells (sp) and the oosphere (o) in the oosporangium depicted in Fig. 1. Note the thick adaxial spiral wall (aw) and the wall (w) between the spiral cells and the oosphere. Chara delicatula, L.M. x1,840.

Fig. 4 Detail of the secondary wall thickenings and the calcine around the germinated oospore depicted in Fig. 2. The compound oosporangial wall shows 4 wall layers (a,b,c,d) and the calcine shows concentric laminations (arrows). Note that the adaxial spiral wall has sloughed off. Chara hispida, x1,600.

1

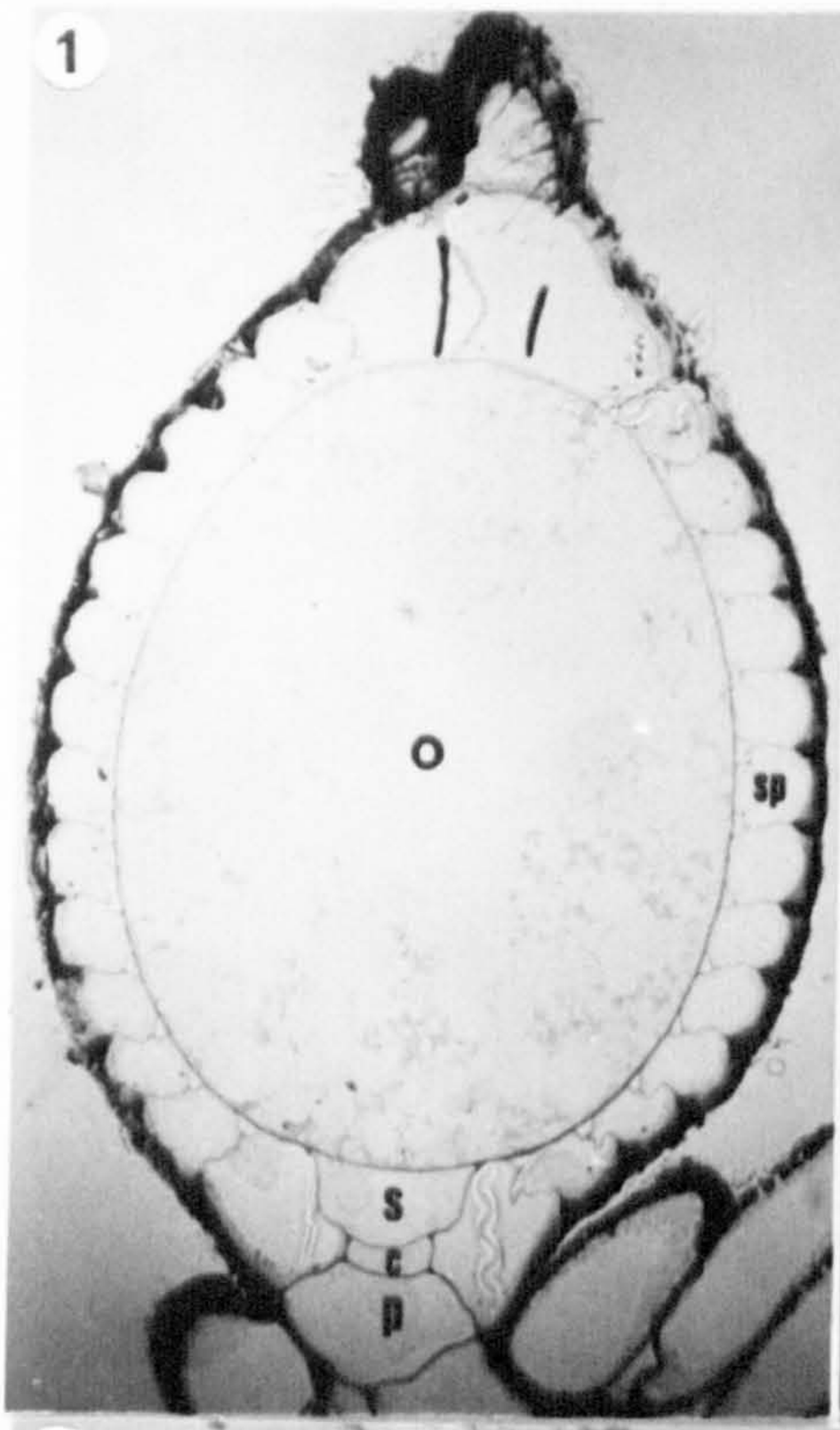

2

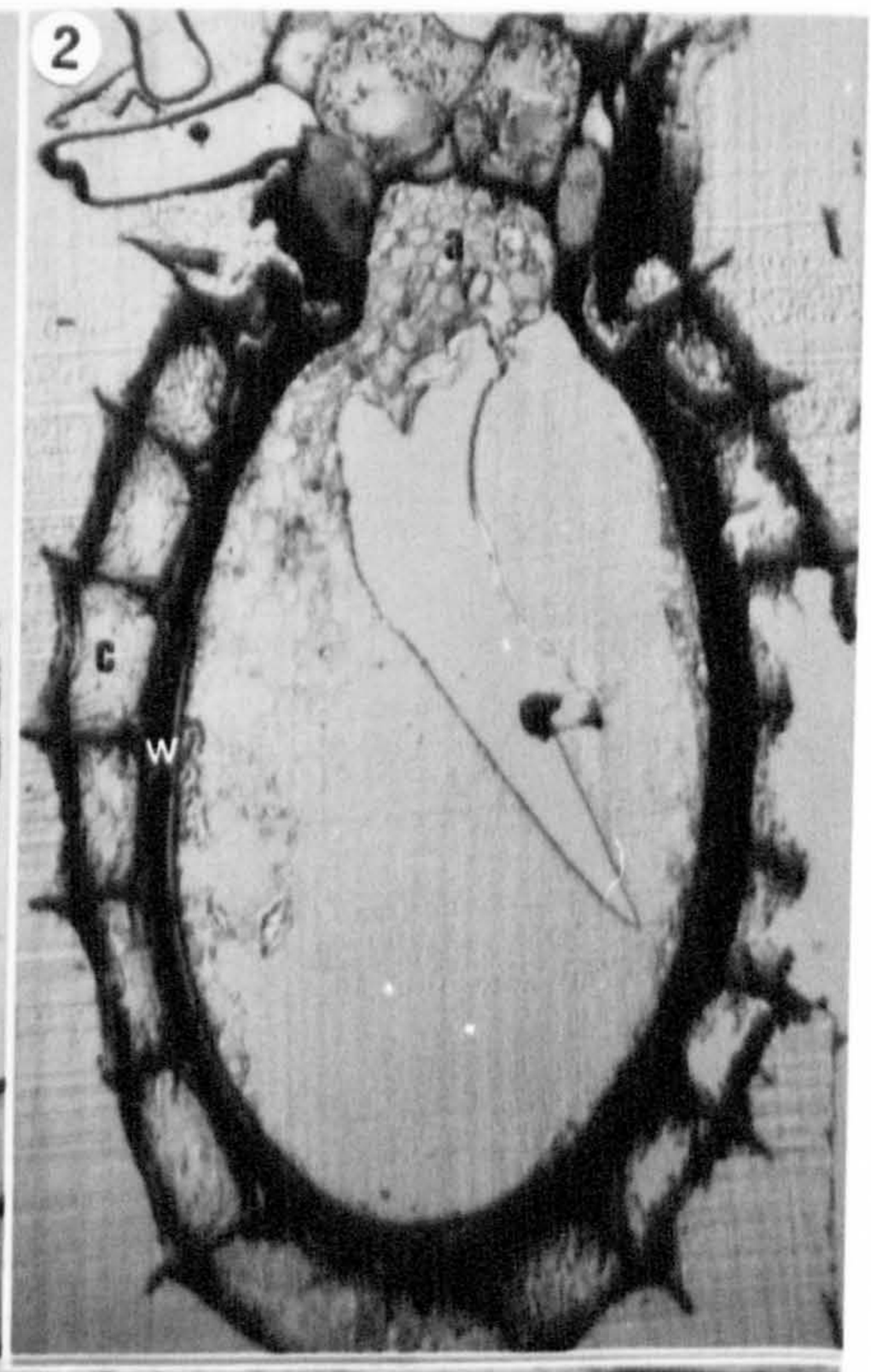

3

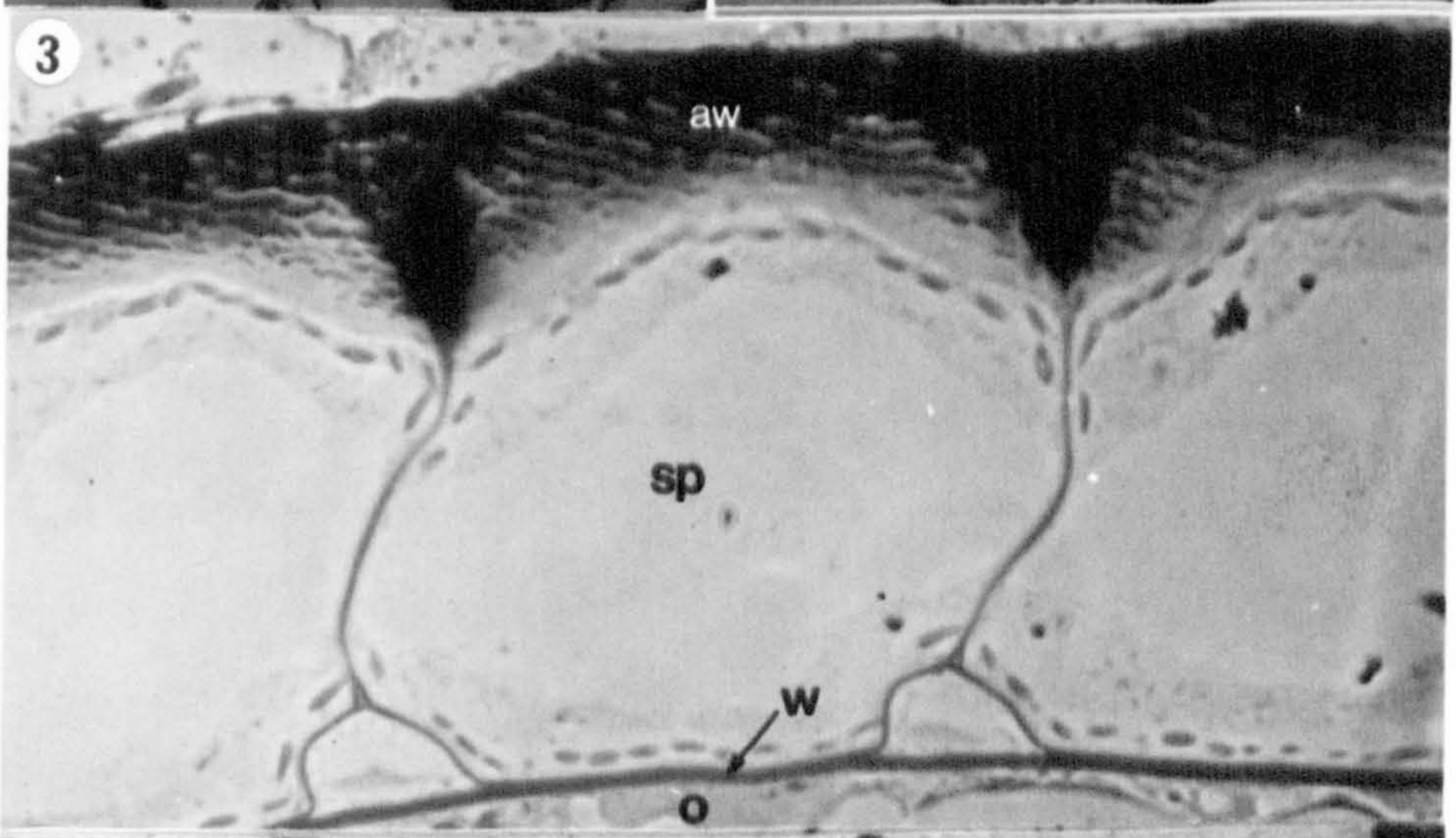

4

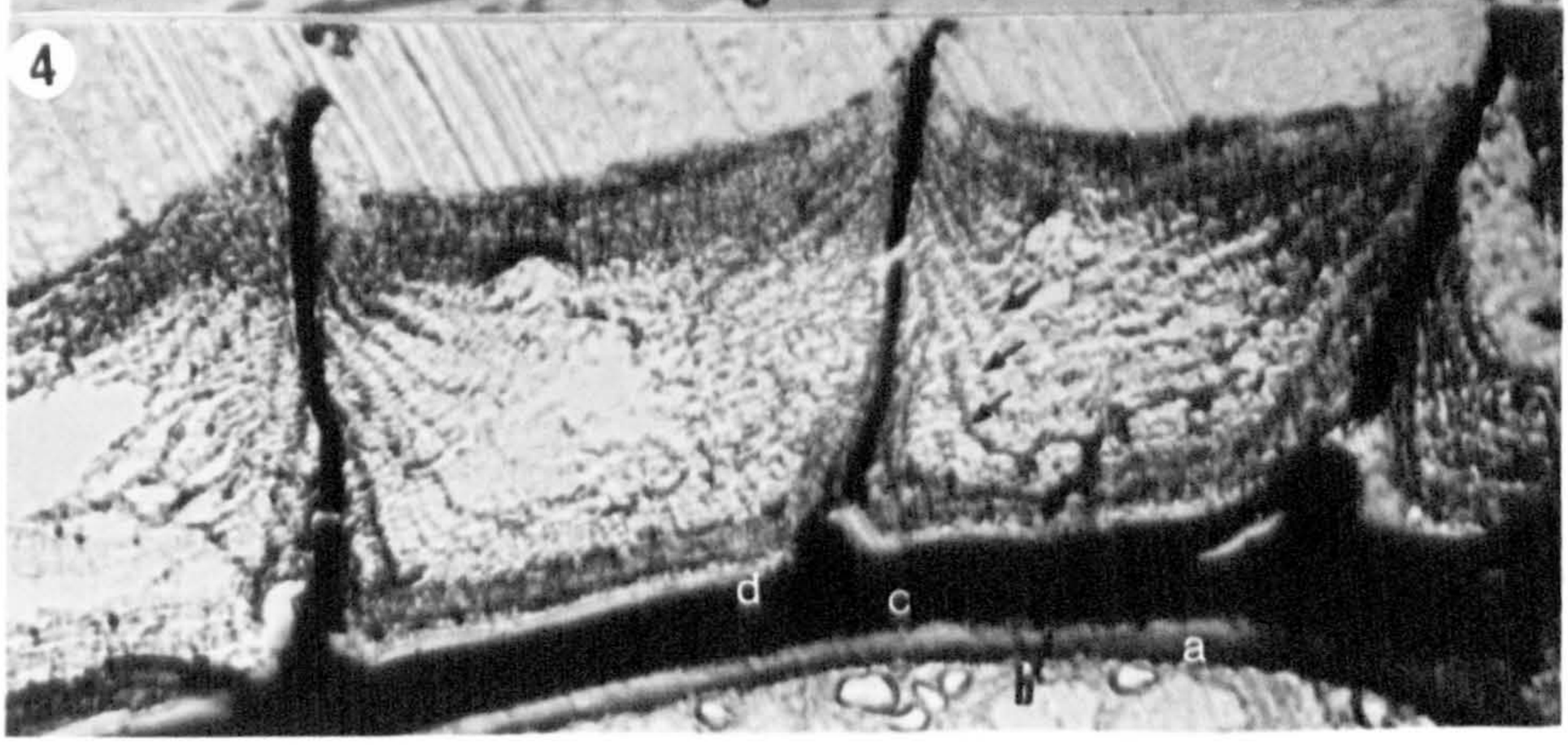

PLATE 12

Fig. 1 Section showing the primary wall (w) between the sterile cell (s) and the oosphere (o). Note the plasmodesmata (p). Chara delicatula, T.E.M. x18,200.

Fig. 2 Section showing the secondary layers associated with the wall between the sterile cell and the oospore . Note in the wall between the two cells there are pits (p) representing the position of plasmodesmata in pre-fertilisation stages: endosporine (2), amorphous layer (3), endosporostine (6). Chara hispida, T.E.M. x23,000.

Fig. 3 Section showing the wall (w) between the sterile cell (s) and the spiral cell (sc). Note the plasmodesmata (p). Chara delicatula, T.E.M. x18,200.

Fig. 4 Section showing calcine (c) deposited against the wall (w) between the sterile cell and the spiral cell . Note the pits (p) in the wall representing the position of plasmodesmata in pre-fertilisation stages. Lamprothamnium papulosum, T.E.M. x13,550.

Fig. 5 Section showing the endosporostine of Lamprothamnium papulosum. Note the crystals (c) have been pulled out of section and heaped together. T.E.M. x20,000.

Fig. 6 Section showing the endosporostine of Chara hispida. Note the crystals (c) in an electron-dense matrix. T.E.M. x10,000.

1
6
W
S
D
2
6
P
P
3
2
3
S
D
W
SG
4
C
W
C
5
C
C
6

PLATE 13

Fig. 1 Section through a compound oosporangial wall of Lamprothamnium papulosum showing that the endosporostine has large holes (h). These holes represent the gaps left by crystals which have been pulled out of section. The supporting electron dense matrix (arrow) appears as a distorted mesh. T.E.M. x6,300.

Fig. 2 Section through a spiral cell of Chara delicatula showing deposition of the endosporostine (6). Note the associated endoplasmic reticulum (er). T.E.M. x32,000.

Fig. 3 Section through a spiral cell of Chara delicatula showing deposition of the endosporostine (6). Note the endoplasmic reticulum (er), the vacuole (v) and the chloroplast (c). T.E.M. x17,000.

Fig. 4 Section through a compound oosporangial wall of Lamprothamnium papulosum showing helicoids in the ectosporostine (7). Note the underlying endosporostine (6). T.E.M. x21,000.

Fig. 5 Section through the compound oosporangial wall of Chara delicatula showing helicoids in the ectosporostine (7) and the amorphous nature of the ornamentation layer (8). Note the differential thickness of the ornamentation layer. T.E.M. x23,000.

Fig. 6 Air dried oosporangium of Chara delicatula showing the profile through a compound oosporangial wall. Note the ectosporostine (7), the protuberances comprising the ornamentation (o), the presence of the ornamentation on the lateral spiral wall (l) and the calcine (c). S.E.M. x2,280.

1
h
2
er
3
v
c
er
6
4
6
5
8
7
6
c

PLATE 14

Fig. 1 Section through the compound oosporangial wall of Nitella opaca showing the three zoned endosporostine (a-c), (a) is amorphous with areolar inclusions, (b) is microfibrillar, (c) is ridged. Note the ectosporostine (7), the primary spiral wall (5), the primary oospore wall (4), the amorphous layer (3) and the endosporine (2). T.E.M. x17,000.

Fig. 2 Section through a weakly calcified germinated oosporangium of Chara hispida. Note the compound oosporangial wall layers; ectosporine (1), endosporine (2), endosporostine (6), ectosporostine (7). The calcine (c) lies immediately on top of the compound oosporangial wall. Note also the depleted oospore cytoplasm (o), with only remnants of starch reserves (s). T.E.M. x2,600.

Fig. 3 Section through a compound oosporangial wall of Nitella opaca showing the helicoidal endosporine (2) and the amorphous layer (3). T.E.M. x32,000.

Fig. 4 Section through a compound oosporangial wall of Nitella opaca showing the primary spiral wall (5), the primary oospore wall (4), the amorphous layer (3) and the endosporine (2). T.E.M. x17,000.

Fig. 5 Section through the lateral wall of a spiral cell of Chara hispida (1) showing the structureless ornamentation layer (8) laid on it. Note the calcine deposited on either side of the wall (c). T.E.M. x14,000.


1
7
C
6
5
4
3
2

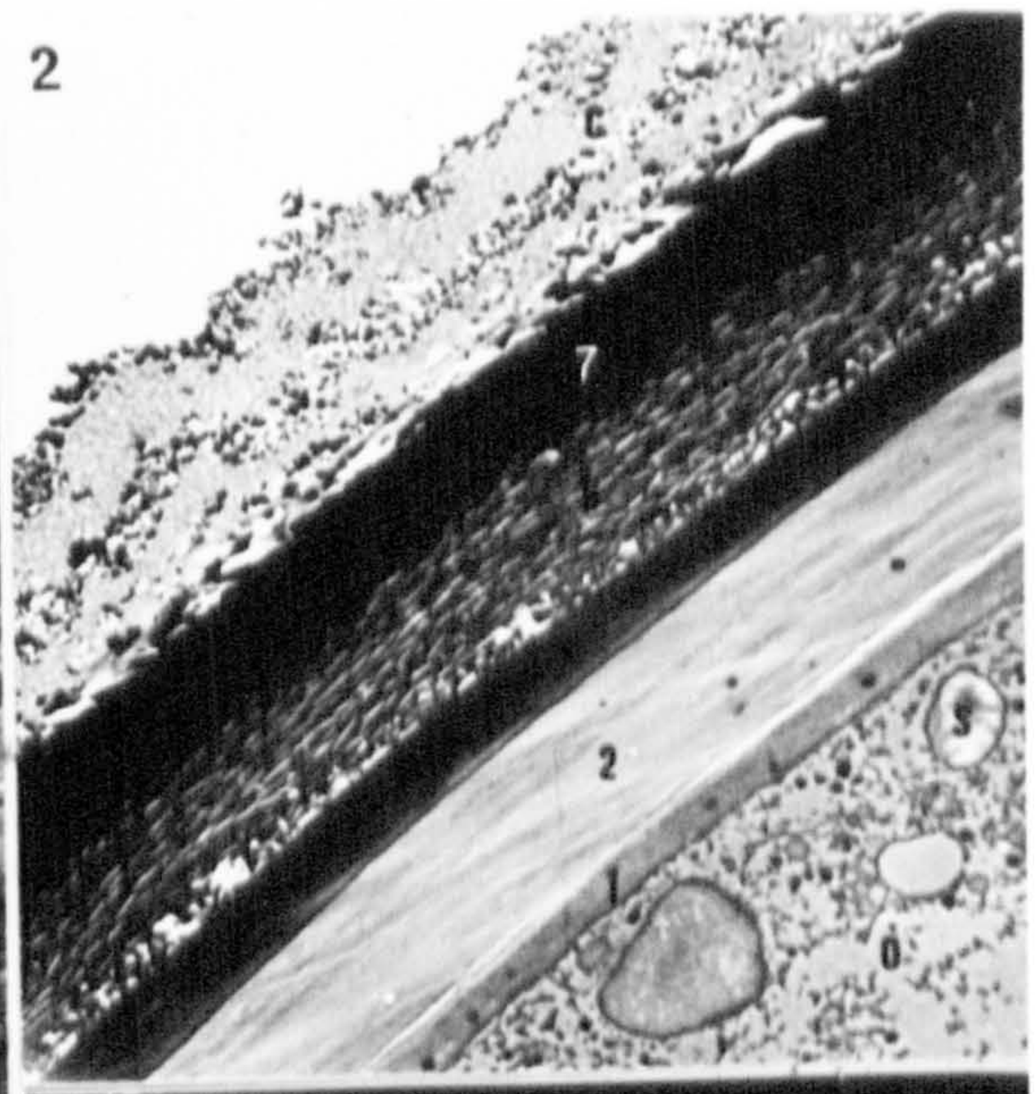
2
C
7
2
1
S
0

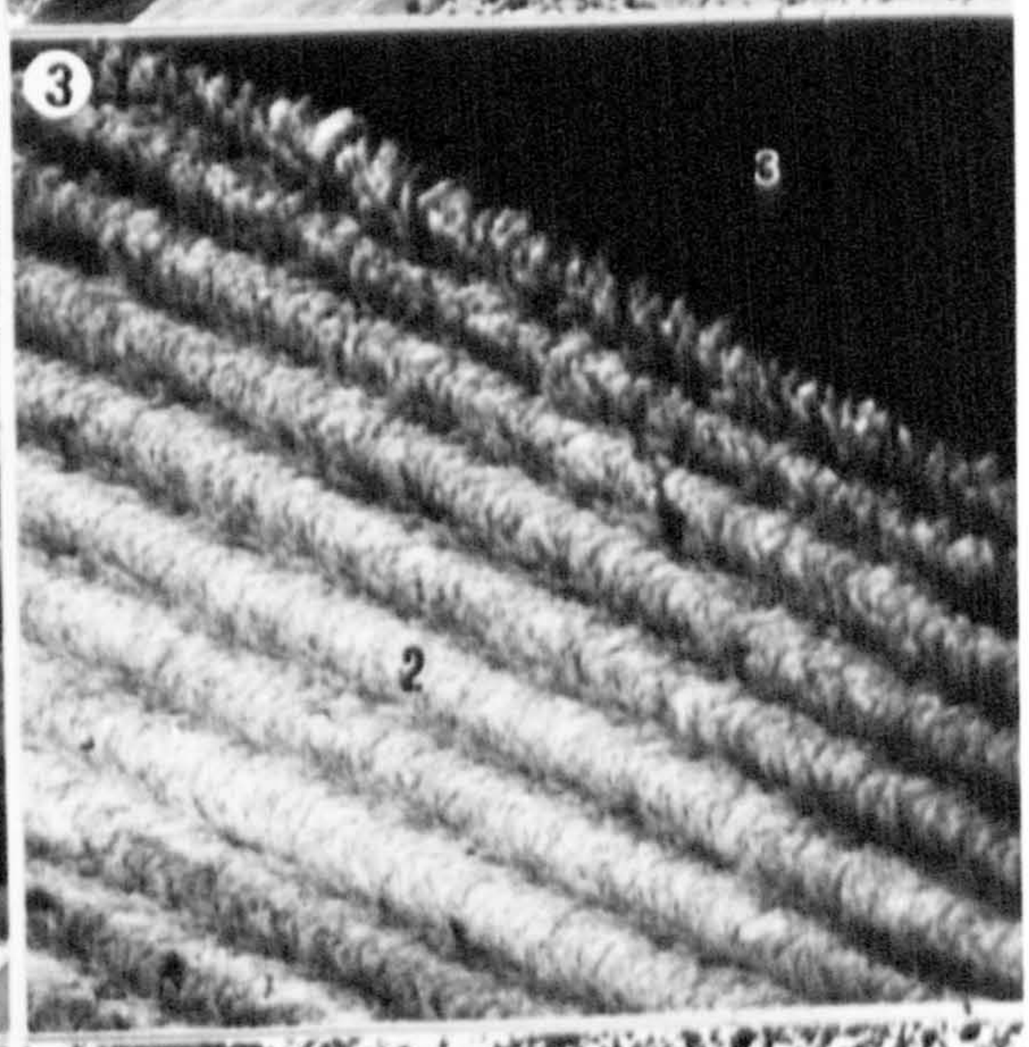
3
3
2

4
5
4
3
2

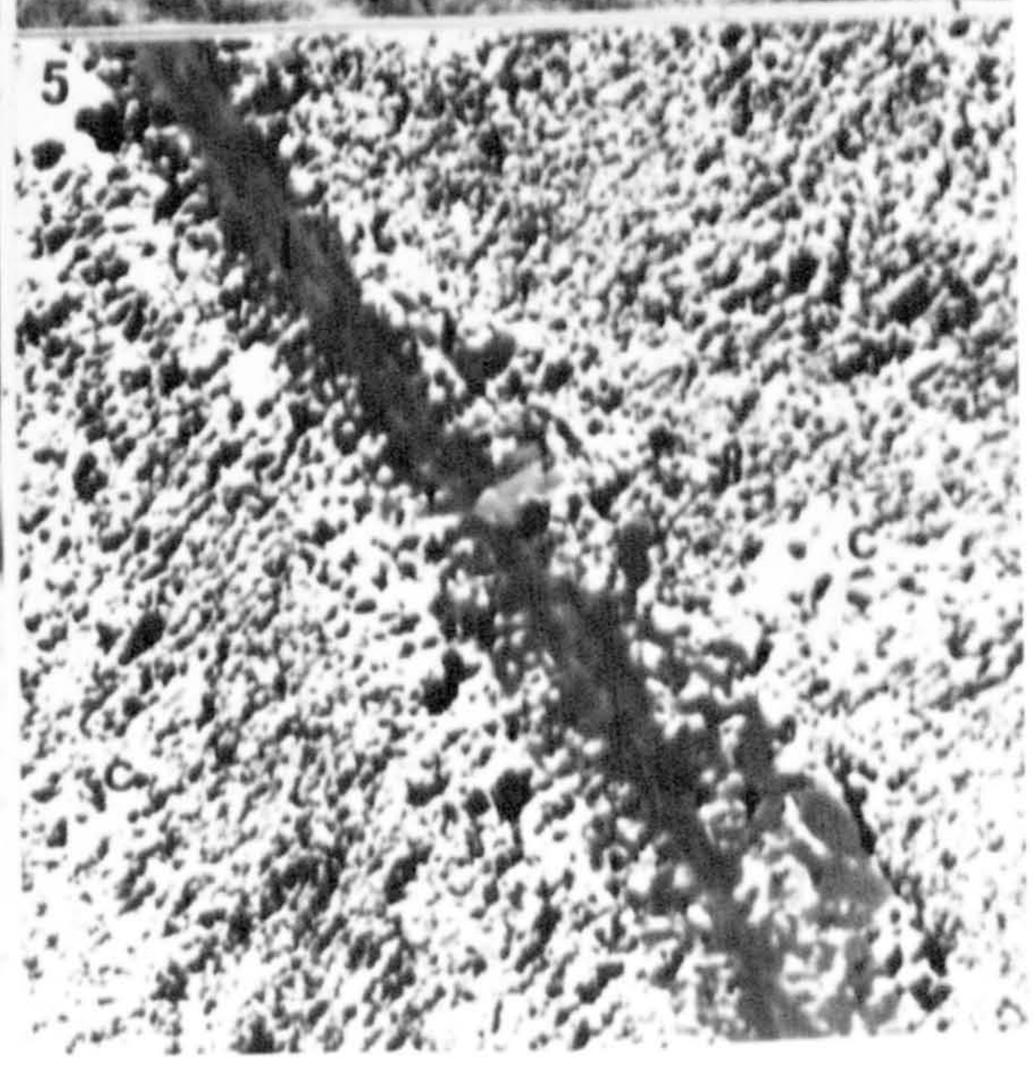
5
C

PLATE 15

Fig. 1 Critical point dried Chara hispida oospore with the calcine removed revealing the compound oosporangial wall. Note the spiralling ridges (arrows). S.E.M. x480.

Fig. 2 Air dried Lamprothamnium papulosum oospore with the calcine removed revealing the compound oosporangial wall. Note at the base of the oospore a ridge (arrows) describing a pentagon. This highlights the position once occupied by the sterile cell. S.E.M. x1,200.

Fig. 3 Air dried Nitella opaca oospore. Note the spiralling ridges (arrows). S.E.M. x430.

Fig. 4 Air dried Nitella opaca oospore. Note at the oospore base the ridge describing a trapezium (tp) adjacent to a ridge describing a triangle (tr). S.E.M. x820.

Fig. 5 Air dried oospore of Nitella translucens showing complex ornamentation (o) on the compound oosporangial wall. Note the lateral spiral walls (l) are extensively covered in the ornamentation layer and form spiralling lamellae. S.E.M. x1,500.

Fig. 6 Air dried Lamprothamnium papulosum oospore with the calcine removed showing the ornamentation on the sterile cell. Note the spiralling pattern of protuberances. S.E.M. x2,100.

Fig. 7 Air dried Lamprothamnium papulosum oospore with the calcine removed showing that the spiralling ridge of secondary thickening alters in height (arrows). Note the spiral cell lateral wall (l) at the ridge apex. S.E.M. x1,400.

Fig. 8 Air dried Lamprothamnium papulosum oospore with the calcine removed showing that the spiralling ridge of secondary thickening alters in thickness (arrows). Note the spiral cell lateral wall (l) at the apex of the ridge. S.E.M. x2,000.

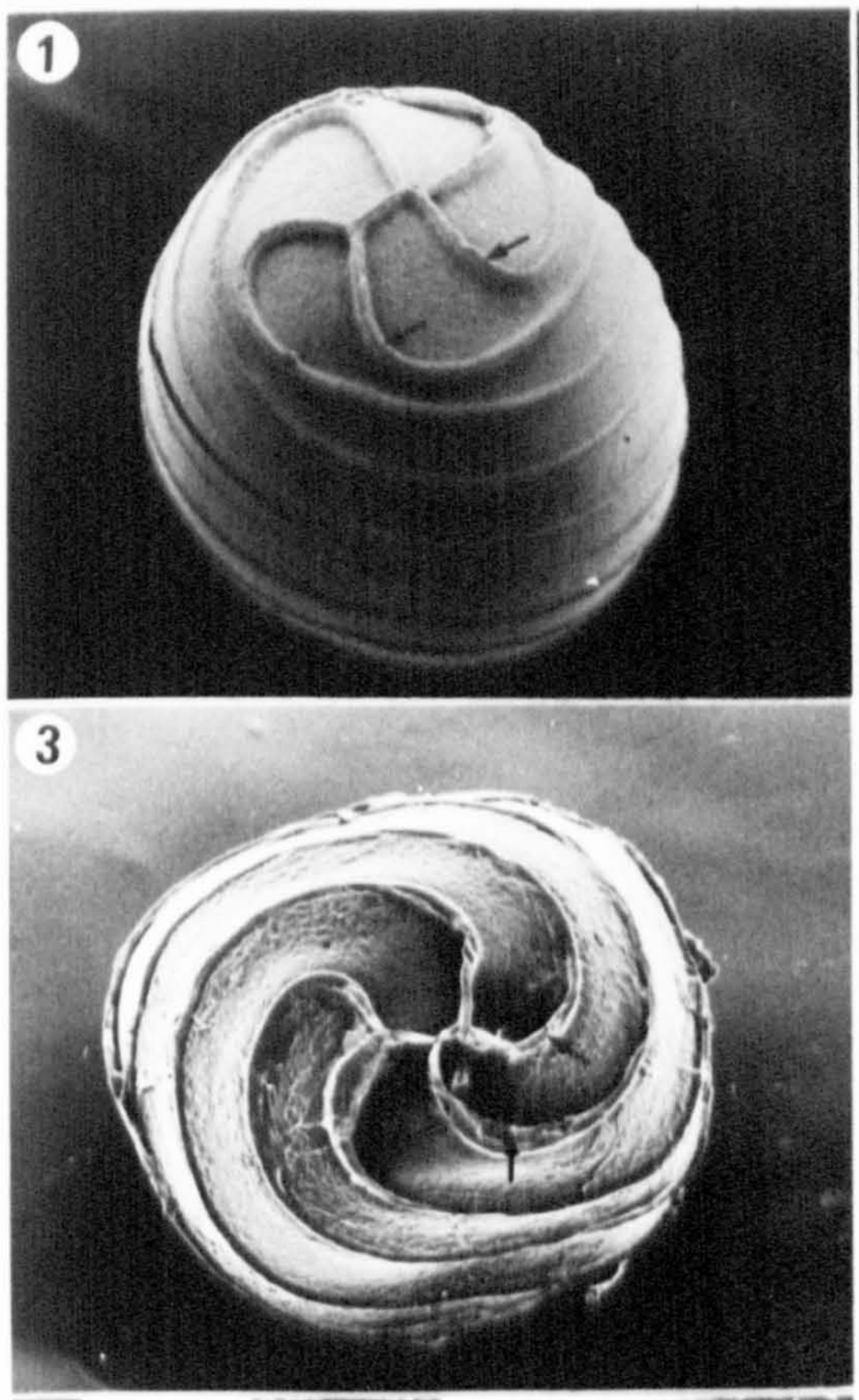
1

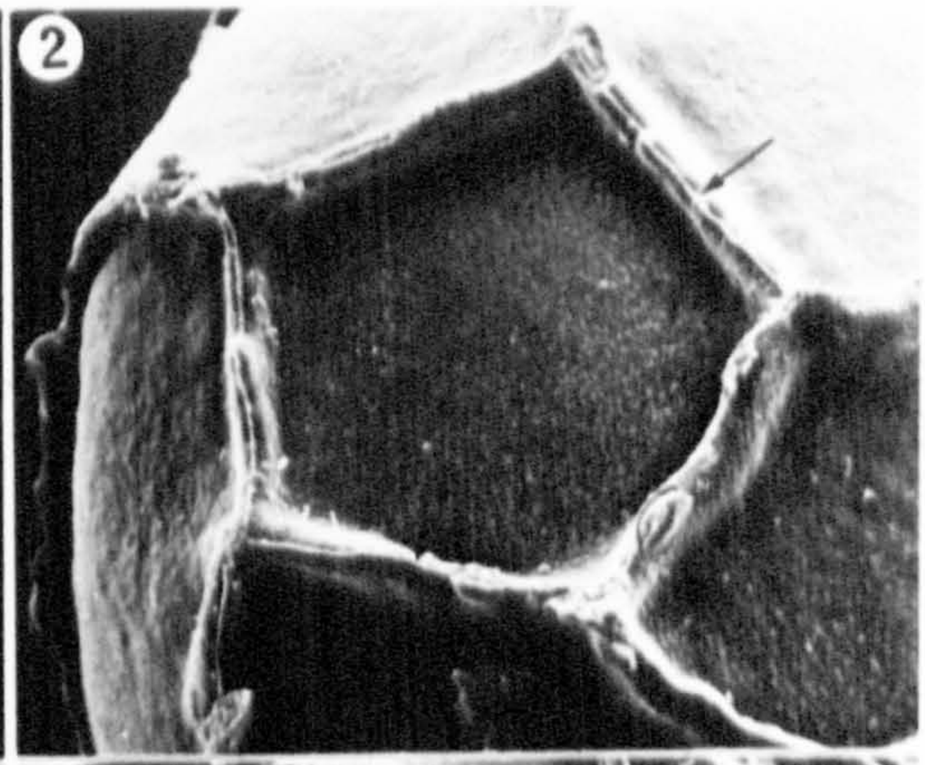
2

3

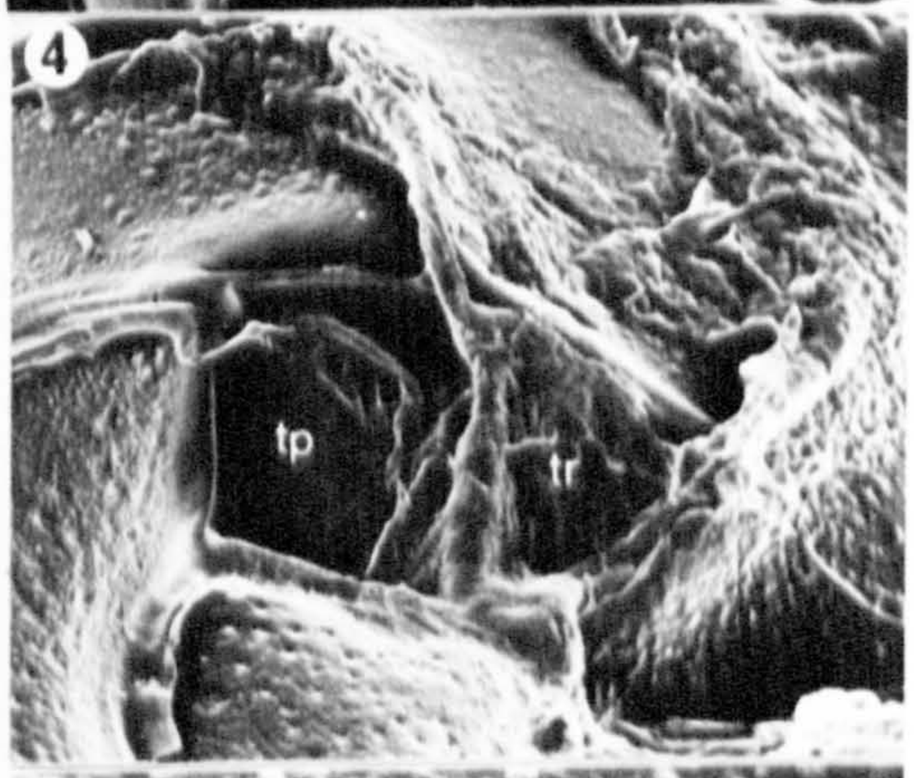
4
tp
tr

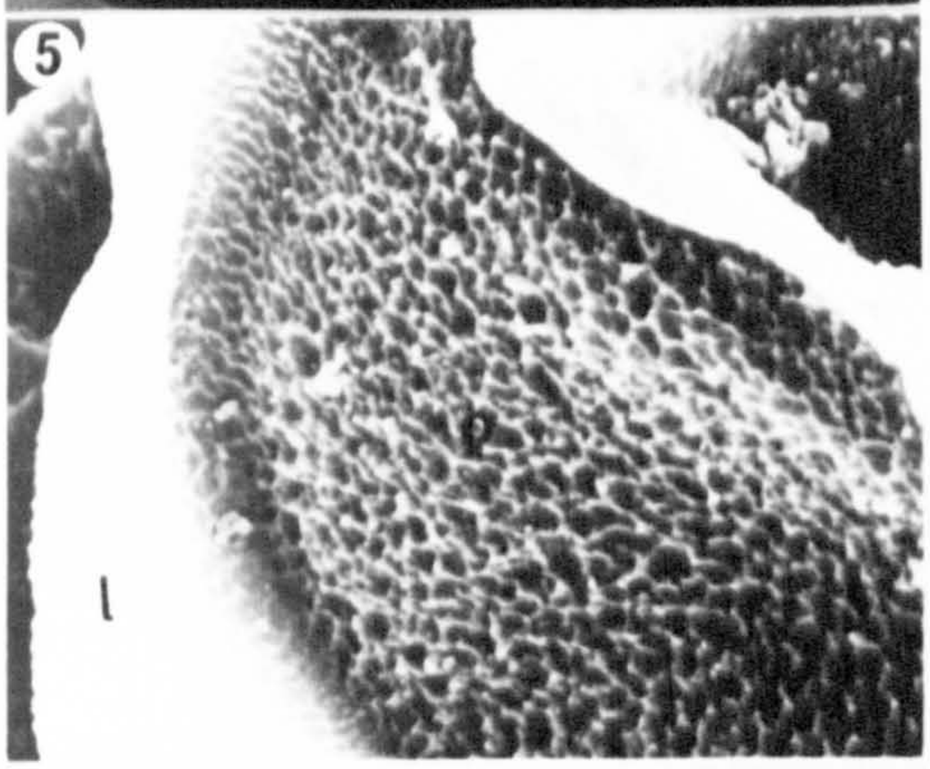
5
p
l


6

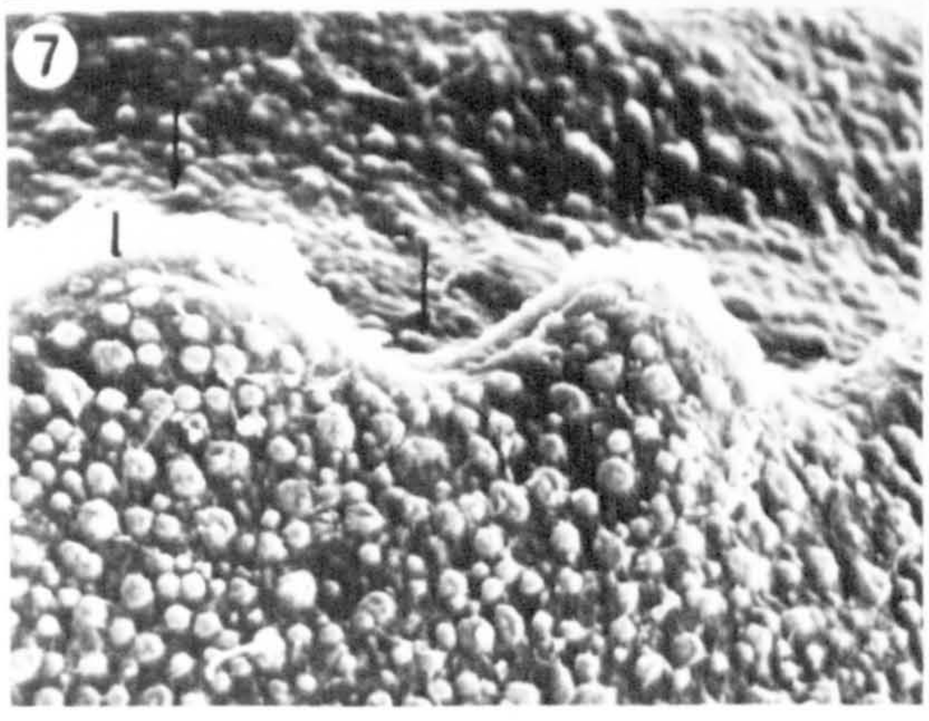
7
l

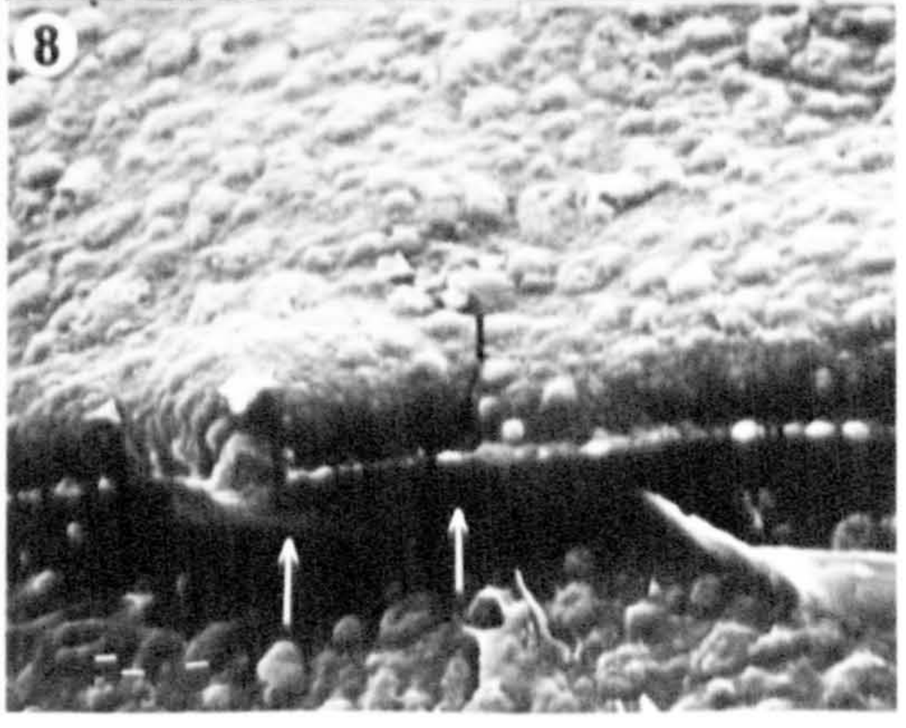
8

PLATE 16

Fig. 1 Critical point dried germinated oospore of Chara hispida. Note the emergent prothallus (p), the rhizoids (r) and that the apices of the spirals have broken off and fallen away during germination. S.E.M. x150.

Fig. 2 A transverse fracture through a germinated Chara hispida oospore. Note that in germination the compound oosporangial wall has torn apart at the spiral ridge (r), and that the ectosporine (1) is continuous with the emergent oospore apex. Note also starch grains (s), the compound oosporangial wall (w), calcine (c) and the spiral cell lateral wall (l). Critical point dried, S.E.M. x680.

Fig. 3 Section through the apex of a germinating Chara hispida oospore. Note the compound oosporangial wall at the apex has been bent backwards (w) with the fracture passing through the ridge of secondary thickening (r). Note also the apical bulge of the oospore (o), the calcine (c) and the first cells of the prothallus (p). L.M. x1,600.

Fig. 4 Stored reserves in a germinated oospore. Note that there are signs of depletion, with reduced size of starch grains (s) and a diffuse cytoplasm (c). Chara hispida, T.E.M. x8,500.

Fig. 5 Section through the apex of a germinated oospore showing the torn endosporine (2) and that the ectosporine (1) is continuous with the emergent oospore. Note that the endosporostine has torn apart (6) and that the stored reserves (r) are in the emergent regions of the cell. Chara hispida, T.E.M. x2,000.

Fig. 6 Detail of the damage caused by germination on the compound oosporangial wall layers. The endosporine (2), the amorphous layer (3), the primary oospore wall (4) and the solid secretion (s) in the intercellular space are torn. The endosporostine (6) shows signs of being pulled apart. Chara hispida, T.E.M. x3,800.

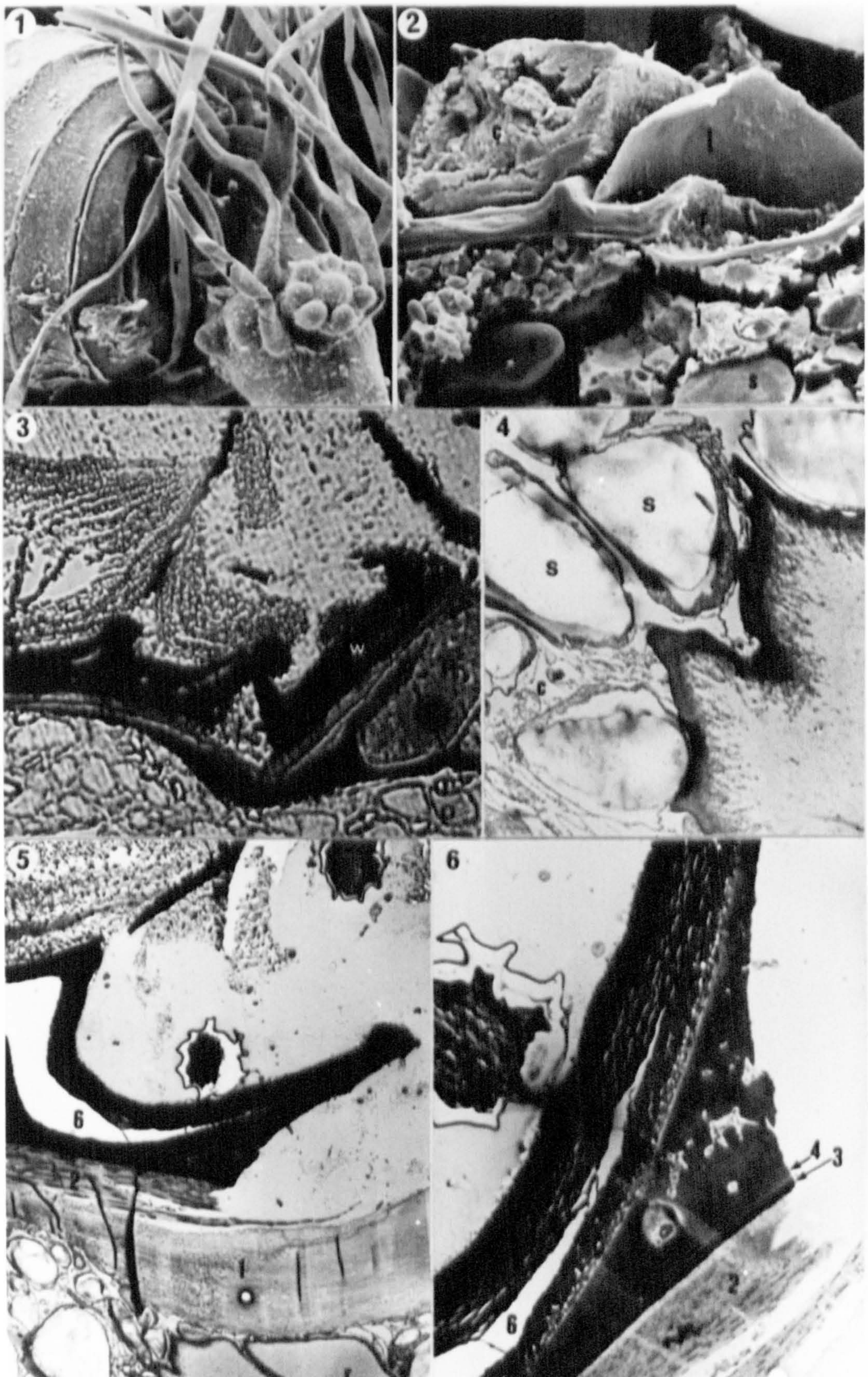
1
2
3
4
5
6

PLATE 17

Fig. 1 Air dried calcified oosporangium of Chara delicatula. The calcine (c) has been fractured and half of the spiral removed revealing the intimate relationship of the calcine with the compound oosporangial wall (w). S.E.M. x730.

Fig. 2 The compound oosporangial wall of Chara delicatula has an ornamentation of protuberances (o). Air dried, S.E.M. x935.

Fig. 3 Calcified oosporangium of Chara hispida showing extracellular calcite caking the outer wall of the spiral cells (sp) and the coronula cells (c). The deposit has been partially removed revealing the underlying spirals (s). Critical point dried, S.E.M. x250.

Fig. 4 The inside of the spirals have pits (arrows) which correspond to the protuberances on the compound oosporangial wall. Air dried, Chara delicatula, S.E.M. x935.

Fig. 5 Calcite crystals (c) on the outside of the spiral cells. Critical point dried, Chara hispida, S.E.M. x18,200.

Fig. 6 Laboratory grown crystals of calcite (c). Air dried, S.E.M. x4,300.

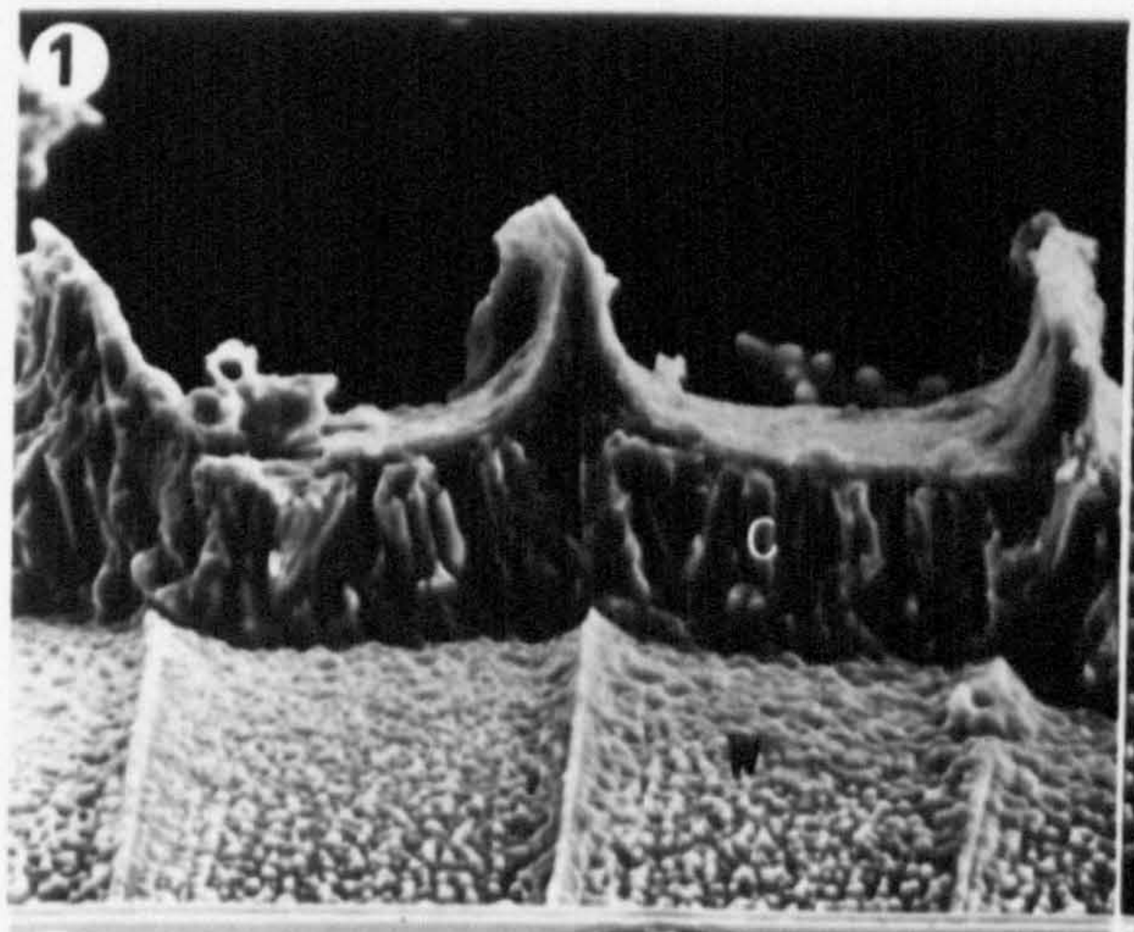
1
C
W

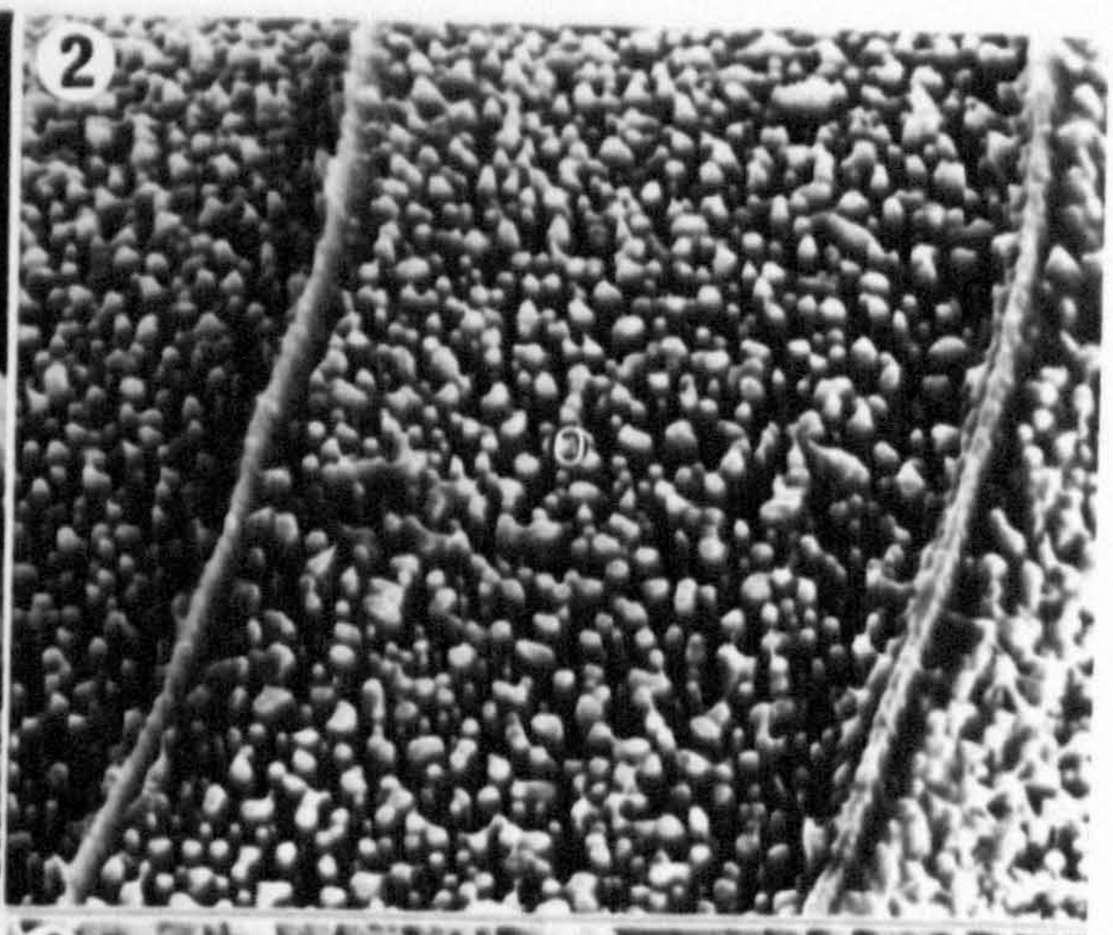
2

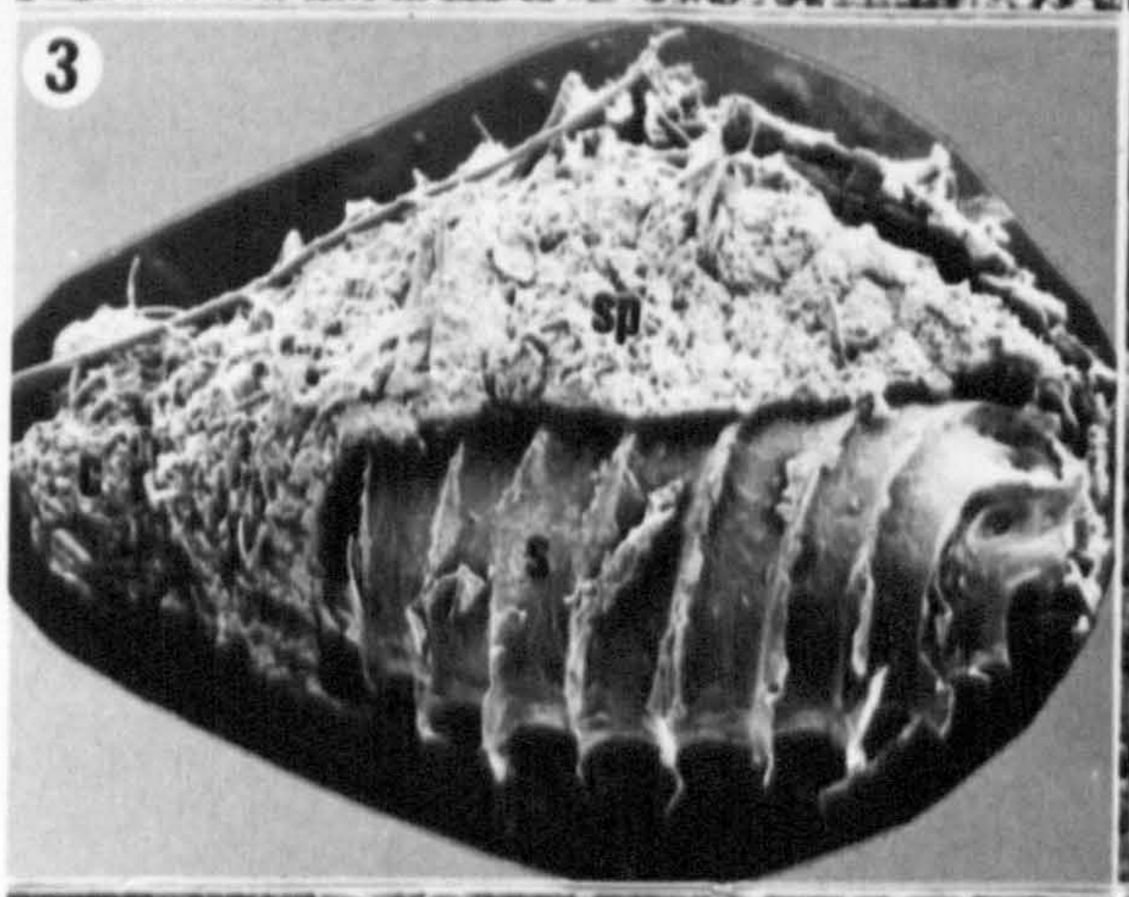
3
sp
C
S

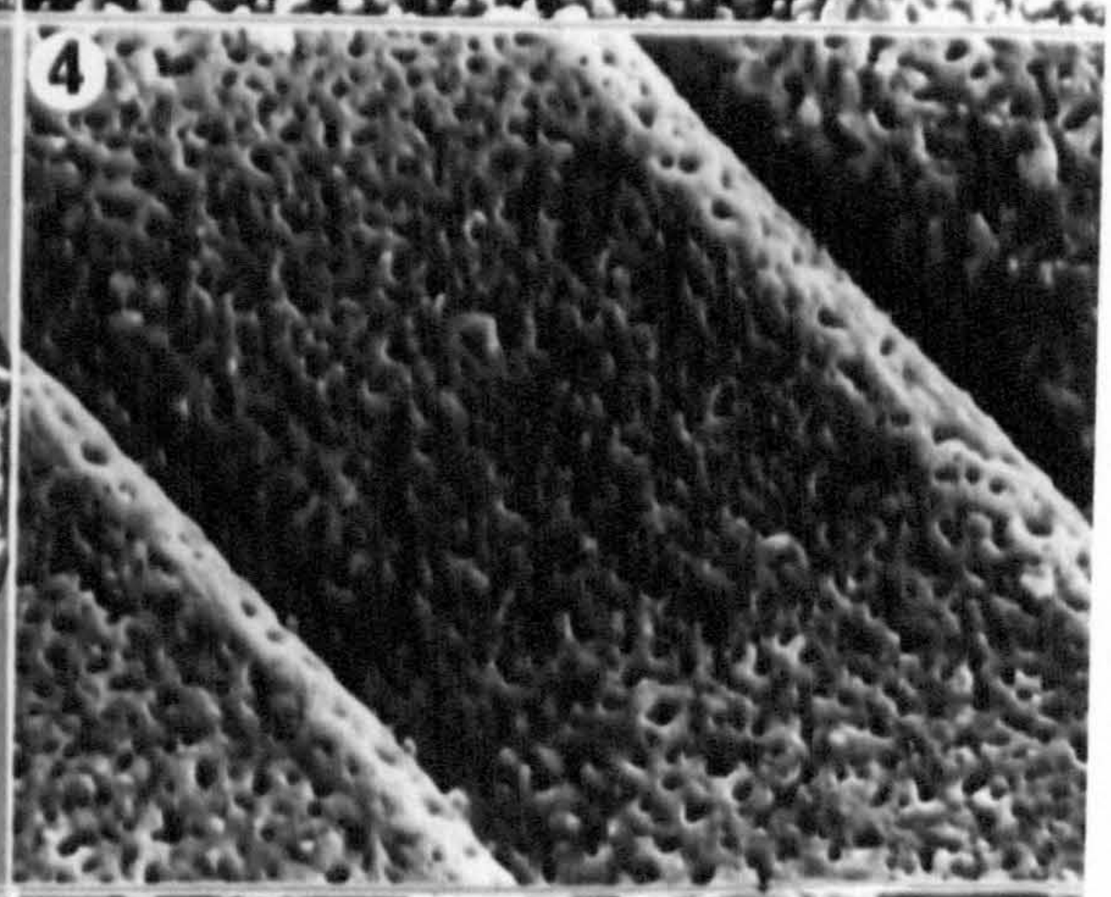
4

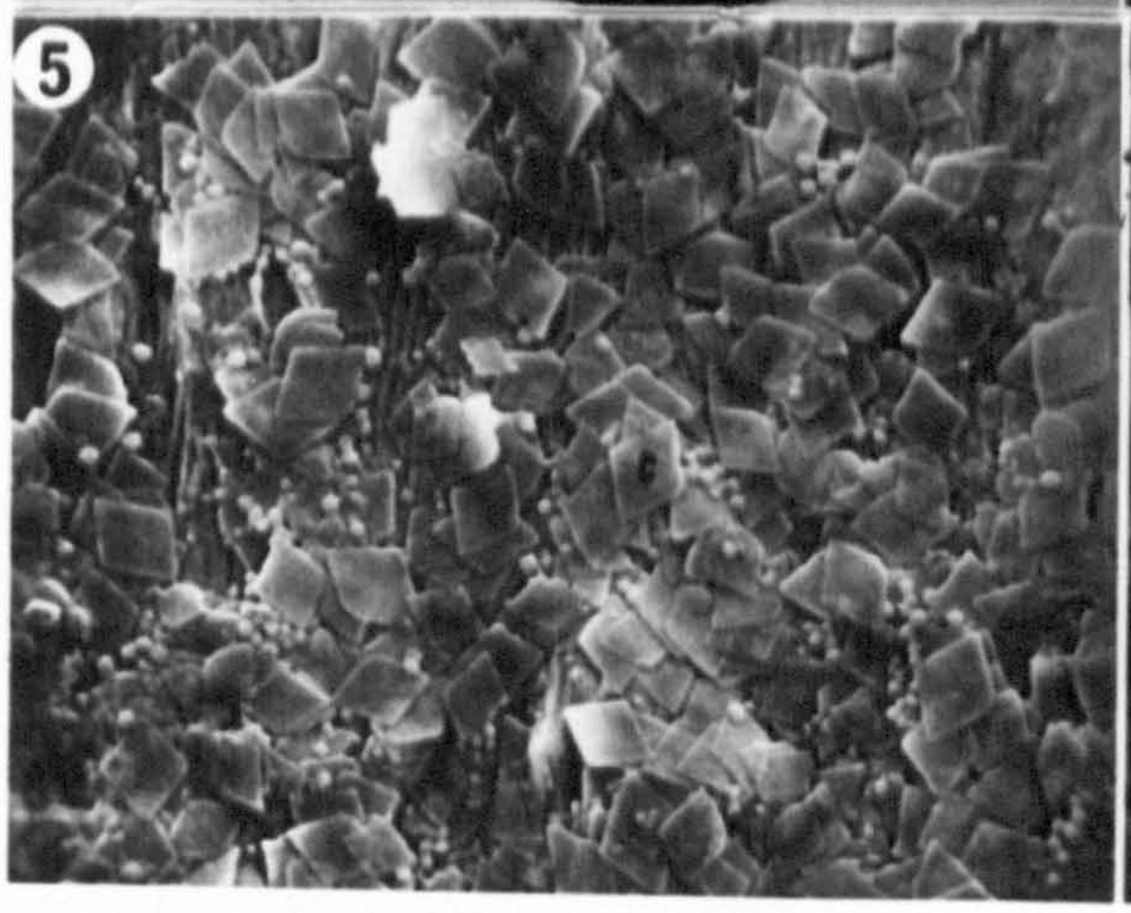
5

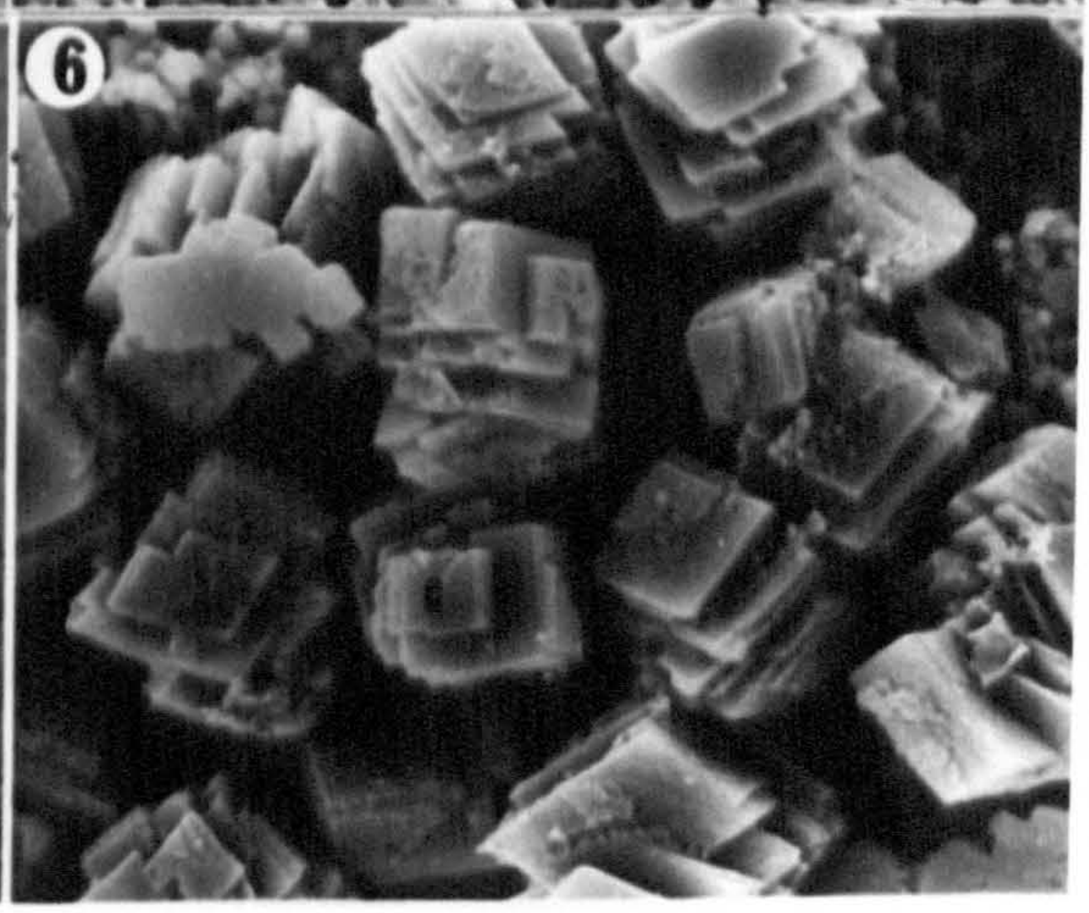
6

PLATE 18

Fig. 1 Weakly calcified Lamprothamnium papulosum oosporangium showing concave spiral profiles (arrows). Note the apex (a) is the most weakly calcified. Air dried, S.E.M. x60.

Fig. 2 Strongly calcified Lamprothamnium papulosum oosporangium showing flat spiral profiles (arrows). Note the apex (a) is the most weakly calcified. Air dried, S.E.M. x60.

Fig. 3 Weakly calcified Lamprothamnium papulosum oosporangium showing the concave spiral profile. Note the spiral cell lateral wall (arrow). Air dried, S.E.M. x430.

Fig. 4 Strongly calcified Lamprothamnium papulosum oosporangium showing the flat spiral profile. Note the spiral cell lateral wall (arrow). Air dried, S.E.M. x430.

Fig. 5 Strongly calcified Chara hispida oosporangium showing the apex to be more weakly calcified. There is a demarcation line where calcine thickness alters (arrow). Air dried, S.E.M. x140.

Fig. 6 Germinated Chara hispida oosporangium showing the spiral apices are fractured and splayed out into 'peg-like' projections (a). Critical point dried, S.E.M. x140.

Fig. 7 Fractured spiral apex shown in Fig. 6 (above). Note the position of fracture (f) and that the spiral is apically expanded (a). Critical point dried, Chara hispida, S.E.M. x200.

Fig. 8 Germinated Chara hispida oosporangium showing the fractured apex of each spiral (f). Critical point dried, S.E.M. x160.

1
2
3
4
5
6
7
8

PLATE 19

Fig. 1 Carborundum ground transverse section of a Chara hispida spiral showing concave bands (thick arrows). Note the indistinct radiating polycrystalline columns (thin arrows). L.M. x250.

Fig. 2 Carborundum ground transverse section of a Lamprothamnium papulosum spiral showing the radiating polycrystalline columns (thick arrows). Note the concave bands (thin arrows). L.M. x350.

Fig. 3 Acid etched (0.1% HCl, 10secs) resin embedded Chara hispida oosporangium. Note the spirals (s), the spiral apex (a) and the basal plate (b). S.E.M. x90.

Fig. 4 Apical region of the specimen depicted in Fig. 3. Note the spirals (s) and the spiral apex (a). S.E.M. x225.

Fig. 5 Spirals of the specimen depicted in Figs. 3 & 4 (above). Note the concave lamellae (large arrows) and the acid insoluble strands (small arrows) that connect the lamellae. Note the acid insoluble endocalcine (e). S.E.M. x550.

Fig. 6 Spiral apex of the specimen depicted in Figs. 3 & 4 (above). Note the closely packed concave lamellae (arrows). S.E.M. x480.

Fig. 7 Acid etched (0.01% HCl, 10secs), resin embedded Chara hispida oosporangium. Note the lamellae (arrows) in the basal plate. S.E.M. x225.

Fig. 8 Acid etched (0.01% HCl, 10secs), resin embedded Lamprothamnium papulosum oosporangium. Note the concave lamellae (arrows) in the spiral. S.E.M. x770.

1

2

3

4

5

6

7

8

PLATE 20

Fig. 1 Section through a calcifying spiral cell of Chara delicatula. Note the plasmalemma (p). Strands / sectioned sheets (s) can be seen outside the plasmalemma. Note the electron dense amorphous crystal nuclei. The holes (h) are formed when calcite crystals are pulled out of section. T.E.M. x10,000.

Fig. 2 Section through 2 spirals of Chara hispida showing concave lamellae (arrows) in the calcine. The central area of calcine (c) sections least well. Note the spiral cell lateral wall (l). Section stained with Reynolds's (1963) lead citrate and uranyl acetate (30% ethanol). T.E.M. x1,000.

Fig. 3 Section through the calcine of Chara hispida showing organic / resinous bands (o) comprising the endocalcine. Note the vertical array of crystal fragments (c) in the calcine . Section stained with Reynolds's (1963) lead citrate. T.E.M. x4,000.

Fig. 4 Section through the endocalcine of Chara hispida showing organic / resinous bands (o) with perpendicularly aligned gaps. Note the electron dense crystal fragments (c). Section stained with Reynolds's (1963) lead citrate. T.E.M. x7,660.

Fig. 5 Section through a spiral of Chara hispida showing the organic / resinous bands (o) of the endocalcine and the vertically aligned crystal fragments (electron dense chips aligned in the direction of the arrows) in the calcine. Section stained with Reynolds's (1963) lead citrate. T.E.M. x2,600.

Fig. 6 Section through the calcine of Chara hispida, showing organic / resinous areas (o), vertically aligned crystal fragments (f) and vertically aligned gaps (g). Section stained with Reynolds's (1963) lead citrate. T.E.M. x7,660.

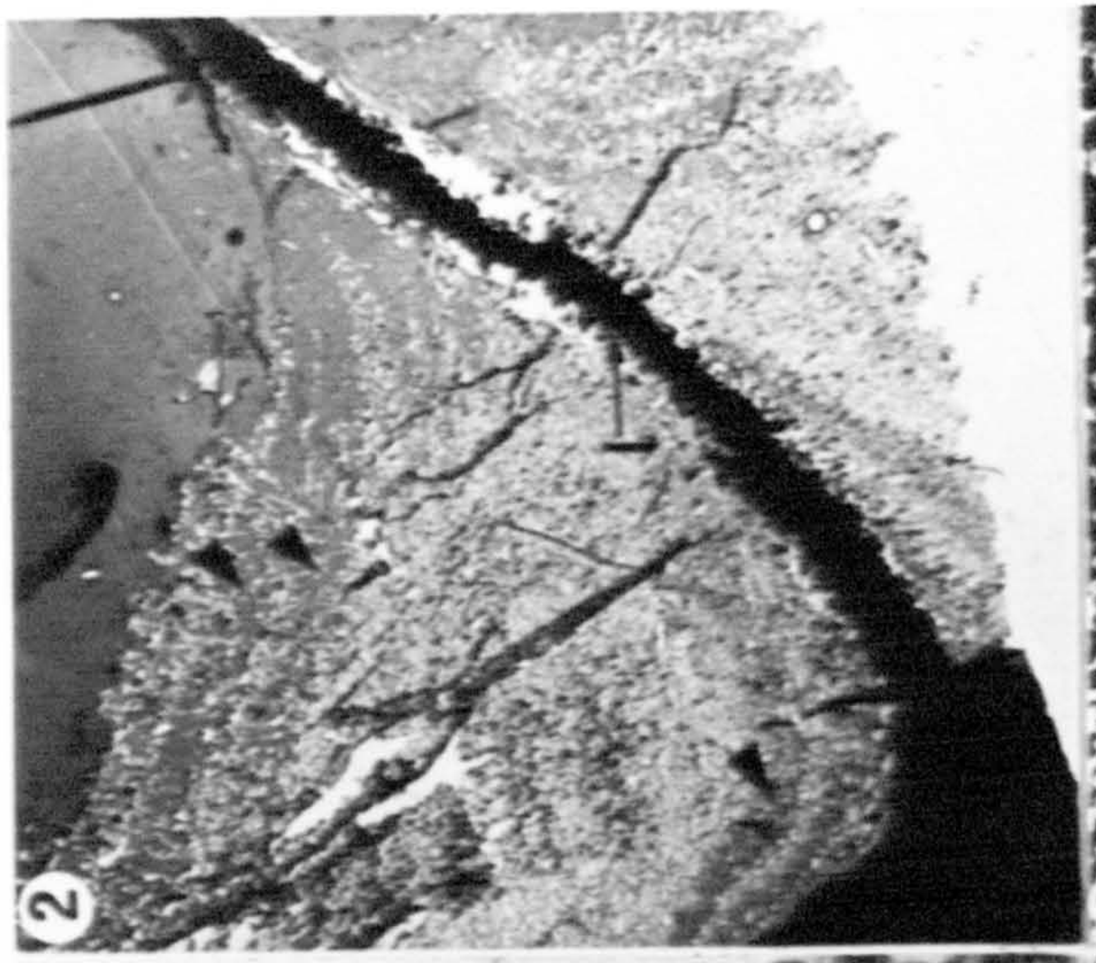

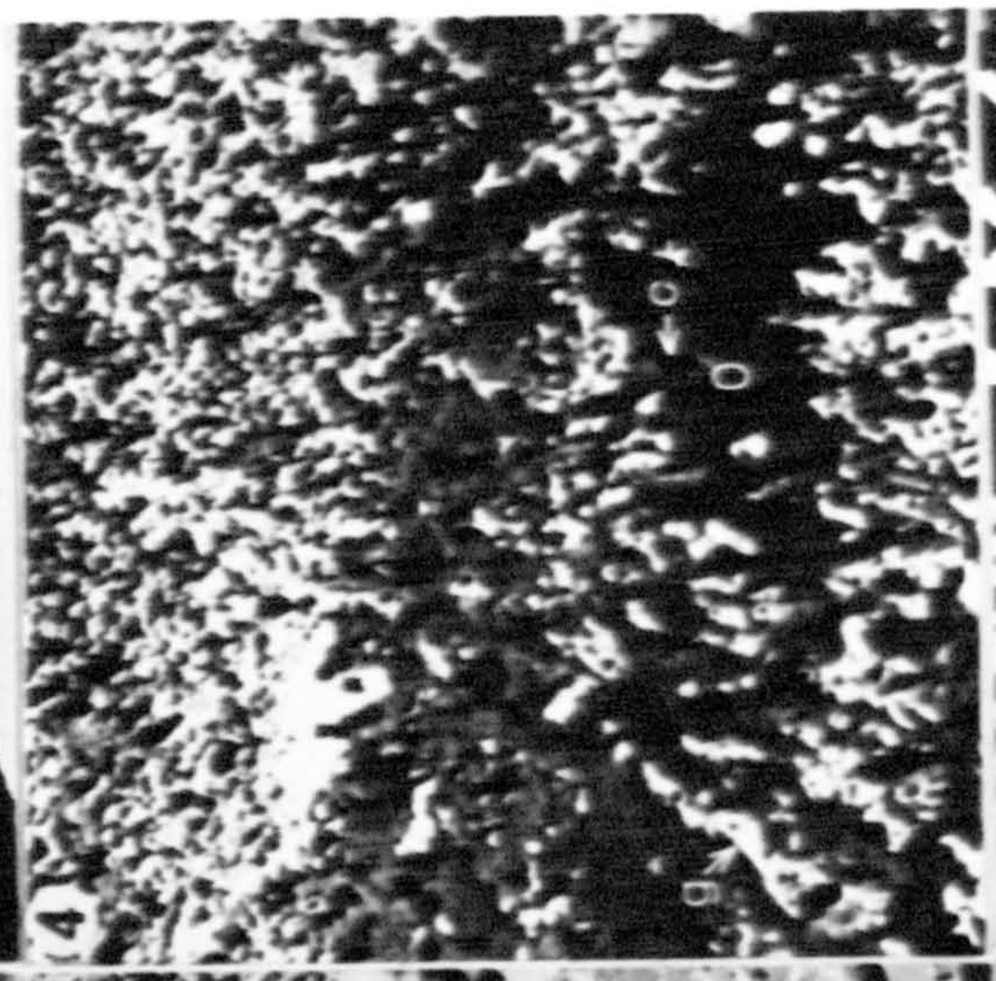

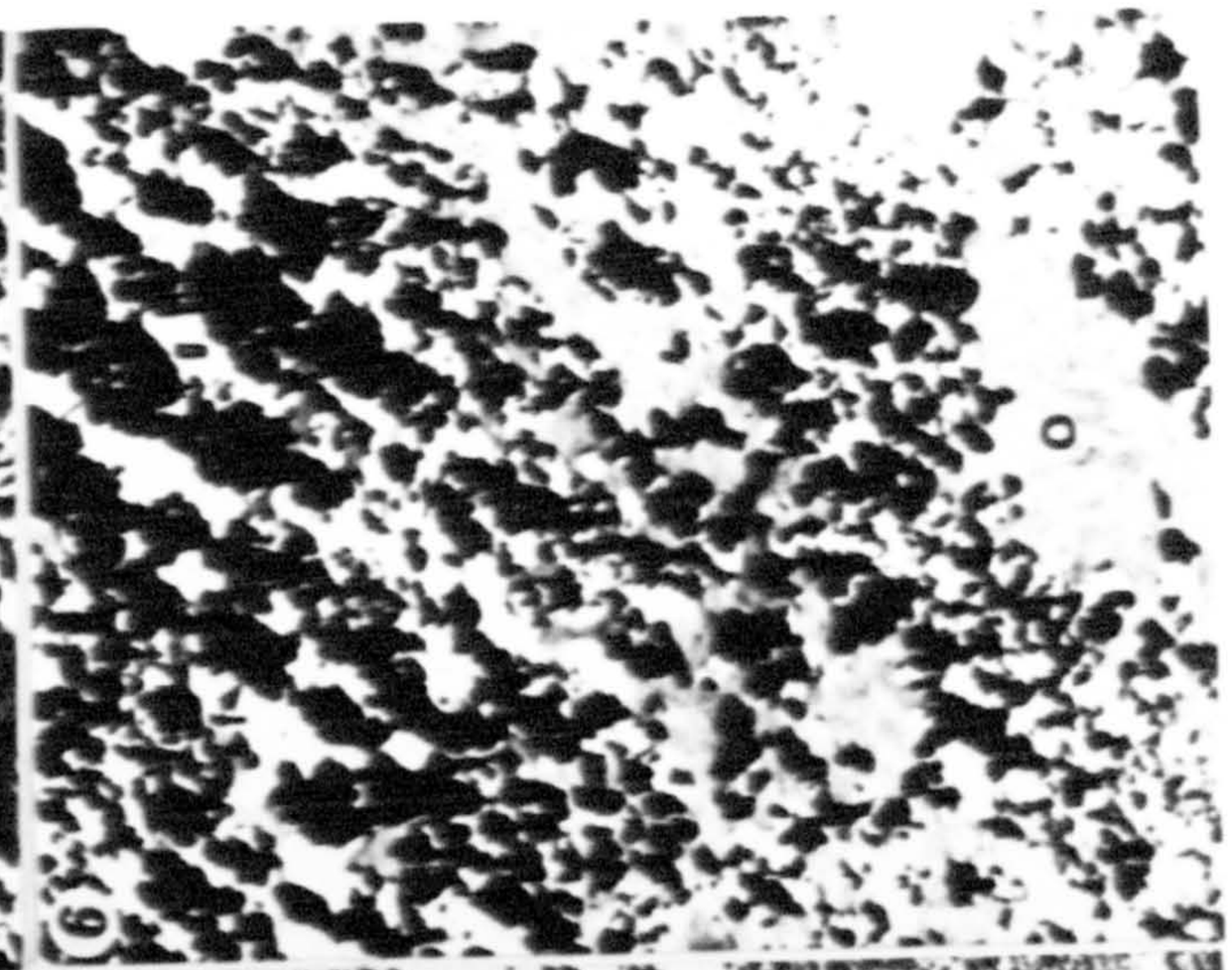

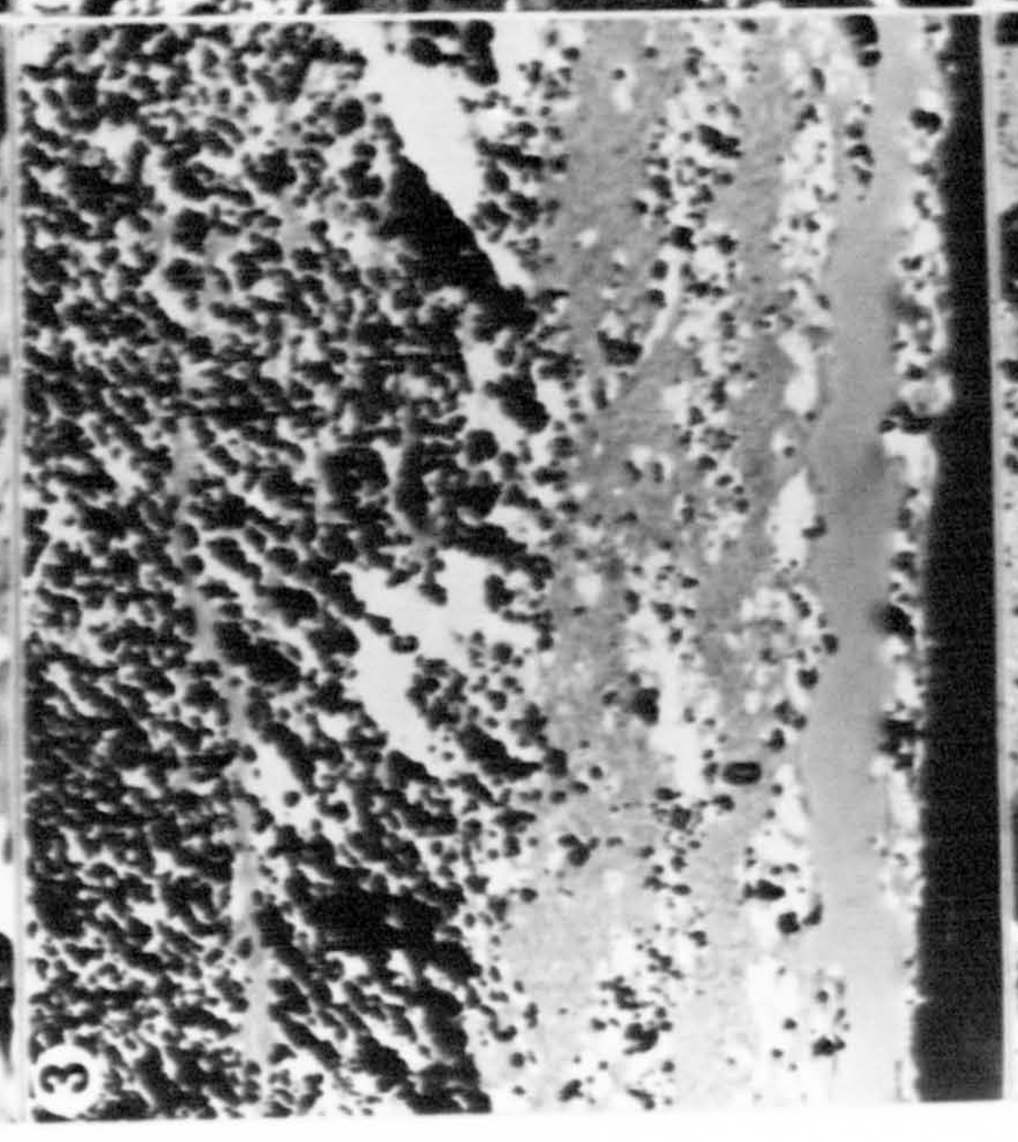

PLATE 21

Fig. 1 Section through Lamprothamnium papulosum calcine showing a complex intricate organic network ramifying throughout (o). Note the concave alignment of organics (arrows). Note also the spiral cell lateral wall (l). T.E.M. x2,500.

Fig. 2 Section through the calcine of Chara hispida showing a complex organic matrix ramifying throughout (o). Note the banding phenomenon in the endocalcine (e), the compound oosporangial wall (w), the ornamentation layer on the spiral cell lateral wall (l). Section stained with Reynolds's (1963) lead citrate and uranyl acetate (30% ethanol). T.E.M. x1,800.

Fig. 3 Section through the calcine of Chara hispida showing a complex organic matrix ramifying throughout (o). Note the banding phenomenon in the endocalcine (e). Section stained with Reynolds's (1963) lead citrate and uranyl acetate (30% ethanol.). T.E.M. x5,500.


1
O
I

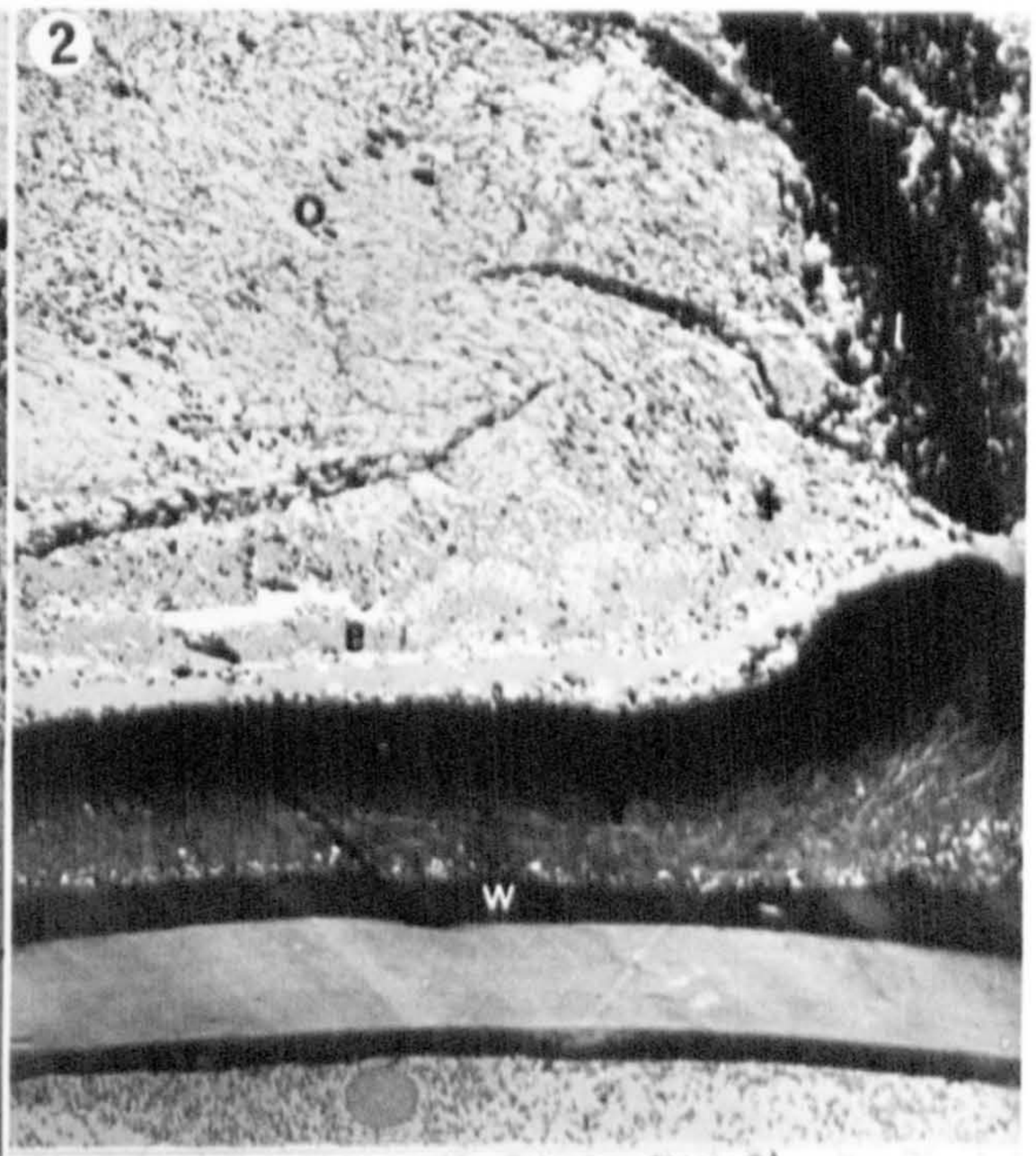
2
O
B
W

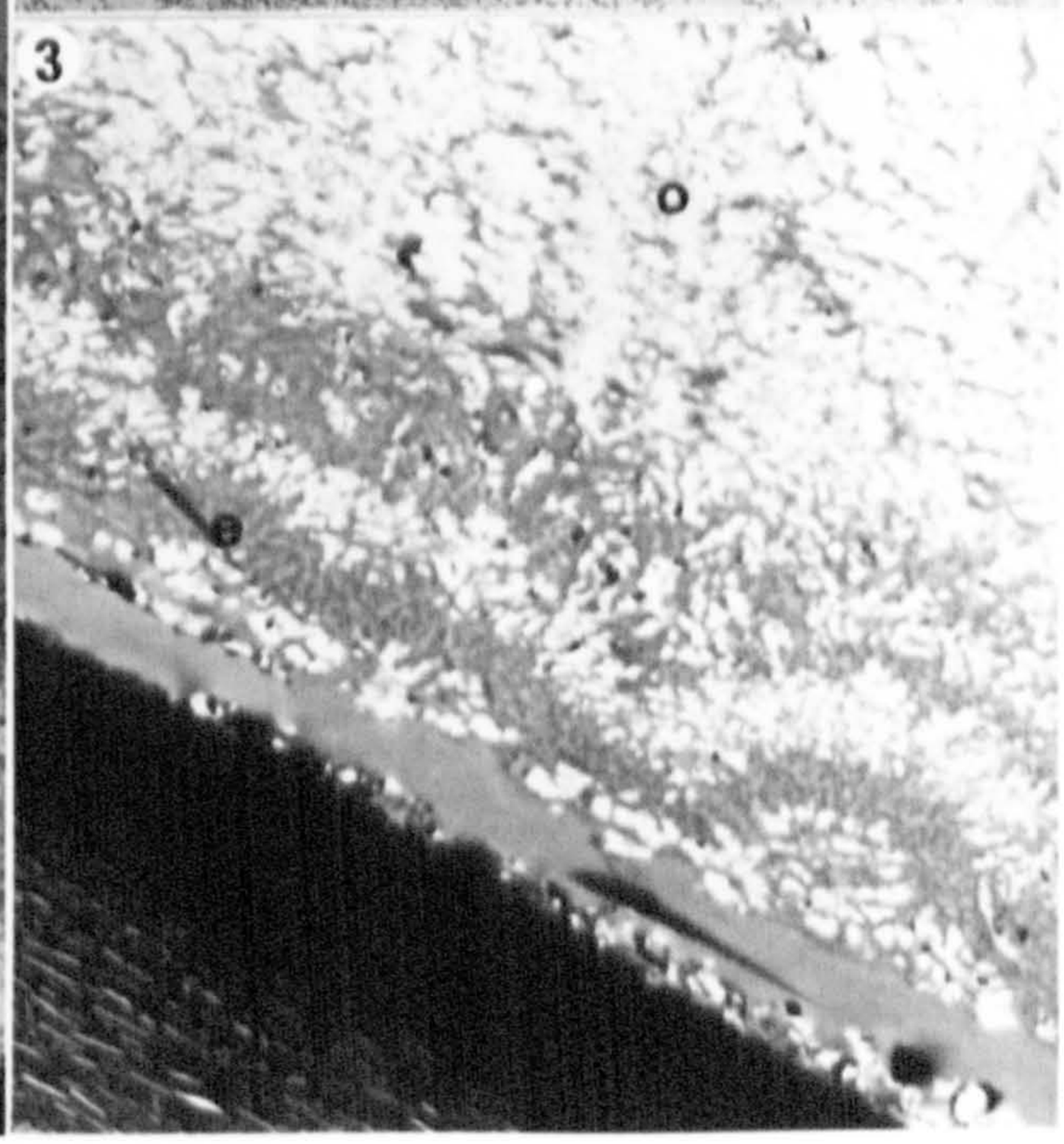
3
O

PLATE 22

Fig. 1 Fractured Chara hispida spirals showing polycrystalline columns (p) and endocalcine (e) at the fractured surface. Air dried, S.E.M. x450.

Fig. 2 Fractured Chara hispida spirals showing polycrystalline columns (p) and endocalcine (e) at the fractured surface. Air dried, S.E.M. x450.

Fig. 3 Fractured Lamprothamnium papulosum spirals showing polycrystalline columns (p) at the fractured surface. Air dried, S.E.M. x620.

Fig. 4 Fractured Lamprothamnium papulosum spiral showing polycrystalline columns and a suture (s) at the change in column direction. Air dried S.E.M. x2,000.

Fig. 5 Fractured Lamprothamnium papulosum spiral showing the suture (s) at the change in direction of the polycrystalline columns(p). Note that there are no tabular crystals. Air dried, S.E.M. x12,500.

Fig. 6 Fractured spirals soaked in tap water for one week. Spiral (b) shows the action of water whilst spiral (a) has refractured after soaking revealing polycrystalline columns. Air dried, Chara hispida, S.E.M. x400.

Fig. 7 Fractured spirals soaked in tap water for five hours showing the loss of polycrystalline colums (p) and the occurrence of a banding phenomenon (arrows). Air dried. Chara hispida, S.E.M. x500.

Fig. 8 Fractured spirals soaked in tap water for five hours. There is a loss of polycrystalline columns and the occurrence of a banding phenomenon (arrows). Air dried, Chara hispida, S.E.M. x870.

1
2
3
4
5
6
7
8

PLATE 23

Fig. 1 Fractured Chara hispida spiral showing the substructure in the polycrystalline columns. The columns are composed of layers of tabular crystals (arrows). Air dried, S.E.M. x6,450.

Fig. 2 Fractured Chara hispida spiral showing the calcine (c) to consist of layers of tabular crystals. Note the outer spiral cell wall (w) has not sloughed away in this specimen but has collapsed on top of the spiral. Air dried, S.E.M. x3,230.

Fig. 3 The spiral surface is the latest formed calcine and has clusters of small crystal stacks (s). Note the fractured surface of the spiral (f). Chara hispida, S.E.M. x3,000.

Fig. 4 Detail of latest formed calcine showing a single stack to be comprised of numerous tabular crystals (arrows). Air dried, Chara hispida, S.E.M. x23,900.

Fig. 5 Fractured spiral of Chara hispida subjected to NaOCl (10% for 5 mins.). The calcine shows layers of tabular crystals that appear the same as those from unprepared calcine. Air dried, S.E.M. x4,000.

Fig. 6 Fractured spiral of Chara hispida subjected to NaOCl (10% for 5 mins.), showing layers of tabular crystals in the calcine. Air dried, S.E.M. x5,500.

Fig. 7 Fractured spiral of Chara hispida showing the endocalcine (e) and the calcine (c). Note the distinctive demarcation between the two types of calcine (arrow). Air dried, S.E.M. x790.

Fig. 8 Underside of the spiral showing the first formed calcine. The crystals (arrows) appear in stacked rows. Air dried, Chara hispida, S.E.M. x5,100

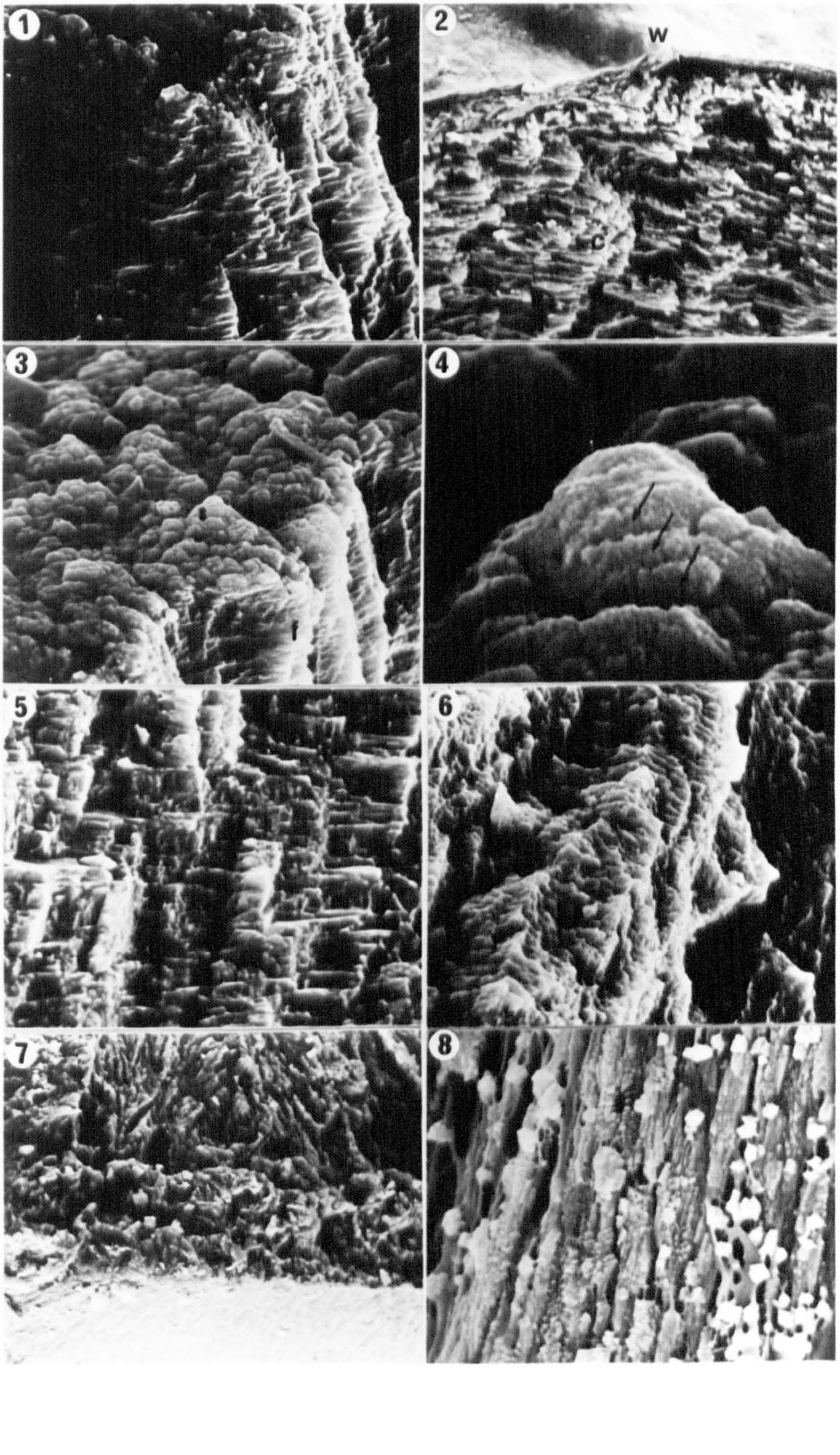
1
2
W
C
3
4
5
6
7
8

PLATE 24

Fig. 1 Fractured Chara hispida spiral soaked in tap water for three days. Note the banding phenomenon and the presence of vertically aligned crystals. Air dried, S.E.M. x2,800.

Fig. 2 Recrystallised calcite forming fimbriate crystals on the fractured spiral surface. Air dried, Chara hispida, S.E.M. x15,600.

Fig. 3 Fractured Chara hispida spiral soaked in tap water for one week. Note the banding phenomenon at the fractured surface. Air dried, S.E.M. x300.

Fig. 4 As in Fig. 3 (above). Air dried, S.E.M. x520.

Fig. 5 Fractured Chara hispida spiral soaked in tap water for one week shows bands. Each band is a complex 3D meshwork that is connected by fibrous strands . Air dried, Chara hispida, S.E.M. x2,100.

Fig. 6 After two weeks soaking in tap water the fractured spiral surface shows isolated bands. Each band is a complex 3D meshwork. Air dried, Chara hispida, S.E.M. x2,600.

Fig. 7 After three weeks soaking in tap water the spiral walls collapse around a central cavity. Air dried, Chara hispida, S.E.M. x150.

Fig. 8 A fractured Lamprothamnium papulosum spiral soaked in tap water for one week. The calcine dissolves away in the centre (c) leaving the less soluble spiral walls. Air dried, S.E.M. x400.

1
2
3
4
5
6
7
8

PLATE 25

Fig. 1 Isolated Chara hispida spiral soaked in tap water for one week showing radiating fans of recrystallised calcite (c) on the lateral spiral wall. Note the fulcrums (f) of the fans are at the base of the lateral wall and that the crystal fans show banding patterns). Air dried, S.E.M. x560.

Fig. 2 The recrystallised calcite fans on the lateral spiral wall (see Fig. 1) are interrupted at intervals (i). This forms bands of long thin crystals (c). Air dried, Chara hispida, S.E.M. x2,300.

Fig. 3 Fractured Chara hispida spiral subjected to pronase for 17 hours shows multiple layers. In addition, a secondary layering (light and dark bands) appears. The darker bands are sunken and have a more disperse layered structure. Air dried, S.E.M. x3,230.

Fig. 4 Greater resolution of the specimen in Fig. 3 (above) shows layers of crystals which are highly pitted (p). Note the strands. within the layers (arrows). Air dried, Chara hispida, S.E.M. x15,600.

Fig. 5 Fractured spiral of Lamprothamnium papulosum subjected to the enzymes zymolyase and proteinase K. A concave banding phenomenon is seen at the fractured spiral surface (f). Air dried, S.E.M. x790.

Fig. 6 Higher resolution of the fractured spiral depicted in Fig. 5. (above). A mesh (m) "blankets" the bands (b). Air dried, Lamprothamnium papulosum, S.E.M. x12,000.

Fig. 7 Fractured spiral of Chara hispida subjected to the enzymes zymolyase and proteinase K. A banding phenomenon (b) is seen at the fractured spiral surface. A "fibrous blanket" covers much of the fractured surface. Air dried, S.E.M. x780.

Fig. 8 Higher resolution of the bands shown at the fractured spiral surface depicted in Fig. 7. Recrystallised calcite (c) is responsible for the bands. Strands (arrows) connect the crystal bands. Air dried, Chara hispida, S.E.M. x6,300.

1
2
c
3
4
5
f
6
b
m
7
m
8
c

PLATE 26

Fig. 1 Fractured Chara hispida calcine subjected to the enzymes zymolyase and proteinase K. The calcine at the fractured surface shows recrystallised calcite (c) and a complex organic mesh of strands (o). Air dried, S.E.M. x8,200.

Fig. 2 Fractured Chara hispida calcine exposed to fast atom beam etching for 20 minutes. The calcine at the fracture surface appears rounded and abraided (arrows). Air dried, S.E.M. x15,000.

Figs. 3-6 Fully developed oosporangia of Chara hispida in lateral view. Note the different oosporangium morphologies. Air dried, S.E.M. x80.

Figs. 7-9 Fully developed oosporangia of Chara delicatula, Air dried.

Fig. 7 Lateral view, S.E.M. x90.

Fig. 8 Apical view, S.E.M. x120.

Fig. 9 Basal view, S.E.M. x120.

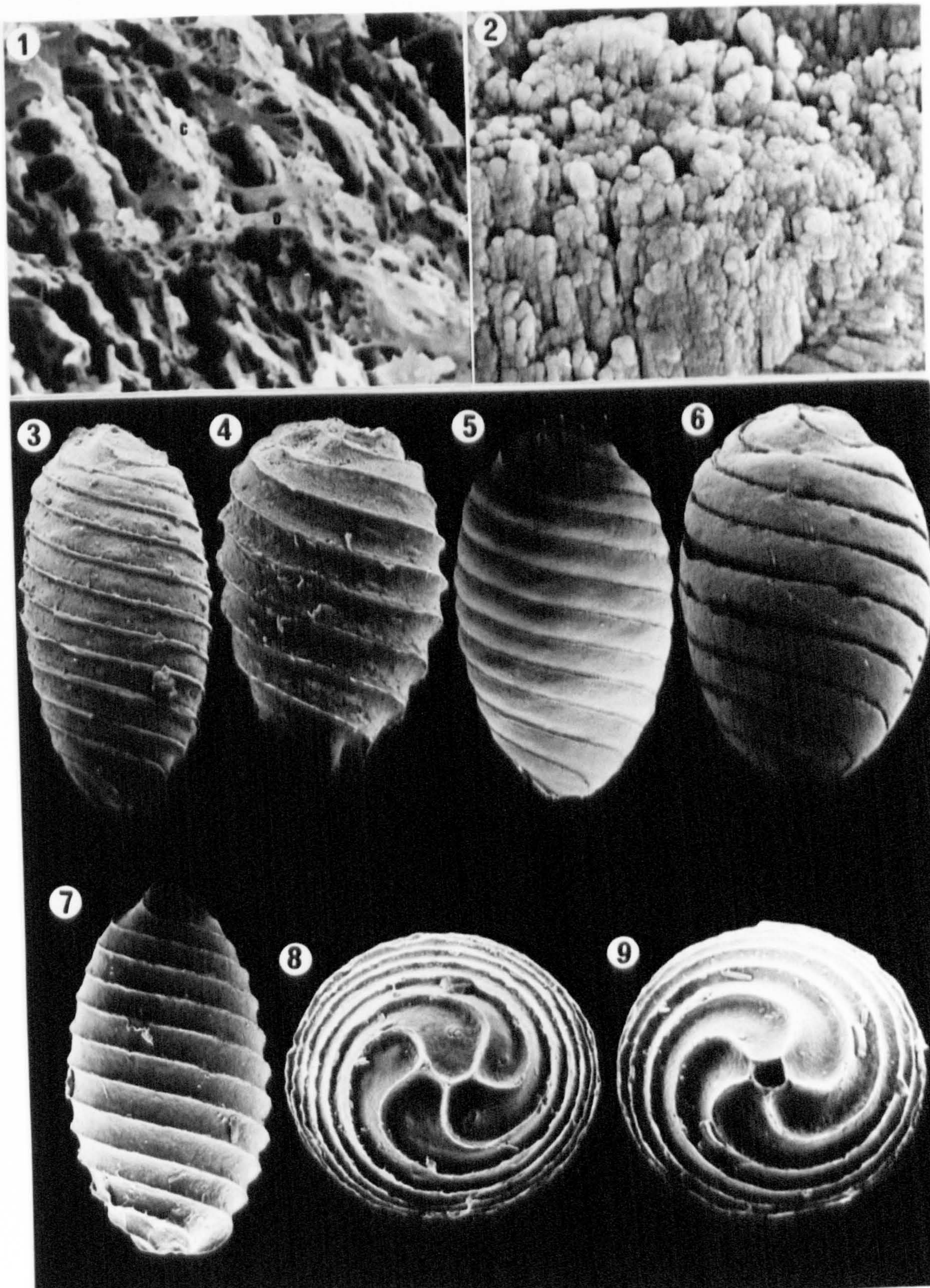
1
c
2
3
4
5
6
7
8
9

PLATE 27

Fig. 1 Ungerminated gyrogonite of Gyrogona showing spirals meeting at the apex. Air dried, S.E.M. x60.

Fig. 2 Germinated gyrogonite of Gyrogona showing fractured spiral apices, giving the "cog-wheel" form of apical pore (ap). Air dried, S.E.M. x60.

Fig. 3 Gyrogonite of Gyrogona showing fractured spiral apices (f). Air dried, S.E.M. x290.

Fig. 4 Gyrogonite of Saportonella maslovi, apical view. Air dried, S.E.M. x60.

Fig. 5 Gyrogonite of Saportonella maslovi showing the weakly calcified apex; interpreted as coronula cell calcine (c). Air dried, S.E.M. x120.

Fig. 6 Gyrogonite of Saportonella maslovi showing the strongly calcified apex; interpreted as coronula cell calcine (c). Air dried, S.E.M. x100.

Fig. 7 Gyrogonite of Rantzieniella nitida showing the "rosette" form of apical pore (ap). S.E.M. x150.

Fig. 8 Gyrogonite of Musacchiella palmeri showing the "stellate" form of apical pore (ap). (The form seems intermediate between the "rosette" form of Rantzieniella and the "cog-wheel" form of Gyrogona). Air dried, S.E.M. x225.

1
2
ap
3
4
5
6
7
ap
8
ap

PLATE 28

Fig. 1 Longitudinal section through a fully calcified oosporangium of Chara hispida showing the post- fertilisation layers, normally associated with the compound oosporangial wall (w) being deposited around the sterile cell (s) and the central cell (c). L.M. x1,600.

Fig. 2 Gyrogonite of Harrisichara, lateral view. Air dried, S.E.M. x120.

Fig. 3 Fully developed, weakly calcified oosporangium of Chara hispida showing the basal cage (c). Air dried, S.E.M. x160.

Fig. 4 Gyrogonite of Harrisichara showing the basal cage (c). Note the calcine ornamentation (o). Air dried, S.E.M. x150.

Fig. 5 Fully developed, strongly calcified oosporangium of Chara hispida showing the basal region. Note there is no basal cage. Air dried, S.E.M. x150.

Fig. 6 Gyrogonite of Harrisichara showing the calcine ornamentation (o). Air dried, S.E.M. x380.

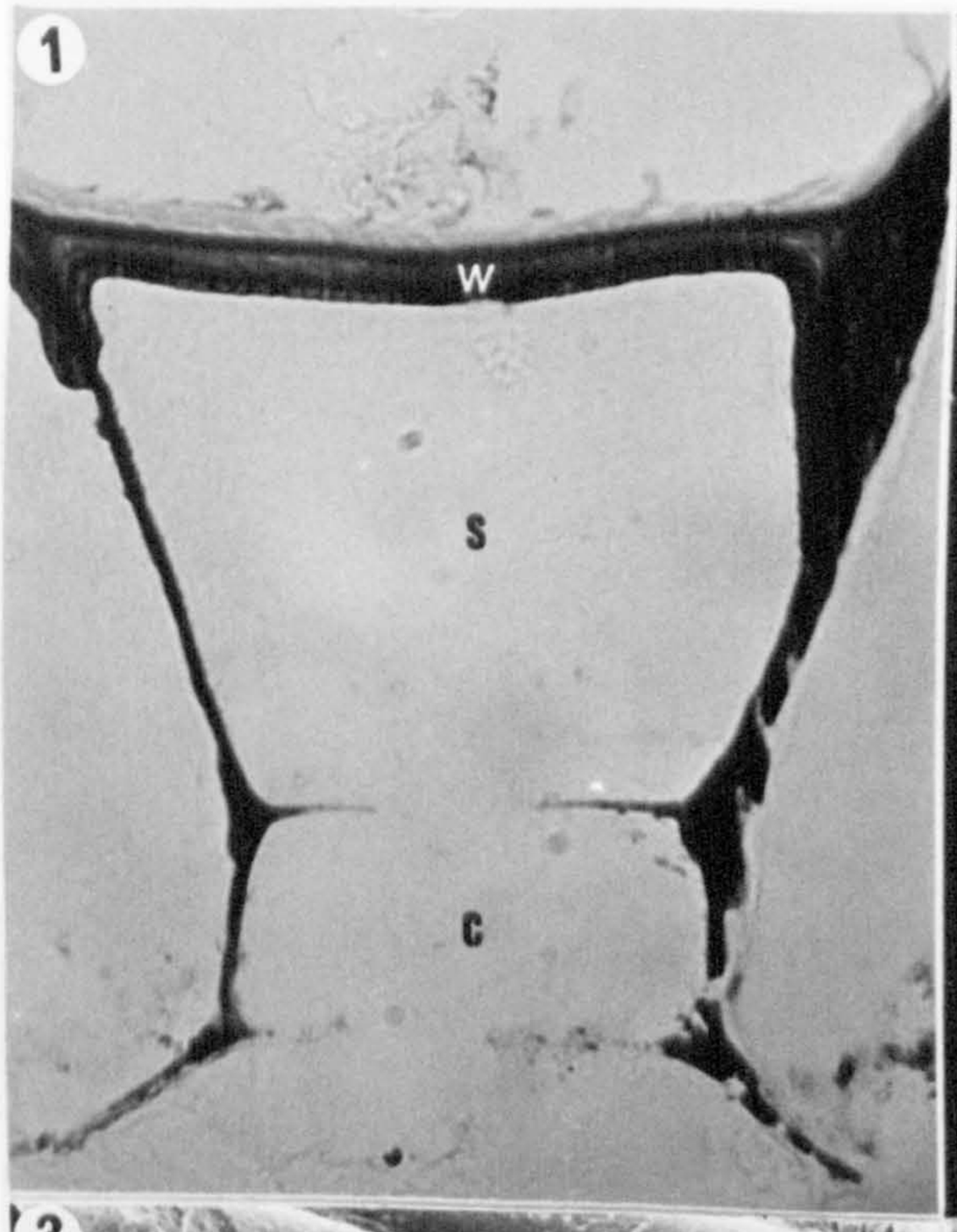
1
W
S
C

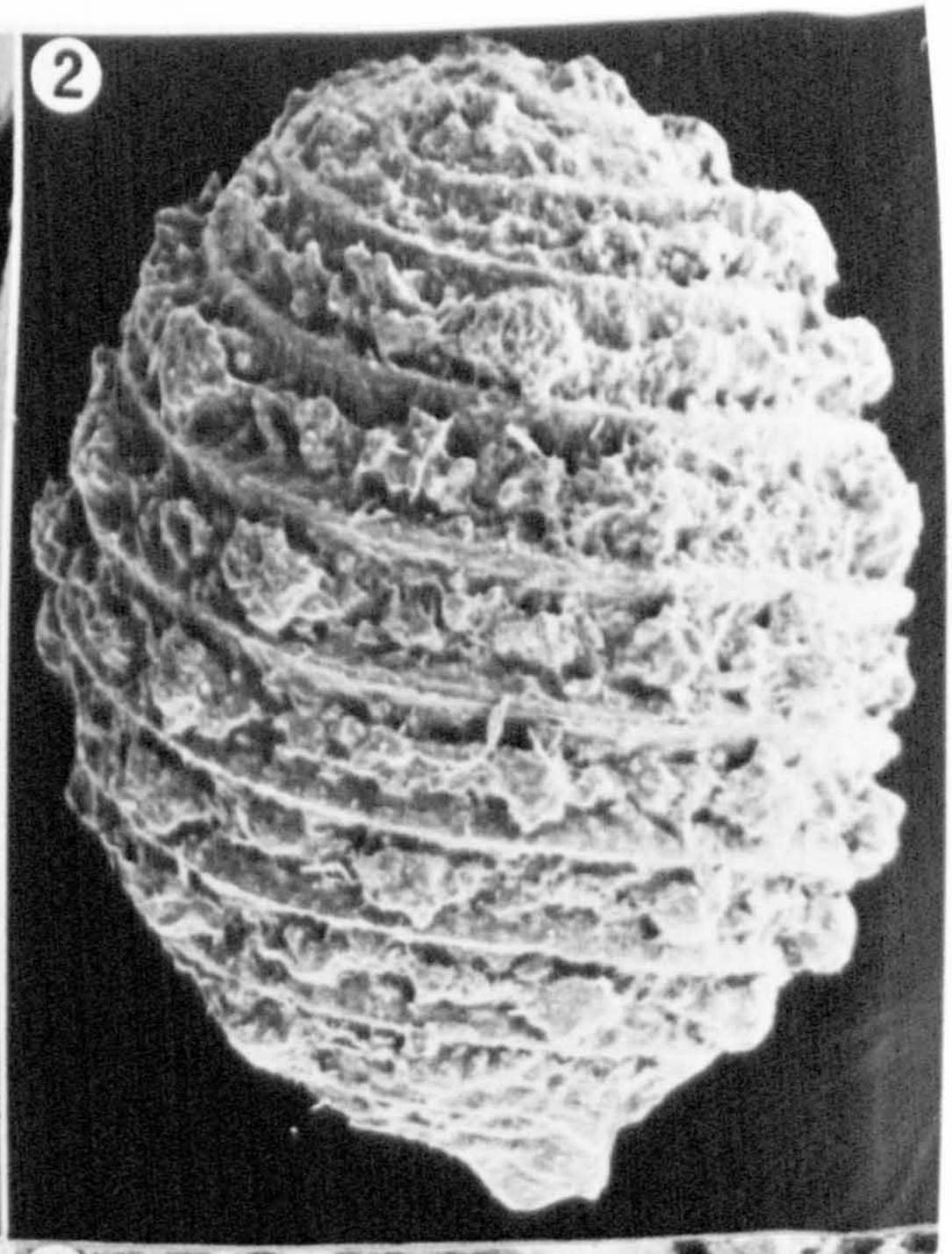
2

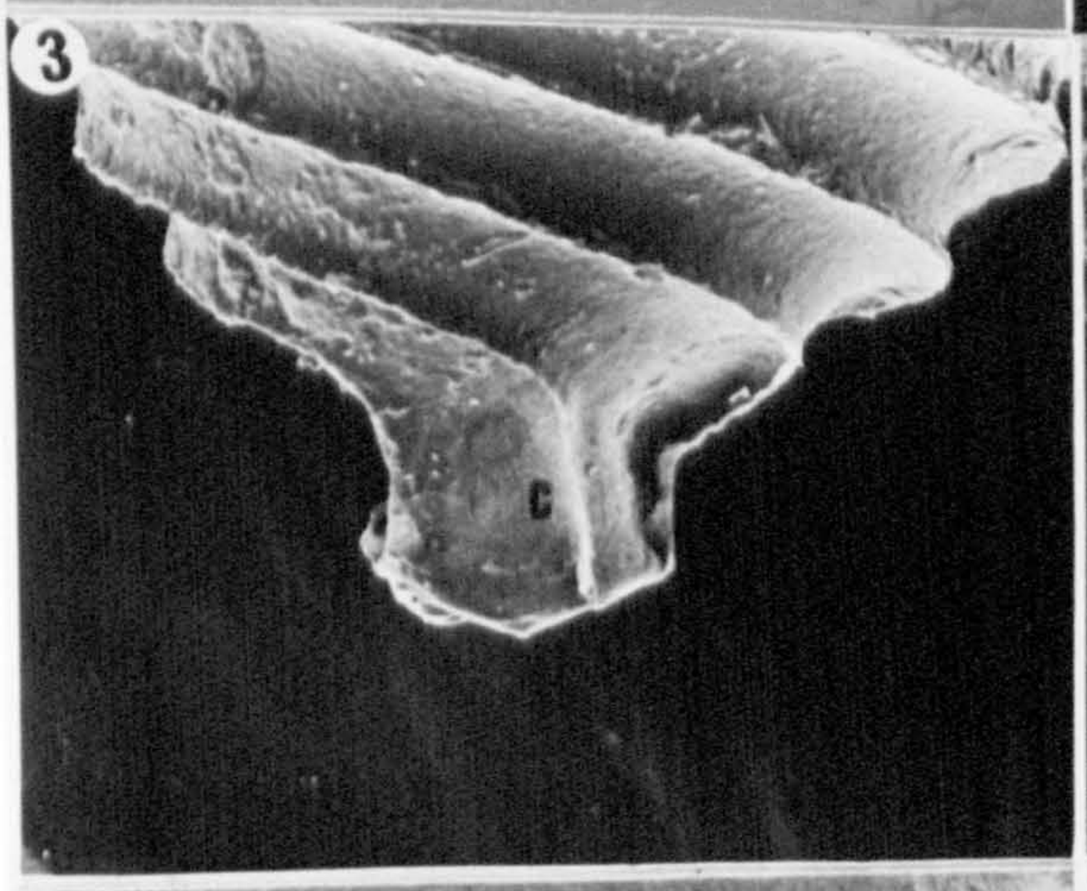
3
C

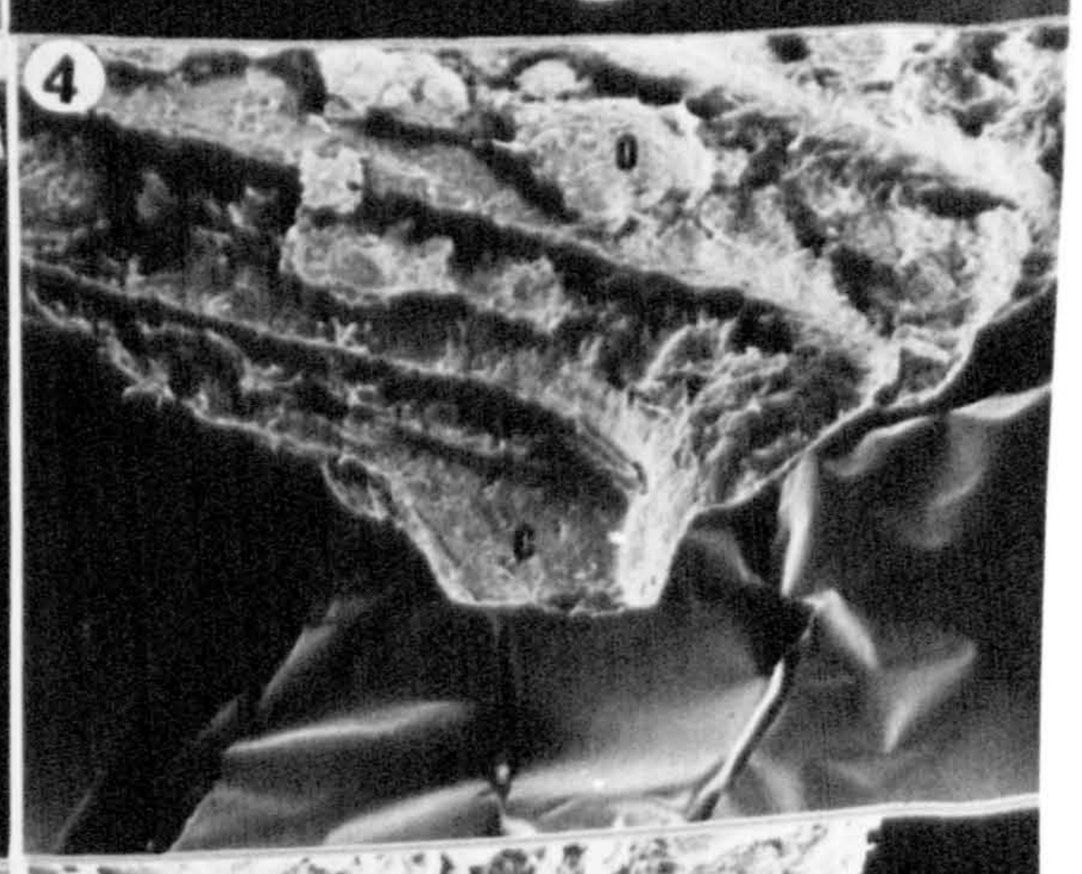
4
O
C

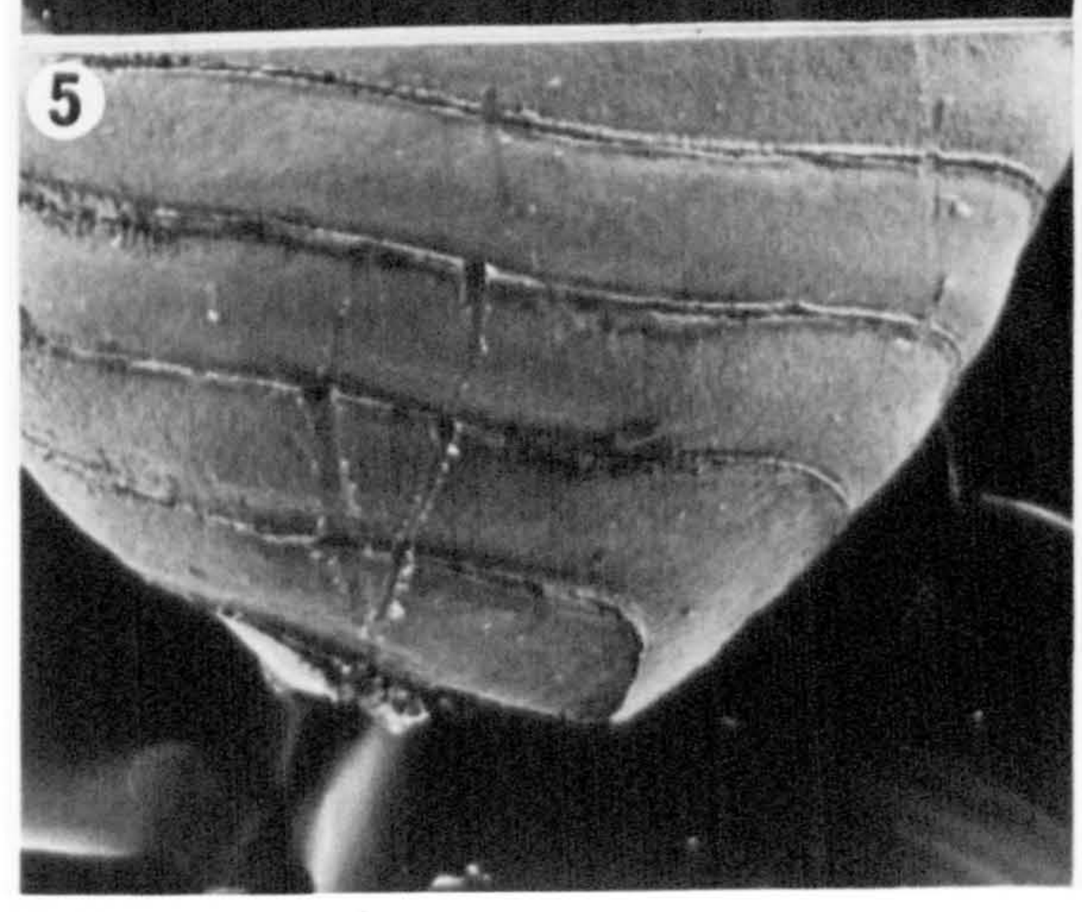
5

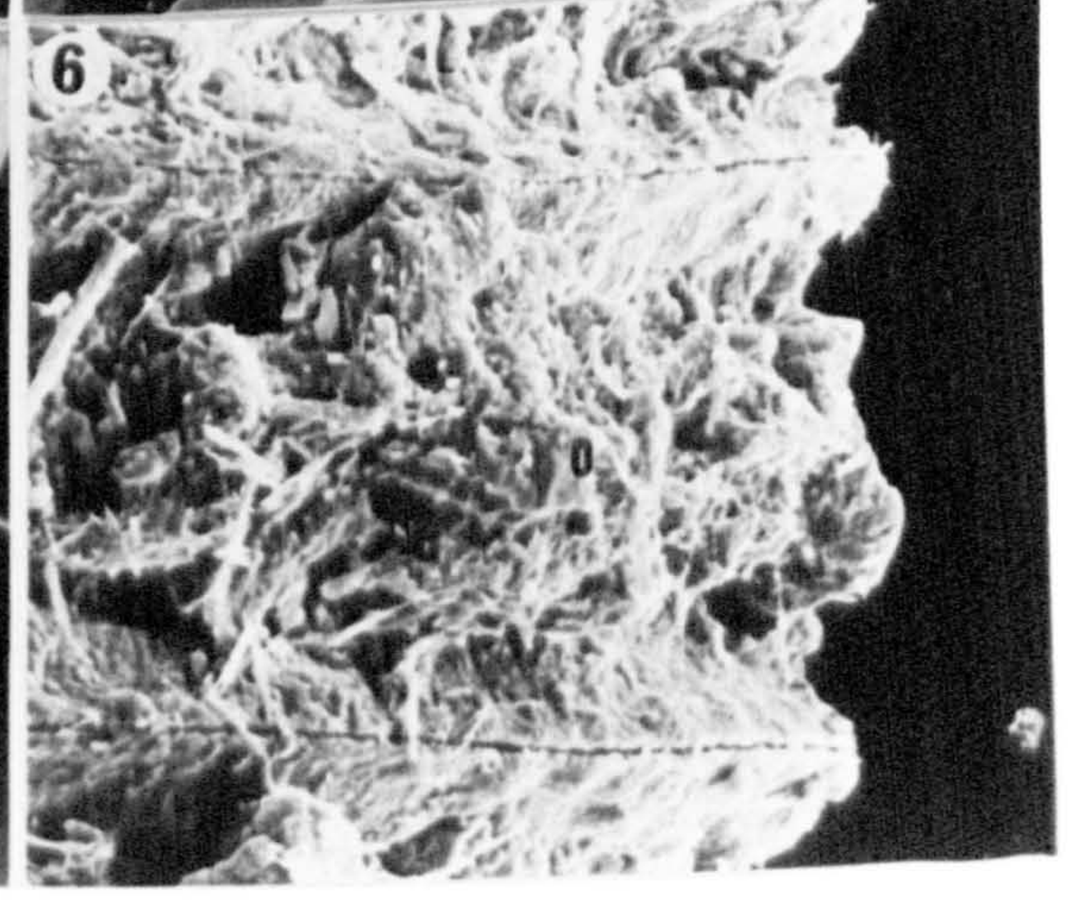
6
O

PLATE 29

Fig. 1 Internal view of the single, undivided basal plate (p) of Lamprothamnium papulosum. Note the spirals (s). Air dried, S.E.M. x190.

Fig. 2 Internal view of the 2 segments of the bipartite basal plate (p) of Musacchiella palmeri. Note the spirals (s). Air dried, S.E.M. x540.

Fig. 3 External view of the bipartite basal plate (p) of Musacchiella douzensis. Air dried, S.E.M. x640.

Fig. 4 External view of the single, undivided basal plate (p) of Porochara westerbeckensis. Note the spirals (s). Air dried, S.E.M. x270.

Fig. 5 Internal view of the spirals of Chara hispida. Note the lateral walls of the spirals (l). Air dried, S.E.M. x500.

Fig. 6 Fractured spirals of Rantzieniella nitida showing that the inner region of the lateral wall is strongly ridged (r). Air dried, S.E.M. x270.

Fig. 7 Internal view of two spirals of Rantzieniella nitida showing the sinusoidal lateral spiral wall (arrow). Air dried, S.E.M. x830.

Fig. 8 Internal view of two spirals of Lamprothamnium papulosum showing the "pillars" (p) at the base of the lateral walls of the spirals. Air dried, S.E.M. x1,550.

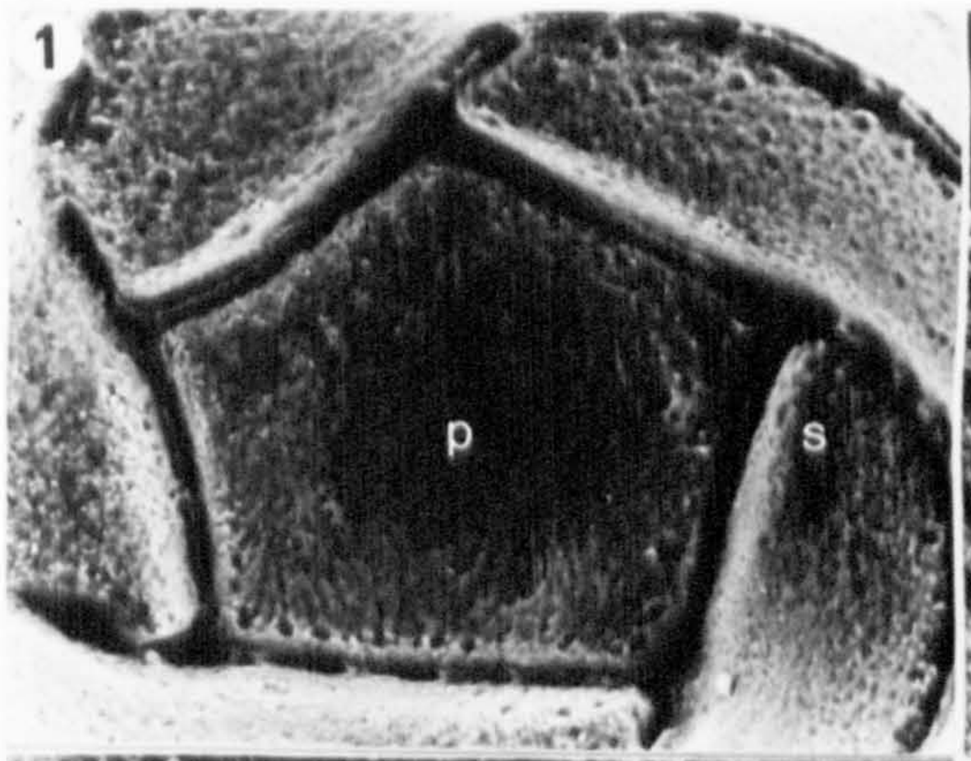
1
p
s

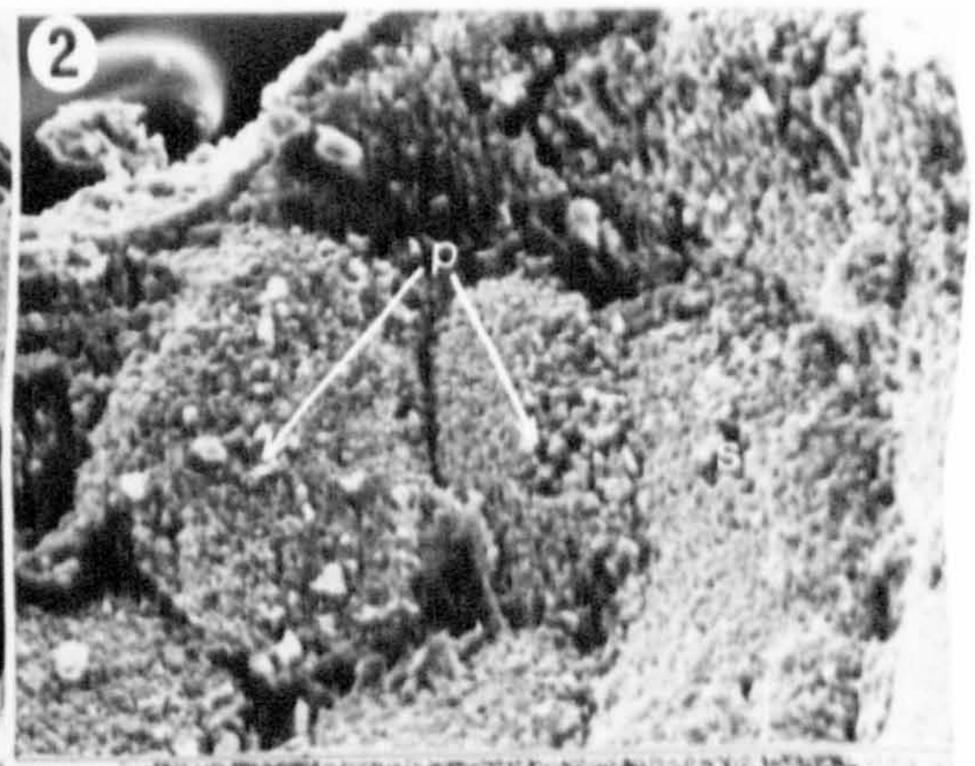
2
p
s

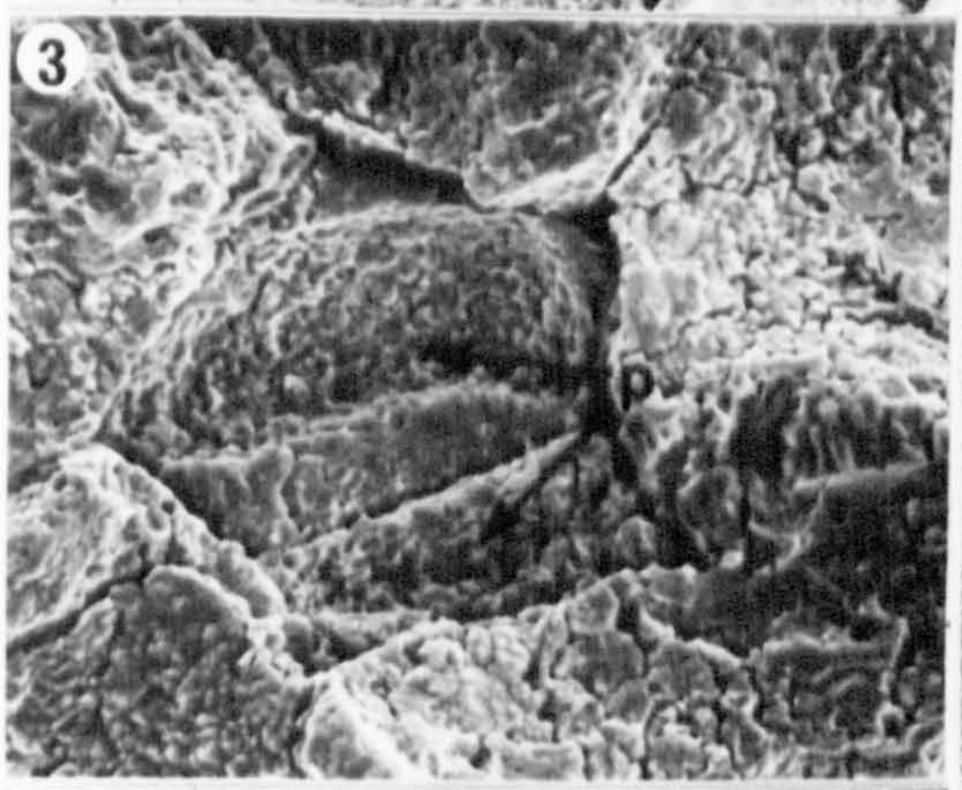
3
p

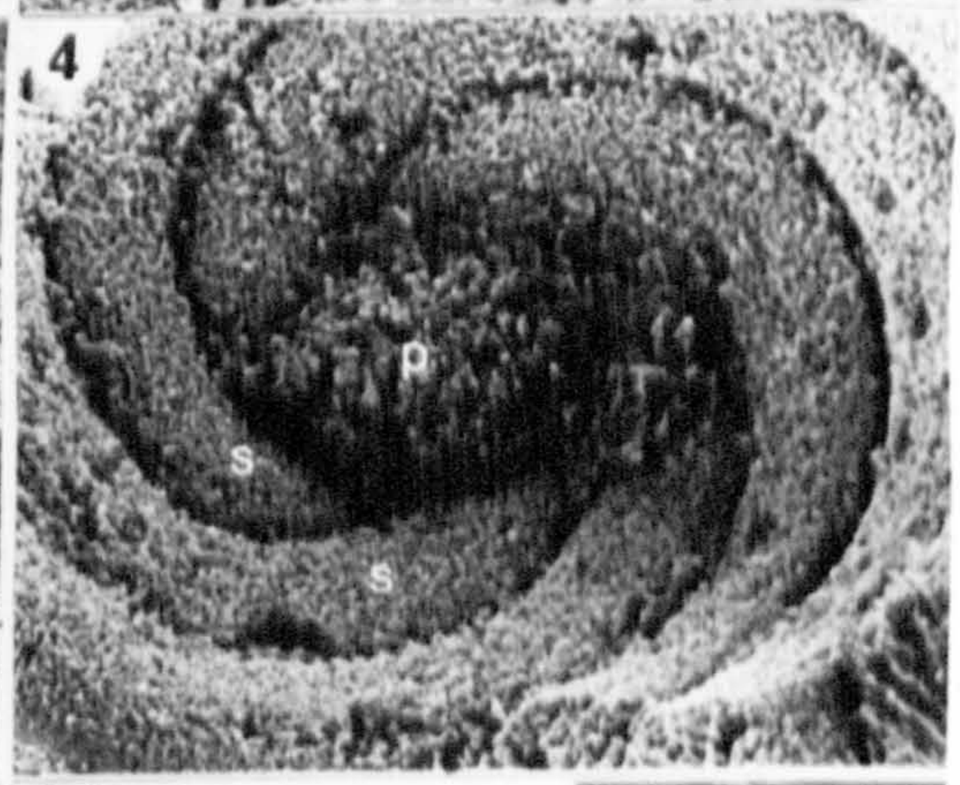
4
p
s
s

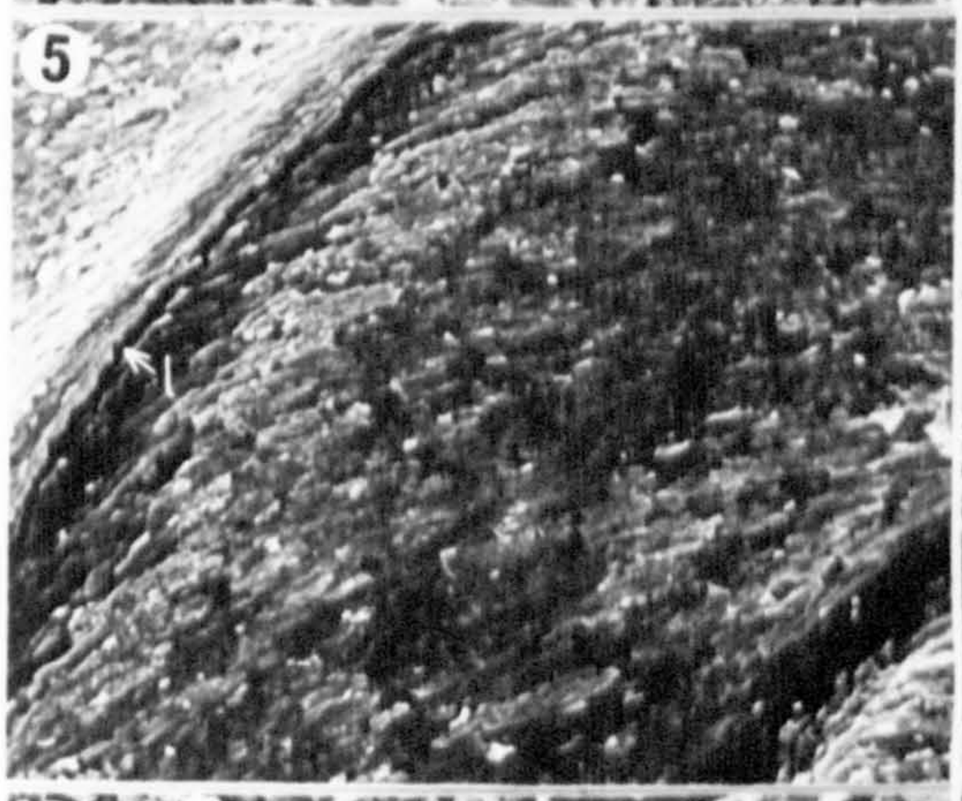
5
l

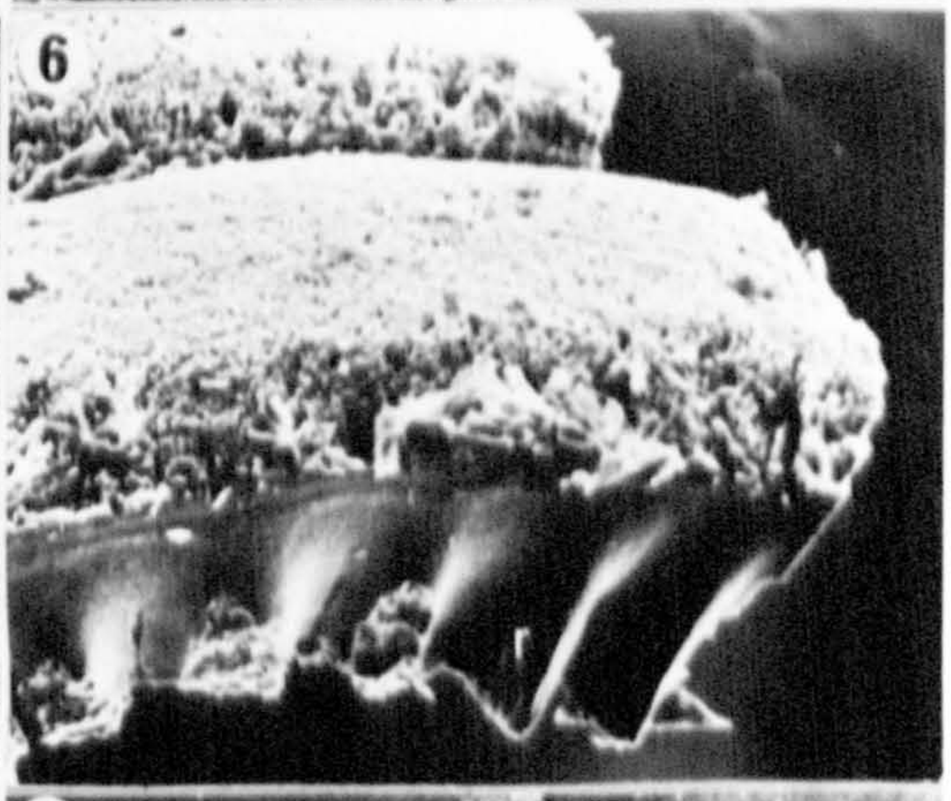
6
l


7


8
p

PLATE 30

Fig. 1 Silicified petrification of Clavator reidi. Note the vertical cells (c) which comprise the utricle. Air dried, S.E.M. x40.

Fig. 2 Longitudinal section through a gyrogonite of Musacchiella palmeri showing the radiating crystals in each spiral (s). L.M. x40.

Fig. 3 Transverse fracture through Musacchiella palmeri spirals showing radiating crystals. Air dried, S.E.M. x900.

Fig. 4 Transverse fracture through Rantzieniella nitida spirals showing radiating crystal needles. Air dried, S.E.M. x370.

Fig. 5 Transverse fracture through Porochara mundula spirals, showing radiating crystals. Note the sparry calcite cast (c) in the centre of the gyrogonite. Air dried, S.E.M. x620.

Fig. 6 Transverse fracture through Porochara mundula spirals showing the crystals (c) . Air dried, S.E.M. x200.

Fig. 7 Transverse fracture through a Gyrogona spiral showing large crystals of secondary calcite (c). Air dried S.E.M. x520.

Fig. 8 Transverse fracture through Saportonella maslovi spirals showing a banding phenomenon in the calcine of each spiral. Air dried, S.E.M. x200.

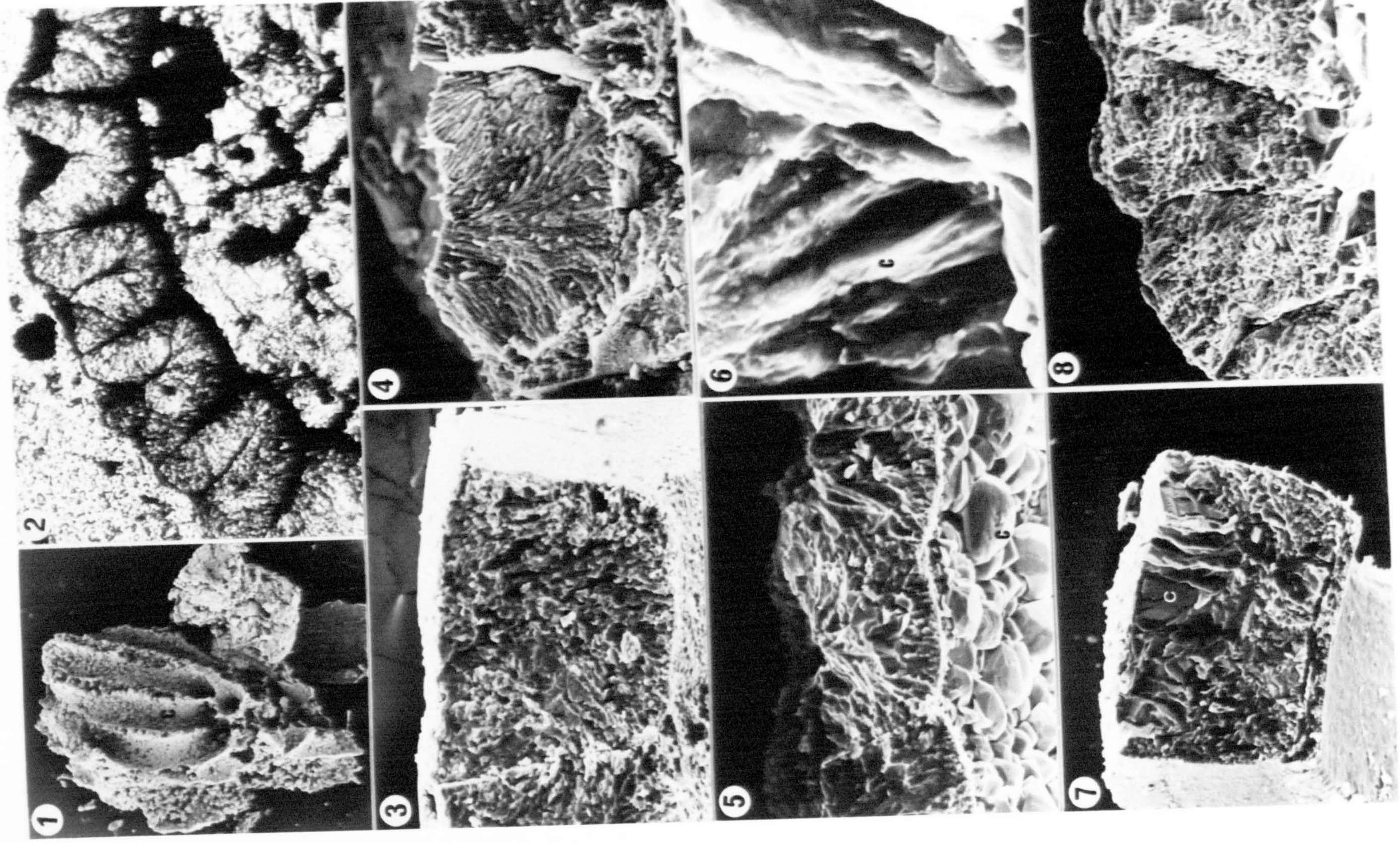
1
2
3
4
5
6
7
8
c
c
c

PLATE 31

All specimens for S.E.M. were air dried

Figs. 1-7 Musacchiella douzensis.

Fig. 1 Lateral view, S.E.M. x 110.

Fig. 2 Apical view, S.E.M. x 155.

Fig. 3 Basal view, S.E.M. x 155.

Fig. 4 External view of base, showing the bipartite basal plate (p). S.E.M. x320.

Fig. 5 The lateral walls of the spirals (l) appear as a spiralling suture in the calcine. S.E.M. x310.

Fig. 6 Transverse section through a gyrogonite showing the radiating crystals in the calcine (c). L.M. x350.

Fig. 7 Detail of the blocky appearance of the calcine as seen on external inspection. S.E.M. x1750.

1

2

3

4

5

6

c

7

PLATE 33

All specimens were air dried.

Figs. 1-9 Porochara westerbeckensis.

Fig. 1 Lateral view; note the broad stout neck at the apex. S.E.M. x110.

Fig. 2 Lateral view, S.E.M. x110.

Fig. 3 Apical view, S.E.M. x110.

Fig. 4 Apical view, S.E.M. x110.

Fig. 5 Basal view, S.E.M. x110.

Fig. 6 Lateral view, gyrogonite shows basal/apical compression. S.E.M. x130.

Fig. 7 Oblique view, gyrogonite is laterally compressed. S.E.M. x130.

Fig. 8 Detail of base; the basal pore (p) is filled with calcite debris which obscures the basal plate. S.E.M. x640.

Fig. 9 Transverse fracture through a spiral (s) showing the radiating calcite crystals in the calcine. S.E.M. x940.

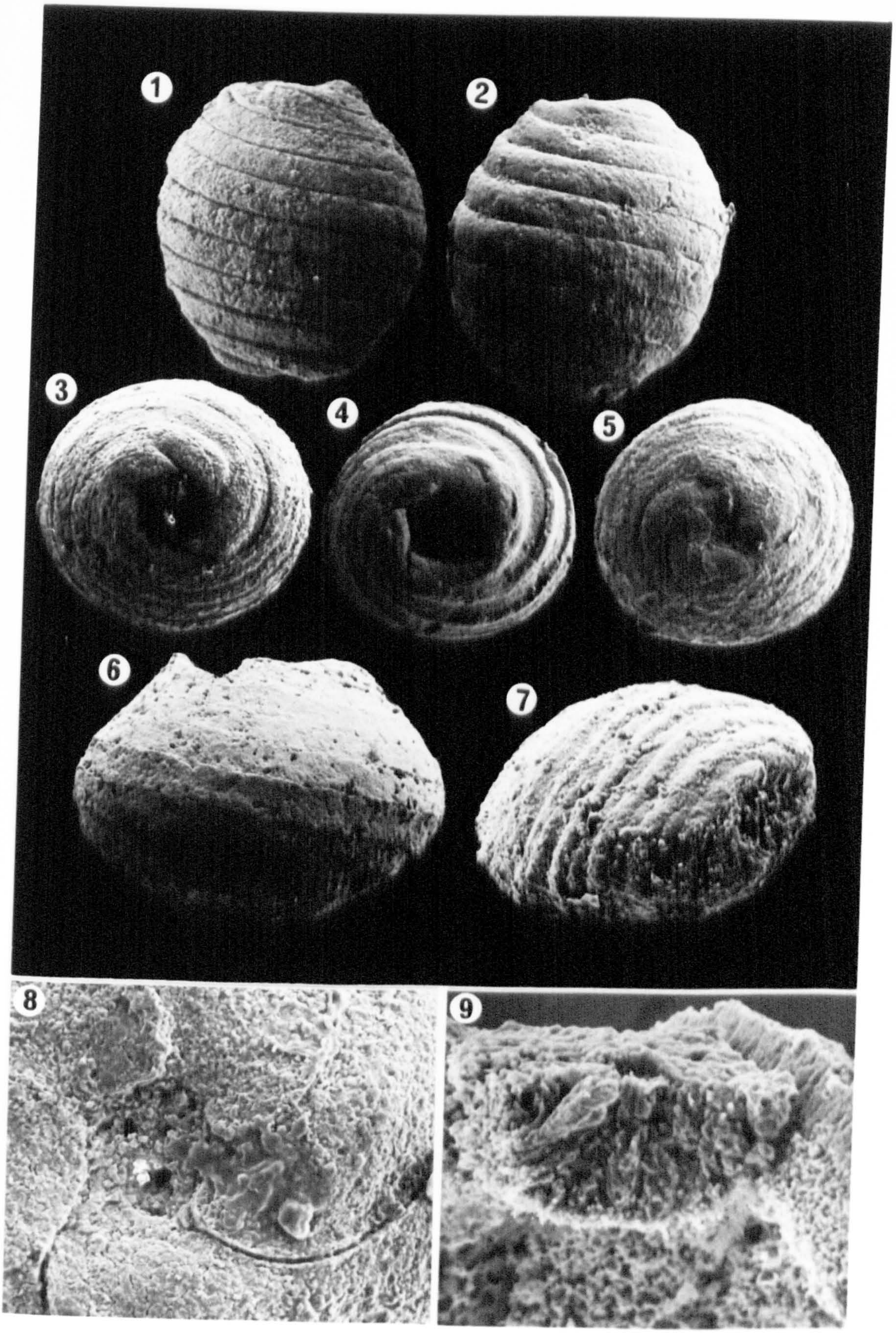
1
2
3
4
5
6
7
8
9

PLATE 34

All specimens were air dried.

Figs. 1-6 Porochara obovata.

Fig. 1 Lateral view, weakly calcified gyrogonite, S.E.M. x115.

Fig. 2 Lateral view, S.E.M. x115.

Fig. 3 Apical view, S.E.M. x115.

Fig. 4 Basal view, S.E.M. x130.

Fig.5 Weakly calcified spirals. Note the calcite debris on the gyrogonite. S.E.M. x640.

Fig. 6 Strongly calcified spiral (s), weakly calcified spiral (w). S.E.M. x300.

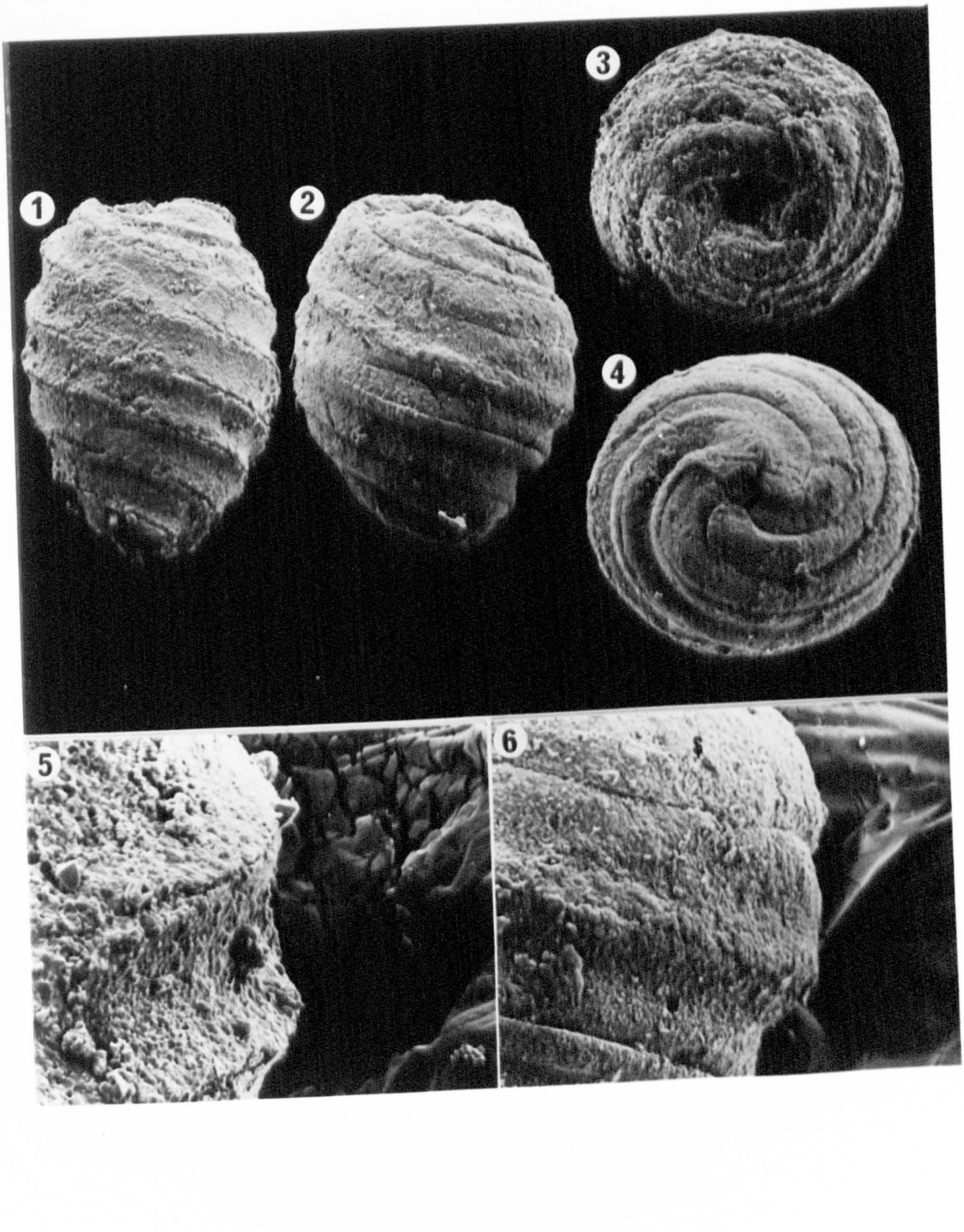
1
2
3
4
5
6

PLATE 35

All specimens were air dried.

Figs. 1-7 Porochara mundula

Fig. 1 Lateral view, S.E.M. x120.

Fig. 2 Lateral view, S.E.M. x90.

Fig. 3 Apical view, S.E.M. x120.

Fig. 4 Basal view, S.E.M. x130.

Fig. 5 Weakly calcified spirals, S.E.M. x370.

Fig. 6 Moderately calcified spirals, S.E.M. x315.

Fig. 7 Strongly calcified spirals, S.E.M. x370.

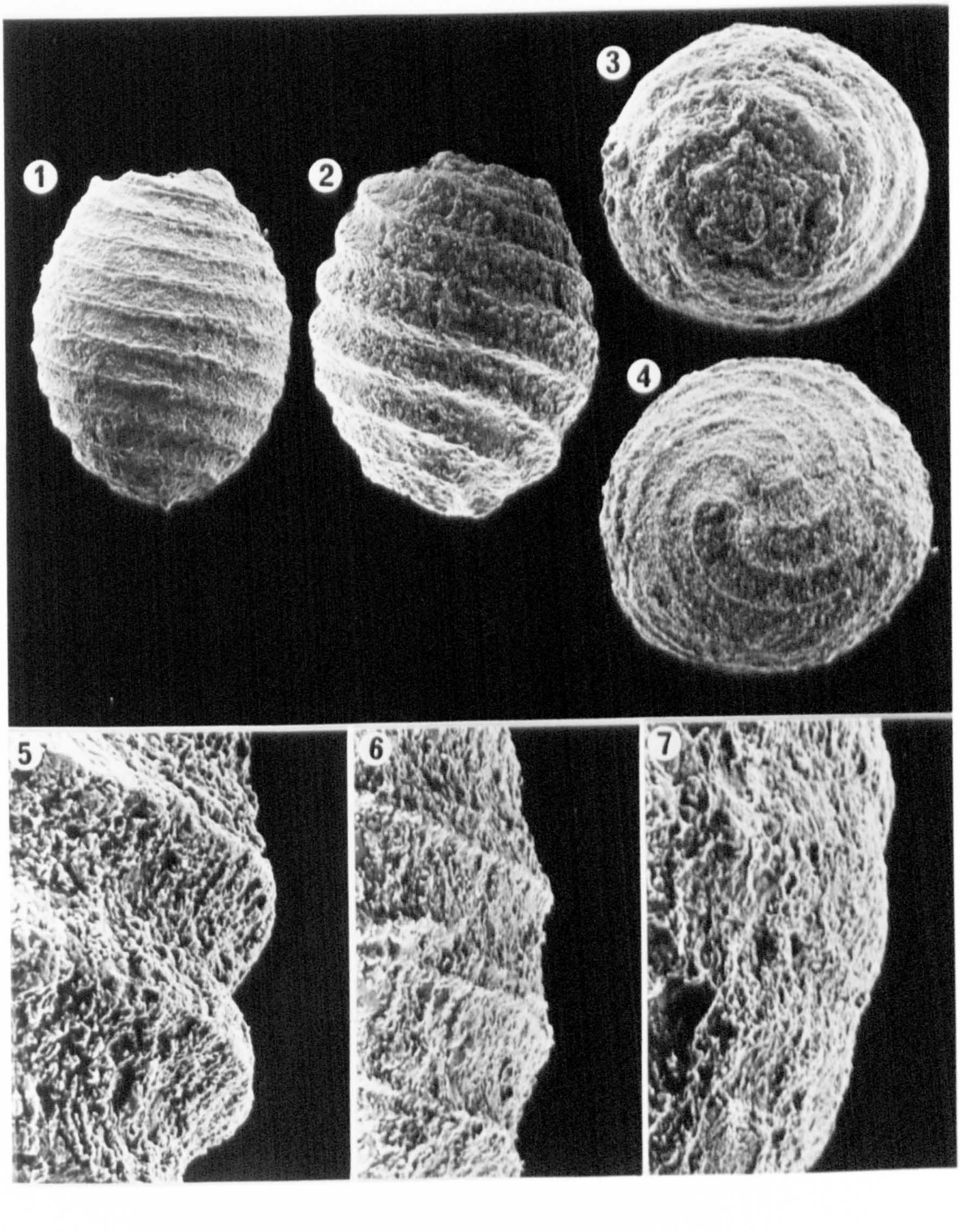
1
2
3
4
5
6
7

PLATE 36

All specimens were air dried

Figs. 1-3 Porochara portoensis

Fig. 1 Lateral view, S.E.M. x140.
2 Lateral view, S.E.M. x140.
3 Apical view, S.E.M. x140.

Fig. 4 Porochara raskyae, lateral view, S.E.M. x90.

Fig. 5 Porochara raskyae, detail of apex, S.E.M. x110.

Fig. 6 Porochara portoensis, detail of base. Note that poor preservation and calcite debris obscures detail of the basal pore (p). S.E.M. x600.

Fig. 7 Fractured spiral (s) of Porochara portoensis showing radiating crystals. Note the sparry calcite cast (c). S.E.M. x1100.

Fig. 8 Porochara raskyae, detail of base. Note that poor preservation and calcite debris obscures detail of the basal pore (p). S.E.M. x140.

Fig. 9 Fractured spiral (s) of Porochara raskyae showing blocky calcite in the calcine. S.E.M. x600.

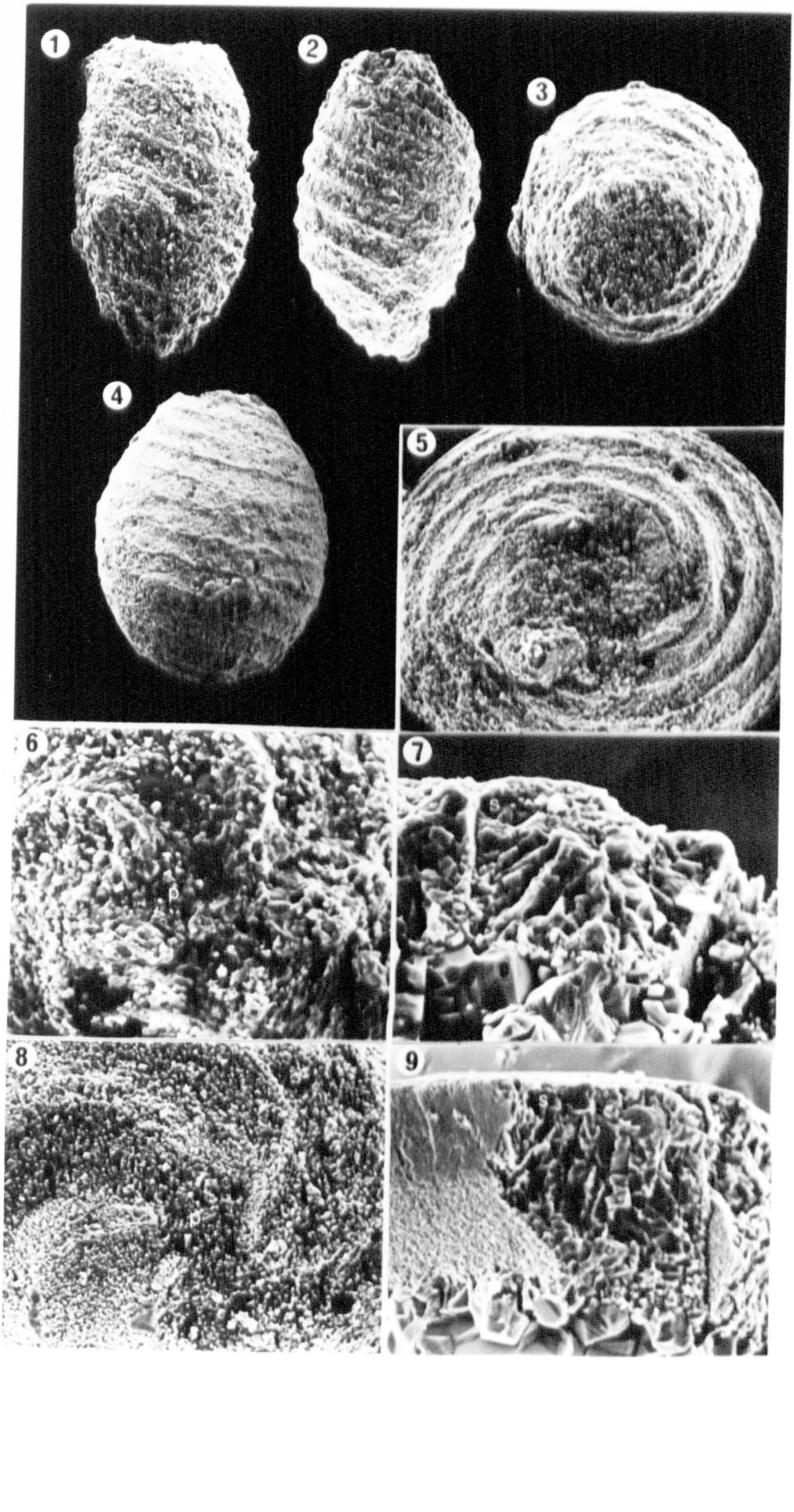
1
2
3
4
5
6
7
8
9